Identifizierung und praktische Anwendung molekularer Marker für eine Verbesserung der Prognosebeurteilung humaner Neuroblastome

Der medizinischen Fakultät
der Universität Leipzig
eingereichte

HABILITATIONSSCHRIFT

zur Erlangung des akademischen Grades

Doctor medicinae habilitatus
(Dr. med. habil.)

vorgelegt

von Dr. med. Axel Weber
geboren am 10. Mai 1974 in Hanau

Leipzig, den 11.01.2011

Verleihungsbeschluss: Leipzig, den 24.04.2012

Bibliographische Beschreibung:

Weber, Axel

Titel der Arbeit:

Identifizierung und praktische Anwendung molekularer Marker für eine Verbesserung der Prognosebeurteilung humaner Neuroblastome

Universität Leipzig, kumulative Habilitationsschrift

Textteil: 129 Seiten einschließlich 8 publizierter Manuskripte, 51 Literaturstellen

Referat:

Die Abschätzung der Prognose für Patienten, insbesondere Kinder mit onkologischen Erkrankungen stellt eine große Herausforderung an die behandelnden Ärzte dar. Vor Beginn einer Therapie werden daher viele Informationen gesammelt, um einen Patienten möglichst gut in eine vordefinierte Risikogruppe stratifizieren und dementsprechend eine mehr oder weniger intensive Therapie anbieten zu können. Diese Einteilungen sind allerdings für keinen Malignomtyp mit 100%-iger Sicherheit möglich. Das ist die Ursache dafür, dass auch in niedrige Risikogruppen eingeteilte Patienten nicht auf die Therapie ansprechen und einen unvorhergesehen schlechten Verlauf zeigen können. Auf der anderen Seite scheint es Patienten zu geben, die trotz initial schlecht eingeschätzter Prognose einen überaschend guten Verlauf nehmen, auf die Therapie gut ansprechen und letztlich geheilt werden können.

Einen Beitrag zu leisten, um die Stratifizierung für Kinder, die an einem Neuroblastom erkrankt sind, zu verbessern und damit zu vermeiden, dass einige Patienten unter- oder andere Patienten übertherapiert werden müssen, ist das Ziel dieser Habilitationsarbeit.

Zu diesem Zweck wurden differentielle, molekulare Marker in primären humanen Neuroblastomen identifiziert und deren prognostische Bedeutung dargestellt. Einzelne dieser Marker (differentiell expremierte mRNAs) wurden in Zellkultursystemen funktionell untersucht, um deren zellbiologische Funktion, die der jeweiligen prognostischen Bedeutung zugrunde liegen kann zu erklären. Desweiteren konnten genomische Merkmale des amplifizierten genomischen Abschnittes auf Chromosom 2p25 um *MYCN* beschrieben werden. Darauf basierend konnte eine patientenindividuelle und tumorzellspezifische PCR entwickelt werden (AFS-PCR), die sich als Marker für den Nachweis einer minimalen Resterkrankung eignet.

Inhaltsverzeichnis

Seite

1. Einleitung 1

2. Publikationen

2.1 Genexpressionsmarker in humanen Neuroblastomen

Hintergrund: 5

Eigene Publikationen: 8

2.2 Funktionelle Untersuchung von differentiell expremierten Genen

Hintergrund: 26

Eigene Publikationen: 29

2.3 Genexpressionsmuster

Hintergrund: 51

Eigene Publikationen: 53

2.4 Amplifikation des genomischen Bereiches Chr2p24-25

Hintergrund: 63

Eigene Publikationen: 66

2.5 Strukturelle Untersuchung des *MYCN* Amplikons und Entwicklung eines MRD Markers

Hintergrund: 82

Eigene Publikationen: 86

2.6 Diskussion und Ausblick 117

2.7 Abkürzungen 119

2.8 Literatur 120

3. Erklärung 124

4.1 Curriculum Vitae 125

4.2 Publikationen 127

Danksagung 129

1. Einleitung

Die Abschätzung der Prognose für Patienten mit onkologischen Erkrankungen stellt eine große Herausforderung an die behandelnden Ärzte dar. Derzeit gibt es keine Parameter, die eine sichere Vorhersage auf das Ansprechverhalten einer diagnostizierten Tumorerkrankung geben können. Vor Beginn einer Therapie werden daher viele Informationen gesammelt, um einen Patienten möglichst gut in eine vordefinierte Risikogruppe stratifizieren und dementsprechend eine mehr oder weniger intensive Therapie anbieten zu können. Diese Einteilungen sind allerdings für keinen Malignomtyp mit 100%-iger Sicherheit möglich. Das ist die Ursache dafür, dass auch in niedrige Risikogruppen eingeteilte Patienten nicht auf die Therapie ansprechen und einen unvorhergesehen schlechten Verlauf zeigen können. Auf der anderen Seite scheint es Patienten zu geben, die trotz initial schlecht eingeschätzter Prognose einen überraschend guten Verlauf nehmen, auf die Therapie gut ansprechen und letztlich geheilt werden können.
Einen Beitrag zu leisten, um diese Stratifizierung für Kinder, die an einem Neuroblastom erkrankt sind, zu verbessern und damit zu vermeiden, dass einige Patienten unter- und andere Patienten übertherapiert werden müssen, ist das Ziel dieser Habilitationsarbeit.

Die Risikoeinteilung von Kindern mit Neuroblastom erfolgte lange Zeit hauptsächlich anhand klinischer, laborchemischer und histopathologischer Kriterien. Bekannte klinische Kriterien sind dabei das Alter bei Diagnosestellung und das Tumorstadium. Säuglinge und Kleinkinder, die jünger als 18 Monate bei Diagnosestellung sind haben dabei eine signifikant bessere Prognose als ältere Kinder (*Cohn et al 2009.*). Die Einteilung der Tumorstadien wird nach der Internationale Stadieneinteilung für Neuroblastome (INSS) vorgenommen *(Evans et al.,1971; Monclair 2009)* (siehe *Tab. 1.1)*. Die Prognose nimmt dabei mit zunehmendem Tumorstadium ab. Eine Besonderheit bei den Neuroblastomen bietet das so genannte Stadium 4s. Dieses Stadium beschreibt Säuglinge mit primär multilokulär manifestierten bzw. metastasierten Tumoren, die ein streng vordefiniertes Metastasierungsmuster aufweisen und trotzdem eine Tendenz zur spontanen Regression zeigen. Zwingt die Tumorlast bei diesen Patienten nicht zur Therapie, kann trotz der teilweise beeindruckenden Klinik auf eine spontane Remission gewartet werden.

Tab 1.1:

Internationale Stadieneinteilung des Neuroblastoms nach INSS (übernommen aus der *NB-97 Studie*)	
Stadium 1	Lokalisierter Tumor mit makroskopisch kompletter Entfernung (mit oder ohne mikroskopischem Resttumor); repräsentative ipsi- und kontralaterale Lymphknoten sind histologisch ohne Tumorbefall. Lediglich unmittelbar am Tumor adhärente, chirurgisch entfernte LK dürfen positiv sein. Außerdem bilaterale Tumore, die makroskopisch komplett reseziert werden können ohne regionalen Lymphknotenbefall.
Stadium 2	Unilateraler Tumor mit makroskopisch inkompletter Entfernung; repräsentative ipsi- und kontralaterale Lymphknoten sind histologisch ohne Tumorbefall. Unilateraler Tumor; regionale, nicht adhärente LK zeigen Tumorbefall; kontralaterale LK sind histologisch negativ.
Stadium 3	Nicht respektabler, unilateraler Tumor mit Überschreiten der Mittellinie mit oder ohne Lymphknotenbefall oder unilateraler Tumor mit kontralateralem Lymphknotenbefall oder nicht resektabler Mittellinientumor mit bilateraler Ausdehnung durch Infiltration oder durch Lymphknotenbefall (bis zur oder über die jeweilige Wirbelkante hinaus)
Stadium 4	Disseminierung des Tumors zu Knochenmark, Knochen, entfernten LK, Leber, und/oder anderen Organen.
Stadium 4s	Lokalisierter Primärtumor wie beim Stadium 1,2a oder 2b und Disseminierung nur in Leber, Haut und/oder Knochenmark. Nur Säuglinge im 1. Lebensjahr. Die Knochenmarksinfiltration ist gering (<10% Tumorzellen im Ausstrich) und mIBG negativ.

Histopathologisch unterscheidet man je nach Differenzierungsgrad zwischen dem Ganglioneurom mit ausdifferenzierten Ganglienzellen und dichtem Schwann-Zell Stroma, dem Ganglioneuroblastom mit Nestern von unreifen Neuroblasten neben ausdifferenzierten Ganglienzellen und Schwann-Zellen und das eigentliche Neuroblastom mit einem einförmigen Zellbild, das von kleinen, runden, Zytoplasma-armen und hyperchromaffinen Zellen geprägt ist, neben denen nur noch wenig oder gar kein Schwann-Zell Stroma zu finden ist. Diese Zellen entsprechen den unreifen Neuroblasten und sind häufig in für das Neuroblastom typischen, so genannten „Homer-Wright-Rosetten“ angeordnet. Die

Differenzierung gegenüber den anderen Tumoren mit ähnlichem Zellbild erfolgt immunhistochemisch über den Nachweis von Neurofilamenten, Synaptophysin und der Neuron-Spezifischen-Enolase. Die bekanntesten Einteilungen in prognostisch unterschiedliche Tumorgruppen nach histopathologischen Kriterien stammen von Hughes und Shimada *(Hughes et al., 1974; Shimada et al., 1984)*. Ein internationaler Konsens ist in der Veröffentlichung des International Neuroblastoma Pathology Committee (INPC) festgehalten (*Shimada et al., 1999*) und wird derzeit in den aktuellen Therapieoptimierungsstudien eingesetzt (in Deutschland: NB-2004 Studie).

Neben diesen Parametern kann der DNA Gehalt der Tumorzellen prognostische Hinweise geben. Flow-Zytometrische Messungen lassen zwei Gruppen von Tumoren unterscheiden, Tumore mit einem diploiden DNA-Gehalt (sog.DNA-Index (DI)=1) und Tumore mit einem hyperploidem DNA-Gehalt (DI>1). Tumore mit einem DI=1 korrelieren mit fortgeschrittenen Stadien (v.a. Stadium 4), ungünstiger Prognose und einem schlechten Ansprechen auf eine zytostatische Therapie. Bei älteren Kindern (ab dem 18. Lebensmonat) können diese Zusammenhänge jedoch nicht mehr eindeutig beobachtet werden, so dass der Einsatz des DI als prognostischer Faktor nur bis zum 2. Lebensjahr sinnvoll erscheint *(Look et al.,1984; Look et al.,1991)*. Die Karyotypisierung der Tumorzellen liefert neben der Aussage über die Ploidie auch zusätzlich Informationen über einzelne, chromosomale Veränderungen wie Deletionen oder Zugewinne von genetischem Material an bestimmten Chromosomenabschnitten.

Die Deletion des kurzen Armes eines Chromosomes 1 (LOH (*loss of heterozygosity*) für Chromosom 1p) ist eine charakteristische Veränderung in Tumoren mit einem diploiden Chromosomensatz und insgesamt schlechterer Prognose. Diese Eigenschaft wird auf die resultierende partielle Monosomie für die entsprechende Region zurückgeführt, in der ein oder mehrere Tumorsuppressorgene vermutet werden *(Brodeur et al., 1977; Franke et al., 1986; Christiansen et al., 1988; Fong et al., 1989)*. LOHs wurden außerdem für die Chromosomenregionen 3p, 4p, 9p und 9q, 11q und 14q beschrieben und zum Teil mit Tumorentstehung und -progression in Verbindung gebracht *(Hallstensson et al., 1997; Caron et al., 1996; Takita et al., 1997; Srivatsan et al., 1991; Suzuki et al., 1989)*. Als weitere zytogenetische Auffälligkeiten weisen vor allem Tumore höherer Stadien so genannte „double-minute-chromosome-bodies“ (dmins), die extrachromosomalen DNA-Abschnitten entsprechen, oder lange, homogen anfärbbare Regionen (HSR (*homogeneously staining regions*)) innerhalb einzelner Chromosomen auf. Beide Veränderungen sind Korrelate amplifizierter Chromosomenabschnitte, die im Falle des Neuroblastoms distalen Regionen des kurzen Armes des Chromosomes 2 entprechen und unter anderem das *MYCN*-Gen enthalten. Die HSR wurden auf 18 von den 24 verschiedenen menschlichen Chromosomen beobachtet und als *MYCN* enthaltende Regionen identifiziert *(Brodeur et al., 1990)*.

Zusätzliche Zugewinne genetischen Materials wurden auf dem langen Arm des Chromosomes 17 (17q21) gefunden und mit einer schlechteren Langzeitprognose assoziiert *(Bown et al., 1999)*.

Die Diagnostik für Kinder mit Neuroblastomen hat sich seit der Entdeckung der *MYCN*-Amplifikation im Jahr 1983 grundlegend geändert (*Schwab et al, 1983)*. Mit dem Nachweis der Amplifikation dieses Onkogenes in ca. 25% aller Neuroblastompatienten konnte zum ersten mal mittels eines spezifischen, molekularen genomischen Markers eine Subgruppe von Patienten identifiziert werden, die eine deutlich schlechtere Überlebenswahrscheinlichkeit aufwiesen, als Patienten ohne *MYCN*-Amplifikation. Dabei ist die prognostische Aussage statistisch gesehen unabhängig von den klinischen und histopathologischen Parametern.

Ein umfassender Überblick über die international konsensuellen Möglichkeiten der Risikoeinteilung mittels der vorgestellten klinischen, histopathologischen und molekolargenetischen Faktoren ist 2009 veröffentlicht worden (*Cohn et al., JCO 2009*). Durch stratifizierungsabhängige Therapieschemata konnte in den letzten 30-40 Jahren zumindest für einen Teil der Neuroblastom-Patienten die Überlebenschancen deutlich verbessert werden *(Moroz et al., Eur J Cancer 2010).*

2. Publikationen

2.1 Genexpressionsmarker in humanen Neuroblastomen

Hintergrund:

Neben den Veränderungen, die das Genom der Neuroblastomzellen spezifisch von dem der übrigen, nicht transformierten Körperzellen unterscheiden können in der Regel auch große Unterschiede im mRNA Expressionsmuster beobachtet werden. Diese können häufig direkt oder indirekt durch genomische Veränderungen erklärt werden.

In *MYCN* amplifizierten Neuroblastomen findet sich daher häufig eine deutlich erhöhte MYCN mRNA Expression im Vergleich zu nicht-*MYCN* amplifizierten Tumoren *(Seeger et al., 1988)*. Diese basiert offensichtlich auf die höhere Anzahl genomischer Kopien von *MYCN*, von denen letztlich auch mehr mRNA transkribiert werden kann. Interessanterweise findet sich jedoch auch in einigen nicht-*MYCN* amplifizierten Neuroblastomen eine sehr hohe MYCN Expression, während es einige, wenige *MYCN* amplifizierte Tumore gibt, die MYCN auf einem niedrigen Level expremieren. Dies führt dazu, dass im Gegensatz zur *MYCN* Amplifikation die MYCN mRNA Expression (hohe MYCN Expression *vs*. niedrige MYCN Expression) keine prognostische Aussagekraft bei Patienten mit Neuroblastom besitzt *(Cohn et al., 2000; Weber at al 2003)*. Dies verdeutlicht, dass die Interpretation von Genexpressionsmarkern eigentlich immer nur in einem Gesamtkontext gewertet werden kann. Dabei ist die Einbeziehung von Faktoren wie Alter des Patienten, Geschlecht, Tumorhistologie, Tumorzellgehalt des untersuchten Gewebes, genomische Veränderungen und Materialentnahmezeitpunkt (vor, während, nach Therapie) notwendig, um zu einer sinnvollen Interpretation zu gelangen. Außerdem ist es wichtig die individuelle RNA Qualität zu beurteilen, da RNA rasch degradieren kann. Hier spielen Faktoren wie Materialentnahmezeitpunkt, Zeit zwischen Entnahme und Fixierung des Gewebes, Isolationsmethoden etc. eine nicht unerhebliche Rolle.

Neben der MYCN-Expression ist die Expression weiterer mRNAs und Proteine für das Neuroblastom beschrieben und Ihre prognostische Eigenschaft auf den Krankheitsverlauf diskutiert worden. Beispiele für prognostisch günstige Expressionsmarker sind das h-Ras-Onkogen und das CD44-Oberflächenprotein *(Tanaka et al., 1988; Gross et al., 1995; Combaret et al., 1996)*. Als prognostisch ungünstig wird die Expression des Bcl2-ProtoOnkogenes, des MDR1-P-Glykoproteines, des src-Protoonkogenes, des Anti-Apoptose-Genes Survivin und des Proliferationsmarkers PCNA beurteilt *(Castle et al., 1993; Dole et al., 1994; Nakagawara et al., 1990; Dhooge et al., 1997; Matsunaga et al., 1991; Adida et al., 1998; Keim et al., 1993)*.

Eigene Publikationen:

Bergmann E, Wanzel M, **Weber A**, Shin I, Christiansen H, Eilers M. Expression of P27(KIP1) is prognostic and independent of *MYCN* amplification in human neuroblastoma. Int J Cancer. 2001 May 20;95(3):176-83.

IF (Stand 2010): 4,772

In dieser Arbeit wurde die Expression von Genen, die eine Rolle in der Regulation des Zellzyklus spielen mit dem Progressionsverhalten und damit der Prognose humaner Neuroblastome korreliert. Dabei konnte die prognostische Relevanz der p27kip Expression in humanen Neuroblastomen beschrieben werden. Eine hohe Expression von p27kip war sowohl für Patienten mit als auch ohne *MYCN* Amplifikation ein gut prognostischer Marker und somit unabhängig von der *MYCN* Amplifikation. Allerdings war die p27kip Expression aufgrund einer deutlichen Korrelation nicht prognostisch unabhängig vom Alter der Patienten und deren Tumorstadien.

Funktionell konnte gezeigt werden, dass die Expression von p27kip in primären Neuroblastomen nicht wie in Zellkulturversuchen invers mit Proliferationsmarkern wie Cyclin-A oder PCNA korreliert. Dies konnte teilweise durch den Umstand erklärt werden, dass p27kip in einigen hoch expremierenden Tumoren über eine Bindung an D-Typ Cyclinen funktionell inaktiviert werden kann. Passend zu diesem Umstand konnte keine prognostische Relevanz für die beiden untersuchten Proliferationsmarker gefunden werden. Damit konnte alleine durch die bekannte Funktion von p27kip als Zellzyklusinhibitor die prognostische Relevanz der p27kip Expression nicht ausreichend erklärt werden.

Diese Arbeit zeigt, dass Untersuchungen in Zellkultursystemen, die Zusammenhänge zwischen Wachstumsverhalten (z.B. Proliferation, Differenzierung, Apoptose) und der differentiellen Expression bestimmter Gene darlegen, keinen direkten Rückschluss auf das Wachstumsverhalten primärer Tumore und damit die Prognose der Patienten erlauben.

Weber A, Huesken C, Bergmann E, Kiess W, Christiansen NM, Christiansen H. Coexpression of insulin receptor-related receptor and insulin-like growth factor 1 receptor correlates with enhanced apoptosis and dedifferentiation in human neuroblastomas. *Clin Cancer Res*. 2003 Nov 15;9(15):5683-92. PMID: 14654552

IF (Stand 2010): 6,747

Zelluläre Proliferation wird maßgeblich durch Wachstumsfaktoren vermittelt. Viele bekannte Wachstumsfaktoren binden extrazellulär an Rezeptoren vom Rezeptor-Tyrosinkinasetyp (RTK) und vermitteln damit ihr proliferationsförderndes Signal nach intrazellulär. Die

Proliferation wird durch Aktivierung des pi3-Kinase- und des MAP-kinase-Signalweges vermittelt. Die Relevanz entsprechender Wachstumsfaktoren und deren RTKs konnte in Neuroblastomen bereits mehrfach gezeigt werden (Christiansen *et al., 1990; Christiansen et al., 1993; Nakagawarat et al., 1993; Kogner et al., 1993; Eggert et al., 2000*). RTK-Proteine bilden in der Zellmembran Dimere, die die eigentliche aktive Form der RTKs darstellen.

Der Insulin-Rezeptor-related-Rezeptor (IRR) ist eine v.a. in ihrem extrazellulären Anteil rudimentäre RTK, für die bisher kein aktivierender oder inhibierender Ligand gefunden werden konnte. Bekannt ist, dass der IRR mit RTKs der gleichen RTK-Familie (Insulin-Rezeptor (IR), Insulin-like-growth-faktor-1-Rezeptor (IGF1-R)) in der Zellmembran Heterodimere bilden kann. Hierdurch kann eine Modulation bei der Ligandbindung an die anderen RTKs und damit der Signalwirkung der Wachstumsfaktoren (Insulin, IGF) erreicht werden.

In der o.g. Arbeit wurde die Expression des IRR in primären humanen Neuroblastomen untersucht. Die IRR Expression korrelierte dabei mit lokalisierten Tumoren (Stadium 1) und dem sehr gut prognostischen Säuglingsstadium (Stadium 4s) sowie mit einem niedrigen Alter (<12 Monate bei Diagnose). Des Weiteren zeigte sich eine positive Korrelation mit einer undifferenzierten Histologie. Durch die Bestimmung der Koexpressionsmuster mit dem IGF1-R, Trk-A und dem NGF-R, erhielten wir einen Hinweis auf eine mögliche Relevanz des IRR für IGF1-R vermittelte Signalwege. Über den IGF1-R wird Proliferation vermittelt und Apoptose inhibiert. Interessanterweise zeigten sich in den IGF1-R / IRR koexpremierenden Tumoren ein signifikant verminderter Apoptotic-Index (AI) und häufiger eine undifferenzierte Histologie (indirekter Hinweis auf vermehrte Proliferation). Da in der untersuchten Kohorte die IGF1-R Expression alleine keinerlei Korrelation zu Apoptose oder Histologie zeigte, kann dies ein Hinweis auf eine relevante Beeinflussung der IGF-1 vermittelten Signaltransduktion durch die Koexpression von IRR mit dem IGF1-R sein.

Klinisch zeigte sich die IRR Expression als prognostisch günstig, unabhängig von der *MYCN* Amplifikation, sowohl in der Gesamtgruppe, als auch in der Untergruppe der IGF1-R expremierenden Tumore.

Int. J. Cancer (Pred. Oncol.): **95,** 176–183 (2001)
© 2001 Wiley-Liss, Inc.

Publication of the International Union Against Cancer

EXPRESSION OF $P27^{KIP1}$ IS PROGNOSTIC AND INDEPENDENT OF *MYCN* AMPLIFICATION IN HUMAN NEUROBLASTOMA

Eckhard Bergmann[1], Michael Wanzel[2], Axel Weber[1], Inhee Shin[1], Holger Christiansen[1] and Martin Eilers[2]*
[1]*Universitäts-Kinderklinik, Marburg, Germany*
[2]*Institute for Molecular Biology and Tumor Research, Marburg, Germany*

Amplification of the *MYCN* gene is significantly associated with an unfavorable prognosis and rapid progression in human neuroblastoma tumors. One potential mechanism by which *MYCN* may cause these effects is by deregulating cell proliferation. Tissue culture experiments support a model in which MYC genes stimulate cell cycle progression by antagonizing the function of the cell cycle inhibitor $p27^{kip1}$. In culture, activation of MYC induces both sequestration of $p27^{kip1}$ by cyclin D complexes and its subsequent proteolytic degradation. We have tested whether this model applies to human neuroblastoma in a retrospective study of 100 primary tumor biopsy samples from neuroblastoma patients with a documented follow-up. Consistent with this hypothesis, *MYCN*-amplified tumors express high levels of both cyclin A and proliferating cell nuclear antigen, 2 marker proteins of cell proliferation. Further, expression levels of $p27^{kip1}$ are of prognostic significance in human neuroblastoma patients. Similar to tissue culture systems, $p27^{kip1}$ is sequestered by cyclin D complexes in a subset of human neuroblastoma samples. Surprisingly, however, expression levels of $p27^{kip1}$ are prognostic independent of *MYCN* amplification, and tumors that have an amplified *MYCN* gene do not express elevated levels of D-type cyclins or contain significantly lower levels of $p27^{kip1}$. Our data do not support a model in which regulation of $p27^{kip1}$ function is an important mechanism by which amplified *MYCN* deregulates cell proliferation in neuroblastoma.
© 2001 Wiley-Liss, Inc.

Key words: *MYCN gene; neuroblastoma; $p27^{kip1}$; cell proliferation*

Progress through the mammalian cell cycle is regulated by cyclin-dependent kinases (CDKs); among other factors, the activity of these kinases is controlled by the levels of specific inhibitory molecules.[1] Two families of CDK inhibitors are known: one family consists of 3 related proteins, p21, p27 and p57, which inhibit CDK2 kinase activity. A second family consists of 4 related "ink4" proteins that specifically inhibit CDK4 and CDK6 kinase activity.[2]

$p27^{kip1}$ acts as a tumor suppressor gene in mice, like other inhibitors of cell cycle progression.[3–6] Despite this fact, mutations of the gene encoding $p27^{kip1}$ are rare in human tumors. However, levels of $p27^{kip1}$ protein are often down-regulated in tumor tissues and are therefore predictive for disease outcome in several human tumors, suggesting that disruption of normal control of $p27^{kip1}$ metabolism is an important event in tumorigenesis.[7–10]

Neuroblastoma represents the second most frequent malignancy in childhood with a relative frequency of 8.3%. The age-standardized incidence rate in Germany between 1989 and 1998 was 1.2 cases per 100,000 children younger than 15 years per year, with a cumulative incidence of 16.9 cases per 100,000 children. The tumors derive from neural crest cells, which migrate during embryogenesis and form the sympathetic nervous system.[11] One of the genetic factors involved in the development of childhood neuroblastoma is the amplification of the *MYCN* gene locus, which occurs in a subset of tumors and is strongly predictive of poor survival.[12,13] The *MYCN* gene encodes a transcription factor that can both positively and negatively regulate gene expression. As with the related *c-myc* protein, enhanced expression of N-Myc stimulates cell proliferation of established cell lines[14] and cooperates with activated alleles of RAS in the transformation of primary fibroblasts.[15]

The mitogenic function of *c-myc* in culture is tightly linked to its ability to regulate the function of $p27^{kip1}$. Activation of Myc strongly stimulates cyclin E/CDK2 kinase;[16,17] this activation is required and can be sufficient to account for the mitogenic properties of Myc.[18,19] Myc regulates cyclin E/CDK2 kinase via p27[20] since no regulation is observed in p27-deficient cells.[21] Myc protein directly stimulates the transcription of the cyclin D2 and cul-1 genes, leading to sequestration and degradation of p27.[22–24] In addition, Myc may indirectly control translation of the cyclin D1 mRNA.[25]

Similarly, regulation of p27 levels has been implicated in the control of proliferation of neuroblastoma cells,[26,27] raising the possibility that deregulation of p27 function is a critical event by which amplification of *MYCN* contributes to the genesis of neuroblastoma. Therefore, in this study we asked whether levels of p27 are of prognostic significance in human neuroblastoma and whether the reduced survival of children with *MYCN*-amplified tumors can be explained in terms of the proposed regulatory circuit linking Myc genes to p27.

MATERIAL AND METHODS

Patients and tissues

Tumor specimens from 100 neuroblastomas from a population of more than 1,000 patients were selected considering distribution of age and stage of the patients. According to the revised international neuroblastoma staging system (INSS) 17 (18%) cases were stage 1, 12 (13%) were stage 2, 18 (19%) were stage 3, 37 (39%) were stage 4 and 10 (10%) were stage 4s. The mean age was 29 months (range 0.2–132 months; median 19.8 months). Histopathologic classification was distributed as follows: 40% stroma-poor undifferentiated (grade 1), 20% stroma-poor differentiated (grade 2) and 40% diffuse stroma-rich tumor samples (grade 3).

Western blot analysis and antibodies

Cellular protein was extracted by lysing 30 mg of tumor tissue with 300 μl of ice-cold lysis buffer (150 mM NaCl, 1% NP-40, 50 mM Tris-buffer pH 8.0, aprotinin 5 mg/ml, leupeptin 5 mg/ml, pepstatin 1 mg/ml, 0.2 M phenylmethanesulfonyl fluoride). Western blotting was carried out as described previously[22] using an enhanced chemiluminescence system (Amersham).

The following antibodies were used: α-mouse IgG peroxidase-conjugated antibody (Amersham); α-rabbit IgG peroxidase-conjugated secondary antibody (Amersham); α-p27 rabbit-polyclonal antibody (Santa Cruz, #sc-528-G); α-cyclin A rabbit-polyclonal antibody (Santa Cruz, #sc-751); α-proliferating cell nuclear antigen (PCNA) mouse monoclonal antibody (Boehringer-Mann-

---

Grant sponsor: Deutsche Krebshilfe.

*Correspondence to: Institute for Molecular Biology and Tumor Research, Emil-Mannkopff-Str. 2, 35033 Marburg, Germany.
Fax: +49-6421-286-5196. E-mail: eilers@imt.uni-marburg.de

Received 13 October 2000; Revised 8 January 2001; Accepted 19 January 2001

TABLE I – SUMMARY OF CLINICAL CHARACTERISTICS AND PRIMARY DATA

	Total number of tumors examined	Number of tumors positive for				
		p27	CyclinA	PCNA	CyclinD1	CyclinD3[3]
MYCN copy number						
>1	21	9	17	16	5	5
<1	79	45	36	36	19[2]	33
Tumor stage						
I	19	11	10	11	3	10
II	12	10	6	7	6	9
III	19	7	10	10	5	6
IV	39	16	21	16	7	10
IVs	11	10	6	8	3	3
Histology[1]						
I	32	15	6	10	6	12
II	18	11	11	11	4	6
III	31	17	21	24	11	11
Age						
>18 months	55	25	24	23	10	19
<18 months	45	29	29	29	14	19

PCNA, proliferating cell nuclear antigen.–[1]Histology of 19 tumors was unknown.–[2]CyclinD1 expression was analyzed in 26 tumors without amplification of *MYCN*.–[3]CyclinD2 was not detected in any tumor.

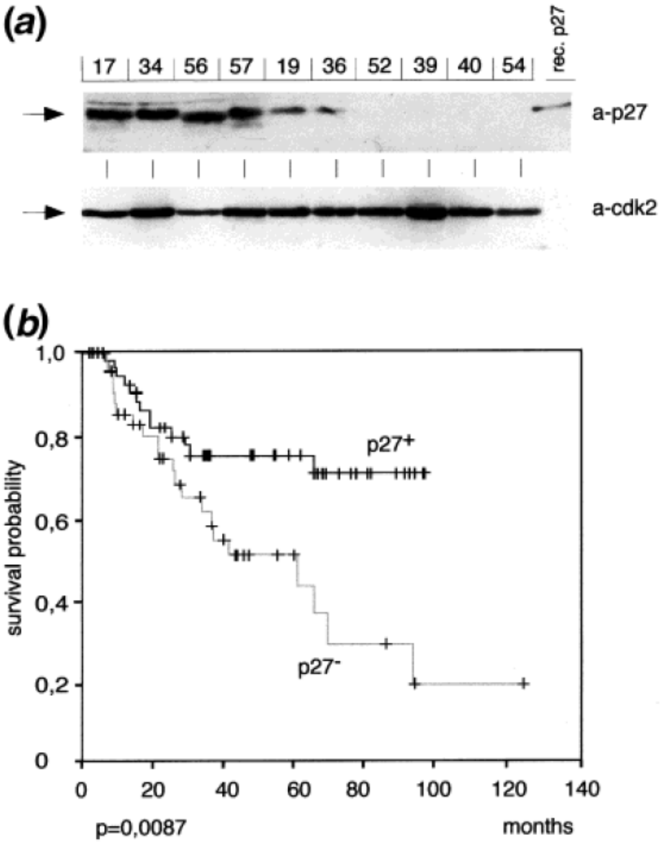

FIGURE 1 – Levels of p27 are prognostic for survival in human neuroblastoma. (*a*) Western blot documenting different expression levels of p27 protein in a group of primary neuroblastoma biopsy samples. The samples represent a group of tumors sorted according to the amount of p27. As a control, the blot was re-probed with antibodies directed against cyclin-dependent kinase-2 (CDK2) (*lower panel*). The lane designated "rec.p27" contains 5 ng recombinant p27. (*b*) Kaplan–Meier diagram documenting increased survival probability of patients with tumors that contain detectable amounts of p27 ($p27^+$) versus patients with tumors lacking detectable p27 ($p27^-$).

heim); α-pRb mouse monoclonal antibody (PharminGen); α-cyclin D1 rabbit polyclonal antibody (Santa Cruz, #sc-246); α-cyclin D2 mouse monoclonal antibody (DCS3; (Bartkova *et al.*[28]); α-cyclin D3 mouse monoclonal antibody (DCS22; (Bartkova *et al.*[28]); α-CDK2 rabbit polyclonal antibody (Santa Cruz, #sc163); and α-Mad rabbit polyclonal antibody (Santa Cruz, #sc222).

Western Blot data on expression of p27, cyclin A, PCNA and cyclin D2 were collected from all tumors in the study.

Histochemistry

Paraffin sections were deparaffinized with xylene for 5 min, rehydrated with descending concentrations of ethanol and microwaved for 10 min in 10 mM citrate buffer (pH 6.0). Endogenous peroxidase activity was blocked by treatment with 3% hydrogen peroxide in methanol. Then sections were incubated with normal horse serum (1:20 dilution) in 0.1 M phosphate-buffered saline (PBS) at pH 6.0 following an overnight incubation with monoclonal p27KIP1 antibody (Transduction laboratories, Lexington, KY) diluted 1:1,000 in PBS. Afterwards slides were treated with a biotin-labeled anti-mouse antibody and incubated with preformed avidin-biotin-peroxidase complex (Vectastain Elite ABC kit; Vector Laboratories, Burlingame, CA). Metal-enhanced diaminobenzidine substrate (DAB, Sigma cat. #D8001) was then added in the presence of horseradish peroxidase. The sections were counterstained with hematoxylin, rehydrated and mounted. Histochemistry of p27 was performed for a total of 14 selected tumors.

Immunedepletion experiments. Pre-cleared cell lysates in immunoprecipitation buffer [50 mM Tris pH 8.0, 150 mM NaCl, 10% glycerol, 1 % NP-40 (Sigma), 50 mM NaF, 80 μM glycerophosphate, 1 mM EGTA, 10 μg each of leupeptin, pepstatin and aprotinin per milliliter] were incubated with the indicated antibody bound to protein G-Sepharose overnight at +4°C on a shaker. This step was repeated with the resulting supernatant of the first immuno-precipitation (IP). Immune complexes bound to protein G-Sepharose were collected by centrifugation and washed several times in immunoprecipitation buffer. Immune-precipitated proteins were resolved by a 12% sodium dodecyl sulfate (SDS) gel followed by the standard protocol for Western blot analysis as described above.

Kinase assays were carried out as described elsewhere.[17]

Statistical analysis

Independence between 2 categorized variables was tested using the Yates-corrected χ^2 test of Pearson. For univariate survival analysis, Kaplan–Meier estimates were calculated. To test for difference in survival between 2 groups, the log-rank test was applied. For multivariate analysis, the Cox proportional hazard model was used. The proportionality assumption was investigated graphically, and 95% confidence intervals (CI) for odds ratios (OR) estimated by the Cox model were obtained using the transformation formula. The molecular markers were coded as follows: *MYCN* = 1 if amplified and 0 otherwise; p27, cyclin A and PCNA = 1 if detected and 0 otherwise.

RESULTS

To explore the potential prognostic value of $p27^{kip1}$ protein levels in human neuroblastoma, we chose 100 samples from a collection of 2,300 primary tumor specimens with a documented mean follow-up time of 47.2 months. This collection reflected the distribution of tumor stages and the percentage of *MYCN*-amplified tumors of the total population of neuroblastoma patients (see Table I for a summary of clinical characteristics and primary data).[29]

Frozen tissue from each tumor was extracted in lysis buffer (see Material and Methods) and extracts were adjusted to equal protein concentration. Aliquots were separated by SDS-polyacrylamide gel electrophoresis and the amount of p27 was determined by a semi-quantitative Western blotting assay. As a control for equal loading, a blot prepared in parallel was probed with α-CDK2 antibodies (see Fig. 1*a*). Extracts that contained low amounts of CDK2 were excluded from the analysis (6 of 100). In these experiments, we found that different tumor samples contained widely varying amounts of p27 protein, ranging from undetectable amounts to approximately 1 ng p27/μg total protein.

Kaplan–Meier analysis showed that levels of p27 protein were predictive for long-term survival of neuroblastoma patients ($p = 0.0087$; $n = 94$) (Fig. 1*b*). The median survival time of patients with tumors expressing p27 was 34.6 months (range 1.6–96 months), and for patients with p27-negative tumors it was 27.9 months (range 6.1–123.2 months).

Immunohistochemistry of a subset of the total tumor samples revealed a close correlation between the signal observed in the Western blot analysis with the signal observed by immunohistochemical staining using an α-p27 polyclonal antiserum and a peroxidase-coupled secondary antibody (Fig. 2*a*). Inspection of several samples taken from an individual tumor revealed that the amount of p27 was homogeneous throughout the entire tumor (not shown). Several tumors of distinct histology were analyzed: in stroma-poor tumors, staining was essentially homogeneous throughout the entire tissue (Fig. 2*a*, top row). In stroma-rich tumors, if positive for p27, a strong staining was observed in the tumor tissue itself; in contrast, the surrounding connective tissue did not stain positive for p27 (Fig. 2*a*, second row). Tumor capsules and fat tissue, where observed, also did not stain positive for p27 (Fig. 2*a*). In an individual tumor, little cell-to-cell variation of staining was observed (Fig. 2*b*).

Taken together, the data show that expression of p27 varies strongly between individual tumors and is homogeneous within the

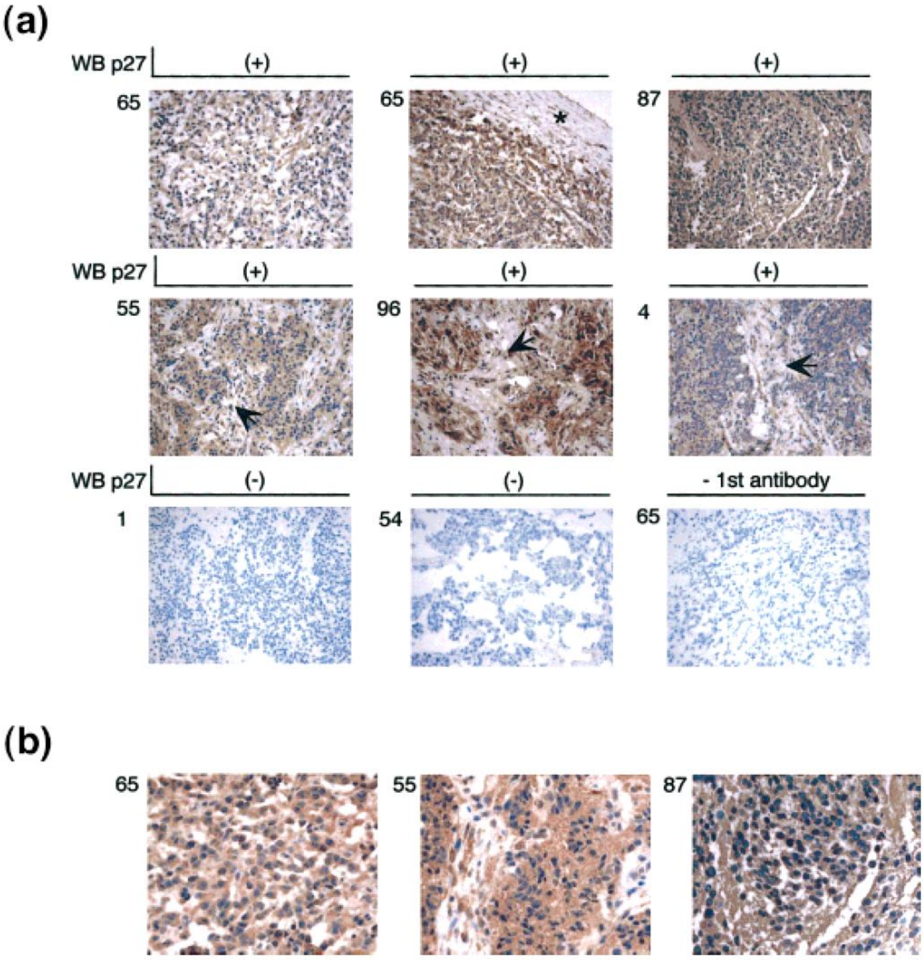

FIGURE 2 – Immunohistochemical detection of p27. Expression of p27 was detected using an immunoperoxidase-coupled secondary antibody; sections were counterstained with hematoxylin. The designations (−) and (+) refer to absence or presence of p27 in the same tumor as determined by Western blotting. (*a*) Tumors 65 and 87 were classified as stroma poor (according to (Shimada *et al.*[30]), and tumors 55, 96 and 4 classified were as stroma rich. The asterisk indicates part of the tumor capsule; black arrows indicate connective tissue; "-1st antibody" designates a control staining in the absence of primary antibody (of tumor 65). (*b*) Higher magnification view of some tumors documenting absence of cell-to-cell variation in p27-positive tumors.

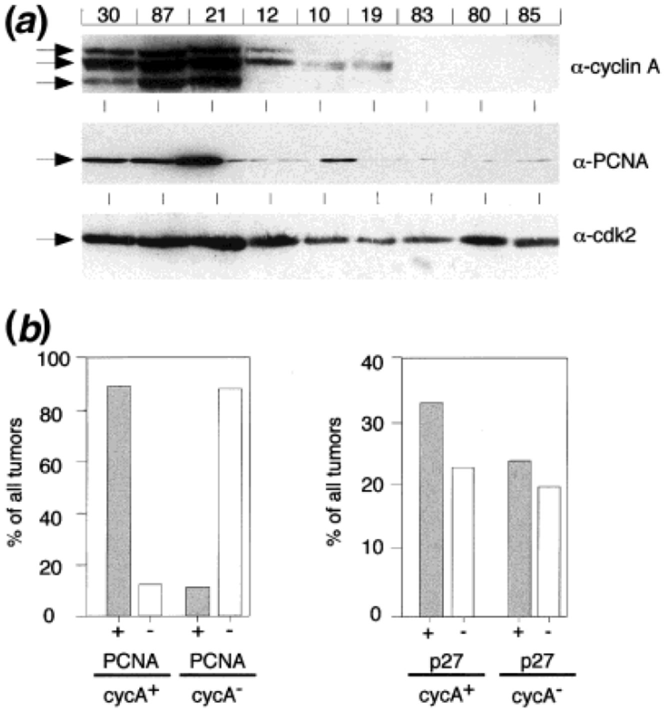

FIGURE 3 – Co-expression of cyclin A and proliferating cell nuclear antigen (PCNA) with p27 in a subset of human neuroblastoma tumors. (*a*) Western blot documenting different expression levels of cyclin A and PCNA proteins in a group of primary neuroblastomas. As a control, the blot was re-probed with antibodies directed against cyclin-dependent kinase-2 (CDK2). Cyclin A migrates as 3 bands presumably to partial proteolytic processing *in vivo* (Bastians *et al.*[39]). (*b*) The panel documents the percentage of tumors that express PCNA or p27 in the subgroups of tumors that do or do not express cyclin A.

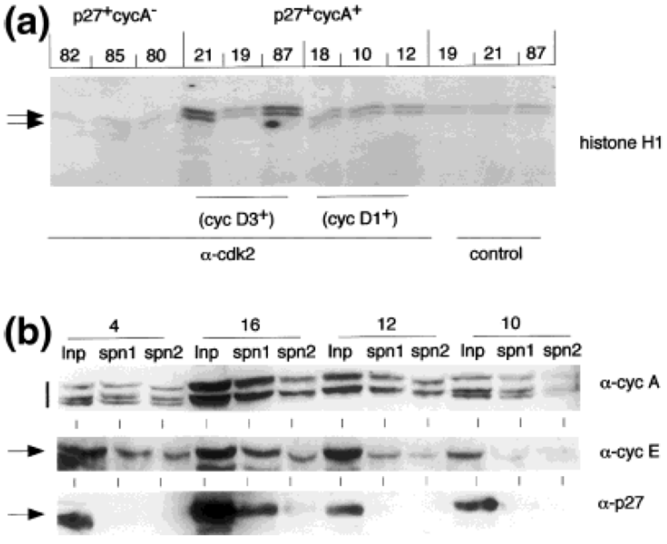

FIGURE 4 – Tumors expressing both p27 and cyclin A contain inhibitor-free cyclin A and cyclin E and active cyclin-dependent kinase-2 (CDK2). (*a*) CDK2 kinase assays documenting the presence of active CDK2 in tumors expressing both cyclin A and p27. As controls, kinase assays from 3 tumors that do not express cyclin A (*left lanes*) and from cyclin A-positive tumors using a control antibody (*right lanes*) are shown. (*b*) Lysates from 4 tumors that express both cyclin A and p27 were either probed directly with antibodies directed against cyclin A, cyclin E or p27 (lanes designated "Inp") or subjected to 2 consecutive rounds of depletion with α-p27 antibodies (lanes "spn1" and "spn2"). Depletion of p27 is documented in the bottom panel.

tumor tissue. Expression levels of p27 are predictive for long-term survival in childhood neuroblastoma.

Because p27 is degraded at the G_1/S transition, proliferating cells often contain much lower amounts of p27 than quiescent cells.[31–34] It was therefore possible that any marker of cell proliferation would yield results that are comparable to those obtained with p27. Indeed, several studies suggested that levels of either PCNA or Ki-67 were prognostic in neuroblastoma patients.[35–37] To test this notion, we probed the same extracts with antibodies directed against PCNA and against cyclin A, a cyclin that is specifically expressed in the S- and G_2-phase of proliferating cells.[38]

Similarly to p27, different tumors contained widely varying amounts of both proteins (Fig. 3*a*). Comparison of the expression level of cyclin A in different tumors with that of PCNA showed that the expression of both proteins was strictly correlated with each other: 90% of all tumors that expressed detectable amounts of PCNA were also positive for cyclin A and vice versa (Fig. 3*b*). The small degree of divergence resulted from a few tumors with low, but detectable expression of 1 protein and undetectable expression of the other. The correlation of expression suggests that the concomitant use of both markers allowed the identification of a subset of highly proliferative tumors.

There was no significant correlation between the expression of cyclin A/PCNA and that of p27 (Fig. 3*b*). Based on both markers, the tumors could be grouped into 4 groups, each of which contained approximately the same number of tumors (p27+/cycA+, p27+/cycA−, p27−/cycA+, p27−/cycA−). The data indicate that expression of p27 and of cyclin A/PCNA are regulated independently of each other in human neuroblastoma. This result is surprising because p27 acts as a negative regulator of cell proliferation by inhibiting CDK2 complexes in the G_1 phase of the cell cycle and thus suppresses expression of cyclin A when expressed ectopically in culture (for review, see Sherr and Roberts[2]). However, a group of tumors expressed high levels of p27 and both cyclin A and PCNA, indicating that a large fraction of cells in these tumors progressed into S and G_2 phase.

To test whether such tumors contained active CDK2 kinase, we prepared lysates from 12 tumors and measured CDK2 kinase activity in these extracts using a standard immune-complex kinase assay (Fig. 4*a*). The results indicate that tumors that contain both cyclin A and p27 contain detectable CDK2 kinase activity, suggesting that p27 is sequestered in non-CDK2 complexes in such tumors. To demonstrate this finding directly, we depleted p27 from 4 such tumors using 2 rounds of immune-depletion with α-p27 antibodies coupled to protein G-Sepharose (Fig. 4*b*). Consistent with the presence of active CDK2 complexes, depletion of p27 did not completely deplete cyclin A or cyclin E from such tumors, confirming that inhibitor-free cyclin-CDK2 complexes exist in these cells.

We considered 2 possibilities as to how p27 might be prevented from binding to CDK2. First, in several tumors p27 has been reported to be inactivated by retention in the cytosol.[40,41] Indeed, higher magnification images of the tumors shown in Figure 2 revealed that p27 staining was observed in both the nucleus and the cytosol, with predominant staining in the cytosol (Fig. 5*a*). However, there was no significant difference in localization of p27 between tumors that did or did not express cyclin A, suggesting that cytosolic localization of p27 does not account for its inability to inhibit CDK2 kinase.

In normal cells stimulated by the addition of growth factors, p27 is sequestered by D-type cyclin complexes (for review, see Sherr and Roberts[2]). To test whether D-type cyclins sequester p27 in human neuroblastoma tumors, we probed extracts of representative tumors with antibodies directed against cyclin D1, D2 and D3 (Fig. 5*b*). In this experiment, tumors that expressed both cyclin A and p27 contained significantly (5- to 10-fold) elevated levels of cyclin

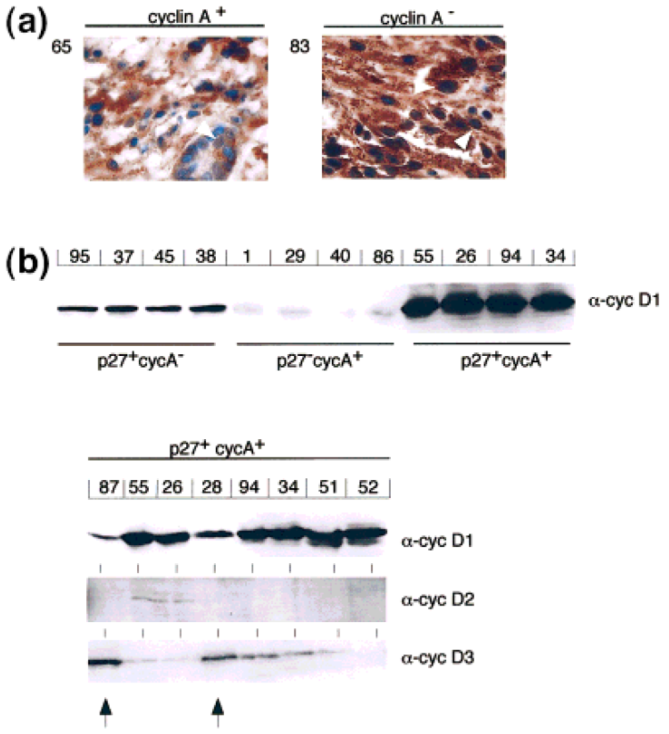

FIGURE 5 – Binding of p27 to cyclins D1 and D3 in human neuroblastoma. (*a*) High magnification view documenting intracellular localization of p27 in a cyclin A-positive and in a cyclin A-negative tumor. White arrows indicate nuclei positive for p27. (*b*) Expression of D-type cyclins in human neuroblastoma. The upper panel shows an α-cyclin D1 Western blot of 12 tumors of the indicated phenotypes. The lower panels show western blots documenting the expression of cyclins D1, D2 and D3 in 8 tumors that express both cyclin A and p27.

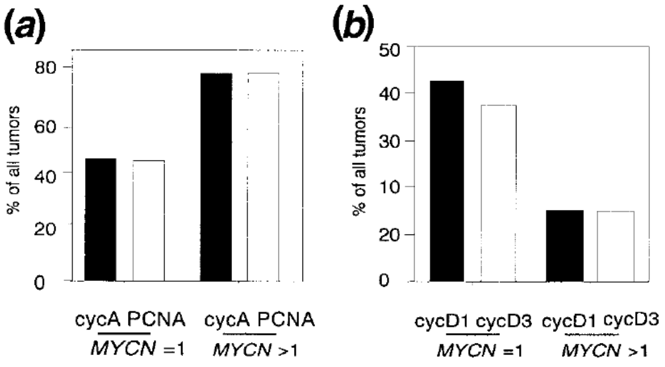

(*c*)

Independent variables		p-values	
1st	2nd	1st var	2nd var
MYCN		0,00137	
p27		0,0087	
p27	*MYCN*	0,0322	0,0099
p27	stage	0,4101	0,0005
p27	age	0,1086	0,0039
p27	histology	0,0447	0,1088

FIGURE 6 – Tumors with an amplification of *MYCN* express cyclin A and proliferating cell nuclear antigen (PCNA). (*a*) Percentage of tumors with detectable expression of cyclin A or PCNA among the tumors that do or do not carry an amplified *MYCN* gene. (*b*) Percentage of tumors that express high levels of cyclins D1 or D3 in the same 2 groups of tumors. (*c*) Uni- and multivariate analysis of expression of p27 and amplification of *MYCN* in relationship to each and of expression of p27 in relationship to tumor stage, histology and age of patient.

D1 relative to either p27$^+$/cyclin A$^-$ or p27$^-$/cyclin A$^+$ tumors, suggesting that p27 is bound to cyclin D1. Re-probing of 15 additional cyclin A$^+$/p27$^+$ tumors showed that all except 3 contained strongly elevated levels of cyclin D1 (Fig. 5*b*): in these, elevated levels of cyclin D3 were found. Cyclin D2 was not expressed at significant levels in any tumor that was analyzed. Direct immunoprecipitation showed that cyclin D1 was bound to p27 in tumors in which the protein is expressed at high levels (not shown). Taken together, the data show that elevated levels of cyclin D1 or cyclin D3 sequester p27 in a subset of human neuroblastoma tumors.

Enhancement of cell proliferation is considered to be an important function of *MYCN* in tumorigenesis. Consistent with the suggestion that amplification of *MYCN* deregulates cell proliferation, more than 80% of the tumors that carry an amplified *MYCN* gene expressed high levels of both cyclin A and PCNA, confirming previous reports[35,36] (Fig. 6*a*).

In contrast to the expectations raised from tissue culture, the large majority of *MYCN* amplified tumors (16 of 21) did not express detectable levels of any D-type cyclin (Fig. 6*b*). Furthermore, expression of either cyclin D1 or D3 was not predictive for survival and was not correlated with amplification of *MYCN*. Because elevated levels of cyclins D1 or D3 were found in all tumors that co-express cyclin A and p27, we concluded that amplification of *MYCN* does not lead to enhanced sequestration of p27 by D-type cyclins.

Also, expression levels of p27 were not reproducibly lowered in *MYCN*-amplified tumors (data not shown) and the total number of p27-positive tumors was only slightly lower in *MYCN*-amplified compared with non-amplified tumors (40% *vs.* 60%). To test whether amplification of *MYCN* was correlated with down-regulation of p27, both univariate and multivariate analysis was performed. Significantly, the analysis showed that the presence or absence of p27 was predictive for prognosis independent of amplification of *MYCN* (Fig. 6*c*). Multivariate analysis also showed that p27 was predictive independent of histology, but was significantly correlated with tumor stage and was therefore not predictive when corrected for tumor stage (Fig. 6*c*). Correction for patient age yielded intermediate *p* values, suggesting that p27 levels might be independently predictive when analyzing larger groups of patients.

Taken together, the data support a model in which amplification of *MYCN* deregulates cell proliferation of neuroblastoma cells *in vivo*, but do not support a model in which cyclin D1-, D2- or D3-mediated inactivation of p27 or enhanced sequestration is a downstream pathway by which amplification of *MYCN* deregulates proliferation in these tumors.

Because *MYCN*-amplified tumors contain high levels of both cyclin A and PCNA and because enhancement of proliferation is considered to be an important function of *MYCN*, one might predict that levels of either cyclin A or PCNA would be indicative of poor prognosis. Surprisingly, this is not the case (Fig. 7*a*). In fact, amplification of *MYCN* (and both tumor stage and age) is highly predictive for poor prognosis among the tumor samples that were analyzed (Fig. 7*a*). To explain this conundrum, we noted that both the average and the median age at diagnosis of patients with tumors that express cyclin A was significantly lower than that of patients with tumors that do not, suggesting that the rate of proliferation of neuroblastoma cells is age-dependent *in vivo*. Indeed, close inspection showed that expression of cyclin A decreased sharply with increasing age of the patient in tumors with a single copy of the *MYCN* gene. In contrast, high expression of cyclin A/PCNA was found in tumors that carry an amplified *MYCN* gene independent of age (Fig. 7*b*). The data suggest that

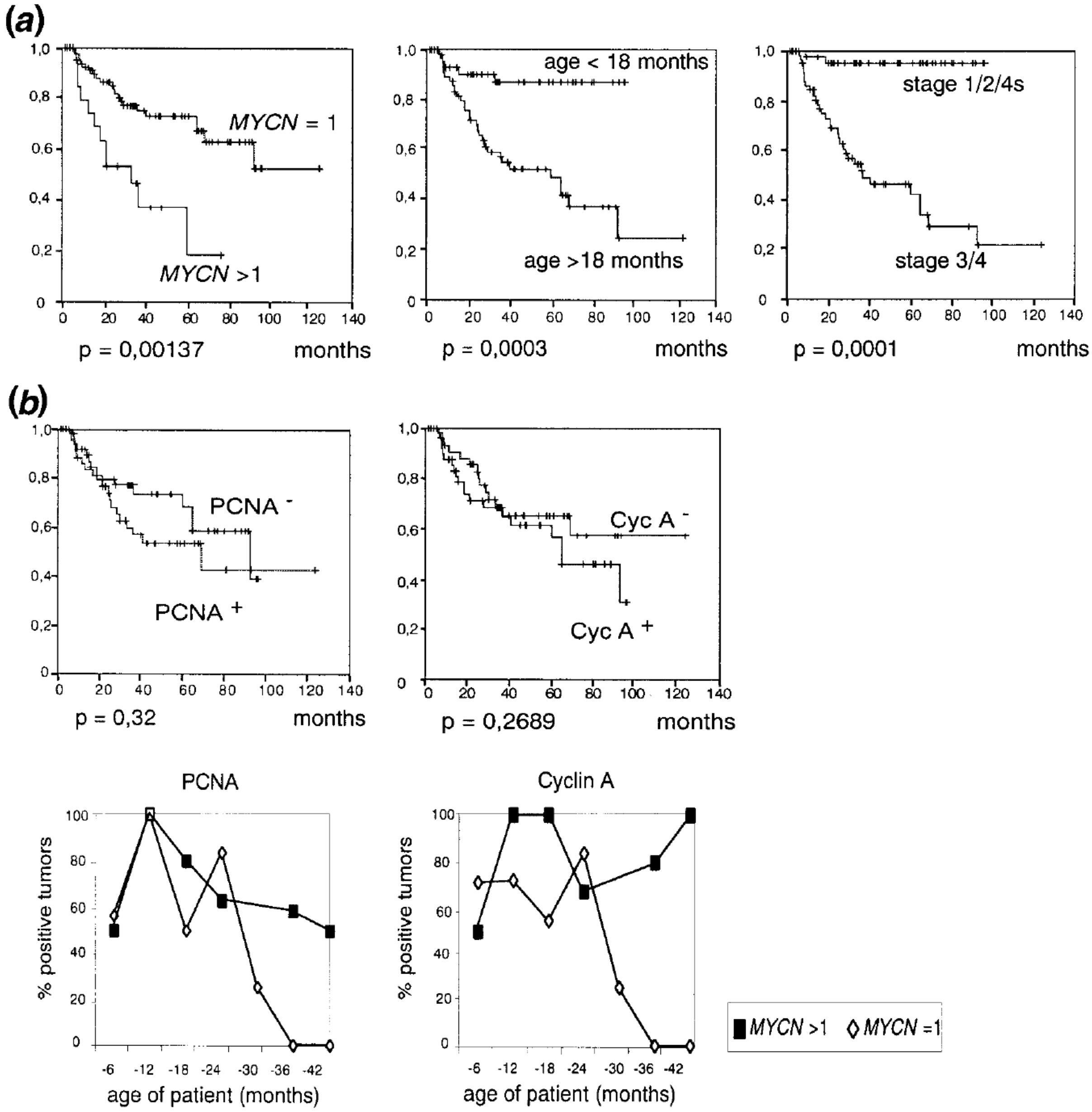

FIGURE 7 – Age-dependence of cyclin A and proliferating cell nuclear antigen (PCNA) expression in human neuroblastoma tumors. (*a*) Kaplan–Meier diagrams for expression of cyclin A and PCNA and, as comparison, for stage, age and amplification of *MYCN*. (*b*) Expression of PCNA (*left*) or cyclin A (*right*) as a function of patient age at diagnosis in tumors that do or do not carry an amplified *MYCN* gene.

neuroblastoma cells undergo a cell cycle arrest *in vivo* with increasing age of the patient and that this arrest does not occur in *MYCN*-amplified tumors. In this view, cyclin A/PCNA levels are not predictive because cells in neuroblastoma tumors, including those from patients with a good outcome, constitute a highly proliferative population during the early postnatal period. Consistent with this view and with other reports,[35,36] detectable cyclin A levels did indicate a lower survival probability in the subgroup of patients over 18 months of age (not shown).

DISCUSSION

In this communication, we reported 3 findings: First, we showed that the levels of the CDK2 kinase inhibitor, p27^{kip1}, are predictive for survival in human neuroblastoma tumors. Unlike the situation found in neuroblastoma cells in culture, however, levels of p27 do not correlate with the degree of cell proliferation at the time of diagnosis, because p27 is bound to cyclins D1 and D3 in a large fraction of the neuroblastomas we analyzed. In tumors expressing high levels of cyclin D1 or cyclin D3, p27 was prevented from binding to CDK2 and active CDK2 kinase was detected. In sharp contrast to p27, expression of marker proteins of cell proliferation, including cyclin A and E (data not shown) and PCNA, does not predict survival in the group of neuroblastomas that we analyzed. This situation contrasts with breast cancer, for example, in which expression of cyclin E and of p27 are both prognostic for survival.[8,9] We conclude from our analysis that the prognostic significance of p27 does not reflect any role in regulating cell proliferation within the primary tumor at the time point of diagnosis.

Our data do not indicate directly why expression of p27 is prognostic in neuroblastomas. Mortality from neuroblastoma usually reflects the appearance of metastases or the recurrence of a tumor at the primary site after initial surgery or chemotherapy.[42,43]

Therefore, mortality and tumor progression reflect proliferative processes that occur usually much later in time and often at different sites from the location of the biopsy of the primary tumor that we analyzed. The presence or absence of p27 may therefore predict the likelihood of such processes.

Second, we noted that expression of cyclin A and PCNA showed a strong decrease with increasing patient age in tumors lacking amplified *MYCN* (Fig. 5). This finding is consistent with a model in which neuroblastomas derive from an uncommitted, highly proliferative precursor cell population, which undergoes a differentiation process and therefore an age-dependent cell cycle arrest *in vivo*.[11] Tumors that carry an amplified *MYCN* gene expressed high levels of cyclin A independent of the age of the patient, suggesting that amplification of *MYCN* enhances proliferation and prevents exit from the cell cycle, consistent with models derived from tissue culture and with previous reports.

Third, our study addressed the potential link between the function of Myc and the regulation of CDK2 activity and the p27 protein. If this regulatory circuit exists in neuroblastomas, one would make 3 predictions: First, *MYCN* amplified tumors should contain elevated levels of cyclin D2 or cyclin D1. Second, such tumors should express low levels of p27. Third, expression levels of p27 and/or cyclin D1/2 should identify the same subset of tumors as *MYCN* amplification and should be able to at least partially substitute for amplification of *MYCN* as a prognostic marker. We found that these predictions were not fulfilled. We found that p27 levels were prognostic independent of *MYCN* amplification and that *MYCN*-amplified tumors did not contain elevated levels of any D-type cyclin; both findings argue against a role for *MYCN* as a critical regulator of p27 protein function in these tumors.

In further studies we tested expression levels of E2F2, a proposed target gene of *c-myc* that links its function to the control of E2F-dependent transcription[44] and of p15*ink4b*, a proposed target of repression by Myc;[45] expression of neither gene was significantly altered in *MYCN* amplified tumors (E. Bergmann, unpublished data).

Several alternative models can be considered to explain the effect of *MYCN* amplification on cell proliferation: First, proliferating somatic cells undergo a decrease in telomere length if they do not express telomerase. Shortened telomeres are recognized as damaged DNA and can induce cell cycle arrest and senescence (for review, see Weinberg[46]). The gene encoding the catalytic subunit of telomerase, *htert*, has been suggested to be a target for activation by Myc.[47–49] Consistent with this model, the expression of *htert* and telomerase activity correlates with amplification of *MYCN* and is highly predictive for poor prognosis in human neuroblastoma.[50,51] We have confirmed these findings for the group of tumors that we analyzed (data not shown). One possibility is, therefore, that amplification of *MYCN* prevents cell cycle exit by inducing *htert* expression. To test this hypothesis, it will be important to determine whether ectopic expression of either *htert* or *MYCN* can immortalize early-stage neuroblastoma cells in culture; such experiments are under way.

Alternatively, many studies have shown that neuroblastoma cells can undergo differentiation processes *in vitro* (*e.g.*, Matsuo and Thiele[27]) and have provided evidence that the proliferation of neuroblastoma *in vitro* and *in vivo* is controlled by neurotrophins and their receptors.[52,53] In culture systems, ectopic expression of *c-myc* can alter the response of cells to neurotrophic factors and block differentiation in response to nerve growth factor;[54,55] similar relationships may hold in neuroblastoma.[56] It is, therefore, equally possible that exit from the cell cycle occurs in response to neurotrophin signaling and that amplification of *MYCN* alters the cellular response to such factors.

ACKNOWLEDGEMENTS

This work was supported by a joint grant from the Deutsche Krebshilfe to Holger Christiansen and Martin Eilers. We are thankful to Fritz Lampert for continuous support of this project.

REFERENCES

1. Morgan D. Principles of CDK regulation. Nature 1995;374:131–4.
2. Sherr CJ, Roberts JM. CDK inhibitors: positive and negative regulators of G_1-phase progression. Genes Dev 1999;13:1501–12.
3. Fero ML, Randel E, Gurley KE, Roberts JM, Kemp CJ. The murine gene p27Kip1 is haplo-insufficient for tumour suppression. Nature 1998;396:177–80.
4. Fero ML, Rivkin M, Tasch M, Porter P, Carow CE, Firpo E, et al. A syndrome of multiorgan hyperplasia with features of gigantism, tumorigenesis, and female sterility in p27(Kip1)-deficient mice. Cell 1996;85:733–44.
5. Kiyokawa H, Kineman RD, Manova Todorova KO, Soares VC, Hoffman ES, Ono M, et al. Enhanced growth of mice lacking the cyclin-dependent kinase inhibitor function of p27(Kip1). Cell 1996; 85:721–32.
6. Nakayama K, Ishida N, Shirane M, Inomata A, Inoue T, Shishido N, et al. Mice lacking p27(Kip1) display increased body size, multiple organ hyperplasia, retinal dysplasia, and pituitary tumors. Cell 1996; 85:707–20.
7. Fredersdorf S, Burns J, Milne AM, Packham G, Fallis L, Gillett CE, et al. High level expression of p27(kip1) and cyclin D1 in some human breast cancer cells: inverse correlation between the expression of p27(kip1) and degree of malignancy in human breast and colorectal cancers. Proc Natl Acad Sci U S A 1997;94:6380–5.
8. Loda M, Cukor B, Tam SW, Lavin P, Fiorentino M, Draetta GF, et al. Increased proteosome-dependent degradation of the cyclin-dependent kinase inhibitor p27 in aggressive colorectal carcinomas. Nat Med 1997;3:231–4.
9. Porter PL, Malone KE, Heagerty PJ, Alexander GM, Gatti LA, Firpo EJ, et al. Expression of cell-cycle regulators p27Kip1 and cyclin E, alone and in combination, correlate with survival in young breast cancer patients. Nat Med 1997;3:222–5.
10. Tan P, Cady B, Wanner M, Worland P, Cukor B, Magi-Galluzzi C, et al. The cell cycle inhibitor p27 is an independent prognostic marker in small (T1a,b) invasive breast carcinomas. Cancer Res 1997;57:1259–63.
11. Maris JM, Matthay KK. Molecular biology of neuroblastoma. J Clin Oncol 1999;17:2264.
12. Brodeur GM, Seeger RC, Schwab M, Varmus HE, Bishop JM. Amplification of N-myc in untreated human neuroblastomas correlates with advanced disease stage. Science 1984;224:1121–4.
13. Schwab M, Ellison J, Busch M, Rosenau W, Varmus HE, Bishop JM. Enhanced expression of the human gene N-myc consequent to amplification of DNA may contribute to malignant progression of neuroblastoma. Proc Natl Acad Sci U S A 1984;81:4940–4.
14. Lutz W, Stohr M, Schurmann J, Wenzel A, Lohr A, Schwab M. Conditional expression of N-myc in human neuroblastoma cells increases expression of alpha-prothymosin and ornithine decarboxylase and accelerates progression into S-phase early after mitogenic stimulation of quiescent cells. Oncogene 1996;13:803–12.
15. Schwab M, Varmus HE, Bishop JM. Human N-myc gene contributes to neoplastic transformation of mammalian cells in culture. Nature 1985;316:160–2.
16. Leone G, DeGregori J, Sears R, Jakoi L, Nevins JR. Myc and Ras collaborate in inducing accumulation of active cyclin E/Cdk2 and E2F. Nature 1997;387:422–6.
17. Steiner P, Philipp A, Lukas J, Godden-Kent D, Pagano M, Mittnacht S, et al. Identification of a Myc-dependent step during the formation of active G_1 cyclin/cdk complexes. EMBO J 1995;14:4814–26.
18. Alevizopoulos K, Vlach J, Hennecke S, Amati B. Cyclin E and c-Myc promote cell proliferation in the presence of p16INK4a and of hypophosphorylated retinoblastoma family proteins. EMBO J 1997;16: 5322–33.
19. Rudolph B, Zwicker J, Saffrich R, Henglein B, Müller R, Ansorge W, et al. Activation of cyclin dependent kinases by Myc mediates transcriptional activation of cyclin A, but not apoptosis. EMBO J 1996; 15:3065–76.
20. Vlach J, Hennecke S, Alevizopoulos K, Conti D, Amati B. Growth arrest by the cyclin-dependent kinase inhibitor p27Kip1 is abrogated by c-Myc. EMBO J 1996;15:6595–604.
21. Beier R, Bürgin A, Kiermaier A, Fero M, Karsunky H, Saffrich R, et al. Induction of cyclin E-cdk2 kinase activity, E2F-dependent transcription, and cell growth by Myc are genetically separable events. EMBO J 2000;21:5813–23.
22. Bouchard C, Thieke K, Maier A, Saffrich R, Hanley-Hyde J, Ansorge

W, et al. Direct induction of cyclin D2 by Myc contributes to cell cycle induction and sequestration of p27. EMBO J 1999;18:5321–33.
23. O'Hagan RC, Ohh M, David G, de Alboran IM, Alt FW, Kaelin WG, Jr., et al. Myc-enhanced expression of cul1 promotes ubiquitin-dependent proteolysis and cell cycle progression. Genes Dev 2000;14:2185–91.
24. Perez-Roger I, Kim S-H, Griffiths B, Sewing A, Land H. Cyclins D1 and D2 mediate Myc-induced proliferation via sequestration of p27Kip1 and p21Cip1. EMBO J 1999;18:5310–20.
25. Rosenwald IB, Lazaris-Karatzas A, Sonenberg N, Schmidt EV. Elevated levels of cyclin D1 protein in response to increased expression of eukaryotic initiation factor 4E. Mol Cell Biol 1993;13:7358–63.
26. Borriello A, Pietra VD, Criscuolo M, Oliva A, Tonini GP, Iolascon A, et al. p27Kip1 accumulation is associated with retinoic-induced neuroblastoma differentiation: evidence of a decreased proteasome-dependent degradation. Oncogene 2000;19:51–60.
27. Matsuo T, Thiele CJ. p27Kip1: a key mediator of retinoic acid induced growth arrest in the SMS-KCNR human neuroblastoma cell line. Oncogene 1998;16:3337–43.
28. Bartkova J, Lukas J, Strauss M, Bartek J. Cell cycle-related variation and tissue-restricted expression of human cyclin D1 protein. J Pathol 1994;172:237–45.
29. Kaatsch P, Haaf G, Michaelis J. Childhood malignancies in Germany—methods and results of a nationwide registry. Eur J Cancer 1995;31A:993–9.
30. Shimada H, Chatten J, Newton WA, Jr., Sachs N, Hamoudi AB, Chiba T, et al. Histopathologic prognostic factors in neuroblastic tumors: definition of subtypes of ganglioneuroblastoma and an age-linked classification of neuroblastomas. J Natl Cancer Inst 1984;73:405–16.
31. Muller D, Bouchard C, Rudolph B, Steiner P, Stuckmann I, Saffrich R, et al. Cdk2-dependent phosphorylation of p27 facilitates its Myc-induced release from cyclin E/cdk2 complexes. Oncogene 1997;15:2561–76.
32. Pagano M, Tam SW, Theodoras AM, Beer Romero P, Del Sal G, Chau V, et al. Role of the ubiquitin-proteasome pathway in regulating abundance of the cyclin-dependent kinase inhibitor p27. Science 1995;269:682–5.
33. Sheaff RJ, Groudine M, Gordon M, Roberts JM, Clurman BE. Cyclin E-CDK2 is a regulator of p27Kip1. Genes Dev 1997;11:1464–78.
34. Vlach J, Hennecke S, Amati B. Phosphorylation-dependent degradation of the cyclin-dependent kinase inhibitor p27. EMBO J 1997;16:5334–44.
35. Kawasaki H, Mukai K, Yajima S, Tanaka R, Takayama J, Takasaki Y, et al. Prognostic value of proliferating cell nuclear antigen (PCNA) immunostaining in neuroblastoma. Med Pediatr Oncol 1995;24:300–4.
36. Keim DR, Hailat N, Kuick R, Reynolds CP, Brodeur GM, Seeger RC, et al. PCNA levels in neuroblastoma are increased in tumors with an amplified N-myc gene and in metastatic stage tumors. Clin Exp Metastasis 1993;11:83–90.
37. Rudolph P, Lappe T, Hero B, Berthold F, Parwaresch R, Harms D, et al. Prognostic significance of the proliferative activity in neuroblastoma. Am J Pathol 1997;150:133–45.
38. Pagano M, Pepperkok R, Verde F, Ansorge W, Draetta G. Cyclin A is required at two points in the human cell cycle. EMBO J 1992;11:961–71.
39. Bastians H, Townsley FM, Ruderman JV. The cyclin-dependent kinase inhibitor p27(Kip1) induces N-terminal proteolytic cleavage of cyclin A. Proc Natl Acad Sci U S A 1998;95:15374–81.
40. Orend G, Hunter T, Ruoslahti E. Cytoplasmic displacement of cyclin E-cdk2 inhibitors p21Cip1 and p27Kip1 in anchorage-independent cells. Oncogene 1998;16:2575–83.
41. Singh SP, Lipman J, Goldman H, Ellis FH, Jr., Aizenman L, Cangi MG, et al. Loss or altered subcellular localization of p27 in Barrett's associated adenocarcinoma. Cancer Res 1998;58:1730–5.
42. Hawkins MM, Kingston JE, Kinnier Wilson LM. Late deaths after treatment for childhood cancer. Arch Dis Child 1990;65:1356–63.
43. Robertson CM, Hawkins MM, Kingston JE. Late deaths and survival after childhood cancer: implications for cure. BMJ 1994;309:162–6.
44. Sears R, Ohtani K, Nevins JR. Identification of positively and negatively acting elements regulating expression of the E2F2 gene in response to cell growth signals. Mol Cell Biol 1997;17:5227–35.
45. Warner BJ, Blain SW, Seoane J, Massagué J. Myc Downregulation by transforming growth factor required for activation of the p15Ink4b G_1 arrest pathway. Mol Cell Biol 1999;19:5913–22.
46. Weinberg RA. Telomeres. Bumps on the road to immortality. Nature 1998;396:23–4.
47. Greenberg RA, O'Hagan RC, Deng H, Xiao Q, Hann SR, Adams RR, et al. Telomerase reverse transcriptase gene is a direct target of c-Myc but is not functionally equivalent in cellular transformation. Oncogene 1999;18:1219–26.
48. Wang J, Xie LY, Allan S, Beach D, Hannon GJ. Myc activates telomerase. Genes Dev 1998;12:1769–74.
49. Wu KJ, Grandori C, Amacker M, Simon-Vermot N, Polack A, Lingner J, et al. Direct activation of TERT transcription by c-MYC. Nat Genet 1999;21:220–4.
50. Hiyama E, Hiyama K, Yokoyama T, Fukuba I, Yamaoka H, Shay JW, et al. Rapid detection of MYCN gene amplification and telomerase expression in neuroblastoma. Clin Cancer Res 1999;5:601–9.
51. Hiyama E, Hiyama K, Yokoyama T, Matsuura Y, Piatyszek MA, Shay JW. Correlating telomerase activity levels with human neuroblastoma outcomes. Nat Med 1995;1:249–55.
52. Nakagawara A, Arima-Nakagawara M, Scavarda NJ, Azar CG, Cantor AB, Brodeur GM. Association between high levels of expression of the TRK gene and favorable outcome in human neuroblastoma. N Engl J Med 1993;328:847–54.
53. Nakagawara A, Brodeur GM. Role of neurotrophins and their receptors in human neuroblastomas: a primary culture study. Eur J Cancer 1997;33:2050–3.
54. Chen J, Chattopadhyay B, Venkatakrishnan G, Ross AH. Nerve growth factor-induced differentiation of human neuroblastoma and neuroepithelioma cell lines. Cell Growth Differ 1990;1:79–85.
55. Maruyama K, Schiavi SC, Huse W, Johnson GL, Ruley HE. myc and E1A oncogenes alter the responses of PC12 cells to nerve growth factor and block differentiation. Oncogene 1987;1:361–7.
56. Nakagawara A, Arima M, Azar CG, Scavarda NJ, Brodeur GM. Inverse relationship between trk expression and N-myc amplification in human neuroblastomas. Cancer Res 1992;52:1364–8.

Vol. 9, 5683–5692, November 15, 2003 Clinical Cancer Research 5

Coexpression of Insulin Receptor-Related Receptor and Insulin-Like Growth Factor 1 Receptor Correlates with Enhanced Apoptosis and Dedifferentiation in Human Neuroblastomas

Axel Weber,[1] Christine Huesken,[1]
Eckhard Bergmann,[1] Wieland Kiess,[2]
Nina M. Christiansen,[1] and Holger Christiansen[1]
[1]University Children's Hospital, Marburg, and [2]Children's Hospital, Leipzig, Germany

ABSTRACT

Purpose: We compared the expression of the insulin receptor-related receptor (IRR) in primary human neuroblastomas with other biological and clinical parameters and the impact of its expression on prognostic outcome.

Experimental Design: We studied 49 neuroblastomas of different clinical stages and histological subtypes for (_a_) IRR, insulin-like growth factor 1 receptor (IGF-1R), TrkA, p75 neurotrophin receptor, and MYCN mRNA expression by reverse transcription-PCR; (_b_) _MYCN_ gene amplification by Southern blot analyses; (_c_) cyclin A protein expression by Western blot analyses indicating proliferation rate; and (_d_) apoptotic index (AI) by terminal deoxynucleotidyl transferase (Tdt)-mediated dUTP nick end-labeling assay.

Results: IRR mRNA expression was found in 25 (51%) neuroblastomas and correlated with stages 1, 2, 3, and 4S disease and with age ≤12 months at diagnosis. IRR was expressed predominantly in neuroblastomas without _MYCN_ gene amplification and coexpressed with IGF-1R, TrkA, and p75 neurotrophin receptor. IRR mRNA expression also correlated with an undifferentiated histology but not with the proliferation rate. In coexpression with IGF-1R, the IRR was associated with enhanced AI. IRR expression was significantly correlated with a good prognosis in all 49 neuroblastomas (6-year survival probability, 91.8% _versus_ 49.7% for IRR nonexpression; $P = 0.003$).

Conclusion: IRR expression is a new marker for a favorable prognosis in neuroblastoma that is independent of _MYCN_ amplification and age at diagnosis. Our data suggest an influence of IRR on IGF signaling via IGF-1R because coexpression of these two receptor tyrosine kinases was significantly correlated with an undifferentiated histology, a high AI, and an advanced survival probability.

INTRODUCTION

Neuroblastoma is the third most common pediatric cancer and is responsible for ~15% of all childhood cancer deaths. It is an embryonal tumor of the postganglionic sympathetic nervous system, which most commonly arises in para- and prevertebral ganglia and in the adrenal gland. The 6-year survival probability of all patients with neuroblastoma is ~60% (own data based on 2030 patients registered from 1980 to 2003). In addition to clinical markers such as stage and age at diagnosis, biological tumor markers have gained increasing importance in determining the prognostic outcome for patients with neuroblastoma. The most extensively studied biological marker for an unfavorable prognostic outcome in patients with neuroblastoma is the amplification of the *MYCN*[3] oncogene (1–3).

MYCN is differentially expressed in neuroblastomas with or without *MYCN* gene amplification and in different clinical stages (4). However, the prognostic impact of MYCN expression is controversial and has not been shown to be of prognostic relevance in most studies (5, 6). Among other biological markers for a favorable prognostic outcome in neuroblastoma are expression of the high-affinity nerve growth factor receptor TrkA (7) and the low-affinity nerve growth factor receptor p75NTR (8–10).

The IGF-1R is of prognostic relevance in a variety of tumor entities and influences apoptosis, differentiation, and proliferation in coexpression with other RTKs (11, 12). In neuroblastoma cells, expression of IGF-1R has been implicated in growth-promoting and antiapoptotic signaling (13). In contrast to its implication in cell survival, proapoptotic action by IGF-1R has been seen in cells that have been triggered to undergo apoptosis through receptors of the death receptor family, such as TNF receptors or p75NTR (14).

Recently, the IRR has been identified as an additional member of the insulin RTK family (15, 16). However, its ligand and biological functions are still unknown. Various ligands activating the IR or the IGF-1R, such as proinsulin, insulin,

---

Received 3/18/03; revised 7/22/03; accepted 8/4/03.
Grant support: This work was supported by the "Deutsche Krebshilfe" (10-1116-Ki2) W. K.'s laboratory is supported by IZKF, Leipzig, Germany. This work contains parts of the doctoral theses of A. W. and C. H. The costs of publication of this article were defrayed in part by the payment of page charges. This article must therefore be hereby marked *advertisement* in accordance with 18 U.S.C. Section 1734 solely to indicate this fact.

Requests for reprints: Holger Christiansen, M.D., Ph.D., Universitaetskinderklinik, Deutschhausstrasse 12, D-35037 Marburg, Germany. Phone: 49-6421-28-62671; Fax: 49-6421-28-66824; E-mail: Holger.Christiansen@mailer.uni-marburg.de; Internet: http://www.neuroblastom.info/.

[3] The abbreviations used are: MYCN, avian myelocytomatosis viral-related oncogene-neuroblastoma derived; TrkA, tyrosine receptor kinase A; P75NTR, P75 neurotrophin receptor; IGF-1R, insulin-like growth factor-1 receptor; RTK, receptor tyrosine kinase; TNF, tumor necrosis factor; IRR, insulin receptor-related receptor; DSR, diffuse-stroma-rich; SP-D, stroma-poor-differentiated; SP-U, stroma poor-undifferentiated; TUNEL, terminal deoxynucleotidyl transferase (Tdt)-mediated dUTP nick end-labeling; M/A, ratio of MYCN to β-actin; AI, apoptotic index; GAPDH, glyceraldehyde-3-phosphate dehydrogenase.

IGF-1, IGF-2, and relaxin, are not able to bind the extracellular domain and activate IRR (17, 18). The functional potential of the tyrosine kinase domain of the IRR was demonstrated by use of receptor hybrids of a known extracellular domain and the intracellular domain of the IRR. Thus, IR substrate-1 and -2 have been identified as receptor substrates of the IRR, implicating a role for the IRR in influencing downstream signaling pathways such the phosphatidylinositol 3′-kinase and the mitogen-activate protein kinase pathway (17).

In contrast to the widespread patterns of expression of the homologous IR and IGF-1R, IRR demonstrates a very restricted cellular distribution in a subset of tissues of neuronal origin, where its appearance is closely associated to that of IR, IGF-1R, and the nerve growth factor receptor TrkA (19, 20). IRR and TrkA appear early in the embryonal development of dorsal root and trigeminal neurons and later, near the time of birth, in sympathetic neurons. This association is highly selective: TrkA mRNA is not detected anywhere else in the developing nervous system in the absence of coordinate IRR expression (20, 21). Furthermore, it was shown recently that IRR is also coexpressed with IGF-1R in neuroblastoma cell lines (22). Coexpression of receptors of the IR family has been shown to influence activation of downstream signaling pathways and cellular biological functions, which might be explained by heterodimerization of the expressed receptor monomers on the cell surface, resulting in different ligand-binding affinities and autophosphorylation status (23–26).

These observations prompted us to study the possible role of IRR expression in primary neuroblastomas. We examined the relationship of IGF-1R, TrkA, and p75NTR mRNA expression with the expression of IRR and correlated this expression pattern to biological effects such as proliferation, apoptosis, and morphological differentiation. We also asked whether *MYCN* amplification/expression status correlates with the IRR expression pattern and whether the IRR might have any prognostic impact on patients with neuroblastoma.

MATERIALS AND METHODS

Patients. We studied tumor specimens from 49 children with neuroblastoma who had been diagnosed in Germany from 1989 to 1997. All neuroblastoma diagnoses were confirmed by histological assessment of a tumor specimen obtained at surgery. The tumors were classified according to the INSS criteria (27). We studied 8 stage 1 (16%), 7 stage 2 (14%), 9 stage 3 (18%), 14 stage 4 (28%), and 11 stage 4S (22%) tumors. The relative incidence rate in our study reflects the relative incidence rate of neuroblastomas in Germany within the investigated time period (1990–1997): stage 1 (19%), stage 2 (12%), stage 3 (20%), stage 4 (39%), and stage 4S (10%).

The median age of the patients at diagnosis was 12.9 months (range, 0.2–131.6 months). Thirteen (26.5%) tumors had a DSR histology, six (12.2%) were SP-D, and 30 (61.2%) were SP-U (28). All patients were treated in a stage-specific manner according to previously described protocols (29). The survival probability of our study population calculated with Kaplan–Meier analysis was 70.5%.

Tissue Preparation. The neuroblastoma specimens were frozen in liquid nitrogen and stored at −80°C for PCR and Southern and Western blot analyses. Portions of the samples (50–60 mg) were fixed in 10% buffered formalin. Serial sections 4-μm in thickness were cut from the same blocks, mounted on poly-L-lysine-coated slides, and used for H&E staining and *in situ* end-labeling of DNA (TUNEL assay).

RNA Extraction and Reverse Transcription. Tumor samples (100 mg each) were homogenized in 1000 μl of RNAzol-B (Biotecx Laboratories Inc., Houston, TX). RNA was isolated after the addition of chloroform according to the guanidinium-isothiocyanate method (30) and finally precipitated with isopropanol. After centrifugation (14000 × *g* for 20 min), the pellet was washed twice with 70% ethanol, vacuum-dried, and dissolved in 50–80 μl of RNase-free distilled water.

We incubated 7500 ng of total RNA at 70°C for 10 min with 1.5 μl of RNase inhibitor (40 units/μl; Promega), 2.5 μl of oligo-primer-p(dT)15 (0.1 nmol/μl; Boehringer-Mannheim) and distilled water in a volume of 42 μl; we then cooled the mixture to 4°C. First-strand cDNA was synthesized with 1.5 μl of Moloney murine leukemia virus reverse transcriptase (SuperScript-II; Invitrogen) in a total volume of 75 μl [15 μl of 5× first-strand buffer (Invitrogen), 7.5 μl of dithiothreitol (0.1 M; Invitrogen), 3 μl of BSA, 1.5 μl of each deoxynucleotide triphosphate (0.01 μmol/μl; Perkin-Elmer), and 0.5 μl of RNasin]. Reverse transcription was performed for 10 min at 25°C and 60 min at 42°C, and finally for 15 min at 75°C to inactivate the enzyme.

Primer Search. Specific primers for the amplification of IRR, IGF-1R, p75NTR, TrkA, MYCN, and β-actin were searched with OLIGO 6.0 (Medprobe); the specificity was controlled with BLAST 2.0 (http://www.ncbi.nlm.nih.gov/blast/blast.cgi). To avoid coamplification of contaminating DNA, primers were located in two subsequent exons. All PCR products were sequenced by the dye-termination procedure on a ALF-express with 5′-Cy5-labeled primers according to the manufacturer's protocol (Pharmacia Biotech); the results were compared with the respective published sequence data (http://www.ncbi.nlm.nih.gov/GenBank/index.html; Table 1).

PCR. PCR was performed in a total volume of 50 μl containing 5 μl of 10× PCR buffer, 2.5 units of *Taq*-polymerase-k (MoBiTec), 1 μl of each deoxynucleotide triphosphate (Perkin-Elmer), 50 pmol of each primer, 200 ng of total cDNA, 1 μl of formamide (Sigma), and 33 μl of distilled water.

The primer sequences and individual PCR conditions (annealing and elongation temperature, time, and cycle number) for each PCR are listed in Table 1. In every PCR, an initial denaturation step at 95°C for 3 min was performed, denaturation during cycling was performed at 95°C for 30 s, and the last cycle was followed by an elongation step at 72°C for 7 min. The reaction was then cooled to 4°C.

In the semiquantitative PCR of *MYCN* relative to β-*actin* (M/A), the first 5 cycles were done only with the *MYCN* primers. After the reaction was cooled to 4°C and the β-actin primers were added, the reaction was continued for 28 cycles, as described by Kinoshita *et al.* (31). PCR conditions have been established for both gene fragments to be in the logarithmic phase at the time of analysis. After agarose gel electrophoresis, the level of *MYCN* expression in each tumor was determined by densitometry and was expressed as the M/A ratio. *MYCN* ex-

Table 1 PCR product length, primer sequences, and PCR conditions

Gene		Primer sequences	PCR conditions
β-*actin*	Upper	5′-ATCTGGCACCACACCTTCTACAATGAGCTGCG-3′	64.5°C for 75 s; 72°C for 90 s; 28 cycles
(838 bp)	Lower	5′-CGTCATACTCCTGCTTGCTGATCCACATCTGC-3′	
MYCN	Upper	5′-AGCGGCGGCGACCACAAGGC-3′	64.5°C for 75 s; 72°C for 90 s; 5 + 28 cycles
(399 bp)	Lower	5′-CGAGTCAGAGTTTCGGGGGCTCAAGC-3′	
p75NTR	Upper	5′-CTGCAACCTGGGCGAGGGTGT-3′	63°C for 60 s; 72°C for 90 s; 40 cycles
(470 bp)	Lower	5′-CTGGGGGTGTGGACCGTGTAA-3′	
TrkA	Upper	5′-GCGCAGAGAACCTGACTGAGCT-3′	60°C for 60 s; 72°C for 90 s; 40 cycles
(442 bp)	Lower	5′-ACGTCGTCCCCCACATCCA-3′	
IRR	Upper	5′-AGGACGGCGACCTCTACCTCAAT-3′	62°C for 60 s; 72°C for 90 s; 40 cycles
(597 bp)	Lower	5′-TGAGTCCGTTGGGGTCTGGTG-3′	
IGF-IR	Upper	5′-ACTTCTGCGCCAACATCCTCA-3′	60°C for 60 s; 72°C for 90 s; 40 cycles
(572 bp)	Lower	5′-CCCTTTAGTCCCCGTCACTTCC-3′	

pression was defined as high for M/A at or above the median and as low for M/A below the median expression level.

Relative to common housekeeping genes (β-*actin* and *GAPDH*), the investigated receptors were found to be expressed at lower levels. Thus, semiquantification of receptor RNA expression was difficult and inaccurate, particularly in comparison with the *MYCN*/β-*actin* PCR. We decided to use a common cDNA-specific PCR with higher cycle number (up to 40) to avoid false-negative results. For a loading control, we equalized the amount of cDNA from each tumor with a *GAPDH* PCR for 26 cycles, which gave comparable specific bands (data not shown). The β-*actin* band in the *MYCN*/β-*actin* PCR was then used as an additional control. Each specific band was regarded as positive expression. Each tumor that was PCR negative was controlled in a second PCR for 50 cycles. None of the controlled tumors turned positive (Fig. 1).

Gel Electrophoresis. The amplified PCR fragments (10 µl of the PCR products) were separated on a 2% agarose gel by electrophoresis, identified by ethidium bromide staining, and documented by the Image Master VDS software (Pharmacia).

***MYCN* Amplification.** For the detection of *MYCN* amplification, the pNB-1 probe (*MYCN* is localized on 2p24.1; ATCC 41011) was used; control hybridization for a single-copy signal was performed with HuCK (IGKC is the immunoglobulin κ constant region, localized on 2p12; ATCC 59172).

DNA Isolation and Southern Blot Analysis. High-molecular-weight DNA was isolated by proteinase K digestion and phenol–chloroform extraction according to standard procedures. We digested 10 µg of DNA from each sample with *Eco*RI, and fragments were separated by 0.8% agarose gel electrophoresis. The DNA was then transferred to Gene Screen Plus membranes (DuPont) by vacuum-blotting (Pharmacia) according to the specifications of the manufacturer. Prehybridization and hybridization were performed according to standard procedures. Filters were washed twice in 0.1× SSC and 0.1% SDS at room temperature for 20 min and three times at 65°C for 30 min. After a brief rinse in 0.1× SSC, autoradiography was performed at −70°C with Kodak XAR-5 film (Fig. 1).

Western Blot Analysis. Cellular protein was extracted by lysing 30 mg of tumor tissue with 300 µl of lysis buffer [NP-40 + 4: 150 mM NaCl, 1% (v/v) NP-40, 50 mM Tris-buffer (pH 8), 5 mg/ml aprotinin, 5 mg/ml leupeptin, 1 mg/ml pepstatin, 0.2 M phenylmethylsulfonyl fluoride]. We separated 30 µg of protein in a 12% gradient SDS–polyacrylamide gel and electroblotted the bands to Hybond-Enhanced Chemiluminescence (ECL) nitrocellulose membrane (Amersham Corp., Arlington Heights, IL). After the membranes were blocked with

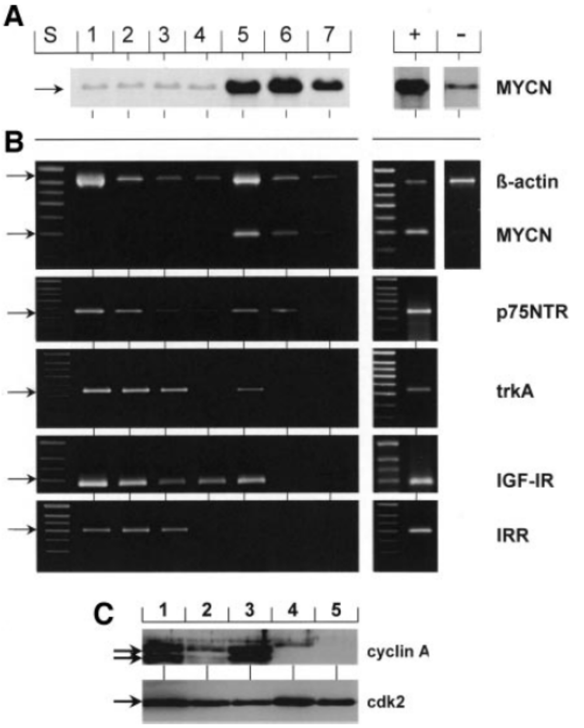

Fig. 1 *A*, seven representative neuroblastomas, examined for MYCN amplification by Southern blot analyses. *Lanes 1–4*, *MYCN* single-copy tumors; *Lanes 5–7*, *MYCN*-amplified tumors. Amplification-positive control (*Lane +*), IMR32 *MYCN*-amplified cell line; negative control (*Lane −*), SHEP *MYCN* single-copy cell line. *B*, same neuroblastomas as in *A*, examined by reverse transcription-PCR for receptor and *MYCN* mRNA expression. Expression of *GAPDH* (data not shown) and β-*actin* was used as an internal control. *Lane S*, length standard. For *MYCN* expression, IMR32 and SHEP cell line cDNAs were used as the positive and negative controls, respectively; for receptor expression, fetal brain cDNA was used as positive control. *C*, cyclin A expression in five neuroblastoma tumors. *Lanes 1* and *3*, neuroblastomas with high cyclin A expression; *Lanes 2* and *4*, neuroblastomas with enhanced expression; *Lane 5*, neuroblastoma with no expression.

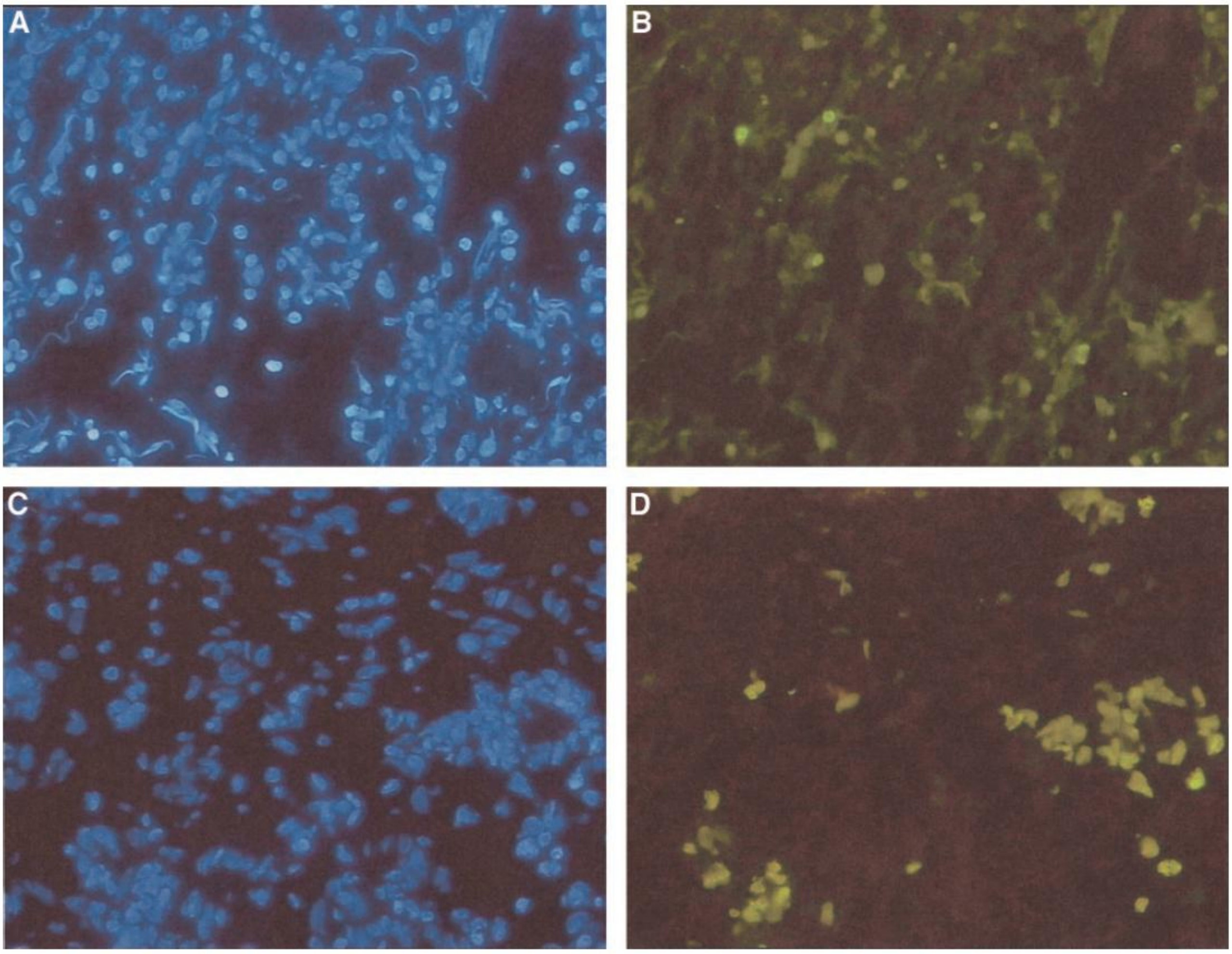

Fig. 2 Apoptosis in neuroblastomas. *A* and *B*, neuroblastoma with low AI (<0.82% TUNEL-positive cells). *C* and *D*, neuroblastoma with high AI (>0.82% TUNEL-positive cells) *A* and *C*, staining with 4′,6-diamidino-2-phenylindole-staining; *B* and *D*, TUNEL assay.

5% nonfat dry milk and 0.1% Tween 20 in Tris-buffered saline, they were incubated at room temperature for 2 h with a 1:400 dilution of a rabbit polyclonal anti-cyclin A antibody (Santa Cruz Biotechnology, Santa Cruz, CA), then with an antirabbit peroxidase-conjugated secondary antibody (Amersham). The blot was finally probed by the ECL Western blotting detection system (Amersham). Equal loading of protein was confirmed by rabbit polyclonal cdk2 antibody (Santa Cruz Biotechnology; Fig. 1).

***In Situ* End Labeling of Fragmented DNA.** The chromatin in apoptotic cells is cleaved at internucleosomal sites. To detect this fragmented DNA, we performed the TUNEL assay, using the *In Situ* Cell Death Detection kit (Boehringer Mannheim). Paraffin-embedded sections (4 μm) were deparaffinized and then incubated with proteinase K (20 μg/ml) in PBS for 15 min at 25°C. Methanol containing 0.3% H_2O_2 was applied to neutralize endogenous peroxidase. The sections were incubated with Tdt enzyme in the presence of a nucleotide mixture. After washing in PBS, the sections were stained with 4′,6-diamidino-2-phenylindole.

Apoptosis was quantitated by determining the percentage of positively stained cells within a field at a magnification of ×400. At least 1000 tumor cells were counted from 10–20 randomly chosen fields per slides assayed, and the counts were averaged to obtain the AI. For every tumor, two slides were evaluated. The median AI of all tumors examined was 0.82% (Fig. 2).

Statistical Analysis. Fisher's exact test was used to examine possible correlations between IRR expression and expression of other receptors (PCR positive *versus* negative), histology (DSR *versus* SP-D/SP-U), AI [low (≤0.82%) *versus* high (>0.82%)], proliferation [low *versus* enhanced/high (high)], *MYCN* amplification *versus* nonamplification, *MYCN* expression [low (M/A ≤0.220) *versus* high (M/A >0.220)], and clinical data (Table 2). Reported *P*s are not corrected for multiple testing.

The 6-year survival probability data for IRR, IGF-1R, TrkA, and p75NTR expression and *MYCN* amplification/expression were evaluated by the Kaplan–Meier method, and differences between survival probability curves were calculated

Table 2 Investigated neuroblastoma patients ($n = 49$) arranged according to receptor RNA expression

				MYCN		RNA[g]						
Stage[a]	Age[b]	Death[c]	Survival[d]	Amp1[e]	RNA[f]	IRR	IGF-1R	p75NTR	TrkA	Cyclin A[h]	AI[i]	Histology[j]
1	0.20	−	72.93	1	−	−	−	−	−	++	Low	3
4s	0.36	−	94.12	1	−	−	−	−	−	ND[k]	ND	3
4s	0.30	−	38.61	1	−	−	+	+	−	ND	ND	2
1	4.36	−	69.46	1	+	−	+	+	+	ND	ND	2
1	9.47	−	68.01	1	−	−	−	+	+	ND	ND	1
1	17.85	−	32.97	1	−	+	−	−	−	−	Low	1
4s	7.56	−	78.77	1	−	+	−	−	+	+	Low	3
4s	0.79	−	66.10	1	+	+	+	−	−	−	Low	3
4s	1.29	+	17.42	10	+	+	+	+	+	ND	ND	3
4s	0.69	−	113.29	1	+	+	+	+	+	ND	ND	3
4s	2.74	−	92.50	1	+	+	+	+	+	ND	ND	3
4s	2.54	−	76.73	1	+	+	+	+	+	ND	ND	2
4s	2.05	−	108.04	1	−	+	+	+	+	−	Low	3
4s	6.99	−	76.33	1	+	+	+	+	+	+	Low	3
4s	9.04	−	35.90	1	+	+	+	+	+	+	ND	3
1	4.36	−	72.30	1	+	+	+	+	+	ND	ND	3
1	11.91	−	112.99	1	−	+	+	+	+	+	High	3
1	12.94	−	66.23	1	−	+	+	+	+	−	High	3
1	18.68	−	67.91	1	+	+	+	+	+	ND	ND	3
2	0.73	−	74.58	1	+	+	+	+	+	ND	ND	3
2	5.81	−	57.82	1	−	+	+	+	+	++	High	3
2	34.06	−	130.52	32	+	+	+	+	+	−	High	3
2	116.85	+	89.60	1	−	+	+	+	+	+	High	1
3	5.97	−	14.36	1	+	+	+	+	+	+	High	3
3	9.11	−	74.45	1	−	+	+	+	+	ND	ND	3
3	10.99	−	58.77	1	+	+	+	+	+	ND	ND	3
3	16.07	−	58.94	1	+	+	+	+	+	−	High	3
3	18.74	−	141.50	1	−	+	+	+	+	+	High	3
4	19.31	−	40.66	1	−	+	+	+	+	+	High	3
4	29.44	+	23.83	1	−	+	+	+	−	+	High	3
4	10.86	+	15.38	40	+	−	+	−	−	++	Low	3
4	12.61	+	39.30	15	+	−	+	−	−	++	Low	1
4	30.56	+	8.09	1	−	−	+	−	−	−	Low	1
4	66.73	+	40.16	1	−	−	+	−	−	+	Low	1
3	11.88	−	81.15	20	+	−	+	−	−	++	High	3
3	59.17	+	92.70	1	−	−	+	+	−	+	Low	1
2	31.68	−	108.64	1	−	−	+	+	−	−	Low	1
3	95.73	−	68.01	15	+	−	+	+	+	ND	ND	2
4	66.46	+	31.71	5	+	−	+	+	+	ND	ND	3
4	57.02	+	12.57	4	+	−	−	+	+	++	High	1
2	13.63	−	90.75	1	−	−	−	+	−	−	High	1
3	30.79	−	114.11	1	−	−	−	+	−	ND	High	1
4	20.16	+	6.50	8	−	−	−	+	−	ND	ND	3
4	30.66	+	21.75	30	+	−	−	+	−	ND	ND	3
4	131.64	+	24.59	1	+	−	−	+	−	−	Low	1
2	47.45	+	18.35	1	−	−	−	−	−	+	High	2
4	34.49	+	6.60	25	+	−	−	−	−	+	Low	2
4	60.19	+	35.77	1	−	−	−	−	−	−	Low	1
4	76.20	−	111.84	1	−	−	−	−	−	−	Low	3

[a] Stage of disease at diagnosis (according to INSS criteria).
[b] Age at diagnosis in months.
[c] +, dead; −, alive.
[d] Survival time in months.
[e] Genomic amplification status of *MYCN* (1, single copy per haploid genome; >1, amplified).
[f] MYCN RNA expression (for criteria see "Materials and Methods").
[g] Receptor RNA expression status.
[h] Expression of cyclin A as parameter for the proliferation rate.
[i] High >0.82%, low ≤0.82% TUNEL-positive cells.
[j] Histology (according to Shimada criteria) with 1 = DSR; 2 = SP-D; 3 = SP-U.
[k] ND, not determined.

Table 3 Six-year survival probabilities (in months) in 49 neuroblastoma patients depending on receptor expression and other variables

Variable	6-Year survival (%)	Survival time (months)		P^a
		Mean	95% confidence interval	
IRR				
Expression	91.8	124.6	108.0–142.3	
Nonexpression	49.7	65.3	46.9–83.7	0.003
TrkA				
Expression	88.5	121.2	102.9–139.4	
Nonexpression	46.6	64.5	45.1–83.8	0.017
p75NTR				
Expression	79.5	108.5	90.3–126.7	
Nonexpression	47.9	65.9	41.8–89.9	0.08
IGF-1R				
Expression	78.5	107.1	88.3–125.8	
Nonexpression	52.6	68.6	43.9–93.3	0.122
MYCN				
Single copy	83.5	114.6	98.4–130.8	
Amplification	27.3	49.3	19.5–79.2	<0.0001
MYCN				
Expression	65.1	92.5	71.1–113.9	
Nonexpression	75.5	104.2	83.0–125.3	0.6
Stage				
Localized (1, 2, 3)	95.7	123.1	105.1–141.1	
Metastatic (4)	12.2	35.0	17.6–52.4	<0.0001
Age at diagnosis				
<12 months	91.1	104.5	92.8–116.1	
>12 months	52.8	78.6	56.2–100.9	0.003
Histology				
DSR or SP-D	53.6	68.0	46.9–89.0	
SP-U	79.6	116.4	98.4–134.3	0.041

[a] Log-rank test.

using the log-rank test (Table 3). Multivariate analysis of IRR expression with respect to MYCN amplification, stage, age at diagnosis, *MYCN* amplification, MYCN expression, expression of other RTKs, and histology was calculated using Cox regression analyses (Table 4). $P < 0.05$ was regarded as significant. Statistical analyses was performed with the SPSS version 10.0 software (SPSS Inc.).

RESULTS

Representative experimental results are shown in Figs. 1 and 2 for the detection of *MYCN* amplification by Southern blot (Fig. 1*A*), RNA expression by reverse transcription-PCR (Fig. 1*B*), cyclin A expression by Western blot (Fig. 1*C*), and the TUNEL assay (Fig. 2) to determine the AI.

IRR Is Predominantly Expressed in Localized and Stage 4S Neuroblastomas. IRR mRNA expression was found in 25 of 49 (51%) primary human neuroblastomas. IRR was expressed in 63% of stage 1, 57% of stage 2, 56% of stage 3, and only 14% of the metastatic disease stage 4 neuroblastomas, but in 82% of disseminated stage 4S neuroblastomas.

Comparison of stages 1, 2, and 3 with stage 4 or stages 1, 2, and 4S with stages 3 and 4 IRR revealed that expression was significantly correlated with stages 1, 2, and 3 ($P = 0.016$) and stages 1, 2, and 4S ($P = 0.002$; Fig. 3).

IRR expression was seen in 70% of neuroblastomas diagnosed in infancy, but in only 35% of tumors diagnosed after the first year of life ($P = 0.022$).

IRR Is Significantly Coexpressed with IGF-1R, TrkA, and p75NTR in Human Neuroblastomas. We found a statistically significant coexpression of IRR with IGF-1R ($P < 0.001$), TrkA ($P < 0.001$), and p75NTR ($P = 0.013$; Table 2).

IGF-1R expression was found in 69% of the investigated neuroblastoma tumors, expression of TrkA in 53%, and expression of p75NTR in 71%, respectively. Similar to the IRR, TrkA was significantly correlated with an age of ≤12 month at diagnosis ($P = 0.021$). There was a trend for preferential expression of the IGF-1R in infants compared with older patients ($P = 0.071$), but p75NTR was not expressed in an age-dependent manner ($P = 0.761$).

IRR Expression Is Correlated with an Undifferentiated Histology. IRR expression was correlated with an undifferentiated histology ($P = 0.0036$), as was TrkA ($P = 0.022$). In contrast to these findings, expression of IGF-1R and p75NTR was not associated with an undifferentiated histology. As expected, deduced from the already known functions of p75NTR, expression of this receptor was correlated with a high AI ($P = 0.003$) as was coexpressed TrkA ($P = 0.003$) but not IRR or IGF-1R. Surprisingly, there was no significant correlation between expression of any of the receptors studied and the proliferation rate.

Coexpression of IRR and IGF-1R Is Correlated with an Undifferentiated Histology and a High AI. In the subgroup of IGF-1R-expressing tumors ($n = 34$), IRR coexpression was significantly associated with an undifferentiated histology ($P = 0.0017$) and a high AI ($P = 0.017$). There was no correlation of IRR/IGF-1R coexpression with the proliferation rate (Fig. 4).

IRR Expression Is Correlated with High *MYCN* Expression in *MYCN*-Nonamplified Neuroblastomas. IRR was expressed in 61% of neuroblastomas without *MYCN* amplification, but in only 18% of *MYCN*-amplified neuroblastomas ($P = 0.018$). In neuroblastomas without *MYCN* amplification, IRR expression was correlated with high *MYCN* expression ($P = 0.02$).

IRR Expression and Prognosis. IRR mRNA expression is a new prognostic marker in neuroblastoma. A 6-year survival probability of 91.8% was seen in neuroblastoma patients with IRR expression in the tumor as compared with 49.7% in patients without IRR expression in the tumor ($P = 0.003$; Table 3; Fig. 5). In a multivariate Cox regression analysis, the prognostic

Table 4 Multivariate Cox regression analysis for IRR expression with respect to different second variables

First variable	Second variable	P^a
IRR expression	Stage (1, 2, 3, *vs.* 4)	0.256
	Age at diagnosis (>12 *vs.* ≤12 month)	0.045
	Histology	0.014
	MYCN amplification	0.037
	MYCN expression	(0.005)
	IGF-1R expression	(0.014)
	TrkA expression	0.147
	p75NTR expression	(0.018)

[a] *P* in parentheses for variables without own prognostic impact.

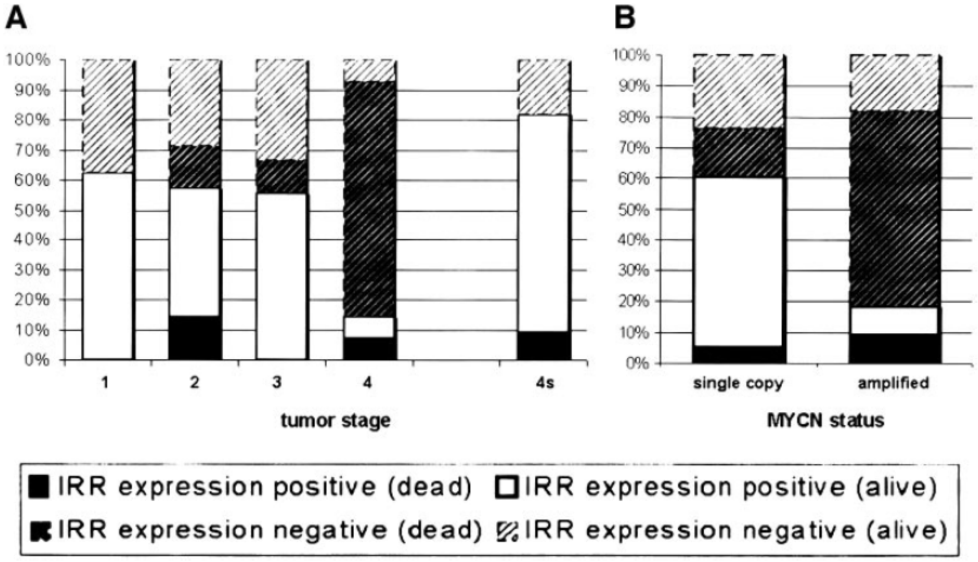

Fig. 3 IRR expression (positive) or nonexpression (negative) according to tumor stage (*A*) and MYCN status (nonamplified *versus* amplified; *B*), further differentiated by outcome (dead or still alive at the writing of the report).

impact of IRR expression was independent of *MYCN* amplification ($P = 0.037$), age at diagnosis (older than 12 months *versus* 12 months or younger; $P = 0.045$) and histological differentiation (DSR and SP-D *versus* SP-U; $P = 0.014$), but it was not independent of stage (1, 2, and 3 *versus* 4; Table 4).

Because the IRR is a heterodimerization partner for IGF-1R, we were interested in the prognostic value of IRR expression in the subgroup of IGF-1R-expressing tumors ($n = 34$). In this subgroup we found a 6-year survival probability of 90.9% for tumors that coexpressed IRR/IGF-1R-*versus* 51.9% in tumors expressing only IGF-1R ($P = 0.0108$; Fig. 5). In multivariate analysis, IRR expression was prognostically independent of IGF-1R expression ($P = 0.014$; Table 4). However, we found no correlation with apoptosis, proliferation, and differentiation for IRR expression in the subgroup of IGF-1R-nonexpressing tumors.

Prognostic Relevance of TrkA, p75NTR, and IGF-1R. TrkA expression was of prognostic significance, and p75NTR approached significance in the 49 neuroblastomas investigated in the present study ($P = 0.017$ and 0.08, respectively). IGF-1R expression was not of prognostic significance ($P = 0.122$; Table 3).

***MYCN* Gene Amplification and MYCN mRNA Expression.** The *MYCN* gene was amplified in 11 (22%) of 49 investigated neuroblastomas. MYCN mRNA expression was strongly correlated with *MYCN* amplification; thus, 10 (91%) of the 11 neuroblastomas with *MYCN* gene amplification but only 14 (37%) of 38 tumors without *MYCN* gene amplification expressed MYCN mRNA at a high level ($P = 0.002$). *MYCN* amplification significantly differentiates an unfavorable prognostic subgroup in this study ($P < 0.0001$). Expression of MYCN RNA was of no prognostic relevance in the group of 49 neuroblastomas ($P = 0.6$).

DISCUSSION

IGFs and their receptors regulate cell proliferation, differentiation, and death of normal and neoplastic cells. They have

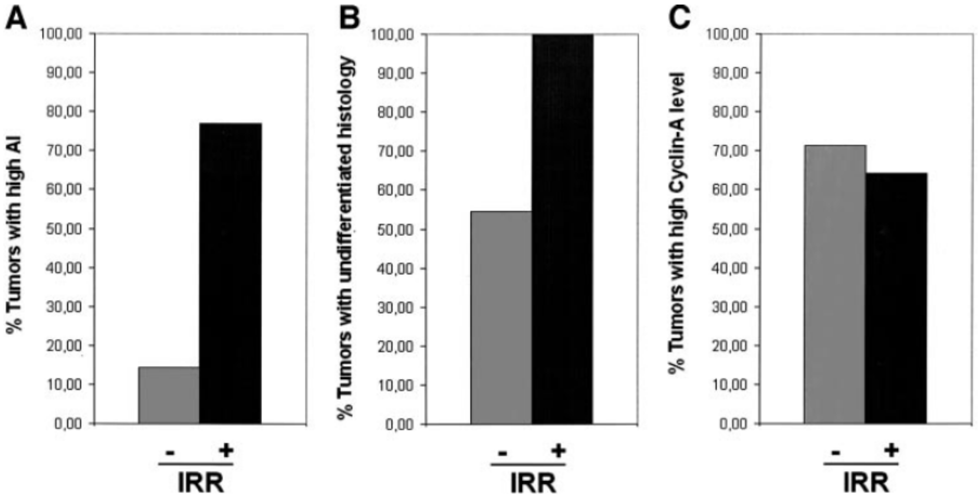

Fig. 4 Subgroups of the IGF-1R-expressing tumors ($n = 34$). IGF-1R/IRR coexpression is associated with a high AI (*A*; $P = 0.0017$) and an undifferentiated histology (*B*; $P = 0.017$). *C*, differences according to expression of the proliferation marker cyclin A are not statistically significant.

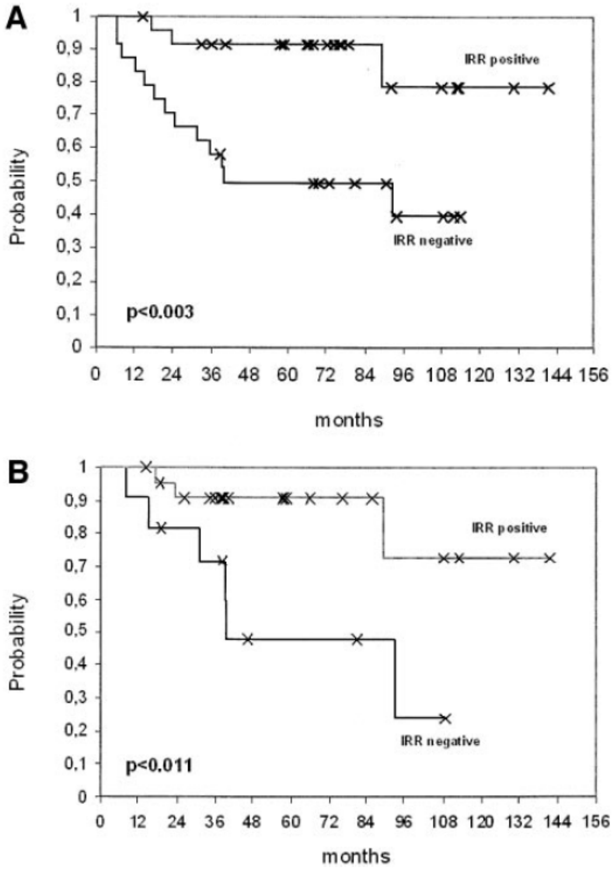

Fig. 5 *A*, Kaplan–Meier analysis for all investigated patients (n = 49). Survival probability of patients with IRR-expressing neuroblastomas (n = 25) *versus* IRR-nonexpressing neuroblastomas (n = 24). *B*, Kaplan–Meier analysis for patients with IGF-1R-expressing neuroblastomas (n = 34). Survival probability of patients with IRR coexpression (n = 23) *versus* IRR-noncoexpressing neuroblastomas (n = 11).

been implicated in the development of the nervous system and in the pathology of neuroblastoma (32, 33). Our study indicates that IRR, a new member of the IR-/IGF receptor family is differentially expressed in primary human neuroblastomas, which is suggestive for a role of the IRR in neuroblastoma biology. We also examined the expression pattern of IGF-1R, TrkA, and p75NTR, which have been previously shown to be expressed in neuroblastoma cells, to investigate the possible interaction of these receptors in concert with IRR on biological effects as proliferation, apoptosis, and differentiation.

Expression of IRR Is a New Prognostic Marker in Neuroblastoma. In the present study, IRR mRNA expression strongly correlated with a favorable outcome in neuroblastoma, which can be attributed to the close association of IRR expression with favorable tumor stages and a predominant expression in neuroblastomas diagnosed in infancy. Expression of TrkA also correlated significantly with a favorable prognosis, whereas expression of p75NTR and IGF-1R showed only a statistical trend toward a better survival probability (Table 3).

In multivariate analysis, the prognostic impact of IRR expression was statistically independent of *MYCN* amplification status and age at diagnosis, but not independent of tumor stage (Table 4).

Independency of *MYCN* amplification and age makes IRR expression interesting for further therapy stratification because at present, in stage 1, 2, 3, and 4S disease, age and *MYCN* amplification are the most commonly used parameters for stratification.

Role of IRR in Neuroblastoma Biology. Dimerization of receptor monomers at the cell surface was shown to be one early event in the activation of the RTKs, leading to autophosphorylation of intracellular domains and further activation of signaling cascades. Physiologically, dimerization is initiated by ligand binding but also by overexpression of receptor monomers exceeding a specific cell surface density threshold for autodimerization (34). We therefore examined the expression pattern of the investigated RTKs themselves and in combination with potential heterodimerization partners that might be important with respect to biological functions. Receptor expression was further compared with proliferation rate (examined by cyclin A protein expression), apoptosis (examined by the TUNEL assay), and morphological differentiation (examined by histology). We showed that IRR expression was strongly correlated with neuroblastomas with an undifferentiated histology, independent of AI and proliferation rate.

Known biological effects of IGF-1R expression in neuroblastoma cells include the induction of proliferation and downregulation of apoptosis (35–38). In contrast to these functions of IGF-1R, the expression pattern of this receptor was not associated with differentiation, proliferation rate, or apoptosis in tumor cells of primary neuroblastomas of our cohort. Missing associations between IGF-1R expression and biological functions might in part be explained by coexpression of IRR and IGF-1R. Recently, Kovacina and Roth (24) showed that these two receptors, when coexpressed, form heterodimeric receptors composed of an $\alpha\beta$-subunit of IGF-1R and another $\alpha\beta$-subunit of IRR and that these heterodimeric receptors are functional RTKs. Our correlative observations of enhanced apoptosis and undifferentiated histology in tumors expressing both receptors in contrast to tumors expressing only IGF-1R indicates an important role of IRR as a coexpression partner for IGF-1R in neuroblastoma cells. This observation is particularly important because an own ligand for IRR has to date not been found. Furthermore, the prognostic outcome of patients with IRR/IGF-1R coexpression was more favorable than that of patients expressing only IGF-1R (P = 0.018; Fig. 4).

In addition to IRR/IGF-1R coexpression, we found a significant coexpression of IRR and TrkA. In multivariate analysis, we showed a dependency of the prognostic impact of IRR expression on TrkA expression. This expression pattern has shown to be important for developing sympathetic and sensory neurons (20). Heterodimerization, however, has only been described for IGF-1R and not for TrkA (24).

Expression of the p75NTR was strongly correlated with a high AI but not to the proliferation rate and, in contrast to IRR, not to an undifferentiated histology; thus, it also exerts its function of inducing apoptosis in more differentiated neuroblastoma cells. Recently, it was shown that p75NTR as a member of the TNF receptor family induces apoptosis in neuroblastoma cells (39–41), which is in accordance with our results. The significant coexpression of p75NTR with the investigated RTKs might explain the correlative trend of RTK expression linked to a higher AI. These results are in accordance with the findings of Niesler *et al*. (14), who observed potentiation of TNF-induced apoptosis by activated IGF-1R.

IRR Is Expressed in Neuroblastomas without *MYCN* Amplification and High *MYCN* Expression. In the present study, *MYCN*-amplified neuroblastomas had higher median MYCN expression compared with neuroblastomas without *MYCN* amplification, which is in accordance with the published literature (4, 5). We found that IRR mRNA expression strongly correlated with neuroblastomas without *MYCN* amplification and that within *MYCN*-nonamplified tumors, IRR was associated with high MYCN expression. This is in accordance with the findings of Cohn *et al.* (6), who described a trend toward a better prognostic outcome for neuroblastomas diagnosed in infancy without *MYCN* amplification and higher MYCN mRNA expression. Finally, these data reflect the complexity of influences on cellular functions by MYC transcription factors, because forced expression of *MYC* oncogenes induces proliferation and prevents differentiation on the one hand, but induces apoptosis on the other (42). The low frequency of IRR expression in *MYCN*-amplified tumors might reflect the developmental stage from which these *MYCN*-amplified neuroblastoma cells are derived.

We conclude that IRR might have a role in the biology and pathogenesis of human neuroblastomas. In agreement with the current literature, we hypothesize that IRR might work as a regulatory partner of IGF-1R in IGF signaling. IRR influences the physiological development of the embryonal nervous system and thus might also play a role in tumorigenesis of malignancies originating from premature neuronal cells. Furthermore, our data indicate that the assessment of IRR expression in neuroblastoma tumors at the time of diagnosis provides confirmative prognostic information, which helps in determining the most appropriate duration and intensity of treatment. Future therapeutic approaches may be aimed at influencing IRR expression in human neuroblastomas and, thus, RTK signaling pathways contributing to the activation of apoptosis.

ACKNOWLEDGMENTS

We thank our colleagues from ~100 German pediatric centers for providing us with neuroblastoma tumor material since 1980. We are grateful to Prof. Dr. Fritz Lampert, former head of the Department of Pediatric Oncology at the Justus-Liebig University of Giessen, for support of our laboratory.

REFERENCES

1. Schwab, M., Alitalo, K., Klempnauer, K. H., Varmus, H. E., Bishop, J. M., Gilbert, F., Brodeur, G., Goldstein, M., and Trent, J. Amplified DNA with limited homology to myc cellular oncogene is shared by human neuroblastoma cell lines and a neuroblastoma tumour. Nature (Lond.), *305:* 245–248, 1983.

2. Brodeur, G. M., Seeger, R. C., Schwab, M., Varmus, H. E., and Bishop, J. M. Amplification of N-myc in untreated human neuroblastomas correlates with advanced disease stage. Science (Wash. DC), *224:* 1121–1124, 1984.

3. Brodeur, G. M., Maris, J. M., Yamashiro, D. J., Hogarty, M. D., and White, P. S. Biology and genetics of human neuroblastomas. J. Pediatr. Hematol. Oncol., *19:* 93–101, 1997.

4. Seeger, R. C., Wada, R., Brodeur, G. M., Moss, T. J., Bjork, R. L., Sousa, L., and Slamon, D. J. Expression of N-myc by neuroblastomas with one or multiple copies of the oncogene. Prog. Clin. Biol. Res., *271:* 41–49, 1988.

5. Bordow, S. B., Norris, M. D., Haber, P. S., Marshall, G. M., and Haber, M. Prognostic significance of MYCN oncogene expression in childhood neuroblastoma. J. Clin. Oncol., *16:* 3286–3294, 1998.

6. Cohn, S. L., London, W. B., Huang, D., Katzenstein, H. M., Salwen, H. R., Reinhart, T., Madafiglio, J., Marshall, G. M., Norris, M. D., and Haber, M. MYCN expression is not prognostic of adverse outcome in advanced-stage neuroblastoma with nonamplified MYCN. J. Clin. Oncol., *18:* 3604–3613, 2000.

7. Nakagawara, A., Arima-Nakagawara, M., Scavarda, N. J., Azar, C. G., Cantor, A. B., and Brodeur, G. M. Association between high levels of expression of the trk gene and favorable outcome in human neuroblastoma. N. Engl. J. Med., *328:* 847–854, 1993.

8. Christiansen, H., Christiansen, N. M., Wagner, F., Altmannsberger, M., and Lampert. F. Neuroblastoma: inverse relationship between expression of N-myc and NGF-r. Oncogene, *5:* 437–440, 1990.

9. Christiansen, N. M., Christiansen, H., Berthold, F., and Lampert, F. Transcriptional activity of N-myc and ngf-r in 50 primary human neuroblastomas as predictor for clinical outcome. Int. J. Oncol., *3:* 853–857, 1993.

10. Kogner, P., Barbany, G., Dominici, C., Castello, M. A., Raschella, G., and Persson, H. Coexpression of messenger RNA for TRK protooncogene and low affinity nerve growth factor receptor in neuroblastoma with favorable prognosis. Cancer Res., *53:* 2044–2050, 1993.

11. Surmacz, E. Function of the IGF-I receptor in breast cancer. J. Mammary Gland Biol. Neoplasia, *5:* 95–105, 2000.

12. Chakravarti, A., Loeffler, J. S., and Dyson, N. J. Insulin-like growth factor receptor I mediates resistance to anti-epidermal growth factor receptor therapy in primary human glioblastoma cells through continued activation of phosphoinositide 3-kinase signaling. Cancer Res., *62:* 200–207, 2002.

13. El-Brady, O., Romanus, J. A., Helman, L. J., Cooper, M. J., Rechler, M. M., and Israel, M. A. Autonomous growth of a human neuroblastoma line mediated by insulin-like growth factor II. J. Clin. Investig., *84:* 829–839, 1989.

14. Niesler, C. U., Urso, B., Prins, J. B., and Siddle, K. IGF-I inhibits apoptosis induced by serum withdrawal, but potentiates TNF-α-induced apoptosis, in 3T3–L1 preadipocytes. J. Endocrinol., *167:* 165–174, 2000.

15. Shier, P., and Watt, V. M. Primary structure of a putative receptor for a ligand of the insulin family. J. Biol. Chem., *264:* 14605–14608, 1989.

16. Hänze, J., Berthold, A., Klammt, J., Gallaher, B., Siebler, T., Kratzsch, J., Elmlinger, M., and Kiess, W. Cloning and sequencing of the complete cDNA encoding the human insulin receptor-related receptor. Horm. Metab. Res., *31:* 77–79, 1999.

17. Zhang, B., and Roth, R. A. The insulin receptor-related receptor. Tissue expression, ligand binding specificity, and signaling capabilities. J. Biol. Chem., *267:* 18320–18328, 1992.

18. Jui, H. Y., Suzuki, Y., Accili, D., and Taylor, S. I. Expression of a cDNA encoding the human insulin receptor-related receptor. J. Biol. Chem., *269:* 22446–22452, 1994.

19. Reinhardt, R. R., Chin, E., Zhang, B., Roth, R. A., and Bondy, C. A. Insulin receptor-related receptor messenger ribonucleic acid is focally expressed in sympathetic and sensory neurons and renal distal tubule cells. Endocrinology, *133:* 3–10, 1993.

20. Reinhardt, R. R., Chin, E., Zhang, B., Roth, R. A., and Bondy, C. A. Selective coexpression of insulin receptor-related receptor (IRR) and TRK in NGF-sensitive neurons. J. Neurosci., *14:* 4674–4683, 1994.

21. Tsuji, N., Tsujimoto, K., Takada, N., Ozaki, K., Ohta, M., and Itoh, N. Expression of insulin receptor-related receptor in the rat brain examined by *in situ* hybridization and immunohistochemistry. Brain Res. Mol. Brain Res., *41:* 250–258, 1996.

22. Elmlinger, M. W., Rauschnabel, U., Koscielniak, E., Haenze, J., Ranke, M. B., Berthold, A., Klammt, J., and Kiess, W. Correlation of type I insulin-like growth factor receptor (IGF-IR) and insulin receptor-

related receptor (IRR) messenger RNA levels in tumor cell lines from pediatric tumors of neuronal origin. Regul. Pept., *84:* 37–42, 1999.

23. Moxham, C. P., and Jacobs, S. Insulin/IGF-I receptor hybrids: a mechanism for increasing receptor diversity. J. Cell. Biochem., *48:* 136–140, 1992.

24. Kovacina, K. S., and Roth, R. A. Characterization of the endogenous insulin receptor-related receptor in neuroblastomas. J. Biol. Chem., *270:* 1881–1887, 1995.

25. Soos, M. A., Whittaker, J., Lammers, R., Ullrich, A., and Siddle, K. Receptors for insulin and insulin-like growth factor-I can form hybrid dimers. Characterisation of hybrid receptors in transfected cells. Biochem. J., *270:* 383–390, 1990.

26. Seely, B. L., Reichart, D. R., Takata, Y., Yip, C., and Olefsky, J. M. A functional assessment of insulin/insulin-like growth factor-I hybrid receptors. Endocrinology, *136:* 1635–1641, 1995.

27. Brodeur, G. M., Pritchard, J., Berthold, F., Carlsen, N. L. T., Castel, V., Castleberry, R. P., De Bernardi, B., Evans, A. E., Favrot, M., Hedborg, F., Kaneko, M., Kemshead, J., Lampert, F., Lee, R. E. J., Look, A. T., Pearson, A. D. J., Philip, T., Roald, B., Sawada, T., Seeger, R. C., Tsuchida, Y., and Voute, P. A. Revisions of the international criteria for neuroblastoma diagnosis, staging, and response to treatment. J. Clin. Oncol., *11:* 1466–1477, 1993.

28. Shimada, H., Chatten, J., Newton, W. A., Sachs, N., Hamoudi, B., Chiba, T., Marsden, H. B., and Misugi, K. Histopathologic prognostic factors in neuroblastic tumors: Definition of subtypes of ganglioneuroblastoma and an age-linked classification of neuroblastomas. J. Natl. Cancer Inst. (Bethesda), *73:* 405–416, 1984.

29. Berthold, F., and Hero, B. Neuroblastoma: current drug recommendations as part of the total treatment approach. Drugs, *59:* 1261–1277, 2000.

30. Chomczynski, P., and Sacchi, N. Single-step method of RNA isolation by acid guanidinium thiocyanate-phenol-chloroform extraction. Anal. Biochem., *162:* 156–159, 1987.

31. Kinoshita, T., Imamura, J., Nagai, H., and Shimotohno, K. Quantification of gene expression over a wide range by the polymerase chain reaction. Anal. Biochem., *206:* 231–235, 1992.

32. Ishii, D. N. Neurobiology of insulin and insulin-like growth factors. *In:* S. E. Loughlin and J. H. Fallon (eds.), Neurotrophic Factors, pp. 415–442. San Diego: Academic Press, 1993.

33. Kiess, W., Koepf, G., Christiansen, H., and Blum, W. F. Human neuroblastoma cells use either insulin-like growth factor-I or insulin-like growth factor-II in an autocrine pathway via the IGF-I receptor. Regul. Pept., *72:* 19–29, 1997.

34. Hempstead, B. L., Rabin, S. J., Kaplan, L., Reid, S., Parada, L. F., and Kaplan, D. R. Overexpression of the trk tyrosine kinase rapidly accelerates nerve growth factor-induced differentiation. Neuron, *9:* 883–896, 1992.

35. Peruzzi, F., Prisco, M., Dews, M., Salomoni, P., Grassilli, E., Romano, G., Calabretta, B., and Baserga, R. Multiple signaling pathways of the insulin-like growth factor 1 receptor in protection from apoptosis. Mol. Cell. Biol., *19:* 7203–7215, 1999.

36. Kurihara, S., Hakuno, F., and Takahashi, S. Insulin-like growth factor-I-dependent signal transduction pathways leading to the induction of cell growth and differentiation of human neuroblastoma cell line SH-SY5Y: the roles of MAP kinase pathway and PI 3-kinase pathway. Endocr. J., *47:* 739–751, 2000.

37. Macaulay, V. M. Insulin-like growth factors and cancer. Br. J. Cancer, *65:* 311–320, 1992.

38. Singleton, J. R., Randolph, A. E., and Feldman, E. L. Insulin-like growth factor I receptor prevents apoptosis and enhances neuroblastoma tumorigenesis. Cancer Res., *56:* 4522–4529, 1996.

39. Bunone, G., Mariotti, A., Compagni, A., Morandi, E., and Della Valle, G. Induction of apoptosis by p75 neurotrophin receptor in human neuroblastoma cells. Oncogene, *14:* 1463–1470, 1997.

40. Kuner, P., and Hertel, C. NGF induces apoptosis in a human neuroblastoma cell line expressing the neurotrophin receptor p75NTR. J. Neurosci. Res., *54:* 465–474, 1998.

41. Bono, F., Lamarche, I., Bornia, J., Savi, P., Della Valle, G., and Herbert, J. M. Nerve growth factor (NGF) exerts its pro-apoptotic effect via the p75NTR receptor in a cell cycle-dependent manner. FEBS Lett., *457:* 93–97, 1999.

42. Bouchard, C., Staller, P., and Eilers, M. Control of cell proliferation by myc. Trends Cell Biol., *8:* 202–206, 1998.

2.2 Funktionelle Untersuchung von differentiell expremierten Genen

Hintergrund:
Die Korrelation von Genexpressionsdaten mit klinischen Parametern lässt eine Hypothesenbildung über funktionelle Zusammenhänge zu, die sich jedoch nicht immer experimentell bestätigen lassen. Ob zum Beispiel die Korrelation eines oder mehrerer Gene aus einem Signalweg mit einer schlechten Prognose dadurch zustande kommt, dass durch diesen Signalweg direkt das Zellwachstum einer onkologischen Erkrankung beeinflusst wird, oder lediglich ein statistischer Zusammenhang besteht, ist ohne funktionelle Untersuchungen in Zellkultur (z.B. an Tumorzelllinien) oder in Tiermodellen (z.B. Maus Tumor-Xenograft Modell) nicht möglich.

In einer Genexpressionsuntersuchung primärer Neuroblastome konnte neben vielen anderen differentiell expremierten Genen auch ein bis dahin noch nicht funktionell beschriebenes Gen, KIAA1538 als in gut prognostischen Neuroblastomen hoch expremiert beschrieben werden (*Berwanger et al., 2002)*. In Datenbankrecherchen, basierend auf der Nukleotidsequenz des KIAA1538 Genes, stellte sich heraus, dass es sich bei dem Genprodukt um einen Transkriptionsfaktor der BTB-POZ Familie handelte. Wir konnten das Gen anschließend erfolgreich aus einer Fetal-Brain-mRNA Library klonieren und sequenzieren. (Die Sequenz ist unter der Accession Nummer: **AY302699** in der NCBI Datenbank veröffentlicht.) Aufgrund der Sequenz-Homologie zu dem Transkriptionsfaktor Kaiso nannten wir das Gen Kaiso-like-1 (KL1). In der offiziellen Nomenklatur ist das Gen unter der Bezeichnung Zbtb4 (Zinc-Finger and BTB-Poz Domain containing Protein 4) geführt. Nach der Klonierung von Zbtb4 erfolgte die funktionelle Untersuchung in verschiedenen Zellkulturexperimenten.

Eigene Publikationen:

Weber A, Marquardt J, Elzi D, Forster N, Starke S, Glaum A, Yamada D, Defossez PA, Delrow J, Eisenman RN, Christiansen H, Eilers M. Zbtb4 represses transcription of P21CIP1 and controls the cellular response to p53 activation. *EMBO J.* 2008 Jun 4;27(11):1563-74. Epub 2008 May 1.

IF (Stand 2010): 8,99

In der zitierten Genexpressionsanalyse, basierend auf einer Microarrayuntersuchung, konnte eine hohe Zbtb4 Expression vor allem in Neuroblastomen des Stadium 1 und in Neuroblastomen ohne Amplifikation von *MYCN* gefunden werden (*Berwanger et al., 2002*). In einer unabhängigen Gruppe primärer Neuroblastome konnten wir mittels RT-PCR-Untersuchung diese Korrelation bestätigen. Mit dieser Korrelation erklärt sich auch die prognostische Aussagekraft der Zbtb4 Expression in einer Kaplan-Meier Überlebensanalyse, die zwar ein statistisch signifikant besseres Überleben für Patienten zeigt, in deren Neuroblastomen Zbtb4 hoch expremiert wir. Dies ist jedoch nicht unabhängig von den anderen prognostischen Faktoren zu werten. Interessanter Weise ist eine hohe Zbtb4 Expression auch in niedrigen Stadien anderer Malignome zu finden, während in hohen Stadien die Zbtb4 Expression herunter reguliert zu sein scheint.

Fortgeschrittene Tumorstadien gehen häufig mit einer relativ erhöhten Resistenz gegenüber Chemotherapeutika einher. In Zellkulturversuchen konnten wir zeigen, dass Neuroblastomzellen, in denen mittels sh-RNA Zbtb4 herunter reguliert wurde eine selektiv erhöhte Resistenz gegenüber Vincristin aufweisen. In den untersuchten Konzentrationen wirkt Vincristin allerdings noch nicht über eine Hemmung der Mikrotubuliarchitektur der Zellen, sondern über eine Aktivierung von p53, das zum Teil an Zytoskelettstrukturen gebunden und damit inaktiv vorliegt. Aus dieser Bindung wird p53 durch niedrig dosiertes Vincristin gelöst und dadurch aktiviert (*Giannakakou et al., 2008*). Durch die Aktivierung von p53 werden zwei hauptsächliche Signalwege vermittelt. Über p21 erhalten die Zellen ein antiproliferatives Signal und können in einen G1-Arrest gehen. Des Weiteren kann über proapoptotische p53-Target Gene (z.B. Puma und Noxa) Apoptose induziert werden. Dabei hängt die Effektivität des Apoptosesignales maßgeblich von der p21 Expression und dem dadurch vermittelten Zellzklusarrest ab. Höhere p21 Level wirken dabei protektiv gegenüber den proapoptotischen Signalen (*Seoane et al., 2002*). In weiteren Versuchen konnten wir zeigen, dass die Expression von p21 direkt von Zbtb4 transkriptionell gehemmt wird. Eine Aktivierung von p53 kann so zu einer vermehrten Apoptose führen.

Letztlich müssen jedoch noch weitere Faktoren eine Rolle bei der p53 Antwort der Neuroblastomzellen eine Rolle spielen, da ja p53 auch von anderen Zytostatika aktiviert wird (z.B. nach Induktion von DNA Doppelstrangbrüchen), die p21 Regulation durch Zbtb4 hier jedoch eine untergeordnete Rolle zu spielen scheint.

Die transkriptionelle Repression des p21 Promotors konnten wir mittels Chromatinimmunoprezipitations-Experimente (ChIP) nachweisen. Dabei ist Zbt4 Teil eines transkriptionellen Repressorkomplexes und bindet unter anderem Miz1 und Sin3a. Dieser Komplex wiederum kann Histondeacetylasen (HDAC) binden und dadurch Promotoren transkriptionell inhibieren.

In dieser Arbeit konnten wir zum ersten Mal einen funktionellen Nachweis erbringen, der die prognostische Bedeutung der Expression von Zbtb4 in humanen Neuroblastomen zumindest teilweise erklären kann.

Ferrandiz N, Martin-Perez J, Blanco R, Donertas D, **Weber A**, Eilers M, Dotto P,Delgado MD, Leon J. HCT116 cells deficient in p21(Waf1) are hypersensitive to tyrosine kinase inhibitors and adriamycin through a mechanism unrelated to p21 and dependent on p53. *DNA Repair* (Amst). 2009 Mar 1;8(3):390-9.

IF (Stand 2010): 4,199

In dieser Arbeit konnte gezeigt werden, dass der CDK Inhibitor p21 in Kolon-Karzinom Zellen keinen direkten Einfluss auf die Sensitivität der untersuchten Zelllinie gegenüber den eingesetzten Kinaseinhibitoren hat. Obwohl eine p21 defiziente Zelllinie (HCT116-p21$^{-/-}$) gegenüber den wildtyp-Zellen eine höhere Sensitivität gegenüber den Kinase Inibitoren aufweist, kann eine Rekonstitution der p21 Expression diese nicht rückgängig machen. Gegenüber dem totalen Knockout von p21 (p21-/-) führt ein vorübergehender Knockdown von p21 durch sh-RNA in wildtyp-HCT116 Zellen nicht zu einem vergleichbaren Phänotyp. Aus diesen Daten folgert, dass neben dem völligen Fehlen von p21 in diesen Zellen weitere Faktoren, zum Beispiel eine erhöhte Stabilisierung von p53 über Abl-Kinasen, für die Medikamentensensitivität eine übergeordnetere Rolle spielen müssen. Dies zeigt sich in der Tatsache, dass im Gegensatz zu einer p21 Überexpression in den p21$^{-/-}$ Zellen eine p53 Herabregulation die Hypersensitivität gegenüber den Kinaseinhibitoren deutlich reduzieren kann.

The EMBO Journal (2008) 27, 1563–1574 | © 2008 European Molecular Biology Organization | All Rights Reserved 0261-4189/08
www.embojournal.org

THE
EMBO
JOURNAL

Zbtb4 represses transcription of *P21CIP1* and controls the cellular response to p53 activation

Axel Weber[1,2,5], Judith Marquardt[1,5], David Elzi[3,5], Nicole Forster[1,5], Sven Starke[2], Andre Glaum[2], Daisuke Yamada[4], Pierre-Antoine Defossez[4], Jeffrey Delrow[3], Robert N Eisenman[3], Holger Christiansen[2] and Martin Eilers[1,*]

[1]Institute of Molecular Biology and Tumour Research (IMT), Marburg, Germany, [2]Center for Children's Medicine, University Hospital Marburg and Giessen, Marburg, Germany, [3]Division of Basic Sciences, Fred Hutchinson Cancer Research Center, Seattle, WA, USA and [4]CNRS UMR218, Institut Curie, Paris, France

In response to stimuli that activate p53, cells can undergo either apoptosis or cell cycle arrest, depending on the precise pattern of p53 target genes that is activated. We show here that Zbtb4, a transcriptional repressor protein, associates with the Sin3/histone deacetylase co-repressor and represses expression of *P21CIP1* as part of a heterodimeric complex with Miz1. *In vivo*, expression of *ZBTB4* is downregulated in advanced stages of multiple human tumours. In cell culture, depletion of *ZBTB4* promotes cell cycle arrest in response to activation of p53 and suppresses apoptosis through regulation of *P21CIP1*, thereby promoting long-term cell survival. Our data suggest that Zbtb4 is a critical determinant of the cellular response to p53 activation and reinforce the notion that p21Cip1 can provide an essential survival signal in cells with activated p53.

The EMBO Journal (2008) **27**, 1563–1574. doi:10.1038/emboj.2008.85; Published online 1 May 2008
Subject Categories: chromatin & transcription
Keywords: apoptosis; cell cycle arrest; Miz1; p21Cip1; p53

Introduction

The p53 tumour suppressor protein orchestrates a broad transcriptional programme in response to both physiological and environmental stress. Activation of p53 can result in either cell cycle arrest or apoptosis and this 'decision' is largely controlled by the exact pattern of p53 target genes that is regulated in response to a specific stimulus.

p53-induced cell cycle arrest is mediated by upregulation of *P21CIP1* which encodes an inhibitor of the Cdk2 kinase, and by suppression of cell cycle regulatory genes that include *CDC25C*, which encodes a phosphatase required for activation of Cdk1 (Vousden, 2006). p53-induced apoptosis is mediated by upregulation of a group of pro-apoptotic genes, most notably *NOXA* and *PUMA*. In addition, non-transcriptional functions of p53 at the mitochondrion have an essential pro-apoptotic function (Mihara *et al*, 2003). Importantly, induction of *P21CIP1* expression by p53 suppresses apoptosis in addition to inhibiting cell cycle progression (see Discussion). As a result, levels of p21Cip1 can be critical determinant of the outcome of p53 activation.

Several factors influence the choice of target genes that are induced in response to activation of p53 under specific circumstances (Vousden, 2006): the p53 protein itself integrates multiple signals that can favour either apoptosis or cell cycle arrest. For example, phosphorylation of serine residues 18 and 23 is required for induction of apoptosis in mice; similarly, phosphorylation of human p53 at residue 46 contributes specifically to activation of pro-apoptotic genes (Chao *et al*, 2006). Also, the ASPP proteins that bind to the p53 protein shift the transcriptional response towards the induction of pro-apoptotic genes and away from cell cycle arrest (Samuels-Lev *et al*, 2001). A second mechanism that allows for the specific regulation of individual p53 target genes is the combinatorial control of many targets of p53 together with other transcription factors. For example, induction of expression of the death receptor DR5 requires cooperation of p53 with NF-κB; also, the Slug repressor protein suppresses p53-dependent induction of *PUMA* in haematopoietic cells (Wu *et al*, 2005).

Conversely, induction of *P21CIP1* expression requires binding of Miz1 to the core *P21CIP1* promoter and, as a consequence, factors that control Miz1 can affect *P21CIP1* expression (Herold *et al*, 2002). One example of this is the Myc protein, which, when deregulated, represses p53-mediated induction of *P21CIP1* through binding to Miz1 and thereby favours apoptosis in response to p53 activation (Seoane *et al*, 2002). Re-expression of *P21CIP1* in Myc-transformed cells inhibits apoptosis and a point mutant of Myc that is unable to bind to Miz1 and therefore to repress *P21CIP1* is unable to induce apoptosis in human fibroblasts. This suggests that repression of *P21CIP1* can be essential for Myc-dependent apoptosis (Seoane *et al*, 2002).

At its amino-terminus, Miz1 contains a POZ protein–protein interaction domain, which can mediate both homo- and heterodimerization among POZ domain proteins. Miz1 heterodimerizes with Bcl-6 to suppress expression of *P21CIP1* during the class switching of immunoglobulin genes in B cells, when p53 is activated in response to the recombination events (Phan *et al*, 2005). We describe now a second POZ domain partner protein of Miz1, Zbtb4. Expression of *ZBTB4* is downregulated in advanced stages of human neuroblastoma and of multiple human solid tumours. Zbtb4 is a transcriptional repressor protein that heterodimerizes with Miz1, represses *P21CIP1* expression and inhibits cell cycle arrest in

---

*Corresponding author. Institute of Molecular Biology and Tumour Research, Phillips University Marburg, Universität Marburg, Emil-Mannkopff-Str. 2, Marburg 35033, Germany. Tel.: +49 6421 286 6410; Fax: +49 6421 286 5196; E-mail: eilers@imt.uni-marburg.de

[5]These authors contributed equally to this work

Received: 19 February 2008; accepted: 2 April 2008; published online: 1 May 2008

response to p53 activation. Conversely, loss of Zbtb4 inhibits apoptosis and favours cell cycle arrest and long-term survival in response to activation of p53. Our data suggest that the expression level of *ZBTB4* is an important determinant of the cellular response to p53 activation.

Results

Zbtb4 expression decreases in human tumours

In human neuroblastoma, advanced tumour stage and amplification of the *MYCN* gene are highly predictive for poor outcome. We have previously performed a microarray analysis of primary human neuroblastomas and identified expression signatures that are specific for individual tumour stages and for *MYCN*-amplified tumours (Berwanger *et al*, 2002). One of the genes that is downregulated in neuroblastomas with poor prognosis encodes Zbtb4, a POZ domain transcriptional repressor protein (Filion *et al*, 2006) (Figure 1A). To extend the microarray data, we measured expression of *ZBTB4* mRNA in 98 independent RNA samples of primary neuroblastomas and confirmed that *ZBTB4* is expressed in a stage-dependent manner, with expression being lowest in stage IV neuroblastoma ($P<0.01$) (Figure 1B). Expression levels of *ZBTB4* are inversely correlated with survival as seen in the Kaplan–Meier analysis (Figure 1C). As *ZBTB4* is expressed in a stage-dependent manner, expression levels of *ZBTB4* did not constitute an independent prognostic parameter in a multivariate analysis, which takes tumour stage into account (not shown).

Data obtained from a publicly available database of tumour expression profiles (www.oncomine.org) showed that downregulation of *ZBTB4* relative to normal tissue occurs in multiple human tumour entities, notably in breast, prostate and lung carcinoma and in glioblastoma (Figure 1D and Supplementary Table 1). In addition, *ZBTB4* is expressed in a stage-specific manner in glioblastoma and in breast, ovarian and prostate carcinoma, with expression being lowest in advanced tumour stages, similar to neuroblastoma (Figure 1E and Supplementary Table 2).

Biological effects of Zbtb4 downregulation

To understand how repression of Zbtb4 affects cell physiology, we used three distinct retroviral expression vectors that express a short hairpin RNA (shRNA) targeting *ZBTB4* (sh*ZBTB4-1,2,3*) or soluble siRNA oligonucleotides that target *ZBTB4* together with scrambled controls. RQ–PCR analysis showed that individual clones of SH-EP neuroblastoma cells stably infected with any of the three *shZBTB4* vectors had 2- to 3-fold lower levels of *ZBTB4* mRNA (Supplementary Figure 1A). Similarly, transfection of either SH-EP or SH-SY5Y

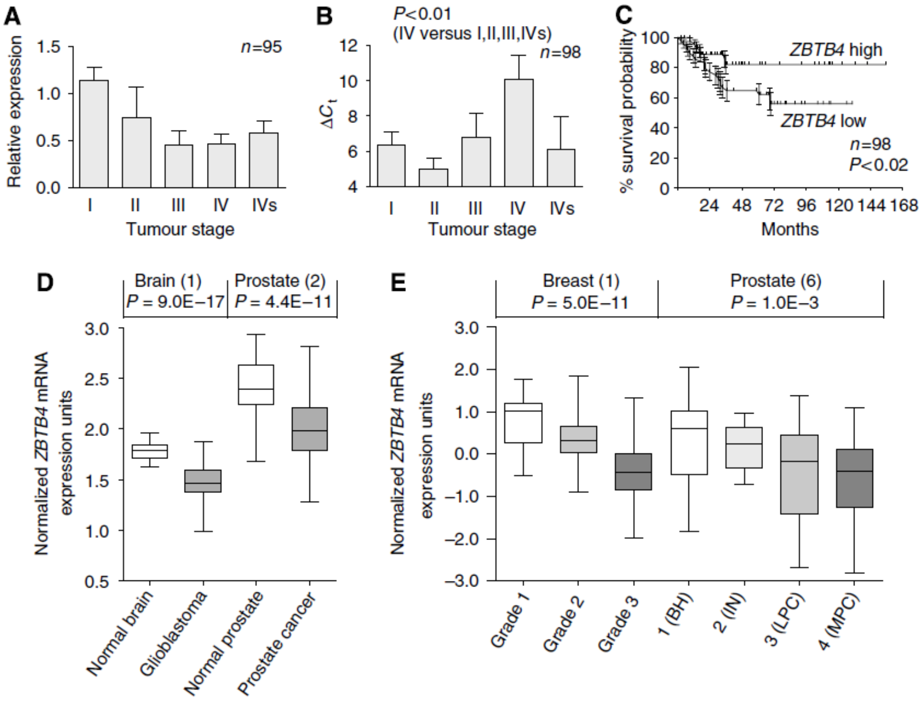

Figure 1 Expression of *ZBTB4* mRNA in human tumours. (**A**) *ZBTB4* is expressed in a stage-dependent manner in human neuroblastoma. The graph is a summary of microarray data of *ZBTB4* mRNA levels observed in different neuroblastoma tumour stages. The data are taken from the original analysis (Berwanger *et al*, 2002). Error bars represent standard error of the mean. (**B**) Confirmation of microarray data. The graph summarizes the RQ–PCR analysis of *ZBTB4* expression in an independent set of 98 primary neuroblastoma tumours. Error bars represent standard error of the mean. (**C**) Expression of *ZBTB4* correlates with patient survival. The graph documents the Kaplan–Meier analysis of neuroblastoma patients with *ZBTB4* mRNA expression levels above (‘high’) and below (‘low’) the mean expression level. (**D**) *ZBTB4* is repressed in glioblastoma and in prostate carcinoma relative to normal tissue. The data are taken from the studies summarized in Table 1, and were obtained from www.oncomine.org. The numbers refer to Table 1. In this and the following panel, data are presented as Box and Whisker graph with error bars representing the 5th and 95th percentile. (**E**) Stage-specific expression of *ZBTB4* in breast and prostate carcinoma. The data are taken from the studies summarized in Table 2. The plots are taken from www.oncomine.org (BH, benign hyperplasia; IN, intraepithelial hyperplasia; LPC, localized prostate carcinoma; MPC, prostate carcinoma metastasis).

neuroblastoma cells with soluble siRNAs targeting *ZBTB4* (si*ZBTB4*) reduced expression levels of *ZBTB4* approximately five-fold relative to control cells (Supplementary Figure 1B). Furthermore, expression of either of the sh*ZBTB4* vectors or transfection of si*ZBTB4* reduced expression levels of a HA-tagged Zbtb4 allele that was stably expressed in SH-EP cells (Supplementary Figure 1C).

Pools of SH-EP cells, which express sh*ZBTB4*, showed no significant change in the rate of proliferation relative to control cells under standard tissue culture conditions (Supplementary Figure 1D). Conversely, ectopic expression of Zbtb4 had little effect on cell growth at moderate expression levels and both stable cell clones and pools expressing moderately elevated levels of Zbtb4 could be established (data not shown and Figure 4). In contrast, expression of approximately 10-fold higher levels of Zbtb4 suppressed colony formation in several tumour cell lines and induced apoptosis, as revealed by the accumulation of cells with a subG1 ($<2n$) content of DNA (Supplementary Figure 1E).

To understand if downregulation of *ZBTB4* confers a selective advantage to tumour cells, we exposed SH-EP cells to a number of drugs that are used in the therapy of neuroblastoma patients, including cisplatin, etoposide, vincristine and retinoic acid (Estlin and Veal, 2003). All drugs suppressed colony formation of control SH-EP cells at the concentrations used in these experiments (Figure 2A). No difference was observed in the response of cells that stably express sh*ZBTB4* towards cisplatin, etoposide or retinoic acid (Figure 2A and data not shown). In contrast, cells expressing sh*ZBTB4* showed an enhanced long-term survival in response to vincristine (Figure 2A and Supplementary Figure 2A). This phenotype was observed in several cell clones with each of the three different shRNAs targeting *ZBTB4*, demonstrating that it did not reflect an off-target effect of an individual shRNA or an artefact due to the selection of an individual clone (Supplementary Figure 2A).

To demonstrate directly that depletion of *ZBTB4* provides a selective advantage in the presence of vincristine, we expressed sh*ZBTB4* together with a GFP marker in SH-EP cells (Figure 2B). The relative abundance of cells expressing either one of three sh*ZBTB4* vectors increased over time in the presence of vincristine relative to cells expressing a control shRNA or to cells expressing GFP alone. In contrast, Zbtb4-depleted cells had no survival advantage in the presence of DMSO, demonstrating that depletion of Zbtb4 provides a specific survival advantage in the presence of vincristine.

To understand the underlying mechanism, we performed FACScan experiments of SH-EP cells before and after addition of vincristine (Figure 2C and Supplementary Figure 2B). Vincristine induced apoptosis in control cells, as documented by the appearance of a cell population with a sub-G1 DNA content. In contrast, vincristine did not induce apoptosis in cells expressing any of the three sh*ZBTB4* vectors. Instead, over 80% of Zbtb4-depleted cells accumulated in the G1 phase of the cell cycle, demonstrating that vincristine induced a temporary arrest or delay in proliferation. To confirm these observations, we monitored cleavage of poly-ADP-ribose-polymerase (PARP), an early marker of apoptosis; consistent with the FACScan data, depletion of Zbtb4 reduced the extent of PARP cleavage in response to vincristine (Figure 2C). We concluded that depletion of Zbtb4 shifted the cellular response to vincristine from apoptosis to a temporary G1 arrest.

In contrast to etoposide or cisplatin, vincristine does not induce DNA damage but exerts its cytostatic effects through interaction with β-tubulin and interference with its function (Jordan *et al*, 1998) (see also Figure 4). At the low concentrations (5 nM) used in these experiments, vincristine does not disrupt the cytoskeleton but activates the tumour suppressor protein p53, potentially by facilitating its nuclear import, which depends on the microtubule-associated motor protein dynein (Giannakakou *et al*, 2000). Consistently, vincristine led to an accumulation of p53 and a p53-dependent induction of p21Cip1 protein expression as well as of *P21CIP1*, *NOXA* and *PUMA* mRNAs (Figure 3A and 5A). At higher concentrations (50 nM), vincristine disrupts the microtubular network, leading to a failure to execute mitosis (Jordan *et al*, 1998). Exposure of either control or Zbtb4-depleted cells to these elevated concentrations of vincristine suppressed colony formation (not shown) and led to an accumulation of cells with $4n$ DNA content, consistent with an arrest in mitosis (Figure 2C and Supplementary Figure 2B). We concluded that depletion of *ZBTB4* does not generally render cells resistant to vincristine, but selectively alters the response to low doses of the drug in the range predicated to activate p53.

Zbtb4 influences p53-mediated p21Cip1 expression

To understand how Zbtb4 shifts the response to vincristine from apoptosis to cell cycle arrest, we analysed how depletion of Zbtb4 affects the expression of a number of p53 target genes including *P21CIP1*, *NOXA* and *PUMA* (Figure 3B). There was no difference in the expression of the pro-apoptotic *BAX*, *PUMA* and *NOXA* between Zbtb4-depleted and control cells, either before treatment with vincristine (Figure 3B) or in response to treatment with the drug (not shown); similarly, the expression of two target genes of p53 that have been implicated in regulation of cell cycle progression, *14-3-3σ* and *BTG2*, was not consistently upregulated by depletion of Zbtb4 (Figure 3B). In contrast, both transient depletion of Zbtb4 using soluble siRNA (Figure 3B) and stable depletion using shRNAs (Figure 3C) led to an increase in expression of *P21CIP1* mRNA and p21Cip1 protein, both in untreated cells and after addition of vincristine (Supplementary Figure 3A). Conversely, stable expression of Zbtb4 from a retroviral vector reduced expression levels of *P21CIP1* mRNA, but had little or no effect on the levels of *PUMA* or *NOXA* mRNAs (Figure 3D and Supplementary Figure 3B). Furthermore, a microarray analysis of cells depleted of Zbtb4 confirmed that induction of *P21CIP1* mRNA was the strongest change in gene expression observed in such cells (Supplementary Figure 4). Taken together, we concluded that Zbtb4 represses transcription of *P21CIP1* both in unstressed cells and in response to vincristine.

To determine whether the enhanced expression levels of *P21CIP1* found in Zbtb4-depleted cells are causal for the resistance to vincristine, we depleted p21Cip1 using stable expression of shRNA in several clones of Zbtb4-depleted SH-EP cells (Figure 3E and Supplementary Figure 3C). Cells were exposed to vincristine and cell survival was measured after 72 h. In these experiments, three independent vectors targeting *P21CIP1* led to a moderate reduction in survival of control cells, and almost completely abolished the survival advantage of Zbtb4-depleted cells in the presence of vincristine. We concluded that depletion of Zbtb4 enhances survival

©2008 European Molecular Biology Organization

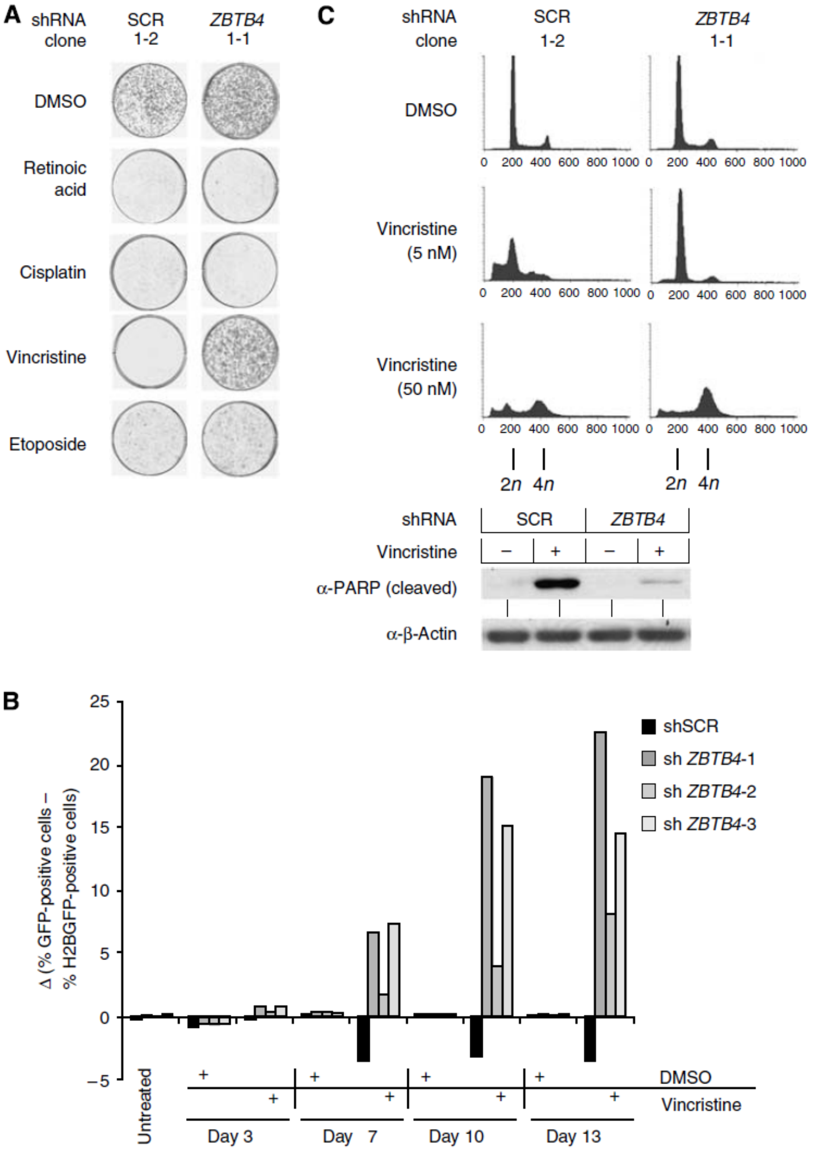

Figure 2 Depletion of Zbtb4 enables neuroblastoma cells to survive in the presence of vincristine. (**A**) Colony assays documenting growth of a control clone of SH-EP cells and a clone expressing the indicated sh*ZBTB4* RNA after treatment with the indicated chemotherapeutic agents. Control (DMSO treated) plates were stained at day 7 and experimental plates stained 14 days after plating. Note that the *ZBTB4* mRNA expression level of this clone is documented in Supplementary Figure 1A. (**B**) Cells expressing sh*ZBTB4* have a survival advantage in the presence of vincristine. SH-EP cells were infected with vectors that express GFP and either a control shRNA vector or one of three distinct sh*ZBTB4* RNAs as indicated. At the indicated time points after infection, the percentage of GFP-positive cells was measured by FACScan. All values were normalized to those obtained from a control plate expressing H2B-GFP. At the start of the experiment, approximately 10% of all cells were positive for GFP. (**C**) Vincristine induces apoptosis in control cells but G1 arrest in Zbtb4-depleted cells. The upper panels document FACS analyses of the DNA content of either a control clone or of a clone expressing sh*ZBTB4* after treatment with DMSO or the indicated concentrations of vincristine for 48 h. The lower panels show immunoblots using antibodies directed against cleaved poly-ADP-ribose-polymerase and β-actin as loading control.

of neuroblastoma cells in response to vincristine at least in part through upregulation of *P21CIP1*.

Induction of p21Cip1 mediates cell cycle arrest downstream of p53; to analyse whether Zbtb4 affects this arrest, we infected SH-EP neuroblastoma cells with control or retroviruses expressing HA-tagged Zbtb4 and treated both cell pools with nutlin, a small molecule inhibitor of the Hdm2 ubiquitin ligase (Vassilev *et al*, 2004). Immunoblots showed that p53 accumulated to a similar extent in both cell pools (Figure 4A). p21Cip1 accumulated in response to nutlin in control cells, but this induction was suppressed in cells expressing ectopic Zbtb4. FACScan analysis showed that SH-EP cells accumulated in the G1 phase of the cell cycle in response to exposure to nutlin for 33 h (Figure 4B); under these conditions, exposure to nutlin did not induce apoptosis (Figure 4B) and elicited only small increases in the levels of *PUMA* and *NOXA* mRNAs (not shown). In contrast to control cells, cells expressing Zbtb4 showed no change in the cell

©2008 European Molecular Biology Organization

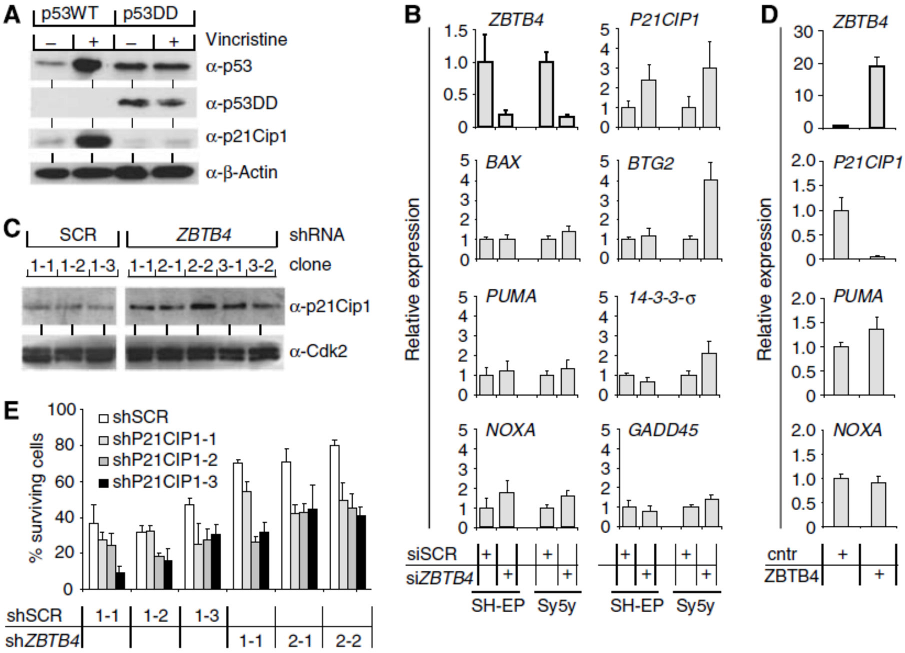

Figure 3 Depletion of Zbtb4 causes resistance to vincristine treatment through upregulation of *P21CIP1*. (**A**) Vincristine induces activation of p53. The panels show immunoblots of SH-EP cells infected with either a control vector (left) or a vector expressing a dominant-negative allele of p53 (p53DD; right) probed with the indicated antibodies. (**B**) Transient depletion of Zbtb4 upregulates *P21CIP1* mRNA levels. The panels document the RQ–PCR analysis of relative mRNA expression level of *ZBTB4*, *P21CIP1*, *14-3-3σ*, *BTG2*, *GADD45*, *PUMA*, *BAX* and *NOXA* in SH-EP and SH-SY5Y neuroblastoma cells transfected with either control or siRNA targeting *ZBTB4*. Cells were harvested 48 h after transfection and expression levels were determined by RQ–PCR. (**C**) Stable depletion of Zbtb4 upregulates p21Cip1 protein. The panels show immunoblots of p21Cip1 and Cdk2 protein levels in indicated SH-EP cell clones stably infected with either control vectors or vectors expressing sh*ZBTB4*. (**D**) Ectopic expression of Zbtb4 represses *P21CIP1*. The panels document the RQ–PCR analysis of the relative mRNA expression level of *ZBTB4*, *P21CIP1*, *PUMA* and *NOXA* in SH-EP cells stably infected with HA-tagged *ZBTB4* vector or a control vector. (**E**) *P21CIP1* is required for protection of SH-EP cells from vincristine-induced apoptosis by depletion of Zbtb4. The indicated SH-EP cell clones stably expressing either sh*ZBTB4* or control shRNA were transiently transfected with vectors expressing sh*P21CIP1* or a scrambled shRNA. At 48 h after transfection, cells were plated in triplicate for vincristine treatment. Cells were treated with either vincristine or DMSO for 3 days; subsequently, the relative cell number was determined. Error bars represent standard error of the mean.

cycle distribution in response to nutlin treatment (Figure 4B). Identical results were obtained after 50 h of treatment, after which the cells became confluent (not shown). Retroviral expression of *P21CIP1* partially restored G1 arrest in cells expressing Zbtb4 in response to nutlin, arguing that suppression of *P21CIP1* causally contributes to the failure of Zbtb4-expressing cells to arrest in response to nutlin (not shown).

We wondered how Zbtb4 affected the cellular response to DNA-damaging agents and exposed SH-EP cells to adriamycin, cisplatin or etoposide in addition to vincristine and nutlin. At the concentrations used, all drugs led to an accumulation of p53 and p21Cip1 and ectopic expression of Zbtb4 repressed this increase in p21Cip1 levels in response to all drugs (Figure 4C). Similar to the responses to nutlin, expression of Zbtb4 reduced the percentage of cells arrested in the G1 phase of the cell cycle in response to all drugs (shown for adriamycin and etoposide in Figure 4D). In contrast to treatment with nutlin, cells treated with DNA-damaging agents accumulated phosphorylated p53 and Chk1, indicative of activation of the ATM and/or ATR kinases (Figure 4C); this correlated with an arrest in the G2 phase in addition to the G1 arrest (Figure 4D). Zbtb4 did not alleviate the G2 arrest in response to these drugs. Our findings are consistent with multiple data demonstrating that cells arrest in the G2 phase independently of p21Cip1 upon exposure to DNA damage (Hirao *et al*, 2000). Taken together, the data show that Zbtb4 specifically suppresses arrest in the G1 phase in response to activation of p53.

Zbtb4 binds to the P21CIP1 promoter

We considered two models on how Zbtb4 might repress expression of *P21CIP1*. First, we tested the hypothesis that Zbtb4 might exert an effect upstream of p53. To address this possibility, we generated clones and pools of SH-EP cells that express a carboxyl-terminal fragment of p53 (p53DD) that exerts an effect as a dominant-negative allele as it sequesters p53 into non-functional heterotetramers (Shaulian *et al*, 1992). As expected, p53DD impaired the ability of SH-EP cells to upregulate *P21CIP1*, *NOXA* and *PUMA* in response to both UV irradiation and to vincristine (Figures 3A and 5A). In contrast, p53DD did not abolish the effect of shRNA targeting Zbtb4 on *P21CIP1* expression in SH-EP cells, arguing that Zbtb4 does not exert an effect upstream of p53 (Figure 5B). To confirm this result, we repeated the experiment in HCT116 colon carcinoma cells and in a clone of these cells, in which both alleles of *P53* have been disrupted. Depletion of Zbtb4 induced expression of *P21CIP1* in both cell types (Figure 5B). We concluded that the effects of Zbtb4 on *P21CIP1* expression are independent of p53.

We then tested the hypothesis that Zbtb4 might directly regulate the activity of the *P21CIP1* promoter. Zbtb4 potently repressed transcription when tethered to DNA through a

©2008 European Molecular Biology Organization

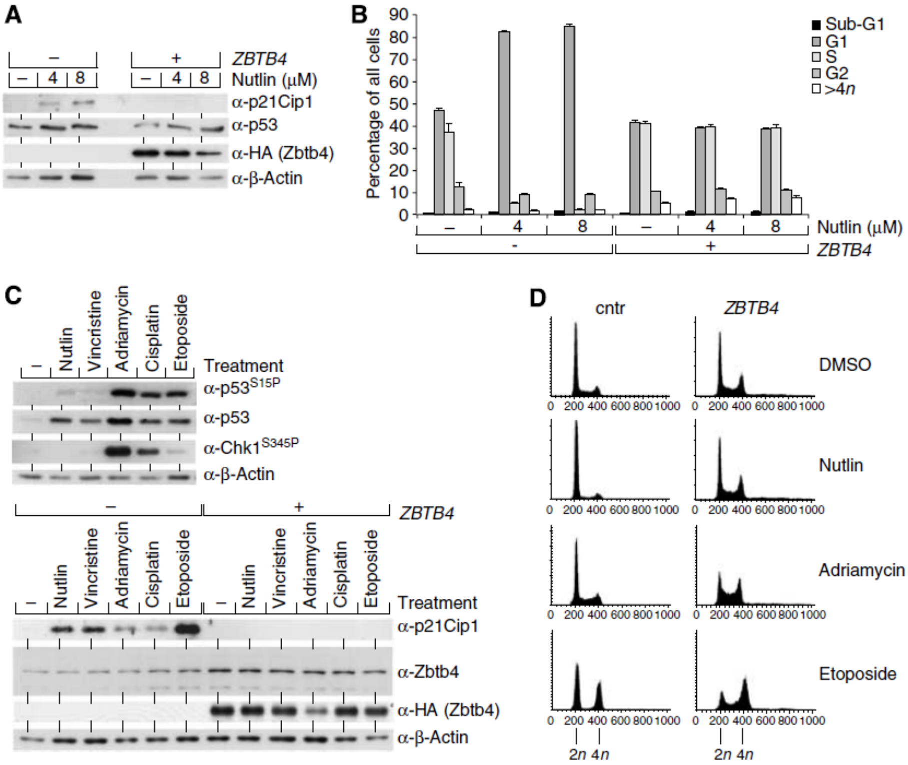

Figure 4 Zbtb4 suppresses cell cycle arrest in response to activation of p53. (**A**) Zbtb4 represses p21Cip1 expression in response to nutlin treatment. SH-EP cells were stably infected with either control retroviruses or viruses expressing HA-tagged Zbtb4. Pools of infected cells were either treated with DMSO as solvent control or with the indicated concentrations of nutlin for 33 h. The panels show immunoblots of cell lysates probed with the indicated antibodies; β-actin served as a loading control. (**B**) FACScan analysis showing the response to nutlin. The panel documents the cell cycle distribution of either control cells or SH-EP cells expressing Zbtb4 after treatment with the indicated concentrations of nutlin for 33 h. Error bars represent the standard deviation of triplicates. (**C**) The upper panels show immunoblots documenting expression of p53, phosphorylated p53 ($p53^{S15P}$) and of phosphorylated Chk1 ($Chk1^{S345P}$) in SH-EP cells treated with the indicated agents. The lower panels show immunoblots documenting expression of p21Cip1, total Zbtb4 and of exogenous Zbtb4 (detected using a HA antibody) in control SH-EP cells and in SH-EP cells expressing Zbtb4; β-actin was used as a loading control. (**D**) FACScan analysis of the responses to nutlin, adriamycin and etoposide of control SH-EP cells and of SH-EP cells expressing Zbtb4.

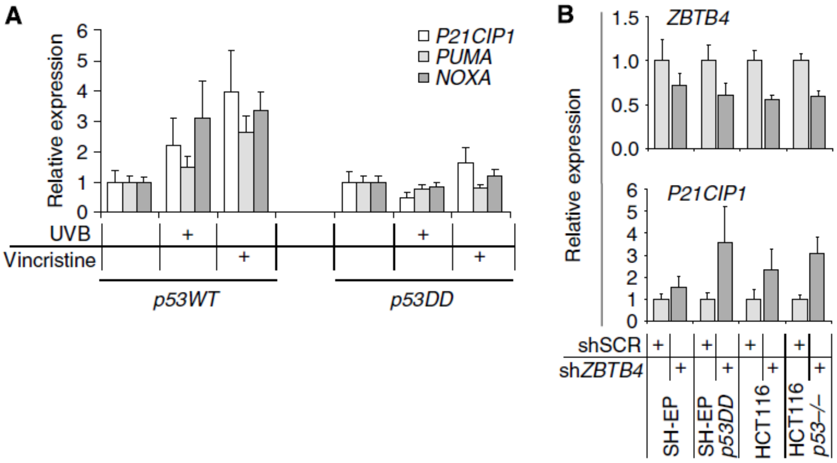

Figure 5 Zbtb4 regulates *P21CIP1* expression independently of p53. (**A**) Expression of a dominant-negative allele of p53 blocks UV- and vincristine-induced upregulation of *P21CIP1*, *NOXA* and *PUMA*. Exponentially growing SH-EP cells were stably infected either with control retroviral vectors or with vectors expressing a carboxyl-terminal fragment of p53 (p53DD). Pools of infected cells were exposed to UVB or treated with 5 nM vincristine or DMSO as a control for 24 h. Cells were harvested and expression of the indicated genes was analysed by the RQ–PCR as before. (**B**) Regulation of *P21CIP1* by Zbtb4 is independent of p53. Control SH-EP cells, SH-EP p53DD-transduced cells, HCT116 cells and HCT116 $p53^{-/-}$ cells were transfected with si*ZBTB4* or control (scrambled) siRNA. At 48 h after transfection, cells were harvested and the expression of *ZBTB4* and *P21CIP1* was determined by the RQ–PCR analysis. Data are plotted as expression relative to an internal standard.

©2008 European Molecular Biology Organization

Gal4-DNA-binding domain (not shown), consistent with previous observations (Filion *et al*, 2006). The *P21CIP1* promoter contains two consensus-binding sites for Zbtb4 (which are identical to the non-methylated Kaiso-binding sites; see Discussion) at −380 and −195 relative to the start site of transcription (Figure 6A). Transient transfection experiments using several reporter plasmids that contain different fragments of the *P21CIP1* promoter showed that Zbtb4 had little effect on basal *P21CIP1* promoter activity in these assays (Figure 6B). To mimic activation of *P21CIP1* in response to DNA damage, we expressed the transcriptional activator Miz1, which is required for DNA damage-induced activation of *P21CIP1* expression (Wanzel *et al*, 2005). Zbtb4 inhibited activation of *P21CIP1* by Miz1. Chromatin immunoprecipitation (ChIP) experiments showed that Zbtb4 binds to the core promoter of the *P21CIP1* gene *in vivo*, but not to a control region located in the 3-untranslated region (3′UTR); shRNA-mediated depletion of Zbtb4 abolished the signal observed in ChIP experiments, documenting the specificity of the antibody (Figure 6C). Taken together, the data show that Zbtb4 binds to the *P21CIP1* promoter *in vivo* and represses its activity.

Surprisingly, Zbtb4 also repressed transcription from promoter fragments spanning from −144 to +16 and from −96 to +16 nucleotides relative to the transcription start site that do not contain any candidate Zbtb4-binding sites (Figure 6A and B). As Zbtb4 can bind to methylated DNA independent of its binding site, we considered the possibility that repression of *P21CIP1* by Zbtb4 reflects methylation of the *P21CIP1* promoter; however, treatment of cells expressing Zbtb4 with the demethylating agent, azacytidine, had no effect on repression of p21Cip1 expression, rendering this possibility unlikely (Supplementary Figure 5). The core *P21CIP1* promoter contains a binding site for the transcription factor Miz1 and the reporter assays described above showed that Zbtb4 repressed Miz1-driven transcription of the *P21CIP1* promoter without affecting the expression of Miz1 protein (Figure 6B and data not shown). Furthermore, ChIPs showed a strong signal for binding of Zbtb4 not only around its cognate-binding site but also at the transcription start site (Figure 6C and D). Although the binding sites are so close that the two primer pairs used to amplify the immunoprecipitated DNA do not completely discriminate between both binding sites (see the low amount of Miz1 binding detected using the primers spanning the Zbtb4-binding sites), the strong signal observed for Zbtb4 around the start site cannot be accounted for by co-amplification of DNA immunoprecipitated through Zbtb4 bound to its cognate-binding site (Figure 6D).

As POZ domain transcription factors can form heterodimers, we wondered whether Zbtb4 heterodimerizes with Miz1. To address this question, we expressed both Miz1- and HA-tagged Zbtb4 by transient transfection in HEK293 cells; in these experiments, α-HA antibodies efficiently co-precipitated Miz1 and vice versa, α-Miz1 antibodies co-precipitated Zbtb4 (Figure 6E). Importantly, α-HA antibodies did not precipitate Miz1 when Zbtb4 was not expressed (Figure 6E). Furthermore, neither monoclonal nor polyclonal control antibodies precipitated Miz1 or Zbtb4 (Figure 6E). We repeated the experiment in the presence of high concentrations of ethidium bromide to exclude the possibility that the co-precipitation was mediated by binding of both proteins to DNA; this did not affect co-immunoprecipitation, demonstrating that both proteins interact independently of their ability to bind DNA (Figure 6E). Consistent with the previous finding that Miz1 interacts with Myc, precipitation of Zbtb4 also co-immunoprecipitated Myc when both proteins were co-expressed by transient transfection; in contrast, Zbtb4 bound less efficiently to MycV394D, a point mutant of Myc that does not bind to Miz1, suggesting that Zbtb4 binds to Myc indirectly through Miz1 (Supplementary Figure 6). To test whether endogenous Zbtb4 interacts with Miz1, we performed immunoprecipitations from colon carcinoma (LS174T) cells, which express high levels of endogenous Miz1 (Figure 6F). Antibodies directed against Zbtb4, but not control antibodies co-precipitated endogenous Miz1 in these experiments, demonstrating that endogenous Miz1 and Zbtb4 interact *in vivo*. Oligonucleotide pulldown experiments showed that both Miz1 and Zbtb4 bound to oligonucleotides spanning either the Zbtb4- or the Miz1-binding sites of the *P21CIP1* promoter, but not to a control oligonucleotide (Figure 6G). Furthermore, Zbtb4 enhanced DNA binding of Miz1 to either site. To test whether Miz1 recruits Zbtb4 to its cognate-binding site *in vivo*, we repeated the ChIP in cells transfected with either scrambled siRNA or siRNA targeting Miz1; depletion of Miz1 reduced binding of Zbtb4 to the *P21CIP1* promoter (Figure 6H). Taken together, we concluded that Zbtb4 and Miz1 form a DNA-binding complex on the *P21CIP1* promoter in human cells.

These data suggest a model in which Zbtb4 represses expression of *P21CIP1* in unstressed cells but that repression is relieved when *P21CIP1* is activated. To test this model, we repeated the ChIPs in cells exposed to the DNA-damaging agent, adriamycin. Exposure to DNA damage induced binding of p53 to its cognate-binding site on the *P21CIP1* promoter; at the same time, binding of endogenous Zbtb4 to the *P21CIP1* promoter was reduced, whereas binding of Miz1 was not affected by DNA damage (Figure 6D). Taken together, these findings support a model in which release of Zbtb4-mediated repression contributes to the activation of the *P21CIP1* promoter in response to DNA damage.

Zbtb4 recruits Sin3a and Sin3b

To understand how Zbtb4 represses *P21CIP1* expression, we monitored histone modifications at the *P21CIP1* promoter in control cells and in cells expressing Zbtb4 using ChIP (Figure 7A). Expression of Zbtb4 led to a decrease in histone H3 acetylation at the *P21CIP1* promoter, suggesting that Zbtb4 recruits a histone deacetylase (HDAC). In contrast, only low levels of histone H3K9 and histone H3K27 methylation, additional modifications that are associated with transcriptional repression, were detected and these were unaffected by Zbtb4. Zbtb4 also induced a decrease in H4K20 methylation, a mark that has been associated with transcriptional elongation. Consistently, the signal was high close to the transcription start site and in the 3′UTR of the *P21CIP1* locus (Figure 7A). To test whether histone deacetylation is critical for Zbtb4-mediated repression, we treated SH-EP cells with two inhibitors of HDACs, trichostatin-A and sodium butyrate. Both inhibitors significantly reduced repression of *P21CIP1*, suggesting that Zbtb4-mediated histone deacetylation mediates repression by Zbtb4 (Figure 7B).

The POZ domain protein Bcl-6 recruits HDAC complexes through binding to Sin3a (Dhordain *et al*, 1998). We therefore

©2008 European Molecular Biology Organization

determined whether Zbtb4 associates with Sin3a and/or Sin3b. Immunoprecipitation of ectopically expressed HA-tagged Zbtb4 co-precipitated endogenous Sin3a from extracts of HEK293 cells (Figure 7C). Furthermore, immunoprecipitation of endogenous Zbtb4 co-precipitated both endogenous Sin3a and Sin3b from HCT116 cell lysates (Figure 7D). Consistent with this observation, immunoprecipitation of exogenous Zbtb4 precipitated significant HDAC activity (Figure 7E). Moreover, shRNA-mediated depletion of the Sin3 complex subunit Sds3, which is required for HDAC binding, results in reduced recruitment of HDAC activity by Zbtb4, indicating that recruitment of HDAC activity by Zbtb4 is dependent on Sin3a or Sin3b (Figure 7E and F). Parallel experiments showed that Zbtb4 co-immunoprecipitates HDAC2, one of the HDACs bound by Sin3, from lysates of transfected cells (not shown). ChIP experiments confirmed that Zbtb4 recruits both Sin3a and Sin3b to the start site of the *P21CIP1* promoter, but not to the 3′UTR (Figure 7G).

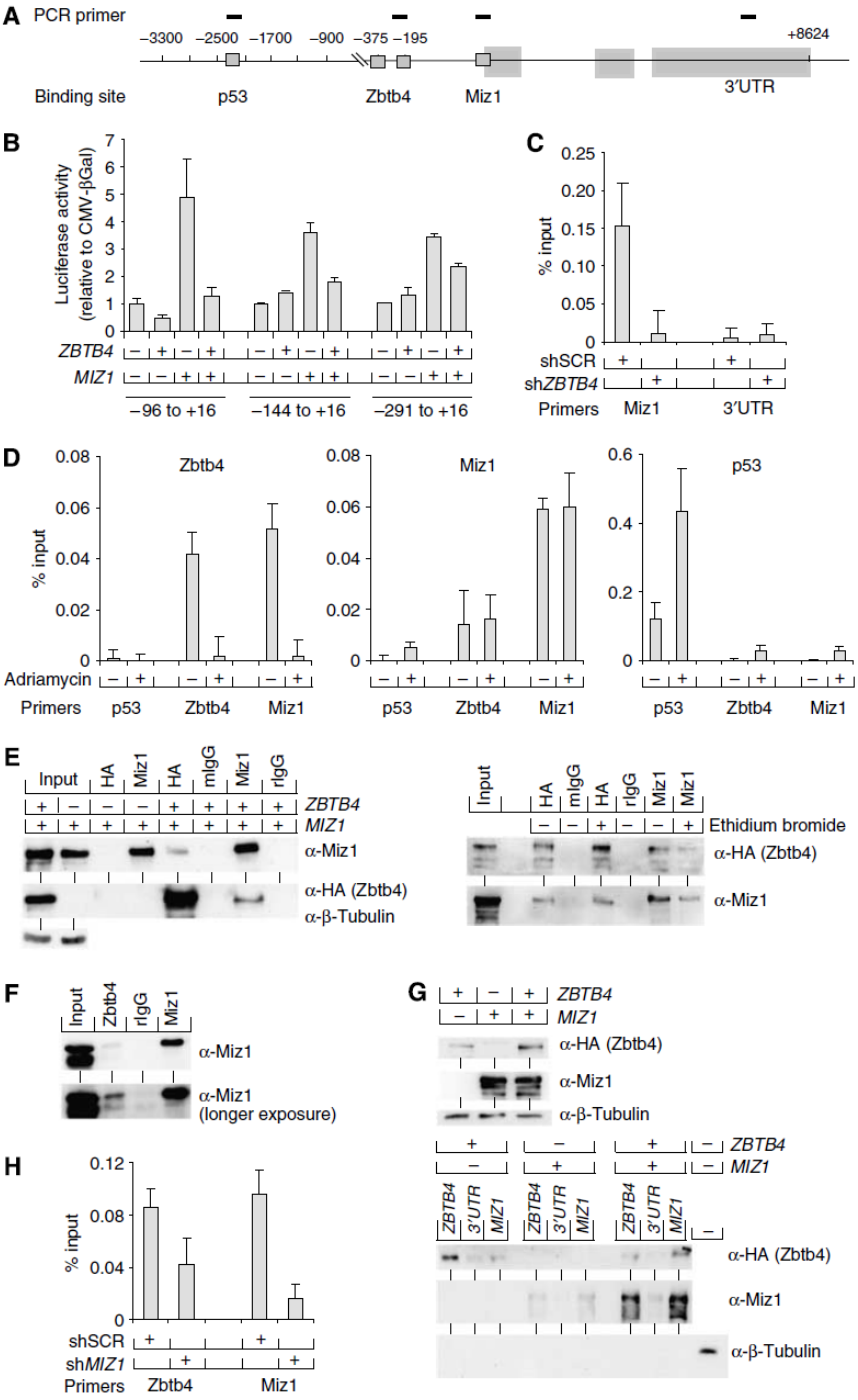

©2008 European Molecular Biology Organization

To demonstrate the functional relevance of this interaction, we carried out expression profiling of HCT116 cells treated with shRNAs to either deplete Zbtb4 or Sin3a and Sin3b (Figure 7H). We identified 192 genes that were upregulated in response to depletion of Zbtb4 and 265 genes that were upregulated in response to co-depletion of Sin3a and Sin3b. The analysis identified 29 genes, among them *P21CIP1*, that were upregulated in response to both Sin3a/b and Zbtb4 depletion. Taken together, our data show that a Zbtb4/Miz1/Sin3 complex represses *P21CIP1* in response to p53 activation and suggests that there is a group of genes that may be similarly repressed by a Zbtb4/Sin3 complex.

Discussion

The POZ domain zinc-finger protein Zbtb4 has been identified based on its homology to the Kaiso protein (Filion *et al*, 2006); Kaiso is a transcriptional repressor protein that binds to methylated DNA sequences in a sequence-independent manner and to non-methylated DNA that contains a Kaiso binding site (KBS) (Daniel *et al*, 2002). Both Zbtb4 and Kaiso are POZ/BTB domain zinc-finger proteins; however, close sequence similarity between both proteins is restricted to the zinc-finger DNA-binding domain. Consequently, Zbtb4 shares with Kaiso the ability to bind both methylated DNA and the KBS (Filion *et al*, 2006). In addition, both Zbtb4 and Kaiso are transcriptional repressor proteins.

We now identify the *P21CIP1* gene, which encodes an inhibitor of the cyclin-dependent kinase Cdk2, as a target for transcriptional repression by Zbtb4. p21Cip1 mediates cell cycle arrest in response to several antimitogenic signals, including activation of p53. Consistent with this notion, Zbtb4 regulates cell cycle arrest under conditions in which p53 is activated by vincristine, which facilitates the nuclear import of p53, or nutlin, which inhibits the Hdm2 E3 ligase that degrades p53 (Giannakakou *et al*, 2000; Vassilev *et al*, 2004). Zbtb4 does not affect the response to genotoxic agents in clonogenic assays and this correlated with its inability to affect the arrest in S and G2 phases in response to such agents. Taken together, our data show that Zbtb4 has little function in regulating the proliferation of unstressed cells but promotes progression through the G1 phase in cells in which p53 is activated.

Paradoxically, however, our interest in Zbtb4 was prompted by the observation that its expression is downregulated in advanced stages of multiple solid tumours, resulting in upregulation of *P21CIP1* expression. Indeed, elevated levels of p21Cip1 are found in several advanced human tumours, suggesting that p21Cip1 can provide a selective advantage during tumorigenesis (Erber *et al*, 1997). Furthermore, *p21cip1*-deficient mice are less susceptible than wild-type mice to Myc-induced mammary tumorigenesis (Bearss *et al*, 2002) and to lymphomagenesis that occurs in *atm*-deficient mice (Wang *et al*, 1997).

Depletion of Zbtb4 suppresses the normal apoptotic response upon vincristine-mediated activation of p53. We show that induction of *P21CIP1* is essential for this suppression. This is consistent with previous observations showing that p21Cip1 can provide critical antiapoptotic signals to cells. Biochemically, this may be mediated indirectly through inhibition of Cdk2 by p21Cip1, as activation of cyclin A/cdk2 complexes can be a critical step in apoptosis (Levkau *et al*, 1998). Alternatively, p21Cip1 inhibits the pro-apoptotic kinases Ask1 and SAPK(JNK) and the cleavage and activation of pro-caspase 3; therefore, the antiapoptotic functions of p21Cip1 may be independent of its ability to regulate Cdk2 activity (Zhan *et al*, 2007).

Importantly, p21Cip1 and Zbtb4 may have critical oncogenic functions independent of the p53 status of a cell. For example, p21Cip1 protects epithelial cells from anoikis by suppressing the expression of the pro-apoptotic BH3-only protein Bim (Collins *et al*, 2005). Anoikis inhibits metastasis, as it eliminates epithelial cells that have detached from the basal membrane and have lost cell–substratum contact. Notably, expression of *ZBTB4* discriminates metastatic from non-metastatic breast, prostate and lung tumours (Supplementary Table 2) and is found in the pan-tumour expression signature that predicts metastasis ($P = 0.003$) (Ramaswamy *et al*, 2003). Downregulation of Zbtb4 may therefore facilitate the escape of tumour cells from anoikis. Furthermore, p21Cip1 has been implicated in maintaining

---

Figure 6 Zbtb4 and Miz1 form a transcriptional repressor complex that represses transcription of *P21CIP1*. (**A**) Scheme of the human *P21CIP1* gene with indicated p53, Miz1 and putative Zbtb4-binding sites. Also indicated are the positions of primers used for the chromatin immunoprecipitation (ChIP) experiments shown below. Shaded grey areas denote exons. (**B**) Zbtb4 represses *P21CIP1* promoter activity. Shown are reporter assays using *P21CIP1* promoter constructs spanning the indicated nucleotides relative to the transcription start site. The graph shows the luciferase activity relative to the standard CMV-βGal after transfection of SH-EP cells with either expression plasmids encoding Zbtb4, Miz1 or both as indicated. The error bars represent the standard deviation of triplicate samples. Controls established that Zbtb4 does not inhibit expression of Miz1 (not shown). (**C**) ChIP demonstrating binding of Zbtb4 to the core of the *P21CIP1* promoter, but not to a control region located in the 3′UTR. Cells were infected with viruses expressing either control shRNA or sh*ZBTB4* as indicated. (**D**) Activation of *P21CIP1* correlates with loss of endogenous Zbtb4 from the *P21CIP1* promoter. The panels show ChIP assays documenting binding of p53, Miz1 and Zbtb4 to the *P21CIP1* promoter in untreated SH-EP cells and in SH-EP cells exposed to adriamycin. For each protein, the difference between specific antibody and control antibody in percentage DNA bound is plotted. (**E**) Zbtb4 binds to Miz1 in lysates of co-transfected cells. HEK293 cells were transfected with expression vectors encoding HA-tagged Zbtb4 and/or Miz1 as indicated. Lysates were immunoprecipitated with the indicated antibodies. The left panels show immunoblots of the immunoprecipitates probed with the indicated antibodies. The right panels document an identical experiment except that 0.1 mg/ml ethidium bromide was added to the lysates before immunoprecipitation to exclude that the observed interaction is mediated by binding of both proteins to DNA. Both antibodies IgG mouse and IgG rabbit were used as controls. (**F**) Endogenous Zbtb4 and Miz1 co-immunoprecipitate in LS174T cells. Rabbit IgG was used as a control. (**G**) Zbtb4 and Miz1 form a DNA-binding complex. HEK293 cells were transfected with expression plasmids encoding Miz1 and/or Zbtb4 as indicated. Biotinylated oligonucleotides spanning the Zbtb4-binding site, the Miz1-binding site or a control sequence (3′UTR) were added and precipitated using avidin-sepharose. Bound proteins were detected by immunoblotting using the indicated antibodies. (**H**) Miz1 recruits Zbtb4 to the core *P21CIP1* promoter. SH-EP cells were transfected either with scrambled siRNA or siRNA targeting *MIZ1*. ChIP assays were performed with control and Zbtb4 antibodies and analysed using the indicated primer pairs. The panel shows the difference between the specific signal and the signal obtained with the control antibody.

©2008 European Molecular Biology Organization

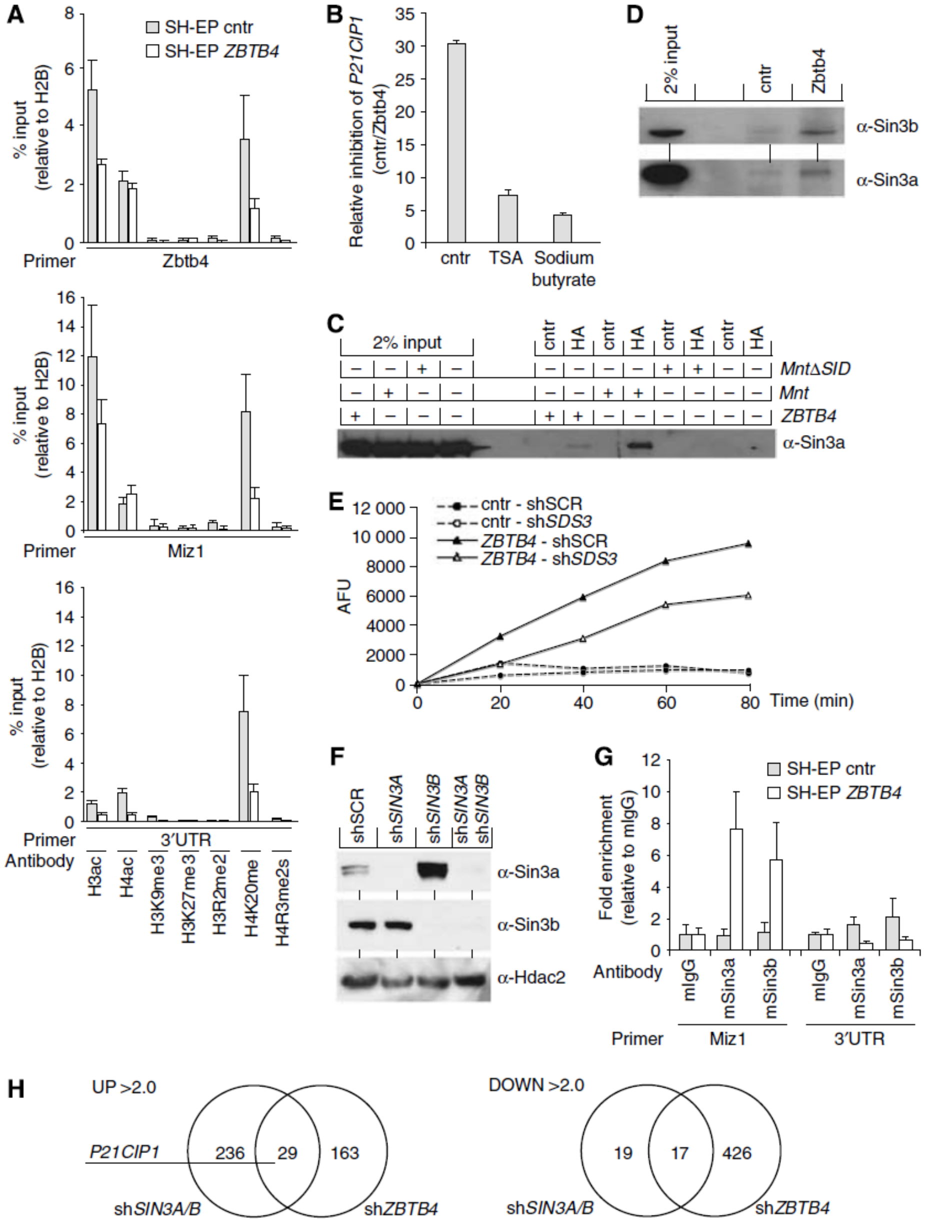

Figure 7 Zbtb4 recruits Sin3a to repress the *P21CIP1* promoter. (**A**) ChIP assays documenting Zbtb4-induced alterations in histone modification at the *P21CIP1* promoter. The assays were performed from either control SH-EP cells or SH-EP cells expressing Zbtb4 using the indicated antibodies. The signals were normalized to precipitations using a H2B antibody. (**B**) Inhibition of histone deacetylation reduces repression of *P21CIP1* by Zbtb4. SH-EP cells were infected with either control retroviruses or retroviruses expressing ectopic Zbtb4. Cell pools were either treated with solvent control or with the histone deacetylase inhibitors trichostatin-A (TSA) or sodium butyrate as indicated. Shown are expression data for *P21CIP1* mRNA relative to a control mRNA derived from the RQ–PCR analysis with error bars representing the standard deviation of the mean. The data are plotted as fold repression by Zbtb4 in each experimental condition. The concentration of TSA used was efficient in inducing overall histone acetylation as determined by immunoblot analysis (not shown). (**C**) Zbtb4 co-immunoprecipitates Sin3a. HEK293 cells were transfected with indicated HA-tagged vectors, and protein lysates were immunoprecipitated with HA antibodies. Associated endogenous Sin3a was visualized by immunoblotting. Here, 2% input of Sin3a is indicated. As a positive control, we used the repressor protein Mnt and a mutated version of Mnt, in which the Sin3a interaction domain had been deleted (MntΔSID) (Hurlin *et al*, 1997). (**D**) Endogenous Zbtb4 co-immunoprecipitates Sin3a and Sin3b. HCT116 whole cell extracts were immunoprecipitated with Zbtb4 or pre-immune antibodies; precipitates were probed with antibodies to mSin3b and mSin3a. Here, 2% of input is shown. (**E**) Association of Zbtb4 with histone deacetylase activity depends on Sds3. HEK293 cells were transfected with constructs expressing Zbtb4 or control vector and simultaneously infected with lentiviruses expressing either control shRNA or shRNA targeting Sds3. At 48 h later, whole cell lysates were prepared and immunoprecipitated with Zbtb4 or normal rabbit serum antibodies. HDAC activity in the immunoprecipitates was analysed. (**F**) Characterization of lentiviral shRNAs targeting *SIN3A* and *SIN3B*. HCT116 cells were infected with lentiviruses expressing the indicated shRNAs. At 48 h after infection, cells were harvested. Immunoblotting was performed with the indicated antibodies. (**G**) Zbtb4 recruits Sin3a and Sin3b to the core *P21CIP1* promoter. Shown are ChIP assays from control SH-EP cells and from SH-EP cells expressing Zbtb4. (**H**) Zbtb4 shares transcriptional targets with Sin3. Comparison of transcripts regulated in Sin3- and Zbtb4-depleted cells relative to control HCT116 cells. Absolute values of the fold changes are indicated as >2.0-fold. The probability of chance of the overlap between sh*SIN3* and sh*ZBTB4* as calculated by the hypogeometric distribution is $<10^{-4}$.

©2008 European Molecular Biology Organization

stem cell pools and suppression of Zbtb4 expression may have a critical role in maintaining quiescence of tumour-initiating cells.

Zbtb4 recruits an mSin3/HDAC complex that is likely to be involved in repression of *P21CIP1* expression. Several HDACs, notably HDAC1, 2 and 3, repress *P21CIP1* in different cell types; therefore, expression of *P21CIP1* is an important target that mediates cell cycle arrest in response to pharmacological inhibition of histone deacetylation (Lagger *et al*, 2003). Upon transient overexpression, Sp1 and Sp3, which bind to the core *P21CIP1* promoter, bind to HDACs and recruit them to the *P21CIP1* gene (Lagger *et al*, 2003). It is less clear whether endogenous Sp proteins recruit HDACs to the *P21CIP1* promoter. In contrast, POZ domain complexes function as dedicated repressor proteins and the Miz1/Zbtb4 complex is a potent repressor of *P21CIP1* promoter activity. In this view, we suggest that this complex may be a key target for cell cycle arrest by inhibition of HDAC activity and levels of Zbtb4 may have prognostic value in determining the response to such drugs.

Materials and methods

Patients

We studied tumour specimens from 98 children with primary neuroblastoma who had been diagnosed from 1981 to 2000. All patients were treated according to previously described protocols with confirmed consent for study procedures.

Cell culture

HEK293 and HeLa cells were grown in DMEM, HCT116 were grown in McCoy's, Ls174T and SH-EP cells were grown in RPMI medium. Where indicated, cells were treated with 4 μM nutlin-3 (Sigma), trichostatin-A (50 ng/ml), 2 and 50 nM vincristine, 40 μM all-*trans* retinoic acid, 0.2 μM etoposide, 0.05 μM cisplatin, 5 mM sodium butyrate or 300 nM azacytidine. UV irradiation experiments used 250 J/m^2 UVB light. Soluble siRNA against *ZBTB4* (Dharmacon) and scrambled were transfected with lipofectamin RNAimax (Invitrogen).

A full-length cDNA encoding HA-tagged Zbtb4 was assembled from PCR-generated fragments, sequenced and inserted into the pCMV and pBabe-puro vectors. Three shRNAs targeting *ZBTB4* and scrambled controls were cloned into pRetroSuper-puro and pRetroSuper-GFP, respectively. shRNAs directed against *P21CIP1* were cloned into pSuper Neo-GFP. ShRNAs directed against *SIN3a*, *SIN3b*, *ZBTB4* and control were cloned into a lentiviral vector derived from the FUGW backbone (courtesy of Valeri Vasioukhin—pLenti-H1). The shRNA sequences are available upon request.

Antibodies

The following antibodies were used: α-HA (HA.11; Covance), α-p21Cip1 (N-20), α-p53 (DO-1), α-Cdk2 (M2), α-mSin3b (H4) (all Santa Cruz Biotechnology), α-β-tubulin (MAB3408; Chemicon), α-Miz1 (10E2, Herold *et al*, 2002; H190, Santa Cruz Biotechnology) and α-Zbtb4 (Filion *et al*, 2006).

Reporter assays and ChIP

The p21Cip1-promoter-luciferase reporter assays have been described in Wu *et al* (2003). ChIP assays were performed as described previously (Bouchard *et al*, 2001) using primers specific for the Miz1-binding site (−32 to +47 relative to the start site of transcription), the promoter-proximal Zbtb4 binding site (−276 to −171), p53-binding site (−2289 to −2164) and a sequence located in the 3′UTR of the gene (+7464 to +7641) as a control. Standard deviations of triplicate were calculated according to the Gaussian error distribution law.

RNA extraction and RQ–PCR analysis

Real-time PCR analysis was performed in triplicate. Relative expression between samples and control was calculated according to the $\Delta\Delta C_T$ relative quantification method using β2-microglobulin as a standard. Primer sequences are available upon request.

HDAC activity

HDAC assays were performed using the Fluor de Lys HDAC assay kit as specified by the manufacturer (Biomol, Plymouth, PA).

Microarray analysis

Expression profiling studies were performed using Affymetrix GeneChip Human U133A 2.0 arrays. Sample labelling and hybridizations were performed with adherence to Affymetrix's standardized protocols. The data sets were subsequently grouped for pairwise analysis consisting of two groups of three biological replicates. The accession number is E-MEXP-1509.

Acknowledgements

We thank Bert Vogelstein for HCT116 p53$^{-/-}$ cells. This study was supported by grants from the AICR (ME), NGFN2 (ME and HC), NIH/NCI grant CA57138 (RNE), NIH training grants T32 CA 09229 and T32 CA09657 (DE) and by Association pour la Recherche contre le Cancer (Grant 3727; P-AD).

References

Bearss DJ, Lee RJ, Troyer DA, Pestell RG, Windle JJ (2002) Differential effects of p21(WAF1/CIP1) deficiency on MMTV-ras and MMTV-myc mammary tumor properties. *Cancer Res* **62:** 2077–2084

Berwanger B, Hartmann O, Bergmann E, Nielsen D, Krause M, Kartal A, Flynn D, Wiedemeyer R, Schwab M, Schäfer H, Christiansen H, Eilers M (2002) Loss of a Fyn-regulated differentiation and growth arrest pathway in advanced stage neuroblastoma. *Cancer Cell* **2:** 377–386

Bouchard C, Dittrich O, Kiermaier A, Dohmann K, Menkel A, Eilers M, Lüscher B (2001) Regulation of cyclin D2 gene expression by the Myc/Max/Mad network: Myc-dependent TRRAP recruitment and histone acetylation at the cyclin D2 promoter. *Genes Dev* **15:** 2042–2047

Chao C, Herr D, Chun J, Xu Y (2006) Ser18 and 23 phosphorylation is required for p53-dependent apoptosis and tumor suppression. *EMBO J* **25:** 2615–2622

Collins NL, Reginato MJ, Paulus JK, Sgroi DC, Labaer J, Brugge JS (2005) G1/S cell cycle arrest provides anoikis resistance through Erk-mediated Bim suppression. *Mol Cell Biol* **25:** 5282–5291

Daniel JM, Spring CM, Crawford HC, Reynolds AB, Baig A (2002) The p120(ctn)-binding partner Kaiso is a bi-modal DNA-binding protein that recognizes both a sequence-specific consensus and methylated CpG dinucleotides. *Nucleic Acids Res* **30:** 2911–2919

Dhordain P, Lin RJ, Quief S, Lantoine D, Kerckaert JP, Evans RM, Albagli O (1998) The LAZ3(BCL-6) oncoprotein recruits a SMRT/mSIN3A/histone deacetylase containing complex to mediate transcriptional repression. *Nucleic Acids Res* **26:** 4645–4651

Erber R, Klein W, Andl T, Enders C, Born AI, Conradt C, Bartek J, Bosch FX (1997) Aberrant p21(CIP1/WAF1) protein accumulation in head-and-neck cancer. *Int J Cancer* **74:** 383–389

Estlin EJ, Veal GJ (2003) Clinical and cellular pharmacology in relation to solid tumours of childhood. *Cancer Treat Rev* **29:** 253–273

Filion GJ, Zhenilo S, Salozhin S, Yamada D, Prokhortchouk E, Defossez PA (2006) A family of human zinc finger proteins that bind methylated DNA and repress transcription. *Mol Cell Biol* **26:** 169–181

Giannakakou P, Sackett DL, Ward Y, Webster KR, Blagosklonny MV, Fojo T (2000) p53 is associated with cellular microtubules and is transported to the nucleus by dynein. *Nat Cell Biol* **2:** 709–717

Herold S, Wanzel M, Beuger V, Frohme C, Beul D, Hillukkala T, Syvaoja J, Saluz HP, Hänel F, Eilers M (2002) Negative regulation

©2008 European Molecular Biology Organization

of the mammalian UV response by Myc through association with Miz-1. *Mol Cell* **10:** 509–521

Hirao A, Kong YY, Matsuoka S, Wakeham A, Ruland J, Yoshida H, Liu D, Elledge SJ, Mak TW (2000) DNA damage-induced activation of p53 by the checkpoint kinase Chk2. *Science* **287:** 1824–1827

Hurlin PJ, Queva C, Eisenman RN (1997) Mnt, a novel Max-interacting protein is coexpressed with Myc in proliferating cells and mediates repression at Myc binding sites. *Genes Dev* **11:** 44–58

Jordan A, Hadfield JA, Lawrence NJ, McGown AT (1998) Tubulin as a target for anticancer drugs: agents which interact with the mitotic spindle. *Med Res Rev* **18:** 259–296

Lagger G, Doetzlhofer A, Schuettengruber B, Haidweger E, Simboeck E, Tischler J, Chiocca S, Suske G, Rotheneder H, Wintersberger E, Seiser C (2003) The tumor suppressor p53 and histone deacetylase 1 are antagonistic regulators of the cyclin-dependent kinase inhibitor p21/WAF1/CIP1 gene. *Mol Cell Biol* **23:** 2669–2679

Levkau B, Koyama H, Raines EW, Clurman BE, Herren B, Orth K, Roberts JM, Ross R (1998) Cleavage of p21Cip1/Waf1 and p27Kip1 mediates apoptosis in endothelial cells through activation of Cdk2: role of a caspase cascade. *Mol Cell* **1:** 553–563

Mihara M, Erster S, Zaika A, Petrenko O, Chittenden T, Pancoska P, Moll UM (2003) p53 has a direct apoptogenic role at the mitochondria. *Mol Cell* **11:** 577–590

Phan RT, Saito M, Basso K, Niu H, Dalla-Favera R (2005) BCL6 interacts with the transcription factor Miz-1 to suppress the cyclin-dependent kinase inhibitor p21 and cell cycle arrest in germinal center B cells. *Nat Immunol* **6:** 1054–1060

Ramaswamy S, Ross KN, Lander ES, Golub TR (2003) A molecular signature of metastasis in primary solid tumors. *Nat Genet* **33:** 49–54

Samuels-Lev Y, O'Connor DJ, Bergamaschi D, Trigiante G, Hsieh JK, Zhong S, Campargue I, Naumovski L, Crook T, Lu X (2001) ASPP proteins specifically stimulate the apoptotic function of p53. *Mol Cell* **8:** 781–794

Seoane J, Le HV, Massague J (2002) Myc suppression of the p21(Cip1) Cdk inhibitor influences the outcome of the p53 response to DNA damage. *Nature* **419:** 729–734

Shaulian E, Zauberman A, Ginsberg D, Oren M (1992) Identification of a minimal transforming domain of p53: negative dominance through abrogation of sequence-specific DNA binding. *Mol Cell Biol* **12:** 5581–5592

Vassilev LT, Vu BT, Graves B, Carvajal D, Podlaski F, Filipovic Z, Kong N, Kammlott U, Lukacs C, Klein C, Fotouhi N, Liu EA (2004) *In vivo* activation of the p53 pathway by small-molecule antagonists of MDM2. *Science* **303:** 844–848

Vousden KH (2006) Outcomes of p53 activation—spoilt for choice. *J Cell Sci* **119:** 5015–5020

Wang YA, Elson A, Leder P (1997) Loss of p21 increases sensitivity to ionizing radiation and delays the onset of lymphoma in atm-deficient mice. *Proc Natl Acad Sci USA* **94:** 14590–14595

Wanzel M, Kleine-Kohlbrecher D, Herold S, Hock A, Berns K, Park J, Hemmings B, Eilers M (2005) Akt and 14-3-3eta regulate Miz1 to control cell-cycle arrest after DNA damage. *Nat Cell Biol* **7:** 30–41

Wu S, Cetinkaya C, Munoz-Alonso MJ, von der Lehr N, Bahram F, Beuger V, Eilers M, Leon J, Larsson LG (2003) Myc represses differentiation-induced p21CIP1 expression via Miz-1-dependent interaction with the p21 core promoter. *Oncogene* **22:** 351–360

Wu WS, Heinrichs S, Xu D, Garrison SP, Zambetti GP, Adams JM, Look AT (2005) Slug antagonizes p53-mediated apoptosis of hematopoietic progenitors by repressing puma. *Cell* **123:** 641–653

Zhan J, Easton JB, Huang S, Mishra A, Xiao L, Lacy ER, Kriwacki RW, Houghton PJ (2007) Negative regulation of ASK1 by p21Cip1 involves a small domain that includes serine 98 that is phosphorylated by ASK1 *in vivo*. *Mol Cell Biol* **27:** 3530–3541

©2008 European Molecular Biology Organization

DNA Repair 8 (2009) 390–399

Contents lists available at ScienceDirect

DNA Repair

journal homepage: www.elsevier.com/locate/dnarepair

HCT116 cells deficient in p21^{Waf1} are hypersensitive to tyrosine kinase inhibitors and adriamycin through a mechanism unrelated to p21 and dependent on p53

Nuria Ferrandiz[a], Jorge Martin-Perez[b], Rosa Blanco[a], Derya Donertas[a], Axel Weber[c], Martin Eilers[c], Paolo Dotto[d], M. Dolores Delgado[a], Javier Leon[a,*]

[a] *Cancer Molecular Biology Group, Instituto de Biomedicina y Biotecnología de Cantabria (IBBTEC) and Dpto.de Biología Molecular, Universidad de Cantabria-CSIC-IDICAN, Santander, Spain*
[b] *Intituto de Investigaciones Biomédicas A. Sols, CSIC, Madrid, Spain*
[c] *Institute for Tumor Biology, University of Marburg, Marburg, Germany*
[d] *Cutaneous Biology Research Center, Massachusetts General Hospital, Charlestown, MA 02129, USA*

ARTICLE INFO

Article history:
Received 28 April 2008
Received in revised form
26 November 2008
Accepted 2 December 2008
Available online 15 January 2009

Keywords:
p53
Adriamycin
Imatinib
Gefitinib
Apoptosis
HCT116
Myc

ABSTRACT

p21^{Waf1} (p21) was described as a cyclin-dependent kinase inhibitor, but other p21 activities have subsequently been described, including its ability to inhibit apoptosis in some models. Comparative work on the human colon cancer isogenic cell lines HCT116 and HCT116p21$^{-/-}$ led to the proposal that p21 protects colon cancer cells against apoptosis by genotoxic drugs. We asked whether p21 also protected from cell death induced by non-genotoxic drugs, such as tyrosine kinase inhibitors. We found that p21-deficient cells were dramatically more sensitive towards imatinib and gefitinib than parental cells. Interestingly, HCT116p21$^{-/-}$ also showed higher basal activity of protein kinases as c-Abl, c-Src, and Akt. We generated HCT116p21$^{-/-}$ sublines with inducible p21 expression and found that p21 did not rescue the hypersensitivity to imatinib. Moreover, down-regulation of p21 by enforced c-Myc expression or by p21 siRNA did not sensitize parental HCT116 cells. We found that, in HCT116p21$^{-/-}$ cells, p53 showed higher stability, higher transcriptional activity and phosphorylation in serines associated with p53 activity. Furthermore, silencing of p53 with siRNA and inactivation of p53 with a dominant negative mutant rescued the hypersensitive response to kinases inhibitors, 5-fluorouracil and adriamycin in HCT116p21$^{-/-}$ cells. Consistently, HCT116p53$^{-/-}$ cells are more resistant to imatinib than parental cells, suggesting that imatinib activity is partly dependent on p53 in colon cancer cells. We conclude that high p53 activity, rather than p21 deficiency, is the mechanism responsible for hypersensitivity to drugs of HCT116p21$^{-/-}$ cells. Therefore the role of p21 on apoptosis of HCT116 colon cancer cells should be re-evaluated.

© 2008 Elsevier B.V. All rights reserved.

1. Introduction

p21$^{Waf1/Cip1}$ (p21 herein after), encoded by the CDKN1A gene, is a member of the Cip/Kip family inhibitors of cell cycle progression. The first discovered and best-studied biochemical activity of p21 is to inhibit Cdks, consistent with its activity as cell cycle inhibitor [1–4]. However, more recent studies have shown that p21 has additional functions as differentiation inducer [5] and as an inhibitor of apoptosis induced by DNA-damaging agents [6–8]. Since cancer cells can escape death induced by chemotherapeutic drugs, this latter p21 activity is of pivotal importance in human cancer therapy.

p21 is a p53 target gene and is a relevant mediator of p53-cell cycle arrest [9–11]. A role of p21 in cancer has been demonstrated in vivo, as p21-null mice develop tumors spontaneously [12] and show increased tumor susceptibility using chemical carcinogenesis [13–16]. Although there are examples of p21 acting as an apoptosis inducer [17–20], the results in most models suggest it has an apoptosis protective effect. One of these cell models consists of the human colon cancer cell line HCT116 and its isogenic derivative HCT116p21$^{-/-}$, generated by disruption of both p21 alleles through homologous recombination [21]. Work with these cell lines suggested that p21 protected from apoptosis induced by adriamycin (doxorubicin) [22]. Later on, many reports have argued for a protective role of p21 against apoptosis induced by DNA-damaging agents and other stimuli as hypoxia using the HCT116 model system (a non-exhaustive list is shown in Supplemental Table 1).

In this work we asked whether p21 also played a role in the cell death induced by non-genotoxic drugs in the HCT116 model. We chose imatinib as the main drug for our studies because it is a tyro-

---

Abbreviations: Chx, cycloheximide; PARP, poy(ADP-ribose)polymerase; PI, propidium iodide.

[*] Corresponding author at: Dpto. de Biologia Molecular, Facultad de Medicina, Avda. Cardenal Herrera Oria, 39011 Santander, Spain. Tel.: +34 942 201952; fax: +34 942 201945.
E-mail address: leonj@unican.es (J. Leon).

1568-7864/$ – see front matter © 2008 Elsevier B.V. All rights reserved.
doi:10.1016/j.dnarep.2008.12.001

sine kinase inhibitor (with higher activity against c-Abl, Bcr-Abl and c-Kit) widely used in human cancer therapy [23,24]. We found that the cytotoxic effect of imatinib, gefitinib and adriamycin was much higher on the p21-deficient HCT116 cells than on parental cells, but, surprisingly, this hypersensitivity was due to p53 overexpression and independent from p21.

2. Materials and methods

2.1. Cell lines, transfections and mice

Colon cancer cell line HCT116 and its isogenic derivatives HCT116p21$^{-/-}$ [21] and HCT116p53$^{-/-}$ cells [22] were grown in RPMI 1640 (Invitrogen) with 8% fetal calf serum and gentamycin (80 μg/ml). HKO-MTp21 cell line was generated cotransfecting HCT116p21$^{-/-}$ cells with the pM6-p21 construct (carrying a Zn^{2+}-inducible p21) [25] and the pLPCX vector in a proportion 6:1. Transfections were carried out with Lipofectamine (Invitrogen) and transfectants were selected with 0.25 μg/ml of puromycin (Sigma). HKO-MTp21 cells were incubated with 75 μM ZnSO$_4$ to induce p21. For silencing of p21, HCT116 cells and derived cell lines were transduced with empty vector (pRetroSuper), and vector carrying two different short-hairpin constructs for human p21 (shp21B and C). The targeted sequences were AACACCTCCTCATGTACAT (shp21B) and GCGACTGTGATGCGCTAAT (shp21C). Overexpression of p21 was achieved by adenoviral infection. HCT116p21$^{-/-}$ cells were infected with adenovirus carrying p21 gene and GFP [26] and 24 h after infection whole-cell protein extracts were analysed by immunoblot. GFP-expressing cells were above 80% in all adenoviral infections. For silencing of p53, HCT116p21$^{-/-}$ cells were transduced with pSuperRetro-shp53 virus [27] and a polyclonal transduced cell line, Hp21KO-shp53, was selected with 0.5 μg/ml of puromycin. Hp21KO-pSR are HCT116p21$^{-/-}$ cells transduced with the empty vector. HCT116p21$^{-/-}$ cells were transfected with an expression vector for pcDNA3-DDp53 [28] and, to allow selection, a vector carrying a puromycin resistance markers (pLPCX) in a proportion 6:1 (DDp53:pLPCX). Transfections were carried out with Lipofectamine and transfectants were selected with 0.5 μg/ml of puromycin. A pool of five transfectants was selected and the presence of the DDp53 isoform analysed by immunoblot. p21-deficient mice (B6;129S2-*Cdkn1a*^{tm1Tyj}/J) [9]were obtained from Jackson Laboratories.

2.2. Proliferation, annexin V binding and cell cycle assays

Proliferation assays were performed to compare the response of cells to drugs. 80,000 cells (for HCT116p21$^{-/-}$) or 50,000 cells (for the other cell lines) were plated on 12-multiwell plates and 24 h after plating, increased concentrations of imatinib (provided by Novartis), gefitinib (provided by Astra-Zeneca), adriamycin (Sigma Chemical Co.), 5-fluorouracil (5-FU) (Sigma Chemical Co.) or SU6656-001 (Biaffin) were added. After 48 h cells were stained with crystal violet (1% in methanol), scanned and subjected to densitometric analysis. Clonogenic assays were performed plating 5000 cells on 6-multiwell plates and after one week colonies where stained as above and counted. For cell cycle analysis the cells were fixed in 90% ethanol at 4 °C, washed with PBS and incubated at 37 °C for 30 min with RNase (200 μg/ml) and 10 μg/ml propidium iodide (PI) (Sigma). The stained cells were analysed by flow cytometry on a FACScan flow cytometer (BD Bioscences) using the CellQuest software. Apoptosis was assessed by annexin V binding. Cells were treated with different imatinib concentrations for 48 h and annexin V binding was determined by flow cytometry and annexin V-phycoerythrin (BD Pharmingen).

2.3. Immunofluorescence staining, immunoblotting and protein kinase assays

Cells were fixed with paraformaldehyde and the presence of phosphorylated H2AX histone (γ-H2AX, monoclonal antibody from Upstate, ref. 05-636) or p21 (polyclonal antibody C-19 from Santa Cruz Biotech.) were detected by immunofluorescence, using a FITC-conjugated secondary antibody (Dako, F0205). Samples were mounted with Vectashield (Vector) containing 4′-6-diamidino-2-phenylindole (DAPI) to stain nuclei and examined under a fluorescence microscope (Zeiss-Axioskop2). Immunoblots were performed as previously described [25]. Blots were revealed with the ECL system (GE Healthcare). Antibodies used were: anti-poy(ADP-ribose)polymerase (PARP) (H-250), anti-phospho-tyrosine (PY20), anti-actin (I-19), anti-p53 (FL-393), anti-Akt1/2 (H136), anti-c-Src (SRC2), anti-Erk2 (C14), anti-phospho-Erk1/2 (E-4), anti-CDK2 (M2) from Santa Cruz Biotech; anti-p53 phosphorylated in serines 6, 9, 15, 20, 37, 46 and 392 (ref. 9919) and anti-phospho Akt (ref. 9271) from Cell Signalling; anti-phospho-c-Src (44-660G) from BioSource; anti-c-Abl (ref. 554104) from BD Pharmingen; anti-p21 (P-184) from Sigma, and anti-α-tubulin antibody provided by Nicholas Cowan (New York University, New York). To assay CDK2 activity, protein extracts (1 mg per assay) were immunoprecipitated with 1.5 μg of CDK2 antibody (same as above) and collected on Gammabind sepharose beads (Pharmacia). Kinase activity was measured on histone H1 (Roche Biochemicals) as a substrate as described [25]. An aliquot of the immunoprecipitate was analysed by immunoblot for p21 and CDK2 expression.

2.4. Reporter–luciferase assays

The transcriptional activity of p53 in HCT116 and HCT116p21$^{-/-}$ was measured with three promoter–luciferase constructs: PG13–Luc, p21–Luc and MDM2–Luc, as well as the promoter-less pGL2-basic vector (Promega) used as negative control. One million of cells were transfected with Lipofectamine and 1 μg of the luciferase constructs plus 0.1 μg of pRL-null for transfection normalization. After 36 h cells were lysed and luciferase activity was assayed with the Dual Luciferase kit from Promega as instructed by the manufacturer. Luciferase activity was normalized to the *Renilla* internal control. Each point corresponds to the mean of two different experiments done in duplicate. Activation is relative to the values obtained with HCT116 cells transfected with the corresponding reporter.

2.5. Gene expression analysis

HCT116 and HCT116p21$^{-/-}$ cells were untreated or treated with 15 μM imatinib for 48 h. Total RNA was extracted (RNeasy kit, Qiagen), labelled and hybridized to a membrane macroarray containing probes for 96 apoptosis-related genes ("Human Apoptosis Gene Array", SuperArray Bioscience Corporation), following the manufacturer indications. The membrane was washed and the radioactivity measured in a Molecular Imager apparatus (BioRad). For each gene the signal was normalized to the control genes in the array, and the ratio between the mRNA levels in control cells and cells treated with imatinib was calculated.

3. Results

3.1. HCT116p21$^{-/-}$ cells are more sensitive to kinase inhibitors

In view of the high sensitivity of HCT116p21$^{-/-}$ to genotoxic drugs, we took advantage of this model to determine whether p21 played a role in the response to drugs that do not directly induce DNA damage such as tyrosine kinase inhibitors in HCT116

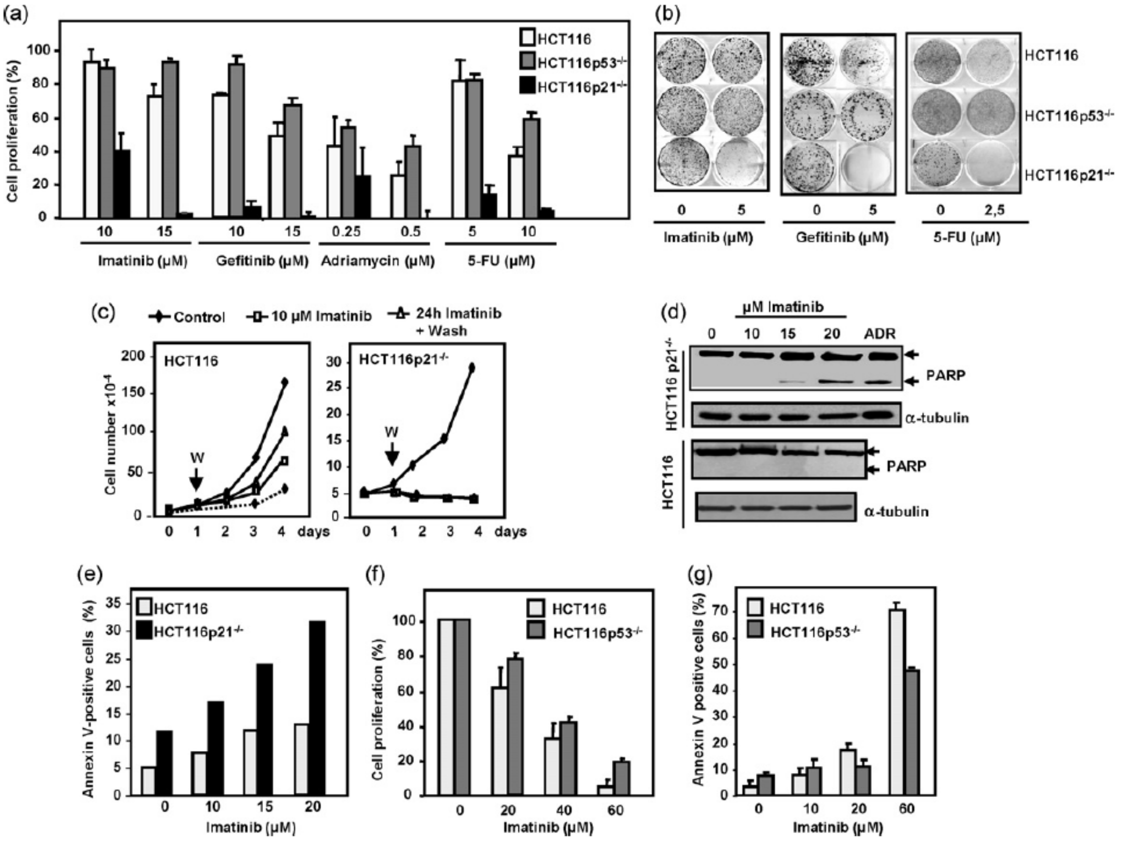

Fig. 1. HCT116p21$^{-/-}$ cells are hypersensitive to the cytotoxic effects of imatinib. (a) Cells of the indicated cell lines were treated with the indicated concentrations of imatinib, gefitinib, adriamycin and 5-FU. Cell proliferation was determined after 48 h and expressed as a percentage of the proliferation of untreated cells. (b) Clonogenic assay of the indicated cell lines treated with imatinib, gefitinib and 5-FU for 5 days after crystal violet staining. (c) Growth curves of the indicated cell lines in the presence of imatinib. "*W*" indicates the time point at which the cells were washed to remove imatinib. Note that the scales for both cell lines are different. Dotted line in the left graph corresponds to untreated HCT116p21$^{-/-}$ for comparison with wild-type HCT116. (d) Apoptosis assessed by the proteolytic cleavage of PARP. HCT116 and HCT116p21$^{-/-}$ cells were treated with the indicated concentrations of imatinib and 0.5 μM adriamycin (ADR) for 48 h. Whole-cell protein extracts were analysed by immunoblot with antibodies anti-PARP and anti-α-tubulin as a loading control. (e) Apoptosis induction by imatinib as assessed by annexin V binding. Cells were treated with different imatinib concentrations for 48 h. Annexin V binding was determined by flow cytometry. (f) Cell proliferation of HCT116 and HCT116p53$^{-/-}$ cells treated with high imatinib concentrations for 48 h. Data are means from three experiments ± S.E.M. (g) Apoptosis induction by imatinib as assessed by annexin V binding in cells treated with high imatinib concentrations for 48 h. Data are means from two experiments ± S.E.M.

and HCT116p21$^{-/-}$. We tested imatinib (which shows higher activity against Bcr-Abl, c-Abl and c-Kit) and gefitinib (with highest specificity against epidermal growth factor receptor). The results demonstrated that p21-deficient cells were dramatically more sensitive against imatinib and gefitinib than parental cells. We also tested p53-deficient cells [29] and found that these cells were more resistant to the kinase inhibitors than the p21-deficient cells (Fig. 1a). As a parallel approach we performed clonogenic assays, which also demonstrated the hypersensitivity of HCT116p21$^{-/-}$ cells to protein kinase inhibitors [30] (Fig. 1b). As positive controls for cell death we used adriamycin and 5-FU and we confirmed the reported hypersensitivity to both drugs of p21-deficient cells [22,31–33] (Fig. 1a and b).

A time–course proliferation assay in response to imatinib confirmed that HCT116p21$^{-/-}$ cells were more sensitive than the parental cells. The imatinib effect on p21-deficient cells was cytotoxic as growth did not resume upon removal of the drug (Fig. 1c). The results also showed that, in the absence of drugs, HCT116p21$^{-/-}$ cells grow ~fivefold slower than parental cells. The cytotoxic effect of imatinib on p21-deficient cells is mediated by apoptosis as demonstrated by proteolytic cleavage of PARP assayed by immunoblot (Fig. 1d), by annexin V binding assayed by flow cytometry (Fig. 1e) and by accumulation of sub-G0/G1 cells (not shown). The effect of imatinib was partly dependent on p53, as p53-deficient cells were more resistant to high imatinib concentrations (20–60 μM) than parental cells, as shown by cell growth assays (Fig. 1f) and annexin V binding (Fig. 1g).

It was surprising that p21 deficiency resulted in such high sensitivity to the tyrosine kinase inhibitors, as well as its partial dependence on p53, in a similar way as genotoxic drugs adriamycin and 5-FU. Therefore, we tested the possibility that imatinib indirectly induces DNA damage in HCT116 cells by assaying the accumulation in the cell nuclei of foci with phosphorylated histone H2AX (γ-H2AX, a marker of genomic damage). The results (Fig. 2a) showed that imatinib did not induce nuclear γ-H2AX foci, contrary to cells treated with adriamycin, which were used as positive control. However, imatinib reached its intracellular targets in HCT116, as autophosphorylation of c-Abl kinase was severely inhibited upon treatment with imatinib (Fig. 2b). Interestingly, basal c-Abl expression and activity were significantly higher in HCT116p21$^{-/-}$ than in parental cells. We did not detect expression of other imatinib targets as c-Kit and EGF receptor in HCT116 (not shown). It was striking the higher level of c-Abl activation observed in HCT116p21$^{-/-}$ cells, and we asked whether other kinases besides c-Abl were hyperactivated in HCT116p21$^{-/-}$ cells. Using phospho-specific antibodies we found an enhanced phosphorylation of Akt, Erk and c-Src kinases in HCT116p21$^{-/-}$ cells as compared to parental cells (Fig. 2c). Imatinib also resulted in the inactivation of the c-Src kinase (Fig. 2d), consistent with the described requirement of c-Abl for c-Src activity [34].

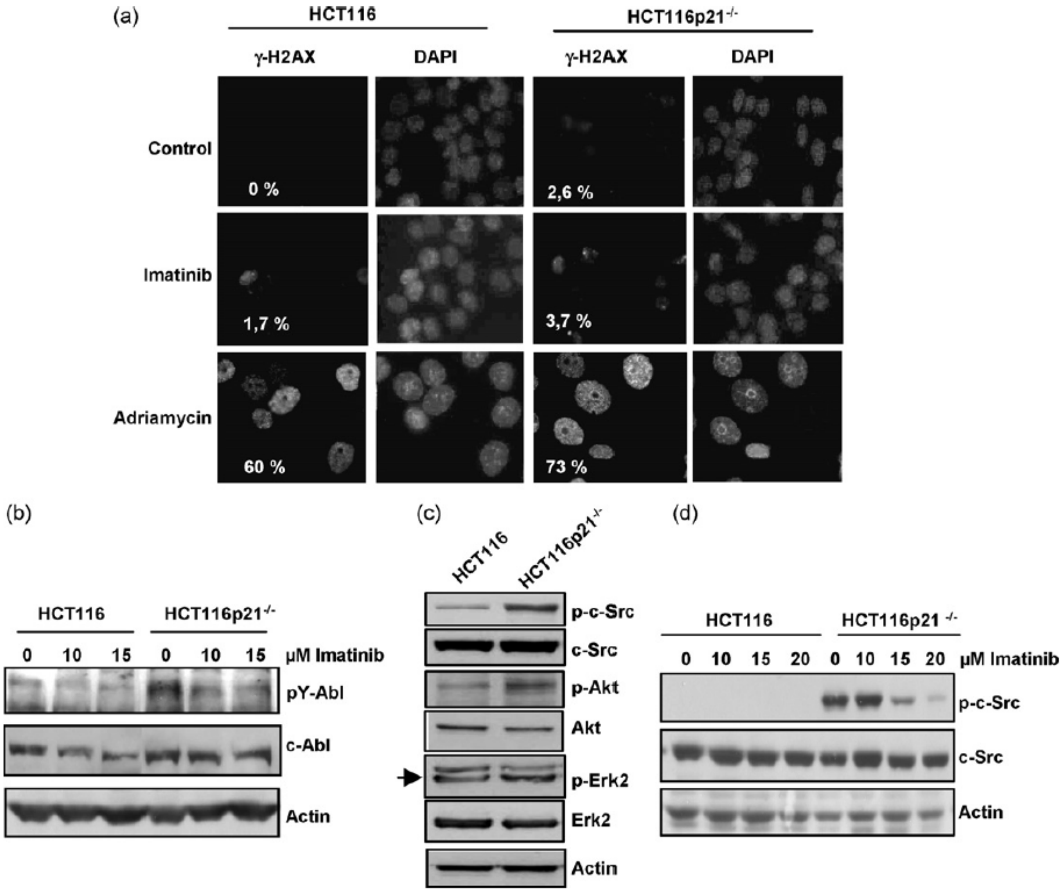

Fig. 2. Imatinib targets in HCT116p21$^{-/-}$. (a) Imatinib does not induce H2AX phosphorylation. Cells were treated with imatinib and (as a positive control) with 0.5 μM adriamycin for 48 h and fixed with paraformaldehyde. The presence of phosphorylated H2AX histone (γ-H2AX) was detected by immunofluorescence. The cells were counterstained with DAPI to stain nuclei and the fraction of positive cells is indicated in each case. Representative images are shown. (b) c-Abl inactivation by imatinib in HCT116 and HCT116p21$^{-/-}$ cells. Cells were incubated for 48 h with imatinib and c-Abl was determined by immunoblot. To determine the phosphorylation of c-Abl the blot was probed with an anti-phospho-tyrosine antibody. Actin levels were also determined to assess protein loading. (c) Protein kinase activation in HCT116p21$^{-/-}$. Cells were lysed and the levels of kinases indicated at the right were determined by immunoblot. Arrow marks the Erk2 band. Actin levels were also determined as a loading control. (d) c-Src inactivation by imatinib in HCT116 and HCT116p21$^{-/-}$ cells. Cells were incubated for 48 h with imatinib and phospho-c-Src and c-Src were determined by immunoblot.

3.2. *p21 deficiency is not responsible for the hypersensitive phenotype of HCT116p21$^{-/-}$ cells*

To directly test whether p21 deficiency is responsible for the hypersensitive phenotype of p21-deficient cells, we generated cell lines with inducible expression of p21. Cells were transfected with an expression vector where the human p21 cDNA is under control of the metallothionein promoter and its expression is induced by Zn^{2+} in the culture media [25]. The kinetics of p21 induction in one selected transfectants (Hp21KO-MTp21) is shown in Fig. 3a. Most of exogenous p21 remains in the cell nuclei, as assessed by immunofluorescence (Fig. 3b). We tested the functionality of the ectopic p21 by assaying the kinase activity of CDK2 upon induction of p21 with Zn^{2+}. The results showed that induction of p21 in Hp21KO-MTp21 resulted in effective inhibition of CDK2 (Fig. 3c). Consistently, induction of p21 reduced the fraction of cells in G1 phase of the cell cycle, as assayed by flow cytometry of PI-stained cells (Fig. 3d), as cells in G1 transverse into G2/M but cannot begin a new S phase. This is consistent with the reported effect of p21 as an inductor of G2 accumulation [35,36].

Having characterized the Hp21KO-MTp21 cell line, we next asked whether restoring p21 expression in HCT116p21$^{-/-}$ cells conferred resistance to imatinib. Surprisingly, the induction of p21 did not alter the sensitivity of the cells towards imatinib, as determined by cell growth (Fig. 3e) and the fraction of apoptotic cells as determined by annexin V binding (Fig. 3f). In addition, induction of p21 in Hp21KO-MTp21 cells did not modify the sensitivity to adriamycin (not shown).

The above results from p21 overexpression suggested that p21 deficiency was not responsible for the enhanced cytotoxic response to drugs. We sought to confirm this by the opposite approach, i.e., decreasing p21 expression in wild-type HCT116 cells through RNA interference. We generated a polyclonal cell line expressing a p21 short-hairpin vector by retroviral transduction. These cells, termed HCT-shp21B, showed reduced levels of p21 protein levels with respect to parental cell line (Fig. 3g). Adriamycin potently upregulated p21, as previously reported [21,37] and we found that HCT-shp21B showed reduced p21 in the presence of adriamycin, as compared to control cells (Fig. 3g). In contrast, imatinib did not modify p21 levels and the cells also showed reduced p21 levels upon treatment with imatinib, with respect to parental cells (Fig. 3g). Thus, we next asked whether p21 suppression modified the cytotoxicity mediated by drugs. We found that the response to adriamycin, 5-fluorouracil, imatinib and gefitinib was similar for HCT116 and HCT-shp21B cell lines (Fig. 3h). Also, HCT-shp21B and parental HCT116 show similar sensitivity to high imatinib concentrations (20–60 μM) (not shown). These results suggest that p21 deficiency is not responsible for the sensitivity to imatinib. In a complementary approach to decrease endogenous p21 we gener-

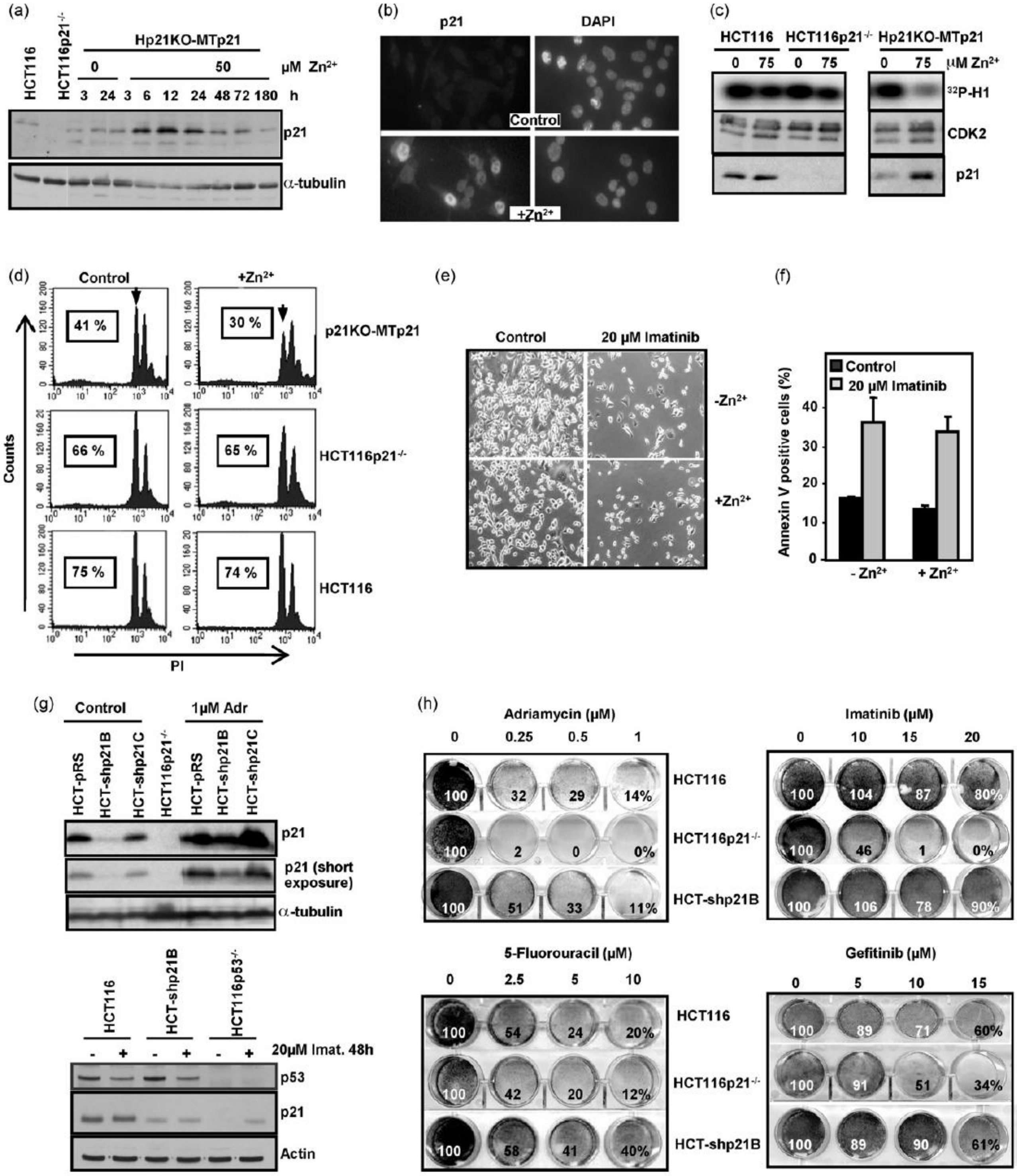

Fig. 3. Ectopic expression of p21 does not rescue the hypersensitive phenotype of HCT116p21$^{-/-}$. (a) Induction of p21 in Hp21KO-MTp21cells. Cells were incubated with 75 μM $ZnSO_4$ for the indicated periods of time and protein extracts were analysed by immunoblot with anti-p21 and anti-α-tubulin antibodies. (b) Induction and nuclear localization of p21 in Hp21KO-MTp21 cells. Immunofluorescence analysis with anti-p21 antibody was performed in cells treated for 12 h with 50 μM $ZnSO_4$. Cells were counterstained with DAPI to stain nuclei. (c) Induction of p21 in Hp21KO-MTcells inhibits activity kinase of CDK2. Cells were incubated with 75 μM $ZnSO_4$ during 24 h. Lysates were immunoprecipitated with anti-CDK2 antibodies and assayed for kinase activity using histone H1 as substrate. Levels of CDK2 and p21 in the immunoprecipitates were determined by immunoblot. (d) Cell cycle analysis of HCT116, HCT116p21$^{-/-}$ and Hp21KO-MTp21 cells treated with 75 μM $ZnSO_4$ for 4 days and assayed for the PI incorporation by flow cytometry. (e) Micrographs of HKO-MTp21 cells treated with 20 μM imatinib for 48 h in the presence and absence of 75 μM $ZnSO_4$ showing similar sensitivity in the presence and absence of the p21 inducer. (f) Apoptosis induction by imatinib as assessed by Annexin V binding. Cells of the indicated cell lines were treated with 20 μM imatinib for 24 h. Annexin V binding was determined as in Fig. 1. (g) Silencing of p21. Lysates were prepared from parental HCT116 and derived cell lines expressing two different short-hairpin constructs for human p21, one competent for silencing (HCT-shp21B) and another used as a negative control (HCT-shp21C), as well as cells transduced with empty vector (HCT-pRS). Cells were treated for 16 h with adriamycin (upper panel) and with imatinib (lower panel) to show p21 levels in the presence of the drugs. p21, α-tubulin and actin were detected by immunoblot. A short exposure of the film is also shown to demonstrate p21 down-regulation in the presence of adriamycin. HCT116p53$^{-/-}$ cells was used as negative control of p53 expression in the lower-panel. (h) Proliferation assay of the indicated cell lines incubated with increased concentrations of adriamycin, 5-fluorouracil, gefitinib and imatinib. The cells were stained with crystal violet after 48 h of treatment. The numbers in the wells represent densitometric units normalized to the value of untreated cells.

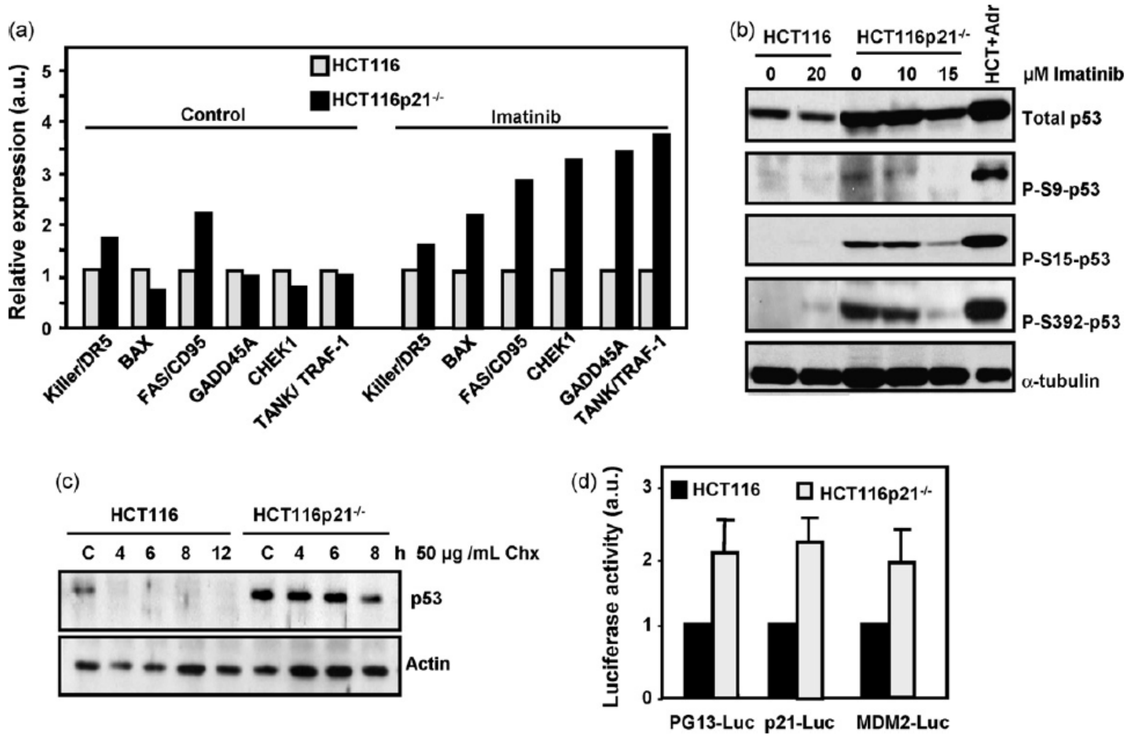

Fig. 4. p53 is stabilized and hyperactivated in HCT116p21$^{-/-}$ cells. (a) Induction of p53-target genes in HCT116p21$^{-/-}$ treated with imatinib. HCT116p21$^{-/-}$ and HCT116 were treated with 15 μM imatinib for 48 h. The RNA was prepared and labelled and the expression of p53 target genes was determined by macroarray hybridization as described in Section 2. Data are normalized to the expression of each gene in parental HCT116 cells. (b) Levels of phosphorylated p53 in HCT116 and HCT116p21$^{-/-}$ cells treated with imatinib for 48 h. Cells were lysed and the immunoblot were prepared using phospho-specific antibodies. As a control, a lysate from HCT116 cells treated with 0.5 μM adriamycin for 48 h (HCT + Adr) was included. (c) Immunoblot of HCT116 and HCT116p21$^{-/-}$ cells treated for the indicated periods of time with 50 μg/ml of cycloheximide (Chx). The blot was probed with anti-p53 and anti-actin antibodies. (d) p53 transcriptional activity of HCT116 and HCT116p21$^{-/-}$ measured with the three indicated luciferase constructs carrying p53-responsive elements. Data are means of two different experiments done in duplicate and are normalized to the values in HCT116 cells. Error bars represent S.E.M.

ated cell lines transfected with an conditional Myc, a transcription factor known to repress p21 expression in many cell lines including HCT116 [38,39]. We generated HCT116 cells expressing c-MycER, a Myc fusion protein which is activated by 4-hydroxytamoxifen. Addition of 4-hydroxytamoxifen to these cells resulted in p21 down-regulation (Supplemental Fig. 1). However, c-Myc activation did not result in a significant change in sensitivity to imatinib or adriamycin, as determined by proliferation assays, annexin V binding and PARP proteolysis (Supplemental Fig. 1). Altogether, the results indicate that p21 deficiency is not responsible for the hypersensitive response of HCT116p21$^{-/-}$ cells to drugs as tyrosine kinase inhibitors or DNA-damaging drugs.

3.3. *p53 is stabilized and hyperactivated in HCT116p21$^{-/-}$ cells*

In an attempt to explain the higher sensitivity of HCT116p21$^{-/-}$ cells to drugs we analysed the expression of genes related to apoptosis through macroarray hybridization. We found that the mRNA expression of several p53 target genes (e.g., GADD45, DR5, CD95, BAX, CHEK1, TRAF1) was up-regulated in response to imatinib in the p21-deficient cells as compared to parental cells (Fig. 4a). This finding suggested that p53 might be involved in the hypersensitive phenotype of HCT116p21$^{-/-}$. Thus, we studied the status of p53 in HCT116p21$^{-/-}$ and found that p53 protein levels were dramatically elevated with respect to parental cells (Fig. 4b), as already observed [40–43]. Most of the p53 mutations found in cancer render a more stable protein, and it was conceivable that mutation in p53 was selected during the multiple passages of the cell line. However, we did not find mutations in exons 2–11 of the p53 gene of the HCT116p21$^{-/-}$ cell line used in our studies (not shown). In contrast we found that in HCT116p21$^{-/-}$ cells but not in the parental cells, p53 was hyperphosphorylated in residues known to be important for p53 stabilization and/or transactivation: Ser-9, Ser-15 and Ser-392 (Fig. 4b). We did not detect significant changes in the phosphorylation of other residues tested (Ser-6, Ser-20, Ser-37, Ser-46) (not shown). It was expected that these modifications would result in increased p53 stability. To determine p53 stability, HCT116 and HCT116p21$^{-/-}$ cells were treated for the indicated periods of time with 50 μg/ml of the protein synthesis inhibitor cycloheximide and the p53 levels were assessed by immunoblot. The results demonstrated that p53 had higher stability in HCT116p21$^{-/-}$ (Fig. 4c). Moreover, reporter–luciferase assays with three different p53-responsive promoters revealed an increased transcriptional activity of p53 in HCT116p21$^{-/-}$ cells (Fig. 4d). Therefore, HCT116p21$^{-/-}$ expressed higher levels of active p53 than the parental cell line.

We next asked whether the elevated p53 levels in HCT116p21$^{-/-}$ cells depended on p21 deficiency. The results (Fig. 5a) revealed that induction of p21 in Hp21KO-MTp21 did not modify p53 levels and p53 phosphorylation. Also, reduction of p21 levels in HCT116 cells (i.e., in HCT-shp21B cells) did not result in increased total p53 levels or phospho-Ser15-p53 levels (Fig. 5b). Moreover, high transient p21 levels achieved by adenoviral infection in HCT116p21$^{-/-}$ cells did not result in any decrease of p53 levels (Fig. 5c). Cells acutely infected with p21 adenovirus did not show any increase in resistance towards imatinib or adriamycin after 24 h of treatment with respect to cells infected with a control virus, assessed by sub-G0/G1 fraction and annexin V binding (not shown). At longer infection times (36–48 h) the p21 virus induced cell death (Fig. 5d). Finally, we could not detect differences in p53 protein levels (as assayed by

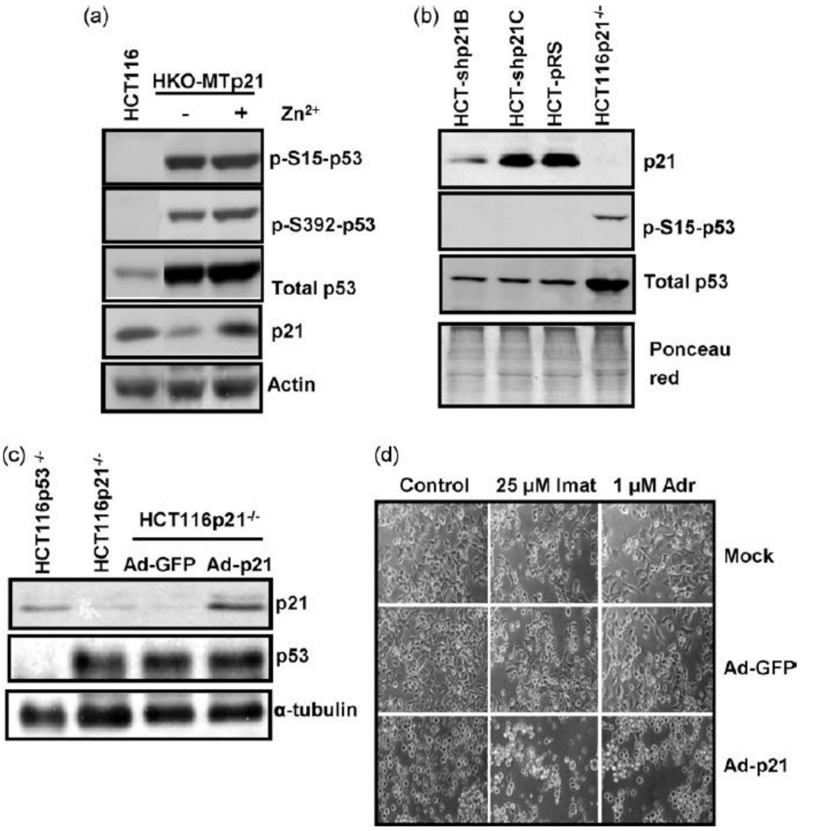

Fig. 5. Induction or repression of p21 does not modify p53 expression in HCT116 cells. (a) Induction of p21 does not modify p53 expression in HCT116. Whole-cell lysates from Hp21KO-MTp21 cells grown in the absence or presence of 50 μM $ZnSO_4$ for 24 h (to induce p21) were analysed by immunoblot with antibodies against p53, p21, actin and Ser-15- and Ser-392-phosphorylated p53. (b) Silencing of p21 does not modify p53 expression in HCT116 cells. Lysates of HCT-shp21B (where p21 is silenced, Fig. 3d), HCT-shp21C (expressing a control siRNA) and HCT-pRS (transduced with the empty virus) were analysed by immunoblot with the antibodies anti-p21, anti-total p53 and anti-phospho-serine-15-p53. The filter was stained with Ponceau Red to assess protein loading. (c) Overexpression of p21 by adenoviral infection does not modify p53 expression in HCT116p21$^{-/-}$ cells. Cells were infected with adenovirus carrying p21 gene and GFP [26] and 24 h after infection whole-cell protein extracts were analysed by immunoblot with antibodies against p21, p53 and α-tubulin. (d) Overexpression of p21 did not confer protection to infected cells. HCT116p21$^{-/-}$ were infected with adenovirus p21 and GFP and 6 h after infection cells were treated with 20 μM imatinib and 1 μM adriamycin and micrographs were taken after 30 h of treatment.

immunoblot) in ascendant colon from p21-deficient mice [9] and parental mice (not shown). In summary, the results indicate that HCT116p21$^{-/-}$ cells express higher p53 levels and exert higher p53 activity than parental cells, and that this was independent from its p21 deficiency.

3.4. *High p53 levels are responsible for the hypersensitive phenotype in HCT116p21$^{-/-}$ cells*

We finally asked whether the increased sensitivity of HCT116p21$^{-/-}$ to drugs was a consequence of the p53 overexpres-

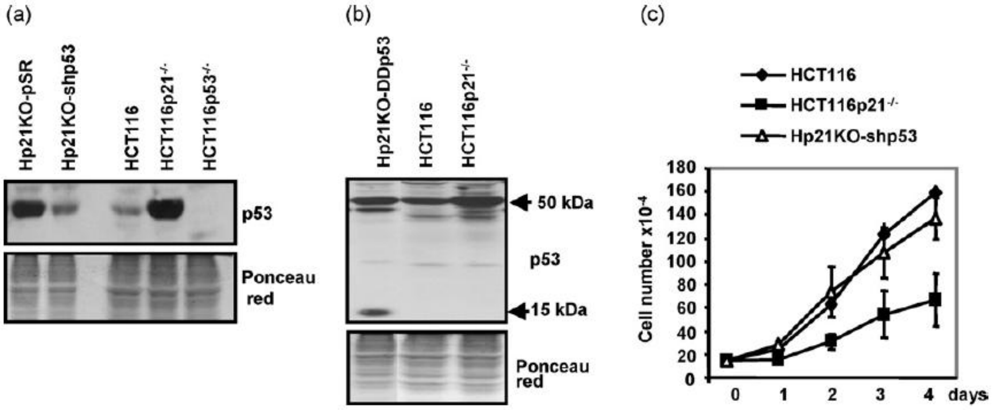

Fig. 6. Impairment of p53 activity in HCT116p21$^{-/-}$ cells rescues the slow-growing phenotype. (a) Silencing of p53 in Hp21KO-shp53 cells. Cell lysates from the indicated cell lines were analysed by immunoblot with anti-p53. The filter was stained with Ponceau Red to assess protein loading. (b) Expression of DDp53. Cell lysates from the indicated cell lines were analysed by immunoblot with anti-p53 antibody. The filter was stained with Ponceau Red to assess protein loading (c) Cell proliferation of HCT116, HCT116p21$^{-/-}$ and Hp21KO-shp53 cells. Cells were plated at equivalent densities in parallel dishes and tripsinized and counted during 4 days. Data are mean from two experiments ± S.E.M.

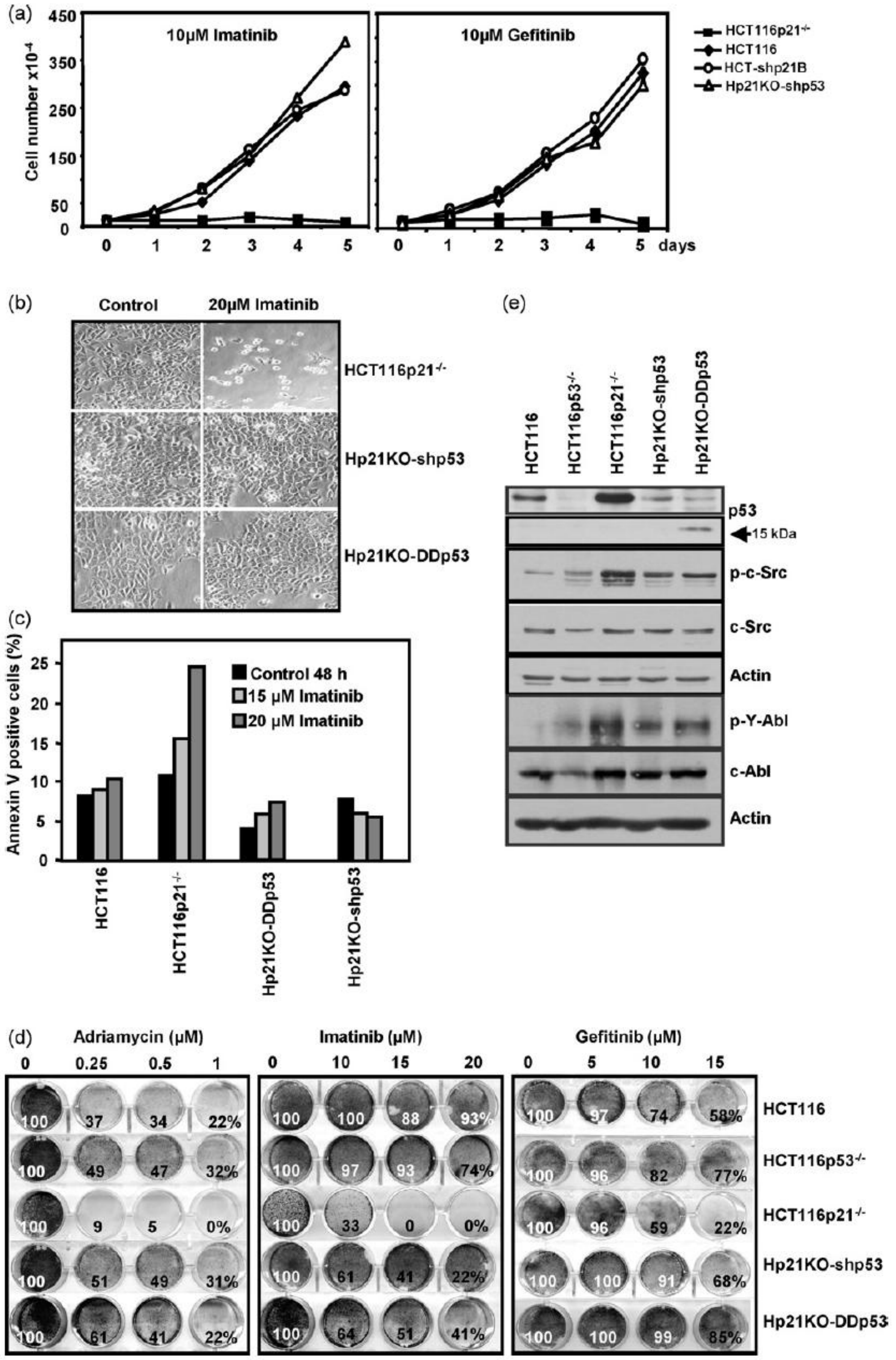

Fig. 7. Hypersensitivity to imatinib of HCT116p21$^{-/-}$ cells depends on high p53 levels and activity. (a) Growth curves of the indicated cell lines in the presence of imatinib and gefitinib. Cells were plated at equivalent densities and tripsinized and counted during 5 days. (b) Micrographs of the indicated cell lines treated with 20 μM imatinib for 48 h showing the reduced sensitivity to imatinib of Hp21KO-shp53 and Hp21KO-DDp53. (c) Cells were treated for 48 h with imatinib and the fraction of cells binding annexin V was determined as in Fig. 1. (d) Proliferation assay of the indicated cell lines incubated with increased concentrations of adriamycin, imatinib and gefitinib. The cells were stained with crystal violet after 48 h of treatment. The numbers in the wells represent densitometric units normalized to the growth of untreated cells. (e) Silencing of p53 protein in HCT116p21$^{-/-}$ down-regulated the activity of c-Src and c-Abl. Whole-cell lysates from HCT116, HCT116p53$^{-/-}$, HCT116p21$^{-/-}$, Hp21KO-shp53, Hp21KO-DDp53 were analysed by immunoblot with antibodies against p53, p-c-Src, c-Src, p-Abl, c-Abl and actin.

sion in HCT116p21$^{-/-}$ cells. To test this hypothesis we generated HCT116p21$^{-/-}$ sublines with reduced p53 expression and tested their response to imatinib and adriamycin. Cells were transduced with retrovirus expressing a short-hairpin p53 [27]. The transduced cells (Hp21KO-shp53) expressed reduced p53 levels (Fig. 6a).

We also generated transfectant HCT116p21$^{-/-}$ cell lines expressing a p53 fragment (DDp53) that acts as a dominant negative p53 mutant [28]. We chose a cell line termed Hp21KO-DDp53 and the expression of DDp53 was confirmed by immunoblot (Fig. 6b). Cell proliferation assays demonstrated that the cell line with reduced p53 (Hp21KO-shp53) grew faster than the parental HCT116p21$^{-/-}$, and at a similar rate than the wild-type HCT116 cells (Fig. 6c).

We next asked whether p53 inactivation in these cells conferred higher resistance to kinase inhibitors. As shown in growth curves of Fig. 7a, silencing of p53 completely rescued the growth inhibition by low imatinib and gefitinib doses, as p21KO-shp53 grew at the same rate than parental HCT116 cells. Confirming our previous results (Fig. 3), the reduction of p21 (i.e., HCT-shp21B cells) did not confer higher sensibility in this assay. The inactivation of p53 with the DDp53 mutant (Hp21KO-DDp53 cells) also reversed the hypersensitive phenotype of HCT116$^{-/-}$ cells to a similar extent than in Hp21KO-shp53 cells (Fig. 7b). Moreover, reduction of p53 levels or p53 activity resulted in increased resistance to the apoptosis induced by imatinib, as assessed by annexin V binding assay (Fig. 7c). Proliferation assays also confirmed that impairment of p53 function reverted the hypersensitive phenotype of HCT116p21$^{-/-}$ cells towards adriamycin, imatinib and gefitinib (Fig. 7d). These results are consistent with the increased resistance to high imatinib concentrations of p53-deficient HCT116, described above (Fig. 1). Thus, reduction of p53 levels or activity rescued the slow growing and the hypersensitive phenotypes of HCT116p21$^{-/-}$. We showed above (Fig. 2) that despite the hypersenstivity to imatinib, HCT116p21$^{-/-}$ cells had higher c-Abl and c-Src protein kinases activity. Thus we asked whether impairment of p53 function would also antagonize these activities. The results demonstrate that c-Abl and c-Src activities are decreased in Hp21KO-shp53 and Hp21KO-DDp53 with respect to parental HCT116p21$^{-/-}$ cells (Fig. 7e). Taken together, our results strongly suggest that p53 is responsible for the hypersensitivity to tyrosine kinases inhibitors in this model.

4. Discussion

We demonstrate here that HCT116p21$^{-/-}$ cells are dramatically more sensitive to imatinib and gefitinib than parental cells. Both inhibitors are now widely used in therapy of human cancer. Our results extend to tyrosine kinase inhibitors the previous observation with DNA-damaging drugs as adriamycin or 5-FU, which are also more cytotoxic to HCT116p21$^{-/-}$ cells [22,31–33]. However, restoring p21 expression in the p21-deficient cells did not modify the hypersensitive response to imatinib and adriamycin, and silencing p21 in parental cells did not confer higher sensitivity to the drugs. Surprisingly, this hypersensitivity is not due to p21 deficiency but to p53 overexpression in HCT116p21$^{-/-}$ cells, as the silencing or inactivation of p53 confers a lower sensitivity towards these drugs, and similar to that of parental cells.

It is noteworthy and previously unnoticed that p53 also confers sensitivity to gefitinib and imatinib, although tenfold higher imatinib concentrations are required to achieve a cytotoxic effect in this colon cancer cells than in chronic myeloid leukemia cells (the major clinical application of imatinib). Conversely to HCT116, chronic myeloid leukemia cells express Bcr-Abl kinase as imatinib target. The dependence on p53 for imatinib response in HCT116, which do not express Bcr-Abl but express c-Abl, extends previous findings in chronic myeloid leukemia where p53 inactivation is associated to imatinib resistance [44,45].

p53 overexpression in HCT116p21$^{-/-}$ was due to enhanced stability of the p53 protein. The reason for this effect in HCT116p21$^{-/-}$ cells is unclear, but it is not dependent on p14^{ARF} and Mdm2 expression [42,46] and our unpublished results. We have shown that HCT116p21$^{-/-}$ cells express high levels of activated c-Abl kinase (Fig. 2b), and it is established that c-Abl stabilizes p53 by inhibiting Mdm2-mediated degradation of p53 (reviewed in [47]). So, high c-Abl expression could explain the stability and elevated p53 levels in HCT116p21$^{-/-}$ cells. It is also noteworthy the high levels of activated kinases (e.g., c-Abl, Akt, c-Src and Erk2) in p21-deficient cells. This is striking as some of these kinases have been associated to cell survival in different systems. We hypothesize that the HCT116p21$^{-/-}$ cell line, besides its deficiency in p21, acquired additional genetic or epigenetic changes during the selection process leading to high basal kinase activity which would stabilize p53 through different pathways. This would result in cells showing a slower growth rate and higher sensitivity to drugs.

Regardless of the mechanism that led to the high-p53 and hypersensitive phenotype of HCT116p21$^{-/-}$ cells, our results invite to reconsider many of the reported conclusions on the anti-apoptotic effect of p21 in colon cancer cells. An anti-apoptotic role for p21 has been demonstrated in several cell culture models from different tissues reviewed in [7,8,48], and can explain the decreased rate of radiation-induced tumorigenesis p21-deficient mice [12,49]. In the HCT116 model, comparative work with HCT116 and HCT116p21$^{-/-}$ cell lines has generated multiple reports arguing that p21 loss sensitizes these cells for apoptosis induced by a number of antitumoral drugs (Supplemental Table 1). Although it is unknown whether our results can be extended to all drugs, the work described here challenge these conclusions as we demonstrate that the hypersensitive phenotype for the drugs tested in our work, depends on the high p53 levels in the HCT116p21$^{-/-}$ cell line and not on the p21 deficiency.

In support of this hypothesis, a recent report indicates that the hypersensitivity to chromium-induced DNA damage in HCT116p21$^{-/-}$ is also mediated by p53 [50]. In vivo inactivation of p21 in mice resulted in a significant increase in the frequency and size of intestinal tumors in two different models of colon carcinogenesis [51,52]. These results are not consistent with the idea that p21 deficiency confers an apoptosis-prone and slow-growth phenotype whereas they are in agreement with our results in the HCT116 model. Moreover, trials in human colorectal cancer with different drugs have failed to demonstrate a favorable prognostic role for elevated p21 expression in overall survival (reviewed in [53]). This observation is at odds with an anti-apoptotic function of p21 in human colon cancer cells. We conclude that p21 does not have a protective effect on drug-induced cell death in the HCT116 model and that the role of p21 in colon cancer cell apoptosis should be re-evaluated.

Conflicts of interest

None.

Acknowledgements

We are indebted to Pilar Frade, Saray Pereda, Maria Aramburu and Elsa Martínez for technical assistance. We are grateful to Dr. Bert Vogelstein for HCT116 cell lines, Carmen Marin and Amancio Carnero for plasmid constructs, Novartis for imatinib and AstraZeneca for gefitinib. NF is funded by a predoctoral fellowship from the Spanish Ministry of Education and Science (MEC) and from the University of Cantabria. Work at the laboratory of JL is funded by MEC grants SAF2005-00461 and Spanish Ministry of Health and Consume (MSC) grant ISCIII-RETIC-RD06/0020. MDD is funded by MSC grant FIS04-1083, and JMP is funded by grants from Fundación de Investigación Médica Mutua Madrileña and MEC grant SAF2006-00371.

Appendix A. Supplementary data

Supplementary data associated with this article can be found, in the online version, at doi:10.1016/j.dnarep.2008.12.001.

References

[1] J.W. Harper, G.R. Adami, N. Wei, K. Keyomarsi, S.J. Elledge, The p21 Cdk-interacting protein Cip1 is a potent inhibitor of G1 cyclin-dependent kinases, Cell 75 (1993) 805–816.

[2] Y. Gu, C.W. Turck, D.O. Morgan, Inhibition of CDK2 activity in vivo by an associated 20K regulatory subunit, Nature 366 (1993) 707–710.

[3] V. Dulic, W.K. Kaufmann, S.J. Wilson, T.D. Tlsty, E. Lees, J.W. Harper, S.J. Elledge, S.I. Reed, p53-dependent inhibition of cyclin-dependent kinase activities in human fibroblasts during radiation-induced G1 arrest, Cell 76 (1994) 1013–1023.

[4] M. Serrano, G.J. Hannon, D. Beach, A new regulatory motif in cell-cycle control causing specific inhibition of cyclin D/CDK4, Nature 366 (1993) 704–707.

[5] O. Coqueret, New roles for p21 and p27 cell-cycle inhibitors: a function for each cell compartment? Trends Cell Biol. 13 (2003) 65–70.

[6] R.H. Weiss, p21Waf1/Cip1 as a therapeutic target in breast and other cancers, Cancer Cell 4 (2003) 425–429.

[7] R.U. Janicke, D. Sohn, F. Essmann, K. Schulze-Osthoff, The multiple battles fought by anti-apoptotic p21, Cell Cycle 6 (2007) 407–413.

[8] A.L. Gartel, A.L. Tyner, The role of the cyclin-dependent kinase inhibitor p21 in apoptosis, Mol. Cancer Ther. 1 (2002) 639–649.

[9] J. Brugarolas, C. Chandrasekaran, J.I. Gordon, D. Beach, T. Jacks, G.J. Hannon, Radiation-induced cell cycle arrest compromised by p21 deficiency, Nature 377 (1995) 552–557.

[10] C. Deng, P. Zhang, J.W. Harper, S.J. Elledge, P. Leder, Mice lacking p21CIP1/WAF1 undergo normal development, but are defective in G1 checkpoint control, Cell 82 (1995) 675–684.

[11] A. Efeyan, M. Collado, S. Velasco-Miguel, M. Serrano, Genetic dissection of the role of p21Cip1/Waf1 in p53-mediated tumour suppression, Oncogene 26 (2007) 1645–1649.

[12] J. Martin-Caballero, J.M. Flores, P. Garcia-Palencia, M. Serrano, Tumor susceptibility of p21(Waf1/Cip1)-deficient mice, Cancer Res. 61 (2001) 6234–6238.

[13] J. Philipp, K. Vo, K.E. Gurley, K. Seidel, C.J. Kemp, Tumor suppression by p27Kip1 and p21Cip1 during chemically induced skin carcinogenesis, Oncogene 18 (1999) 4689–4698.

[14] A.J. Poole, D. Heap, R.E. Carroll, A.L. Tyner, Tumor suppressor functions for the Cdk inhibitor p21 in the mouse colon, Oncogene 23 (2004) 8128–8134.

[15] G.I. Topley, R. Okuyama, J.G. Gonzales, C. Conti, G.P. Dotto, p21(WAF1/Cip1) functions as a suppressor of malignant skin tumor formation and a determinant of keratinocyte stem-cell potential, Proc. Natl. Acad. Sci. U.S.A. 96 (1999) 9089–9094.

[16] R.J. Jackson, R.W. Engelman, D. Coppola, A.B. Cantor, W. Wharton, W.J. Pledger, p21Cip1 nullizygosity increases tumor metastasis in irradiated mice, Cancer Res. 63 (2003) 3021–3025.

[17] M.A. Shibata, K. Yoshidome, E. Shibata, C.L. Jorcyk, J.E. Green, Suppression of mammary carcinoma growth in vitro and in vivo by inducible expression of the Cdk inhibitor p21, Cancer Gene Ther. 8 (2001) 23–35.

[18] V. Chopin, C. Slomianny, H. Hondermarck, X. Le Bourhis, Synergistic induction of apoptosis in breast cancer cells by cotreatment with butyrate and TNF-alpha, TRAIL, or anti-Fas agonist antibody involves enhancement of death receptors' signaling and requires P21(waf1), Exp Cell Res. 298 (2004) 560–573.

[19] S. Kondo, B.P. Barna, Y. Kondo, Y. Tanaka, G. Casey, J. Liu, T. Morimura, R. Kaakaji, J.W. Peterson, B. Werbel, G.H. Barnett, WAF1/CIP1 increases the susceptibility of p53 non-functional malignant glioma cells to cisplatin-induced apoptosis, Oncogene 13 (1996) 1279–1285.

[20] K. Fujiwara, S. Daido, A. Yamamoto, R. Kobayashi, T. Yokoyama, H. Aoki, E. Iwado, N. Shinojima, Y. Kondo, S. Kondo, Pivotal role of the cyclin-dependent kinase inhibitor p21WAF1/CIP1 in apoptosis and autophagy, J. Biol. Chem. 283 (2008) 388–397.

[21] T. Waldman, K.W. Kinzler, B. Vogelstein, p21 is necessary for the p53-mediated G1 arrest in human cancer cells, Cancer Res. 55 (1995) 5187–5190.

[22] F. Bunz, P.M. Hwang, C. Torrance, T. Waldman, Y. Zhang, L. Dillehay, J. Williams, C. Lengauer, K.W. Kinzler, B. Vogelstein, Disruption of p53 in human cancer cells alters the responses to therapeutic agents, J. Clin. Invest. 104 (1999) 263–269.

[23] R. Capdeville, E. Buchdunger, J. Zimmermann, A. Matter, Glivec (STI571, imatinib), a rationally developed, targeted anticancer drug, Nat. Rev. Drug Discov. 1 (2002) 493–502.

[24] B.J. Druker, Perspectives on the development of a molecularly targeted agent, Cancer Cell 1 (2002) 31–36.

[25] M.J. Munoz-Alonso, J.C. Acosta, C. Richard, M.D. Delgado, J. Sedivy, J. Leon, p21Cip1 and p27Kip1 induce distinct cell cycle effects and differentiation programs in myeloid leukemia cells, J. Biol. Chem. 280 (2005) 18120–18129.

[26] V. Devgan, C. Mammucari, S.E. Millar, C. Brisken, G.P. Dotto, p21WAF1/Cip1 is a negative transcriptional regulator of Wnt4 expression downstream of Notch1 activation, Genes Dev. 19 (2005) 1485–1495.

[27] T.R. Brummelkamp, R. Bernards, R. Agami, A system for stable expression of short interfering RNAs in mammalian cells, Science 296 (2002) 550–553.

[28] T. Bowman, H. Symonds, L. Gu, C. Yin, M. Oren, T. Van Dyke, Tissue-specific inactivation of p53 tumor suppression in the mouse, Genes Dev. 10 (1996) 826–835.

[29] F. Bunz, A. Dutriaux, C. Lengauer, T. Waldman, S. Zhou, J.P. Brown, J.M. Sedivy, K.W. Kinzler, B. Vogelstein, Requirement for p53 and p21 to sustain G2 arrest after DNA damage, Science 282 (1998) 1497–1501.

[30] R.S. Herbst, M. Fukuoka, J. Baselga, Gefitinib—a novel targeted approach to treating cancer, Nat. Rev. Cancer 4 (2004) 956–965.

[31] I. Sturm, B. Rau, P.M. Schlag, P. Wust, B. Hildebrandt, H. Riess, S. Hauptmann, B. Dorken, P.T. Daniel, Genetic dissection of apoptosis and cell cycle control in response of colorectal cancer treated with preoperative radiochemotherapy, BMC Cancer 6 (2006) 124.

[32] T.A. Chan, P.M. Hwang, H. Hermeking, K.W. Kinzler, B. Vogelstein, Cooperative effects of genes controlling the G(2)/M checkpoint, Genes Dev. 14 (2000) 1584–1588.

[33] M. Mahyar-Roemer, K. Roemer, p21 Waf1/Cip1 can protect human colon carcinoma cells against p53-dependent and p53-independent apoptosis induced by natural chemopreventive and therapeutic agents, Oncogene 20 (2001) 3387–3398.

[34] A. Sirvent, A. Boureux, V. Simon, C. Leroy, S. Roche, The tyrosine kinase Abl is required for Src-transforming activity in mouse fibroblasts and human breast cancer cells, Oncogene 27 (2008) 3494–3500.

[35] NiculescuF A.B. III, X. Chen, M. Smeets, L. Hengst, C. Prives, S.I. Reed, Effects of p21(Cip1/Waf1) at both the G1/S and the G2/M cell cycle transitions: pRb is a critical determinant in blocking DNA replication and in preventing endoreduplication, Mol. Cell. Biol. 18 (1998) 629–643.

[36] V. Dulic, G.H. Stein, D.F. Far, S.I. Reed, Nuclear accumulation of p21Cip1 at the onset of mitosis: a role at the G2/M-phase transition, Mol. Cell. Biol. 18 (1998) 546–557.

[37] R. Ravizza, M.B. Gariboldi, L. Passarelli, E. Monti, Role of the p53/p21 system in the response of human colon carcinoma cells to Doxorubicin, BMC Cancer 4 (2004) 92.

[38] J. Seoane, H.V. Le, J. Massague, Myc suppression of the p21(Cip1) Cdk inhibitor influences the outcome of the p53 response to DNA damage, Nature 419 (2002) 729–734.

[39] S. Wu, C. Cetinkaya, M.J. Munoz-Alonso, N. von der Lehr, F. Bahram, V. Beuger, M. Eilers, J. Leon, L.G. Larsson, Myc represses differentiation-induced p21CIP1 expression via Miz-1-dependent interaction with the p21 core promoter, Oncogene 22 (2003) 351–360.

[40] D. Javelaud, F. Besancon, Inactivation of p21WAF1 sensitizes cells to apoptosis via an increase of both p14ARF and p53 levels and an alteration of the Bax/Bcl-2 ratio, J. Biol. Chem. 277 (2002) 37949–37954.

[41] E.V. Broude, Z.N. Demidenko, C. Vivo, M.E. Swift, B.M. Davis, M.V. Blagosklonny, I.B. Roninson, p21 (CDKN1A) is a negative regulator of p53 stability, Cell Cycle 6 (2007) 1468–1471.

[42] P.G. Hemmati, G. Normand, B. Verdoodt, C. von Haefen, A. Hasenjager, D. Guner, J. Wendt, B. Dorken, P.T. Daniel, Loss of p21 disrupts p14 ARF-induced G1 cell cycle arrest but augments p14 ARF-induced apoptosis in human carcinoma cells, Oncogene 24 (2005) 4114–4128.

[43] D. Sohn, F. Essmann, K. Schulze-Osthoff, R.U. Janicke, p21 blocks irradiation-induced apoptosis downstream of mitochondria by inhibition of cyclin-dependent kinase-mediated caspase-9 activation, Cancer Res. 66 (2006) 11254–11262.

[44] H.G. Wendel, E. de Stanchina, E. Cepero, S. Ray, M. Emig, J.S. Fridman, D.R. Veach, W.G. Bornmann, B. Clarkson, W.R. McCombie, S.C. Kogan, A. Hochhaus, S.W. Lowe, Loss of p53 impedes the antileukemic response to BCR-ABL inhibition, Proc. Natl. Acad. Sci. U.S.A. 103 (2006) 7444–7449.

[45] Z. Goldberg, Y. Levav, S. Krichevsky, E. Fibach, Y. Haupt, Treatment of chronic myeloid leukemia cells with imatinib (STI571) impairs p53 accumulation in response to DNA damage, Cell Cycle 3 (2004) 1188–1195.

[46] N. Burri, P. Shaw, H. Bouzourene, I. Sordat, B. Sordat, M. Gillet, D. Schorderet, F.T. Bosman, P. Chaubert, Methylation silencing and mutations of the p14ARF and p16INK4a genes in colon cancer, Lab. Invest. 81 (2001) 217–229.

[47] Y. Levav-Cohen, Z. Goldberg, V. Zuckerman, T. Grossman, S. Haupt, Y. Haupt, C-Abl as a modulator of p53, Biochem. Biophys. Res. Commun. 331 (2005) 737–749.

[48] I.B. Roninson, Oncogenic functions of tumour suppressor p21(Waf1/Cip1/Sdi1): association with cell senescence and tumour-promoting activities of stromal fibroblasts, Cancer Lett. 179 (2002) 1–14.

[49] J. Martin-Caballero, J.M. Flores, P. Garcia-Palencia, M. Collado, M. Serrano, Different cooperating effect of p21 or p27 deficiency in combination with INK4a/ARF deletion in mice, Oncogene (2004).

[50] R. Hill, A.M. Leidal, P.A. Madureira, L.D. Gillis, H.K. Cochrane, D.M. Waisman, A. Chiu, P.W. Lee, Hypersensitivity to chromium-induced DNA damage correlates with constitutive deregulation of upstream p53 kinases in $p21^{-/-}$ HCT116 colon cancer cells, DNA Repair 7 (2008) 239–252.

[51] W.C. Yang, J. Mathew, A. Velcich, W. Edelmann, R. Kucherlapati, M. Lipkin, K. Yang, L.H. Augenlicht, Targeted inactivation of the p21(WAF1/cip1) gene enhances Apc-initiated tumor formation and the tumor-promoting activity of a Western-style high-risk diet by altering cell maturation in the intestinal mucosal, Cancer Res. 61 (2001) 565–569.

[52] W. Yang, A. Velcich, I. Lozonschi, J. Liang, C. Nicholas, M. Zhuang, L. Bancroft, L.H. Augenlicht, Inactivation of p21WAF1/cip1 enhances intestinal tumor formation in $Muc2^{-/-}$ mice, Am. J. Pathol. 166 (2005) 1239–1246.

[53] J.I. Geller, K. Szekely-Szucs, I. Petak, B. Doyle, J.A. Houghton, P21Cip1 is a critical mediator of the cytotoxic action of thymidylate synthase inhibitors in colorectal carcinoma cells, Cancer Res. 64 (2004) 6296–6303.

2.3 Genexpressionsmuster

Hintergrund:

Neben der Identifizierung einzelner Gene, die in der Genese eines bestimmten Malignomes (z.B. Neuroblastom) auch potentiell eine funktionelle Bedeutung haben können (*Berwanger et al., 2002, Weber et al., 2008*), können über Microarrayuntersuchungen auch ganze Genexpressionsmuster dargestellt werden, die eine Prognose-relevante Zuordnung von Patienten in verschiedene Subgruppen zulassen. Dabei ist die funktionelle Bedeutung der einzelnen Gene nebensächlich.

In einer vorangegangenen Studie konnten Oberthuer und Kollegen ein Genexpressionsmuster von 144 Genen identifizieren, mit dem unabhängig von anderen klinischen Parametern eine prognostische Einteilung der n=77 untersuchten Neuroblastomen möglich war (*Oberthuer et al., 2006*).

In einer weiteren Studie wurde dieses Genexpressionsmuster nun an einer weiteren, unabhängigen Patientenkohorte auf seine Eignung als prognostischer Marker hin untersucht.

Eigene Publikation:

Oberthuer A, Hero B, Berthold F, Juraeva D, Faldum A, Kahlert Y, Asgharzadeh S, Seeger R, Scaruffi P, Tonini GP, Janoueix-Lerosey I, Delattre O, Schleiermacher G, Vandesompele J, Vermeulen J, Speleman F, Noguera R, Piqueras M, Bénard J, Valent A, Avigad S, Yaniv I, **Weber A**, Christiansen H, Grundy RG, Schardt K, Schwab M, Eils R, Warnat P, Kaderali L, Simon T, Decarolis B, Theissen J, Westermann F, Brors B, Fischer M. Prognostic impact of gene expression-based classification for neuroblastoma. *J Clin Oncol*. 2010 Jul 20;28(21):3506-15.

IF (Stand 2010): 17,793

In dieser Studie konnte der aus dem Genexpressionsprofil der zuvor 144 identifizierten Gene entwickelte Zuordnungsalgorithmus (**P**rediction **a**nalysis for **m**icroarrays (PAM)-Classifier) an insgesamt n=440 weiteren, international rekrutierten Neuroblastompatienten validiert werden. 125 Patienten wurden dabei prospektiv untersucht. Der PAM-Classifier zeigte sich sowohl in den retrospektiv, als auch in den prospektiv untersuchten Patienten als zuverlässiger und hoch signifikanter Prädiktor sowohl für das Ereignis-freie-Überleben (event free survival (EFS)) als auch das Gesamt-Überleben (overall survival (OS)). Mittels des PAM-Classifiers konnte auch in aufgrund klinischer Eigenschaften gebildeter Untergruppen (z.B. Stadien, Alter) zwischen gut und schlecht prognostischen Neuroblastomen unterschieden werden. Die größte Signifikanz erreichte der PAM-Classifier in der Untergruppe der Patienten mit einem niedrigen Risiko (niedriges Tumorstadium (1, 2 oder 3), Alter <18 Monate bei Diagnosestellung, keine *MYCN* Amplifikation). In der Untergruppe der Hoch-Risiko Patienten, die bei Diagnosestellung ein Stadium 4 aufwiesen aber keine *MYCN* Amplifikation nachgewiesen hatten (n=66), konnte mit dem PAM-Classifier keine prognostisch relevante Aussage getroffen werden. Des Weiteren konnte der PAM-Classifier auch in der Untergruppe der *MYCN* amplifizierten Patienten (Stadium unabhängig) (n=64) nicht zwischen guter und schlechter Prognose unterscheiden. Die Relevanz der Betrachtung dieser Subgruppen ist jedoch fraglich, da die Anzahl der beobachteten Patienten in solchen Untergruppen, bezogen auf die ohnehin sehr schlechte Prognose, relativ klein ist.

VOLUME 28 · NUMBER 21 · JULY 20 2010

JOURNAL OF CLINICAL ONCOLOGY

ORIGINAL REPORT

Prognostic Impact of Gene Expression–Based Classification for Neuroblastoma

André Oberthuer, Barbara Hero, Frank Berthold, Dilafruz Juraeva, Andreas Faldum, Yvonne Kahlert, Shahab Asgharzadeh, Robert Seeger, Paola Scaruffi, Gian Paolo Tonini, Isabelle Janoueix-Lerosey, Olivier Delattre, Gudrun Schleiermacher, Jo Vandesompele, Joëlle Vermeulen, Frank Speleman, Rosa Noguera, Marta Piqueras, Jean Bénard, Alexander Valent, Smadar Avigad, Isaac Yaniv, Axel Weber, Holger Christiansen, Richard G. Grundy, Katharina Schardt, Manfred Schwab, Roland Eils, Patrick Warnat, Lars Kaderali, Thorsten Simon, Boris DeCarolis, Jessica Theissen, Frank Westermann, Benedikt Brors, and Matthias Fischer

From the University of Cologne, Cologne; University Clinic Mainz, Mainz; University of Leipzig, Leipzig; German Cancer Research Center, Heidelberg, Germany; Children's Hospital Los Angeles, Los Angeles, CA; National Institute for Cancer Research, Genoa, Italy; Institut Curie, Paris; Institut Gustave Roussy, Villejuif, France; Ghent University Hospital, Ghent, Belgium; University of Valencia, Valencia, Spain; Schneider Children's Medical Center of Israel, Petah Tikva; Tel Aviv University, Tel Aviv, Israel; and University of Leicester, United Kingdom.

Submitted December 4, 2009; accepted May 5, 2010; published online ahead of print at www.jco.org on June 21, 2010.

Supported by Grants No. 50-2719-Fi1 and 106847 (M.F.) from the Deutsche Krebshilfe, 01GS0456 (M.F., A.O., F.B.) from the Bundesministerium für Bildung und Forschung through the National Genome Research Network 2, 01GS0895 (M.F.) from the National Genome Research Network plus, and RD06/0020/0102 (R.N.) from the Red Temática de Investigación Cooperativa en Cáncer, and by Auerbach-Stiftung, the Italian Neuroblastoma Foundation (P.S. and G.P.T.), Competence Network Pediatric Oncology and Hematology, and the Fördergesellschaft Kinderkrebs-Neuroblastom-Forschung e.V.

Authors' disclosures of potential conflicts of interest and author contributions are found at the end of this article.

Corresponding author: Matthias Fischer, MD, University Children's Hospital of Cologne, Department of Pediatric Oncology, Kerpener Str. 62, 50924 Cologne, Germany; e-mail: matthias.fischer@uk-koeln.de.

© 2010 by American Society of Clinical Oncology

0732-183X/10/2821-3506/$20.00

DOI: 10.1200/JCO.2009.27.3367

ABSTRACT

Purpose
To evaluate the impact of a predefined gene expression–based classifier for clinical risk estimation and cytotoxic treatment decision making in neuroblastoma patients.

Patients and Methods
Gene expression profiles of 440 internationally collected neuroblastoma specimens were investigated by microarray analysis, 125 of which were examined prospectively. Patients were classified as either favorable or unfavorable by a 144-gene prediction analysis for microarrays (PAM) classifier established previously on a separate set of 77 patients. PAM classification results were compared with those of current prognostic markers and risk estimation strategies.

Results
The PAM classifier reliably distinguished patients with contrasting clinical courses (favorable [n = 249] and unfavorable [n = 191]; 5-year event free survival [EFS] 0.84 ± 0.03 *v* 0.38 ± 0.04; 5-year overall survival [OS] 0.98 ± 0.01 *v* 0.56 ± 0.05, respectively; both $P < .001$). Moreover, patients with divergent outcome were robustly discriminated in both German and international cohorts and in prospectively analyzed samples ($P \leq .001$ for both EFS and OS for each). In subgroups with clinical low-, intermediate-, and high-risk of death from disease, the PAM predictor significantly separated patients with divergent outcome (low-risk 5-year OS: 1.0 *v* 0.75 ± 0.10, $P < .001$; intermediate-risk: 1.0 *v* 0.82 ± 0.08, $P = .042$; and high-risk: 0.81 ± 0.08 *v* 0.43 ± 0.05, $P = .001$). In multivariate Cox regression models based on both EFS and OS, PAM was a significant independent prognostic marker (EFS: hazard ratio [HR], 3.375; 95% CI, 2.075 to 5.492; $P < .001$; OS: HR, 11.119, 95% CI, 2.487 to 49.701; $P < .001$). The highest potential clinical impact of the classifier was observed in patients currently considered as non–high-risk (n = 289; 5-year EFS: 0.87 ± 0.02 *v* 0.44 ± 0.07; 5-year OS: 1.0 *v* 0.80 ± 0.06; both $P < .001$).

Conclusion
Gene expression–based classification using the 144-gene PAM predictor can contribute to improved treatment stratification of neuroblastoma patients.

J Clin Oncol 28:3506-3515. © 2010 by American Society of Clinical Oncology

INTRODUCTION

Neuroblastoma accounts for roughly 8% of childhood cancers and 15% of pediatric oncology deaths.[1] The natural courses of the disease are remarkably heterogeneous. Whereas therapy-resistant progression is frequently observed in older children with disseminated disease, spontaneous regression or differentiation into benign ganglioneuroma occurs regularly in infants. Accordingly, treatment protocols vary from a wait-and-see approach for patients with expected spontaneous regression to intense multimodal treatments for high-risk patients. The broad range of clinical phenotypes and the divergence of corresponding therapeutic regimens make accurate risk estimation at the time of diagnosis an essential prerequisite for therapeutic decisions. Currently, clinical trials stratify patients into prognostic subgroups with expected low, intermediate, and high risk of death from disease by using a limited number of variables, including stage of disease,[2] age at diagnosis,[3,4] *MYCN* amplification,[5] histopathologic classification,[6] allelic loss of chromosomal regions at 1p and 11q,[7,8] and DNA ploidy.[9,10] While

Information downloaded from jco.ascopubs.org and provided by at UNIVERSITAETSKLINIKUM LEIPZIG on August 27, 2010 from 139.18.235.200
Copyright © 2010 American Society of Clinical Oncology. All rights reserved.

such classification systems largely succeed in discriminating patients with divergent outcome, some low- and intermediate-risk patients still die from disease, which indicates the presence of biologically unfavorable tumors in these subgroups. Moreover, results from neuroblastoma mass screening programs[11-13] and recent prospective clinical trials[14] indicated that the frequency of spontaneous regression might have been underestimated in the past, suggesting that chemotherapy may be spared in a substantial fraction of children.

In recent years, several studies provided strong evidence that clinically relevant neuroblastoma subgroups differ molecularly on both the genomic and the transcriptome level.[15] It has therefore been suggested that risk assessment of neuroblastoma patients could be

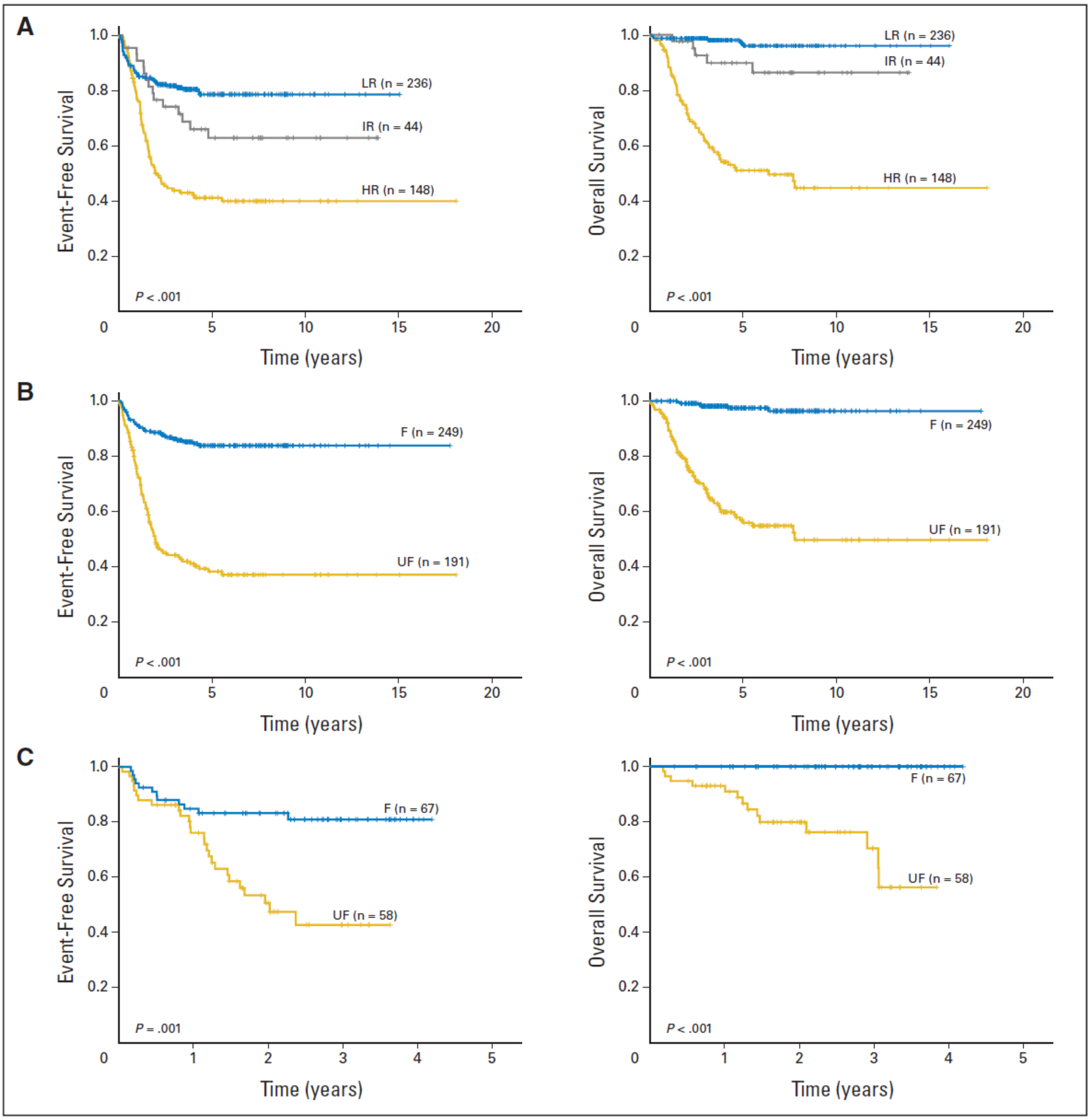

Fig 1. Comparison of neuroblastoma risk stratification according to the German neuroblastoma trial NB2004, the 144-gene prediction analysis for microarrays (PAM) classifier, and prognostic performance of the classifier in prospectively analyzed patients. Kaplan-Meier estimates for event-free survival and overall survival for (A) all 440 patients stratified according to the NB2004 trial, (B) the same 440-patient set according to classification results of the 144-gene PAM classifier, and (C) 125 patients whose tumor samples had been collected and analyzed prospectively, according to classification results of the 144-gene PAM classifier. LR, low risk; IR, intermediate risk, HR, high risk; F, favorable; UF, unfavorable.

Information downloaded from jco.ascopubs.org and provided by at UNIVERSITAETSKLINIKUM LEIPZIG on August 27, 2015 from 139.18.235.208
Copyright © 2010 American Society of Clinical Oncology. All rights reserved.

Table 1. Summary of Kaplan-Meier Estimates for EFS and OS Based on the Classification Result of the 144-Gene PAM Prediction After Subdividing Patients Into Subcohorts According to Either Single Prognostic Markers or Combinations of Prognostic Markers

	PAM Favorable			PAM Unfavorable			
Marker	Survival Probability	SD	No. of Patients	Survival Probability	SD	No. of Patients	*P*
Total cohort (n = 440)			249			191	
5-year EFS	0.84	0.03		0.38	0.04		< .001
5-year OS	0.98	0.01		0.56	0.04		< .001
Stage 1 (n = 100)			87			13	
5-year EFS	0.97	0.02		0.39	0.19		< .001
5-year OS	1.0			0.82	0.12		< .001
Stage 2 (n = 72)			58			14	
5-year EFS	0.83	0.05		0.41	0.16		.005
5-year OS	1.0			0.42	0.21		< .001
Stage 3 (n = 73)			41			32	
5-year EFS	0.78	0.07		0.35	0.09		.002
5-year OS	1.0			0.59	0.10		.001
Stage 4 (n = 142)			33			109	
5-year EFS	0.72	0.08		0.34	0.05		< .001
5-year OS	0.84	0.07		0.49	0.05		.001
Stage 4S (n = 53)			30			23	
5-year EFS	0.73	0.11		0.61	0.10		.061
5-year OS	1.0			0.83	0.08		.018
< 18 months of age (n = 284)			202			82	
5-year EFS	0.85	0.03		0.54	0.06		< .001
5-year OS	1.0			0.79	0.05		< .001
> 18 months of age (n = 155)			46			109	
5-year EFS	0.78	0.07		0.28	0.05		< .001
5-year OS	0.87	0.06		0.43	0.05		< .001
MYCN amplification (n = 64)			1			63	
5-year EFS	1.0			0.34	0.06		.30
5-year OS	1.0			0.34	0.07		.31
Del/Imb 1p36 (n = 92)			22			70	
5-year EFS	0.86	0.07		0.49	0.06		.001
5-year OS	0.91	0.06		0.53	0.07		.003
Del/Imb 11q (n = 79)			27			52	
5-year EFS	0.77	0.08		0.28	0.08		< .001
5-year OS	0.88	0.07		0.62	0.08		.022
NB2004 low risk (n = 236)			194			42	
5-year EFS	0.85	0.03		0.48	0.10		< .001
5-year OS	1.0			0.75	0.10		< .001
NB2004 intermediate risk (n = 44)			17			27	
5-year EFS	1.0			0.36	0.10		< .001
5-year OS	1.0			0.82	0.08		.042
NB2004 high risk (n = 148)			28			120	
5-year EFS	0.67	0.09		0.35	0.05		.001
5-year OS	0.81	0.08		0.43	0.05		.001
Stages 1 to 3 *MYCN* single-copy (n = 222)			183			39	
5-year EFS	0.88	0.02		0.35	0.1		< .001
5-year OS	1.0			0.72	0.1		< .001
Stages 4 and 4S *MYCN* single copy < 18 months of age (n = 85)			48			37	
5-year EFS	0.83	0.06		0.57	0.09		.004
5-year OS	1.0			0.86	0.06		.009
Stage 4 *MYCN* single copy > 18 months of age (n = 66)			15			51	
5-year EFS	0.46	0.13		0.32	0.07		.10
5-year OS	0.64	0.13		0.49	0.08		.35
NB2004 low-risk + intermediate-risk (n = 289)			218			71	
5-year EFS	0.87	0.02		0.44	0.07		< .001
5-year OS	1.0			0.80	0.06		< .001
German patients total cohort (n = 325)			197			128	
5-year EFS	0.83	0.03		0.39	0.05		< .001
5-year OS	1.0			0.62	0.06		< .001

(continued on following page)

Information downloaded from jco.ascopubs.org and provided by at UNIVERSITAETSKLINIKUM LEIPZIG on August 27, 2010 from 139.18.235.208
Copyright © 2010 American Society of Clinical Oncology. All rights reserved.

Table 1. Summary of Kaplan-Meier Estimates for EFS and OS Based on the Classification Result of the 144-Gene PAM Prediction After Subdividing Patients Into Subcohorts According to Either Single Prognostic Markers or Combinations of Prognostic Markers (continued)

	PAM Favorable			PAM Unfavorable			
Marker	Survival Probability	SD	No. of Patients	Survival Probability	SD	No. of Patients	*P*
German patients prospectively analyzed (n = 125)			67			58	
3-year EFS	0.81	0.05		0.43	0.08		.001
3-year OS	1.0			0.70	0.08		< .001
International patients total cohort (n = 115)			52			63	
5-year EFS	0.89	0.05		0.33	0.06		< .001
5-year OS	0.91	0.04		0.44	0.06		< .001

Abbreviations: EFS, event-free survival; OS, overall survival; PAM, prediction analysis for microarrays; Del, deletion; Imb, imbalance; NB2004, German neuroblastoma trial.

improved by complex molecular markers. We have previously reported on a prognostic gene expression–based classifier[16] that had been designed on a training set of 77 patients to distinguish patients requiring intense chemotherapy from those who may recover following a wait-and-see strategy. In this study, we now determine the prognostic value of this classifier in a validation cohort of 440 primary neuroblastoma patients from multiple international pediatric oncology centers, 125 of which were examined prospectively, and evaluate its potential utility as a prognostic marker in clinical practice.

PATIENTS AND METHODS

Patients

This study consisted of 440 patients from nine centers in eight countries: Belgium, n = 9 (2.0%); France (two centers), n = 29 (6.6%); Germany, n = 325 (73.9%); Israel, n = 7 (1.6%); Italy, n = 17 (3.9%); Spain, n = 14 (3.2%); United Kingdom, n = 5 (1.1%); and United States, n = 34 (7.7%). Tumors of 125 patients diagnosed with neuroblastoma after October 1, 2004, were analyzed prospectively as part of the German neuroblastoma trial NB2004. All patients were registered in the respective clinical trials with informed consent. Patients' age at diagnosis ranged from 0 to 305 months (median age, 12 months). Median follow-up for patients without fatal events was 4.7 years (range, 0.3 to 18.1 years). Five-year event-free survival (EFS) of the total cohort was 0.65 $\pm$ 0.02, and 5-year overall survival (OS) was 0.80 $\pm$ 0.02. Stage was classified according to the International Neuroblastoma Staging System (INSS)[2]: stage 1, n = 100 (*MYCN* amplified [MNA], n = 3); stage 2, n = 72 (MNA, n = 3); stage 3, n = 73 (MNA, n = 15); stage 4, n = 142 (MNA, n = 38); and stage 4S, n = 53 (MNA, n = 5). Response to treatment was defined according to the revised criteria of the International Neuroblastoma Response Criteria (INRC)[2]. Chromosomal alterations were defined according to the guidelines of the European Neuroblastoma Quality Assessment Group.[17]

Gene Expression Analyses and Supervised Classification

Gene expression profiles were generated as dye-flipped, dual-color replicates from 1 μg of total tumor RNA using customized 11K oligonucleotide microarrays as described.[16] A detailed description of the experimental procedures is indicated in the Patients and Methods section of the Appendix (online only). All raw and normalized microarray data are available at the ArrayExpress database (http://www.ebi.ac.uk/arrayexpress; Accession: E-MTAB-161). Supervised class prediction analysis was performed using the nearest shrunken centroids method (prediction analysis for microarrays [PAM])[18]), expression values of 144 predefined signature genes, and classification rules as described.[16]

Statistical Analysis

Kaplan-Meier estimates for EFS and OS were calculated and compared by log-rank test. Recurrence, progression, and death from disease were considered as events. Cox regression models were applied using a stepwise variable selection procedure recommended by Collett[19] to analyze the prognostic value of potentially prognostic factors. Model building is fully described in the Patients and Methods section of the Appendix.

RESULTS

Prognostic Performance and Robustness of the 144-Gene PAM Classifier

To test the predictive power of the 144-gene PAM classifier, 440 neuroblastoma specimens reflecting the full spectrum of the disease's courses were collected from eight different countries (Data Supplement Table DS1). Risk stratification according to the German neuroblastoma trial NB2004[20,21] was applied to all patients: 236 were categorized as low risk, 44 as intermediate risk, and 148 as high risk. Three patients could not be stratified because of missing *MYCN* status, and nine patients could not be differentiated between low or intermediate risk because of missing chromosome 1p status. Risk stratification according to NB2004 significantly discriminated patients with different EFS and OS (NB2004 low risk: 5-year EFS, 0.79 $\pm$ 0.03 and 5-year OS, 0.96 $\pm$ 0.02; intermediate risk: 5-year EFS, 0.63 $\pm$ 0.08 and 5-year OS, 0.90 $\pm$ 0.05; high risk: 5-year EFS, 0.41 $\pm$ 0.04 and 5-year OS, 0.51 $\pm$ 0.05; all $P < .001$; Fig 1A). In comparison, application of the 144-gene PAM classifier also significantly discriminated patients with divergent outcome (PAM favorable [n = 249]: 5-year EFS, 0.84 $\pm$ 0.03 and 5-year OS, 0.98 $\pm$ 0.01; PAM unfavorable [n = 191]: 5-year EFS, 0.38 $\pm$ 0.04 and 5-year OS, 0.56 $\pm$ 0.04; both $P < .001$; Fig 1B). All Kaplan-Meier analyses are summarized in Table 1.

To evaluate the robustness of the classifier, patient cohorts obtained from German and from international centers were analyzed separately (n = 325 and n = 115, respectively). In both cohorts, PAM reliably distinguished patients with divergent EFS and OS ($P < .001$ each, Data Supplement Figs DS3 and DS4). Additionally, the prognostic performance of the classifier was determined in a set of patients whose tumor specimens had been collected and analyzed prospectively as part of the NB2004 trial (n = 125). Again, patients with favorable and unfavorable clinical courses were accurately discriminated (PAM favorable [n = 67]: 3-year EFS, 0.81 $\pm$ 0.05 and 3-year OS, 1.0; PAM unfavorable [n = 58]: 3-year EFS, 0.43 $\pm$ 0.08 and 3-year OS, 0.70 $\pm$ 0.08; both $P \leq .001$, Fig 1C).

© 2010 by American Society of Clinical Oncology

Information downloaded from jco.ascopubs.org and provided by at UNIVERSITAETSKLINIKUM LEIPZIG on August 27, 2013 from 139.18.235.208
Copyright © 2010 American Society of Clinical Oncology. All rights reserved.

Performance of the PAM Classifier Within Patient Subgroups Defined by Current Prognostic Markers

Next, we assessed PAM classification results in patient subgroups defined by currently used prognostic markers. Intriguingly, the PAM predictor correctly identified all children with fatal outcome in the cohort of patients age $<$ 18 months of age with stage 1, 2, 3, and 4S disease and in patients with amplified *MYCN* (Data Supplement Figs DS1A-DS1C, DS1E, DS2A, and DS2C). Furthermore, significant discrimination of contrasting outcome was observed in patients with stage 4 disease, age $>$ 18 months, and those with an allelic deletion of 1p or 11q (Data Supplement Figs DS1D, DS2B, DS2D, and DS2E).

Despite these results, it was appreciated that current risk stratification is based on a combination of several of the above-mentioned single markers. Therefore, the performance of the PAM classifier was evaluated in subcohorts of patients considered as low, intermediate, and high risk, according to the NB2004 trial. Of 236 patients classified as low risk by NB2004, 194 were also classified as favorable by PAM and had an excellent outcome (5-year EFS, 0.85 ± 0.03 and 5-year OS, 1.0). The 42 patients classified as unfavorable by PAM had a significantly worse EFS and OS (0.48 ± 0.10 and 0.75 ± 0.10, respectively; both $P < .001$; Fig 2A). Likewise, intermediate-risk patients predicted as unfavorable by PAM (n = 27) had a poor EFS of 0.36 ± 0.10 and an OS of 0.82 ± 0.08, whereas no events were observed in those 17 intermediate-risk patients who were classified as favorable by PAM ($P < .001$ for EFS and $P = .042$ for OS; Fig 2B). Finally, within the cohort of 148 NB2004 high-risk patients, gene expression–based classification also separated subgroups with significantly differing EFS and OS (favorable [n = 28]: EFS, 0.67 ± 0.09 and OS, 0.81 ± 0.08 *v* unfavorable [n = 120]: EFS, 0.35 ± 0.05 and OS, 0.43 ± 0.05; both $P = .001$; Fig 2C).

Multivariate Cox Regression Analysis

To further assess the performance of the PAM classifier, multivariable Cox regression models were applied to analyze the prognostic value of the following potentially explanatory prognostic factors with respect to EFS and OS: age at diagnosis, tumor stage, *MYCN* status, chromosome 1p status, chromosome 11q status, the Shimada classification, and PAM (Table 2). While both the Shimada system and PAM were independent prognostic markers in the model based on EFS (PAM hazard ratio [HR], 3.375; 95% CI, 2.075 to 5.492; $P < .001$), the PAM classifier, the Shimada system, and amplified *MYCN* were significant independent prognostic markers in the model based on OS (PAM HR, 11.119; 95% CI, 2.487 to 49.701; $P < .001$). In addition, the PAM classifier turned out to be an independent prognostic marker for neuroblastoma risk estimation in separate Cox regression models that considered the total NB2004 stratification system and the PAM classifier with respect to both EFS and OS ($P < .001$ each; Table 2).

Potential Clinical Utility of the PAM Classifier

To identify patients in whom gene expression–based risk estimation using the PAM classifier might result in a real clinical benefit, we determined the prognostic value of this predictor in clinically relevant subgroups of patients defined by combinations of prognostic markers. In 222 patients with localized (stages 1-3) *MYCN*-nonamplified disease, the 144-gene predictor accurately classified all patients who succumbed to disease as unfavorable (favorable [n = 183]: 5-year EFS, 0.88 ± 0.02 and 5-year OS, 1.0 *v* unfavorable [n = 39]: 5-year EFS, 0.35 ± 0.10 and 5-year OS, 0.72 ± 0.10; both $P < .001$; Fig 3A). Likewise, the cohort of patients with *MYCN*-nonamplified metastatic disease (stages 4 and 4S) and age $<$ 18 months at diagnosis (n = 85) was separated by PAM into subcategories with significantly differing EFS and OS (favorable [n = 48]: 5-year EFS, 0.83 ± 0.06 and 5-year OS, 1.0 *v* unfavorable [n = 37]: 5-year EFS, 0.57 ± 0.09 and 5-year OS, 0.86 ± 0.06; $P = .004$ and $P = .009$, respectively; Fig 3B).

In contrast, the classifier did not perform convincingly in patients age $>$ 18 months with *MYCN*–single-copy stage 4 disease (n = 66). Here, 15 favorably classified patients had a 5-year EFS of 0.46 ± 0.13 and 5-year OS of 0.64 ± 0.13, while 51 unfavorably classified patients had a 5-year EFS of 0.32 ± 0.07 and a 5-year OS of 0.49 ± 0.08 ($P = .101$ and $P = .350$, respectively; Fig 3C). It has to be noted, though, that five of six favorably predicted patients with fatal outcome were non-German patients (Data Supplement Figs DS3D and DS4D), which may indicate either a less robust performance of the predictor in this subgroup, influences of different ethnic backgrounds, different therapeutic concepts, or logistic difficulties in handling and shipping of the specimens.

The combination of nonamplified localized disease and nonamplified metastatic disease in patients age $<$ 18 months largely corresponds to all NB2004 low- and intermediate-risk patients (with the exception of an age 12 months cutoff for patients with metastatic disease in NB2004) and to non–high-risk patients in risk stratification systems of other cooperative trials. We therefore determined the prognostic performance of the PAM classifier in the combined NB2004 low- and intermediate-risk groups (n = 289). This analysis also included those nine patients for whom no discrimination between low or intermediate risk could be performed because of missing chromosome 1p status. As highlighted in Figure 3D, PAM classified 218 patients of this subgroup who had an excellent outcome as favorable (5-year EFS, 0.87 ± 0.02 and 5-year OS, 1.0), while all patients with fatal outcome of disease were among the 71 patients who were classified as unfavorable (5-year EFS, 0.44 ± 0.07 and 5-year OS, 0.80 ± 0.06; both $P < .001$). The prognostic significance of the PAM classifier for non–high-risk patients was further supported by a multivariate Cox regression analysis that included the variables of tumor stage, age at diagnosis, Shimada classification, chromosome 1p status, chromosome 11q status, and the NB2004 risk group. Here, PAM was the only independent prognostic marker for EFS (HR, 4.298; 95% CI, 2.416 to 7.644; $P < .001$; Data Supplement Table DS2). The finding that current low- and intermediate-risk patients with divergent tumor behavior can be separated accurately by the 144-gene PAM classifier is shown by Appendix Figure A1 (online only). Two dominant contrasting gene expression patterns are readily distinguishable in a hierarchical clustering analysis of these non–high-risk patients that was performed using gene expression information from the 144 genes of the PAM classifier.

DISCUSSION

In this study, we evaluated the clinical utility of a previously defined gene expression–based classifier for neuroblastoma patients. This classifier, built on a previous set of 77 neuroblastomas with maximally contrasting clinical courses (ie, patients who died from disease *v* patients who survived event-free without chemotherapy) was designed to reliably discriminate tumors programmed to undergo spontaneous

Information downloaded from jco.ascopubs.org and provided by at UNIVERSITAETSKLINIKUM LEIPZIG on August 27, 2016 from 139.18.235.208
Copyright © 2010 American Society of Clinical Oncology. All rights reserved.

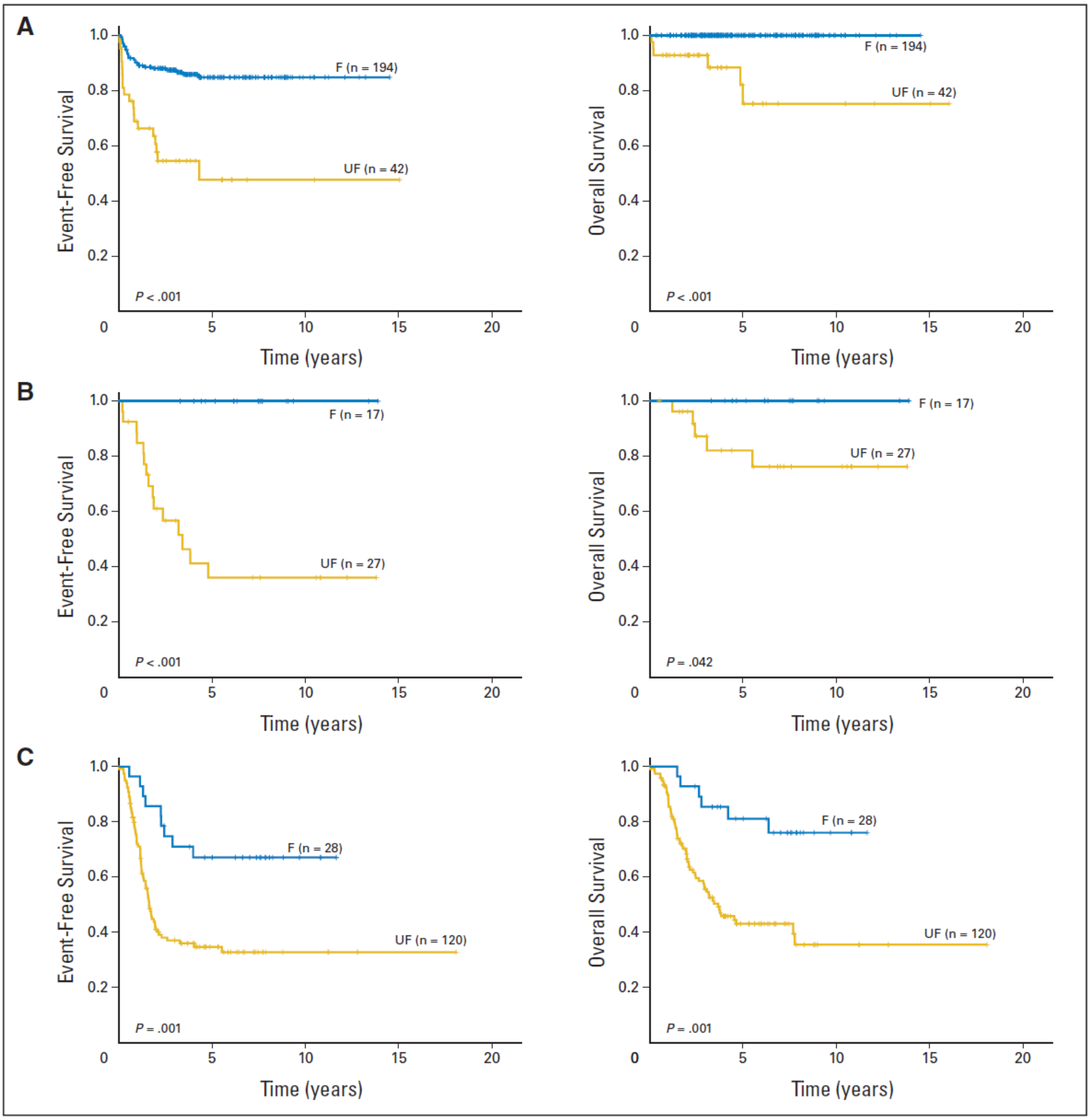

Fig 2. Kaplan-Meier estimates for event-free survival and overall survival for all patients according to their classification by the 144-gene prediction analysis for microarrays (PAM) predictor after subcategorization into (A) low-risk (n = 236), (B) intermediate-risk (n = 44), and (C) high-risk (n = 148) groups as defined by the German neuroblastoma trial NB2004. F, favorable; UF, unfavorable.

regression from those with an aggressive phenotype.[16] In recent years, it has become clear that the disease labeled "neuroblastoma" encompasses a wide range of biologic subtypes that are reflected by differing gene expression patterns.[12,13,22-24] However, the clinical impact of classifiers resulting from several well-conducted gene expression–based approaches[16,25-27] still needs to be validated by testing these markers in new, comprehensive patient cohorts. Moreover, strategies for integrating such classifiers into risk stratification systems have to be devised.

To evaluate whether our 144-gene PAM classifier results in a clinical benefit for neuroblastoma patients, we conducted a collaborative, multinational study that resulted in the largest available set of genome-wide neuroblastoma expression data (total cohort, n = 517; validation cohort used in this study, n = 440). Using this set, we

© 2010 by American Society of Clinical Oncology

Information downloaded from jco.ascopubs.org and provided by at UNIVERSITAETSKLINIKUM LEIPZIG on August 27, 2013 from 139.18.235.206
Copyright © 2010 American Society of Clinical Oncology. All rights reserved.

Table 2. Multivariate Cox Regression Models for the Complete Cohort of Patients Based on EFS and OS Considering Single Prognostic Markers and the PAM Classifier and the NB2004 Stratification System and the PAM Classifier

Marker	No. of Patients	Available Cases	Hazard Ratio	95% CI	*P*
Model considering single prognostic markers and the PAM classifier based on EFS	440	347*			
Age (> 18 months *v* < 18 months)					N/S
Stage (4 *v* 1, 2, 3, 4S)					N/S
MYCN (amplified *v* normal)					N/S
Status 1p (altered *v* normal)					N/S
Status 11q (altered *v* normal)					N/S
Shimada (UF *v* F)			**2.013**	**1.268 to 3.195**	**.002**
PAM (UF *v* F)			**3.375**	**2.075 to 5.492**	**< .001**
Model considering single prognostic markers and the PAM classifier based on OS	440	344*			
Age (> 18 months *v* < 18 months)					N/S
Stage (4 *v* 1, 2, 3, 4S)					N/S
***MYCN* (amplified *v* normal)**			**2.563**	**1.432 to 4.588**	**.002**
Status 1p (altered *v* normal)					N/S
Status 11q (altered *v* normal)					N/S
Shimada (UF *v* F)			**6.954**	**2.375 to 20.361**	**< .001**
PAM (UF *v* F)			**11.119**	**2.487 to 49.701**	**< .001**
Model considering the NB2004 risk stratification system and the PAM classifier based on EFS	440	428			
NB2004 (high risk *v* low risk + intermediate risk)			**1.494**	**1.026 to 2.174**	**.034**
PAM (UF *v* F)			**4.274**	**2.783 to 6.562**	**< .001**
Model considering the NB2004 risk stratification system and the PAM classifier based on OS	440	428			
NB2004 (high risk *v* low risk+ intermediate risk)			**5.845**	**2.977 to 11.476**	**< .001**
PAM (UF *v* F)			**8.770**	**3.629 to 21.197**	**< .001**

NOTE. Bold font indicates statistical significance ($P < .05$).
Abbreviations: EFS, event-free survival; OS, overall survival; PAM, prediction analysis for microarrays; NB2004, German neuroblastoma trial; N/S, not significant; UF, unfavorable; F, favorable.
*At last step.

observed that our classifier reliably discriminated the contrasting courses of this multifaceted disease. Importantly, all children who died from disease but were currently considered not to be at high risk were accurately classified as unfavorable.

Furthermore, the reliability of the classifier is emphasized by an in-depth review of patients' clinical courses. Here, a highly divergent quality of events was observed in patients who received a favorable PAM classification compared with patients classified as unfavorable. In the combined NB2004 low- and intermediate-risk cohort, 27 events were observed in 218 patients with a favorable PAM prediction. Of these, 11 had stage 4S-related events, and 13 had small locoregional events. All these patients survived after either no treatment, local surgical intervention, or low-intensity chemotherapy. Only three patients (all < 12 months of age) showed stage 4–related events and were treated according to the high-risk protocol. To date, all of them are event-free survivors, legitimizing the hypothesis that they suffered from stage 4 disease with a less aggressive tumor biology. In contrast, 34 events were observed in those 71 non–high-risk patients classified as unfavorable by PAM. Of them, 11 patients succumbed to disease. Of the 23 surviving patients with events, six suffered from metastatic progression and three had multiple locoregional events entailing treatment according to the high-risk protocol. Seven of the remaining patients were cured by limited treatment, consistent with a misclassification of tumors with a more benign clinical phenotype. The remaining events did not allow a clear-cut interpretation because of short follow-up time. Nonetheless, these data strongly support the notion that the PAM classifier can serve as a prognostic marker for early identification of patients currently considered non–high-risk who require more intensive treatment.

In contrast, current high-risk patients (ie, patients with amplified *MYCN* and those with nonamplified stage 4 disease and age > 18 months) may not benefit from our PAM classifier. Although PAM significantly separated patients with divergent outcome in this cohort, it was observed that PAM classification results and *MYCN* amplification were almost completely concordant (63 of 64 patients, Data Supplement Fig DS2C), while patients with divergent clinical courses were not separated reliably in the nonamplified high-risk subgroup (Fig 3C). Yet, prognostic gene expression–based classification of these cohorts appears feasible by classifiers specifically generated for this cohort.[25]

Given the clinical importance of correct assignment, it is axiomatic that any proposed classifier has to be robust and reproducible. It is therefore reassuring that prospective classification of patients by the PAM classifier, which has been performed in Germany since October 2004, reveals an exceptionally accurate discrimination of patients with differing clinical courses (Fig 1C). In addition, we observed highly similar classification results in children from Germany and children from other countries (Data Supplement Figs DS3 and DS4). These findings underscore the general applicability of our classifier as a prognostic marker for neuroblastoma patients. Our study is, to the best of our knowledge, the first work that relies on both retrospectively (n = 315) and prospectively (n = 125) analyzed neuroblastoma patients from different countries and that clearly proposes a strategy of how to adjust future therapeutic strategies for neuroblastoma patients using gene expression–based classification results. While it

Information downloaded from jco.ascopubs.org and provided by at UNIVERSITAETSKLINIKUM LEIPZIG on August 27, 2013 from 139.18.235.208
Copyright © 2010 American Society of Clinical Oncology. All rights reserved.

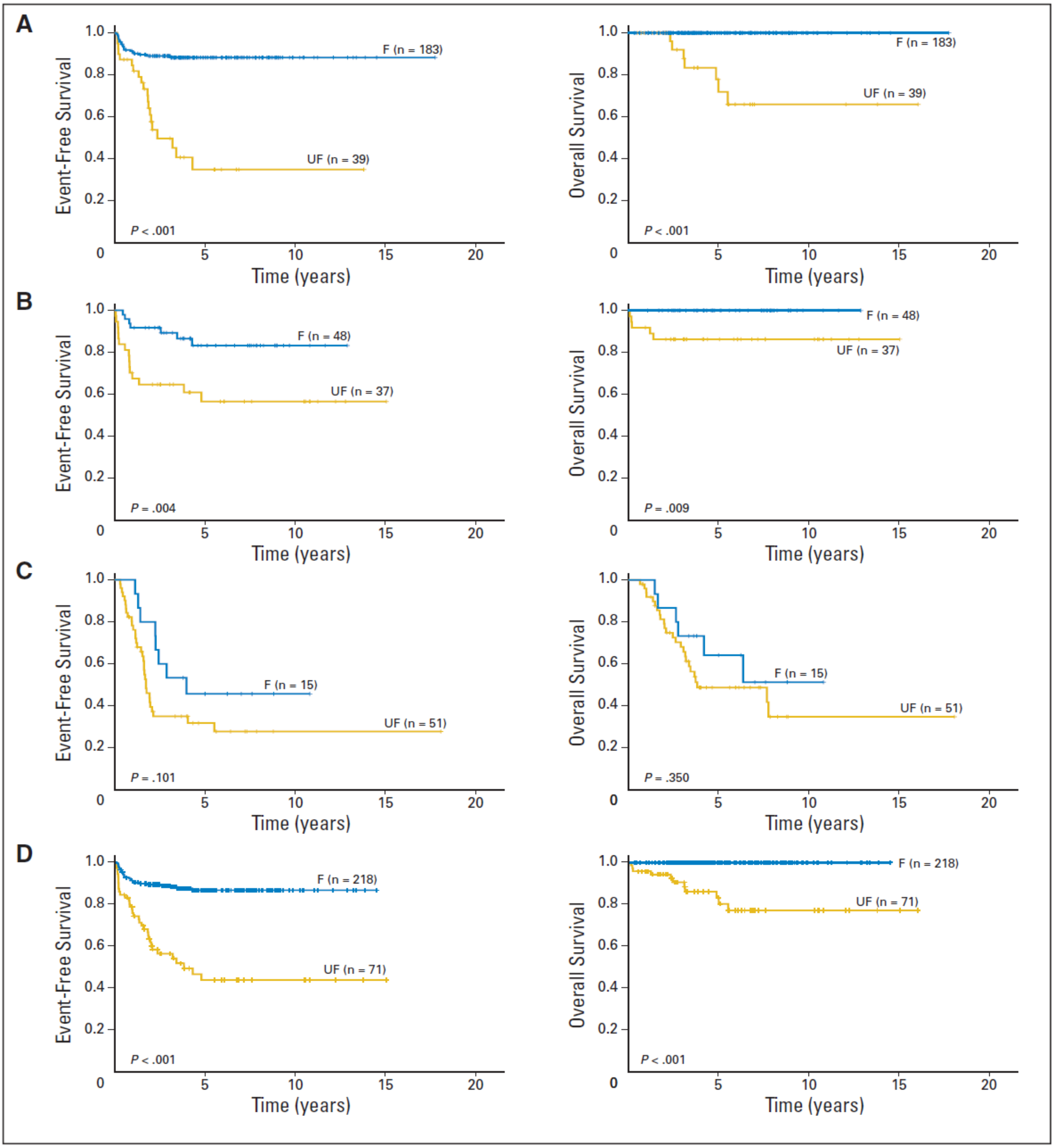

Fig 3. Kaplan-Meier estimates for event-free survival and overall survival for patients divided into clinically relevant subgroups defined by combinations of current prognostic markers with *MYCN* single-copy (A) localized (stages 1 to 3) disease, (B) metastatic (stages 4 and 4S) disease and age < 18 months at diagnosis, (C) stage 4 disease and age > 18 months at diagnosis, and (D) the combined cohort of NB2004 low- and intermediate-risk patients. F, favorable; UF, unfavorable.

is possible to transfer this classifier from the microarray to a real-time reverse transcriptase polymerase chain reaction approach as it has been described by others,[24] we consider the implementation of a microarray-based assay in future clinical trials more reasonable because of the high number of classifier genes (n = 144) and the additional information generated in a comprehensive microarray experiment that can be used in future studies.

It appears reasonable to assume that the robustness of the PAM classifier in part is attributed to the mechanistic relevance of the signature genes. Although the molecular mechanisms of spontaneous

© 2010 by American Society of Clinical Oncology

Information downloaded from jco.ascopubs.org and provided by at UNIVERSITAETSKLINIKUM LEIPZIG on August 27, 2010 from 139.18.235.208
Copyright © 2010 American Society of Clinical Oncology. All rights reserved.

regression, differentiation, and tumor progression still have to be elucidated, recent studies have documented that specific pathways may determine neuroblastoma tumor behavior. In this context, it has been suggested that high Myc pathway activity is associated with the aggressive behavior of neuroblastoma, which may be conferred by MycN in *MYCN*-amplified tumors and by c-Myc in *MYCN*–single-copy tumors.[28,29] Accordingly, we have recently shown that both our predictor and other prognostic multigene classifiers consistently comprise direct Myc targets that are upregulated in unfavorable neuroblastomas.[29] Furthermore, it has been reported that high-risk neuroblastomas are characterized by low expression levels of genes involved in neuronal differentiation, which may either mirror the developmental stage of the tumor precursor cells or indicate that physiologic differentiation processes are disrupted in aggressive neuroblastoma.[26,28,30,31] In line with this hypothesis, numerous classifier genes downregulated in adverse tumors have been implicated in neuronal differentiation,[16] several of which have previously been shown to be associated with a favorable neuroblastoma phenotype (eg, *NTRK1, SCG2*[28], and *SYN3, DST, CNR1,* and *MAP7*[30]). Thus, there is increasing evidence that the signature genes of different classifiers consistently represent the same mechanistically relevant features of distinct tumor subtypes.

In conclusion, our data strongly suggest that risk estimation using the PAM classifier improves the accuracy of discrimination of true low-risk patients who may need no chemotherapy at all from patients with aggressive tumors who require intense cytotoxic treatment. Such precise prediction of the clinical courses will prevent significant treatment-associated damages in true low-risk patients elicited by unnecessary therapies. In contrast, therapy intensification has to be considered for patients with aggressive disease who have previously been misclassified to be at low risk to ensure an appropriate first-line treatment of these children. On the basis of these results, we therefore propose to implement the PAM classifier as a prognostic marker for risk estimation of current non–high-risk neuroblastoma patients in future risk stratification systems.

AUTHORS' DISCLOSURES OF POTENTIAL CONFLICTS OF INTEREST

The author(s) indicated no potential conflicts of interest.

AUTHOR CONTRIBUTIONS

Conception and design: André Oberthuer, Frank Westermann, Benedikt Brors, Matthias Fischer
Financial support: Frank Berthold, Matthias Fischer
Administrative support: Frank Berthold, Manfred Schwab, Roland Eils, Frank Westermann, Benedikt Brors, Matthias Fischer
Provision of study materials or patients: Barbara Hero, Frank Berthold, Shahab Asgharzadeh, Robert Seeger, Paola Scaruffi, Gian Paolo Tonini, Isabelle Janoueix-Lerosey, Olivier Delattre, Gudrun Schleiermacher, Jo Vandesompele, Joëlle Vermeulen, Frank Speleman, Rosa Noguera, Marta Piqueras, Jean Bénard, Alexander Valent, Smadar Avigad, Isaac Yaniv, Axel Weber, Holger Christiansen, Richard G. Grundy, Thorsten Simon, Boris DeCarolis, Jessica Theissen
Collection and assembly of data: André Oberthuer, Barbara Hero, Yvonne Kahlert, Katharina Schardt
Data analysis and interpretation: André Oberthuer, Barbara Hero, Frank Berthold, Dilafruz Juraeva, Andreas Faldum, Patrick Warnat, Lars Kaderali, Benedikt Brors, Matthias Fischer
Manuscript writing: André Oberthuer, Matthias Fischer
Final approval of manuscript: André Oberthuer, Barbara Hero, Frank Berthold, Dilafruz Juraeva, Andreas Faldum, Yvonne Kahlert, Shahab Asgharzadeh, Robert Seeger, Paola Scaruffi, Gian Paolo Tonini, Isabelle Janoueix-Lerosey, Olivier Delattre, Gudrun Schleiermacher, Jo Vandesompele, Joëlle Vermeulen, Frank Speleman, Rosa Noguera, Marta Piqueras, Jean Bénard, Alexander Valent, Smadar Avigad, Isaac Yaniv, Axel Weber, Holger Christiansen, Richard G. Grundy, Katharina Schardt, Manfred Schwab, Roland Eils, Patrick Warnat, Lars Kaderali, Thorsten Simon, Boris DeCarolis, Jessica Theissen, Frank Westermann, Benedikt Brors, Matthias Fischer

REFERENCES

1. Maris JM, Hogarty MD, Bagatell R, et al: Neuroblastoma. Lancet 369:2106-2120, 2007

2. Brodeur GM, Pritchard J, Berthold F, et al: Revisions of the international criteria for neuroblastoma diagnosis, staging, and response to treatment. J Clin Oncol 11:1466-1477, 1993

3. Evans AE, D'Angio GJ, Randolph J: A proposed staging for children with neuroblastoma: Children's Cancer Study Group A. Cancer 27:374-378, 1971

4. London WB, Castleberry RP, Matthay KK, et al: Evidence for an age cutoff greater than 365 days for neuroblastoma risk group stratification in the Children's Oncology Group. J Clin Oncol 23:6459-6465, 2005

5. Brodeur GM, Seeger RC, Schwab M, et al: Amplification of N-myc in untreated human neuroblastomas correlates with advanced disease stage. Science 224:1121-1124, 1984

6. Shimada H, Ambros IM, Dehner LP, et al: The International Neuroblastoma Pathology Classification (the Shimada system). Cancer 86:364-372, 1999

7. Brodeur GM, Fong CT, Morita M, et al: Molecular analysis and clinical significance of N-myc amplification and chromosome 1p monosomy in human neuroblastomas. Prog Clin Biol Res 271:3-15, 1988

8. Attiyeh EF, London WB, Mossé YP, et al: Chromosome 1p and 11q deletions and outcome in neuroblastoma. N Engl J Med 353:2243-2253, 2005

9. Cohn SL, Pearson AD, London WB, et al: The International Neuroblastoma Risk Group (INRG) classification system: An INRG Task Force report. J Clin Oncol 27:289-297, 2009

10. Look AT, Hayes FA, Nitschke R, et al: Cellular DNA content as a predictor of response to chemotherapy in infants with unresectable neuroblastoma. N Engl J Med 311:231-235, 1984

11. Yamamoto K, Ohta S, Ito E, et al: Marginal decrease in mortality and marked increase in incidence as a result of neuroblastoma screening at 6 months of age: Cohort study in seven prefectures in Japan. J Clin Oncol 20:1209-1214, 2002

12. Schilling FH, Spix C, Berthold F, et al: Neuroblastoma screening at one year of age. N Engl J Med 346:1047-1053, 2002

13. Woods WG, Gao RN, Shuster JJ, et al: Screening of infants and mortality due to neuroblastoma. N Engl J Med 346:1041-1046, 2002

14. Hero B, Simon T, Spitz R, et al: Localized infant neuroblastomas often show spontaneous regression: Results of the prospective trials NB95-S and NB97. J Clin Oncol 26:1504-1510, 2008

15. Fischer M, Spitz R, Oberthür A, et al: Risk estimation of neuroblastoma patients using molecular markers. Klin Padiatr 220:137-146, 2008

16. Oberthuer A, Berthold F, Warnat P, et al: Customized oligonucleotide microarray gene expression-based classification of neuroblastoma patients outperforms current clinical risk stratification. J Clin Oncol 24:5070-5078, 2006

17. Ambros PF, Ambros IM: Pathology and biology guidelines for resectable and unresectable neuroblastic tumors and bone marrow examination guidelines. Med Pediatr Oncol 37:492-504, 2001

18. Tibshirani R, Hastie T, Narasimhan B, et al: Diagnosis of multiple cancer types by shrunken centroids of gene expression. Proc Natl Acad Sci U S A 99:6567-6572, 2002

19. Collett D: Strategy for model selection, in: Modelling Survival Data in Medical Research. London, United Kingdom, Chapman & Hall, 1994, pp 78-83

20. Simon T, Spitz R, Faldum A, et al: New definition of low-risk neuroblastoma using stage, age, and 1p and MYCN status. J Pediatr Hematol Oncol 26:791-796, 2004

21. Oberthuer A, Theissen J, Westermann F, et al: Molecular characterization and classification of neuroblastoma. Future Oncol 5:625-639, 2009

22. Brodeur GM: Neuroblastoma: Biological insights into a clinical enigma. Nat Rev Cancer 3:203-216, 2003

© 2010 by American Society of Clinical Oncology

Information downloaded from jco.ascopubs.org and provided by at UNIVERSITAETSKLINIKUM LEIPZIG on August 27, 2010 from 139.18.235.208
Copyright © 2010 American Society of Clinical Oncology. All rights reserved.

23. Maris JM: The biologic basis for neuroblastoma heterogeneity and risk stratification. Curr Opin Pediatr 17:7-13, 2005

24. Vermeulen J, De Preter K, Naranjo A, et al: Predicting outcomes for children with neuroblastoma using a multigene-expression signature: A retrospective SIOPEN/COG/GPOH study. Lancet Oncol 10:663-671, 2009

25. Asgharzadeh S, Pique-Regi R, Sposto R, et al: Prognostic significance of gene expression profiles of metastatic neuroblastomas lacking MYCN gene amplification. J Natl Cancer Inst 98:1193-1203, 2006

26. Ohira M, Oba S, Nakamura Y, et al: Expression profiling using a tumor-specific cDNA microarray predicts the prognosis of intermediate risk neuroblastomas. Cancer Cell 7:337-350, 2005

27. Wei JS, Greer BT, Westermann F, et al: Prediction of clinical outcome using gene expression profiling and artificial neural networks for patients with neuroblastoma. Cancer Res 64:6883-6891, 2004

28. Fredlund E, Ringnér M, Maris JM, et al: High Myc pathway activity and low stage of neuronal differentiation associate with poor outcome in neuroblastoma. Proc Natl Acad Sci U S A 105:14094-14099, 2008

29. Westermann F, Muth D, Benner A, et al: Distinct transcriptional MYCN/c-MYC activities are associated with spontaneous regression or malignant progression in neuroblastomas. Genome Biol 9:R150, 2008

30. Fischer M, Oberthuer A, Brors B, et al: Differential expression of neuronal genes defines subtypes of disseminated neuroblastoma with favorable and unfavorable outcome. Clin Cancer Res 12:5118-5128, 2006

31. Bénard J, Raguénez G, Kauffmann A, et al: MYCN-non-amplified metastatic neuroblastoma with good prognosis and spontaneous regression: A molecular portrait of stage 4S. Mol Oncol 2:261-271, 2008

***Journal of Clinical Oncology* — The ideal place to publish your research**

- Impact Factor of 17.157: *JCO*'s published articles were cited 97,639 times and accounted for fully 9.7% of all oncology journal citations in 2008.
- Maximum Exposure: More than 25,000 of the world's leading oncology professionals receive *JCO* and more than 180,000 unique visitors per month visit jco.org.
- Outstanding Reputation: With an acceptance rate of just 20%, *JCO* publishes only the very best articles in the field.
- International Coverage: *JCO* is available globally in 28 countries and in 15 international editions.
- Rapid Turnaround: *JCO* averages just 9 weeks from final manuscript acceptance to online publication.
- No Exclusivity Clause: *JCO* authors may reproduce or reuse their own material published in *JCO* for educational purposes at no charge.
- No Submission Charges: *JCO* has no submission, color, or page charges.

To submit a manuscript, visit submit.jco.org.

ASCO
American Society of Clinical Oncology

© 2010 by American Society of Clinical Oncology

Information downloaded from jco.ascopubs.org and provided by at UNIVERSITAETSKLINIKUM LEIPZIG on August 27, 2016 from 139.18.235.208
Copyright © 2010 American Society of Clinical Oncology. All rights reserved.

2.4 Amplifikation des genomischen Bereiches Chr2p24-25

Hintergrund:

Die amplifizierten, distalen Abschnitte des kurzen Armes des Chromosomes 2 enthalten das *MYCN*-Protoonkogen, welches dadurch in >4 bis hin zu 300-facher Kopieenzahl pro Zellkern vorliegen kann. Das ist in 20-25% der Tumore bei Erstdiagnose der Fall und geht mit einer schlechten Prognose, unabhängig von Tumorstadium und Alter bei Diagnosestellung einher *(Brodeur et al., 1995)*. Patienten, in deren Tumoren eine *MYCN* Amplifikation nachgewiesen wurde werden als Hochrisiko-Patienten gewertet. Dementsprechend intensiv sind die Therapieregime bei diesen Kindern aufgebaut (Operation(-en), Polychemotherapie bis hin zu ablativer Chemotherapie mit autologer Stammzellretransfusion und Konsolidierungstherapie mit Retinolsäure). Dies geht einher mit teilweise schweren Nebenwirkungen und therapiebedingten Todesfällen. Interessanterweise zeigt sich mit zunehmender Nachbeobachtungsdauer, dass eine recht konstante Zahl von Patienten (25-30%) mit *MYCN* amplifiziertem Neuroblastom auf die intensive Therapie ansprechen und als Langzeitüberlebende (LZÜ) definiert werden können (LZÜ=Überleben >6 Jahre nach Diagnosestellung; danach ist in allen Untergruppen die Wahrscheinlichkeit im weiteren Verlauf an der Erkrankung zu versterben <1% (*eigene Daten*)).

Der genomische Status von *MYCN* ist heute einer der wichtigsten Stratifizierungsparameter bei Diagnose eines Neuroblastomes geworden. Die Mechanismen, die zu einer Amplifikation des genomischen Bereiches um *MYCN* herum führen sind dagegen weitgehend unbekannt.

Eigene Publikationen:

Weber A, Imisch P, Bergmann E, Christiansen H. Coamplification of *DDX1* correlates with an improved survival probability in children with *MYCN*-amplified human neuroblastoma. *J Clin Oncol*. 2004 Jul 1;22(13):2681-90.

IF (Stand 2010): 17,793

Neben der Amplifikationshöhe (=Kopieenzahl) der amplifizierten genomischen Abschnitte (ampGA) ist deren Ausdehnung um *MYCN* nach temoler- und centromerwärts eine interessante Eigenschaft der jeweiligen Neuroblastome. Die Ausdehnung der ampGA bestimmt dabei, welche Gene neben *MYCN* ebenfalls amplifiziert in den Zellen vorliegen. Da die ampGA sich über mehrere Megabasen in beide Richtungen hin erstrecken können und die mit *MYCN* koamplifizierten Gene wie MYCN selbst in der Regel auch in den Zellen überexpremiert werden ist eine Beeinflussung des Tumorwachtumsverhaltens und damit auch der Prognose durch diese Eigenschaft denkbar. Diese Hypothese haben wir an einer Kohorte von n=98 primären Neuroblastomen untersucht, indem wir das Vorhandensein einer Coamplifikation von 7 Genen um *MYCN* herum mittels Multiplex-PCR analysiert haben. Für die Untersuchung wurde nur Patienten ausgewählt, die entweder bereits an ihrer Erkrankung verstorben waren oder als Langzeitüberlebende (Überlebenszeit > 72 Monate) definiert waren.

Unsere Ergebnisse zeigten, dass Patienten, deren Tumore eine Koamplifikation der Genes *DDX1* aufweisen, eine höhere Wahrscheinlichkeit zum Langzeitüberleben und damit eine bessere Gesamtprognose haben, als Patienten ohne diese Koamplifikation (*Weber et al., 2004*). Das für *DDX1* kodierende Gen liegt auf dem kurzen Arm von Chromosom 2 in direkter Nachbarschaft zu *MYCN*. Diese physikalische Nähe führt in ca. 60-70% der Fälle in *MYCN* amplifizierten Neuroblastomen zu einer Koamplifikation von *DDX1*. Die Koamplifikation von *DDX1* wurde erstmals von R. Godbout und Mitarbeitern beschrieben (*Godbout et al., 1993*). Auch für weitere, telomerseits von *MYCN* gelegene Gene ist ein Trend hin zu einem Überlebensvorteil erkennbar (*NAG, NSE1*) (eigene Daten). In der gleichen Arbeit konnten wir eine direkte Korrelation der Koamplifikationshäufigkeit der untersuchten Gene mit deren physikalischer Nähe (Entfernung in Basen) telomerwärts und centromerwärts zu *MYCN* zeigen (Figur 1 ; *Weber et al., 2004*).

Die prognostische Bedeutung der Koamplifikation von *DDX1* wird in der aktuellen Literatur kontrovers diskutiert, jedoch konnten in verschiedenen Kollektiven statistische Trends, die einen Überlebensvorteil für Patienten mit *DDX1* koamplifizierten bzw. überexpremierenden Neuroblastomen zeigen, beobachtet werden. *(Kaneko et al. 2007, Deferrari et al. 2007)*

Weber A, Starke S, Bergmann E, Christiansen H. The coamplification pattern of the *MYCN* amplicon is an invariable attribute of most *MYCN*-amplified human neuroblastomas. *Clin Cancer Res*. 2006 Dec 15;12(24):7316-21.

IF (Stand 2010): 6,747

Sowohl die Amplifikationshäufigkeit (Kopieenzahl pro haploidem Genom) als auch die Amplikonstruktur eines amplifizierten Chromosomenabschnittes können sich im zeitlichen Verlauf und unter Selektionsdruck in etablierten Zellkulturmodellen verändern (*Hahn et al., 1992*).

Wir untersuchten eine Kohorte von n=33 *MYCN* amplifizierten Neuroblastomen auf die Konsitienz der Kopieenzahl der ampGA und deren Ausdehnung nach Beginn der Chemotherapie und bei Auftreten eines Rezidives. Dabei konnten wir zeigen, dass die Amplifikationshöhe nach Beginn der Chemotherapie abnehmen kann, während die Ausdehnung der ampGA, ausgedrückt durch das untersuchte Koamplifikationsmuster, immer konstant bleibt. Im Falle der untersuchten Rezidive zeigte sich eine durchschnittlich höhere Kopieenzahl der ampGA im Vergleich zu Tumorgewebe bei Diagnosestellung, die Ausdehnung der ampGA war hier jedoch bis auf eine Ausnahme ebenfalls konstant.

Diese Ergebnisse haben eine große Relevanz, da die *MYCN* Amplifikation in Ihrer Architektur (Ausdehnung der individuellen ampGA) eine feststehende Eigenschaft der einzelnen Neuroblastome zu sein scheint. Die Kopienzahl der ampGA unterliegt einer gewissen Schwankung, jedoch konnten wir in keinem der untersuchten Patienten einen Verlust oder eine vollständige Veränderung der *MYCN*-Amplikons nachweisen.

VOLUME 22 · NUMBER 13 · JULY 1 2004

JOURNAL OF CLINICAL ONCOLOGY

ORIGINAL REPORT

Coamplification of *DDX1* Correlates With an Improved Survival Probability in Children With *MYCN*-Amplified Human Neuroblastoma

Axel Weber, Patricia Imisch, Eckhard Bergmann, and Holger Christiansen

From the Children's Hospital, Pediatric Hematology and Oncology, University of Marburg, Marburg, Germany.

Submitted July 25, 2003; accepted April 2, 2004.

This work contains parts of the doctoral theses of Patricia Imisch.

Authors' disclosures of potential conflicts of interest are found at the end of this article.

Address reprint requests to Holger Christiansen, MD, The Children's Hospital of Marburg, Pediatric Oncology and Hematology, Neuroblastoma Research Laboratory, Deutschhausstrasse 12, 35037 Marburg, Germany; e-mail: Holger .Christiansen@staff.uni-marburg.de.

© 2004 by American Society of Clinical Oncology

0732-183X/04/2213-2681/$20.00

DOI: 10.1200/JCO.2004.07.192

ABSTRACT

Purpose
Amplification of the *MYCN* oncogene at chromosome 2p24-25 identifies an aggressive subtype of human neuroblastoma with a poor clinical outcome. Differences in amplicon structure and coamplification of genes telomeric and centromeric to the *MYCN* oncogene have previously been described. A relevant role of gene coamplification for neuroblastoma pathogenesis remains elusive.

Patients and Methods
We analyzed 98 primary neuroblastoma tumors with *MYCN* amplification for coamplification of seven additional genes at chromosome 2p24-25 (*DDX1, NAG, NSE1, LPIN1*, EST-*AA581763, SMC6,* and *SDC1*). Two semiquantitative multiplex polymerase chain reactions were used to obtain the amplification status of the target genes in relation to a reference gene on chromosome 2q (*Inhibin-beta-b*). Furthermore, mRNA expression pattern of coamplified genes in a subset of tumors was analyzed.

Results
Our results show that the frequency of gene coamplification on 2p24-25 in neuroblastoma is correlated directly to the physical distance to *MYCN*. Coamplification is correlated to an upregulated gene expression for DDX1 and NAG. Coamplification of the *DDX1* gene within 400kb telomeric to *MYCN* identifies a subgroup of advanced stage neuroblastoma tumors with a more favorable outcome ($P = .027$, log-rank test). A high expression level of DDX1 is associated with a trend towards a better survival probability ($P = .058$, log-rank test).

Conclusion
Our results indicate that *DDX1* coamplification correlates with a better prognosis and improved patient survival in *MYCN*-amplified neurobastoma.

J Clin Oncol 22:2681-2690. © 2004 by American Society of Clinical Oncology

INTRODUCTION

Neuroblastoma is the most common extracranial solid cancer in childhood and responsible for approximately 15% of all childhood cancer deaths. The 6-year overall survival probability of all patients with neuroblastoma is approximately 60%.

Amplification of the *MYCN* oncogene is the most extensively studied biologic marker for an unfavorable prognostic outcome in patients with neuroblastoma.[1-3] The overall survival probability for patients with *MYCN* amplification is less than 30% in the first 6 years after diagnosis (authors' own data of 216 patients with *MYCN*-amplified neuroblastoma). Because of the poor prognosis, these patients are treated by combination of high-dose chemotherapy, surgical therapy, and different experimental therapy strategies depending on the therapy protocol. However, some *MYCN*-amplified tumors can be distinguished by a better response to the combined treatment resulting in a better prognosis for the individual patient, as 7% of patients with *MYCN*-amplified neuroblastoma survive more than 72 months after initial diagnosis and survival probability after 72 months is more than 95% for these patients (authors' own unpublished data of 1,443 patients registered from 1981 to 2000). Thus, amplification of

Information downloaded from jco.ascopubs.org and provided by at UNIVERSITAETSKLINIKUM LEIPZIG on August 27, 2013 from 139.18.235.208
Copyright © 2004 American Society of Clinical Oncology. All rights reserved.

the *MYCN* gene does not seem to be a death warrant per se, because long-time survival is possible for patients even with *MYCN* amplified neuroblastoma.[4]

Amplification of *MYCN* can be found in double minutes and homogenously staining regions.[5] The role of coamplification of additional genes close to the *MYCN* locus on 2p24-25 for the progression of the disease or resistance to therapy in neuroblastoma tumors is still unclear. Coamplification of different genes in close distance to *MYCN* had been reported previously.[6-11] Furthermore, a diversity in amplicon structure and size was observed in more detailed genomic analyses.[12]

To get further information of the amplicon structure and the clinical relevance of coamplified genes within *MYCN*-amplified tumors, we investigated seven genes located in different distances telomeric and centromeric to *MYCN* on 2p24-25 for coamplification in a cohort of 98 primary neuroblastoma tumors with known *MYCN* gene amplification and a long-time follow-up.[13]

DDX1 (DEAD/H-BOX 1) is a putative RNA helicase containing the characteristic D(Asp)-E(Glu)-A(Ala)-D(Asp)-box conserved sequence motif. Proteins of this family have been described to be involved in RNA processing, and thus to influence transcription, splicing, translation, and intracellular transport of different RNA subfamilies.[14] Genes of the DEAD/H protein family were found to be involved in tumorigenesis and cellular proliferation,[15] as well as in antiproliferative processes.[16] The preferential expression pattern of DDX1 in cells of neuronal origin and the coamplification with *MYCN* in neuroblastoma and retinoblastoma cell lines was first described in 1993.[17] Several authors described coamplification of *DDX1* in neuroblastoma cell lines and primary tumors as well.[6,8-10,18-20] Some authors described a trend towards a worse prognosis for patients with *DDX1* coamplified tumors.[6-11] Because of the relative homogeneity regarding prognosis of the neuroblastoma patients in these studies, statistical significance was not obtained.

The *NAG* (neuroblastoma amplified gene) gene locus encodes for a 155.9 kDa protein, including domains for nuclear-localization, coil-coil-, and leucine-zipper-motifs. The function of *NAG* is yet unknown. Coamplification of *NAG* within the *MYCN* amplicon has been reported first by Wimmer et al.[10,21] Recently, Scott et al[11] characterized the amino acid sequence and the genomic structure of *NAG* systematically, and found an association of *NAG* coamplification and lower stage disease in human neuroblastoma with *MYCN* amplification.

Non-SMC element 1(NSE-1) is described to be a structural maintenance complex component of a smc5/smc6 complex involved in chromosome structure organization, DNA repair, and cellular proliferation.[22] LPIN1 is a nuclear protein required for normal adipose tissue development, differentiation, and metabolism processes.[23] As the region in close vicinity centromeric to *MYCN* is lacking yet known genes, we investigated the coamplification of the expressed sequence tag (EST) *AA581763* that is located 87kb centromeric to *MYCN*. This EST was identified as a spliced EST in a kidney tumor cDNA library (NCI-CGAP_Kid6, Homo sapiens EST library) predicting an encoded gene in this region. Structural maintenance complex protein 6 (SMC6) is a chromatin bound protein described to act as a regulating factor in cellular proliferation and cell division processes.[24] Thus, a second gene for a protein belonging to the same DNA organizing SMC-complex is located in a close distance of 3000 kb around *MYCN*, as it is shown for *NSE1*.[22] Syndecan1 (SDC1) is a cell surface proteoglycan acting as a receptor for the extracellular matrix and represents a protein critical for WNT1-induced tumorigenesis in the mouse mammary gland.[25,26]

In this study, we investigated a large cohort of *MYCN*-amplified human neuroblastomas with a long mean follow-up time of 48.6 months for the patients alive. Our results show a direct dependency of coamplification frequency on the physical distance to *MYCN*. Coamplification of *DDX1* and *NAG* are both correlated to an upregulated mRNA expression. Furthermore, our data provide statistical evidence that coamplification of *DDX1* correlates with an improved survival probability for patients with *MYCN*-amplified neuroblastoma.

PATIENTS AND METHODS

Patients

We studied primary tumor specimens from 98 children with *MYCN*-amplified neuroblastoma diagnosed in Germany from 1981 to 2000. The investigated cohort is representative for the group of *MYCN*-amplified neuroblastomas during this time period, regarding age at diagnosis, disease stage, and the follow-up time.

All neuroblastoma diagnoses were confirmed by histologic assessment of a tumor specimen obtained at surgery. The tumors were classified according to the International Neuroblastoma Staging System criteria.[27] Our study group consisted of four stage 1 patients, one stage 2 patient, 25 stage 3 patients, 60 stage 4 patients, and eight stage 4S tumors. The median patient age at diagnosis was 20.5 months (range, 0.03 to 164.9 months). The median follow-up time for all 98 patients was 20.9 months (range, 0.36 to 138.9 months). The median follow-up time of the patients that died of the disease was 15.8 months ($n = 63$) compared with 42.2 months for patients alive ($n = 35$). All patients were treated according to previously described protocols with confirmed consent for therapy and study procedures.[28,29]

Because of limited availability of comparable amounts of tumor tissue, a subset of 19 neuroblastoma specimens was selected for gene expression analyses to ensure material homogeneity used for RNA isolation and cDNA synthesis in order to get comparable results. The median age at diagnosis of this subset was 25.8 months (range, 1.3 to 78.6 months). The median follow-up time for the 19 patients was 20.6 months (range, 2.3 to 92.5 months).

Information downloaded from jco.ascopubs.org and provided by at UNIVERSITAETSKLINIKUM LEIPZIG on August 27, 2010 from 139.18.235.208
Copyright © 2004 American Society of Clinical Oncology. All rights reserved.

Tissue Preparation

The neuroblastoma specimens were frozen in liquid nitrogen directly after surgical excision and stored at −80°C until preparation for investigation.

DNA Extraction

DNA was extracted from tumor samples of 50 mg each with the Qiagen DNA extraction kit (Qiagen, Hilder, Germany) following the manufacturer's protocol.

RNA Extraction

Tumor samples of 100 mg each were homogenized in 1,000 μL RNAzol-B (Biotecx Laboratories Inc, Houston, TX). RNA was isolated after adding chloroform according to the guanidinium-isothiocyanate method.[30]

Reverse Transcription

Reverse transcription was performed using Super-Script-II MMLV reverse transcriptase (Invitrogen, Carlsbad, CA) following the manufacturer's protocol.

MYCN Amplification (Southern Blot; reference method)

For the detection of *MYCN* amplification, the pNB-1 probe (*MYCN* is localized on 2p24.1, ATCC 41,011) was used; control hybridization for a single copy signal was performed with HuCK (immunoglobin kappa constant region is localized on 2p12, ATCC 59,172).[31]

Primer Design

Primer for the amplification of *MYCN, DDX1, NAG, NSE1, LPIN1, EST-AA581763, SMC6, SDC1, Inhibin-beta-b,* and Beta-actin were designed with OLIGO 6.0 (Medprobe, Oslo, Norway). The specificity was controlled with actual BLAST data (http://www.ncbi.nlm.nih.gov/blast/blast.cgi). For genomic polymerase chain reaction (PCR), one primer was located in an exon and the second in an adjacent intron. For reverse transcriptase PCR, primers were located in two subsequent exons. All PCR products showed specific bands of the expected size.

Multiplex PCR

PCR was performed in a total volume of 50 μL using 2.5 Units Taq-polymerase-k (MoBiTec, Göttingen, Germany). Primer sequences and individual PCR conditions of each PCR reaction are listed in Appendix Table A1 (online only).

The first multiplex-PCR for evaluation of the genomic amplification status contained the primer pairs of *MYCN, DDX1, NAG, LPIN1, SDC1,* and *Inhibin-beta-b* on chromosome 2q13 as single copy reference. The second multiplex-PCR contained the primer pairs of *NSE1, EST-AA581763, SMC6,* and again *MYCN* as amplification status control and *Inhibin-beta-b* as single copy reference. The amplified PCR fragments (10 μL of the PCR reaction) were separated in a 2% agarose gel by electrophoresis, identified by ethidium bromide staining, and documented by the Image Master VDS software (Amersham Biosciences, Piscataway, NJ). Relative band intensity of each specific PCR-band was calculated with Image Master VDS software. The amplification status was expressed as relative band intensities of the genes of interest on 2p24-25 to the band intensitiy of the reference gene *Inhibin-beta-b* (ratio, *target gene/inhibin-beta-b*).

To define the single copy status of the band intensity for each gene, we used human placental and kidney DNA as single copy reference. Fifteen separate PCR reactions were done with either placental and kidney DNA. Mean and standard deviation for the ratios of the single copy status for each gene were determined. Double of the standard deviation above the mean ratio was defined as threshold. A positive amplification status was defined as a band intensity ratio (*target gene/Inhibin-beta-b*) above the threshold. To verify our assays, we compared the amplification status of *MYCN* determined by the PCR-threshold in both multiplex PCRs for all 98 tumors with a reference method (southern blot, described above). All of the investigated neuroblastoma tumors were defined as *MYCN* amplified in both of our PCR-assays.

Real-Time PCR

Real-time PCR was performed in a total volume of 50 μL as previously described, but containig 5 μL SYBR Green (Roche, Alameda, CA). Primer sequences and PCR conditions are listed in Appendix Table A1.

Threshold cycles were determined using the iCycler PCR detection system and automated computer software (Biorad; Laboratories, Hercules, CA) following the manufacturer's protocols. Expression analysis of beta-actin and the target genes were perfomed simultaneously in one experiment. Each experiment was performed twice. The mean Ct-values of each sample were used to perform mathematical analysis. Relative expression pattern of the target genes to beta-actin in each sample and in relation to the mean of the whole investigated population was performed using the $2^{-\Delta\Delta Ct}$ method.[32] Thus, a high expressing tumor was defined by expressing the target gene in relation to beta-actin above the mean of the investigated population.

Distance Calculation

The distance of the coamplified genes to *MYCN* was determined using current BLAT (BLAST-like alignment tool) alignment information[13] for each gene on chromosome 2p24-25. Information on gene localization is given with a base-count for start and end on the according chromosome. The base-count closest to *MYCN* was used for physical distance calculation.

Statistical Analysis

The Fisher's exact test was used to examine possible correlations between coamplification and expression of investigated genes. The Spearman-Rho test was used to evaluate the correlation between coamplification frequency and physical distance of coamplified genes. Survival data for amplification status and expression of the investigated genes were determined by the Kaplan-Meier method, and differences between survival curves were calculated using the log-rank test. Reported *P* values were not corrected for multiple testing.

Multivariate analysis was perfomed using the Cox regression analysis. Statistical analyses were performed with the SPSS version 10.0 software (SPSS Inc, Chicago IL). *P* values of ≤ .05 were regarded as significant.

RESULTS

Gene Coamplification Frequency Within the MYCN Amplicon Correlates With the Physical Distance to MYCN

Ninety-eight primary neuroblastoma tumor samples with known *MYCN* amplification were investigated with two multiplex PCR for coamplification of seven genes on chromosome 2p24-25 (Fig 1). All tumors showed positive *MYCN*-amplification status in Southern blot analysis (data

Information downloaded from jco.ascopubs.org and provided by at UNIVERSITAETSKLINIKUM LEIPZIG on August 27, 2010 from 139.18.235.206
Copyright © 2004 American Society of Clinical Oncology. All rights reserved.

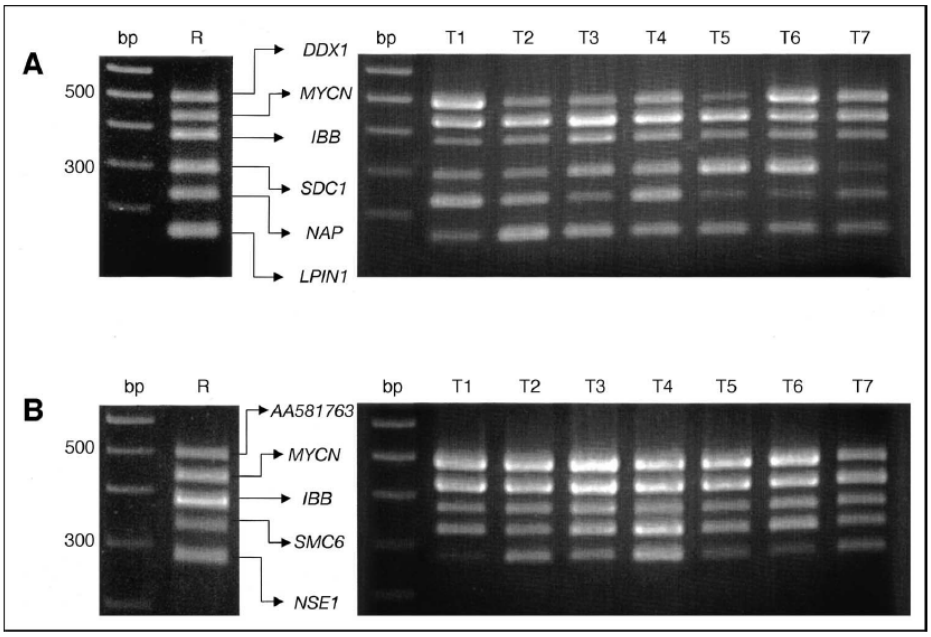

Fig 1. Coamplification on chromosome 2p24-25. (A) Six-fold polymerase chain reaction (PCR) for *Inhibin-beta-b, MYCN, DDX1, SDC1, NAP,* and *LPIN1*; (B) five-fold PCR for *Inhibin-beta-b, MYCN, EST-AA581763, SMC6,* and *NSE1*. bp, molecular weight marker; r, healthy human kidney DNA was used as single-copy reference; T1-T7, seven of the 98 investigated tumors with different combinations of coamplification pattern.

not shown). In accordance to Southern blot analysis, *MYCN*-amplification status was found to be positive in both multiplex PCRs in all 98 tumor samples.

Besides *MYCN* amplification 64 (65.3%) of the investigated tumors showed coamplification for *DDX1*, 42 (42.9%) for *NAG*, 21 (21.4%) for *NSE1*, five (5.1%) for *LPIN1*, 89 (90.8%) for EST-*AA581763*, 12 (12.2%) for *SMC6*, and four (4.1%) for *SDC1*. No tumor sample was found to be coamplified for all seven investigated genes. The most extensive amplicon size included both marginal genes (*LPIN1* and *SDC1*), but showed a deleted region containing the *SMC6* locus.

With consideration of current gene mapping data, our results show that the frequency of gene coamplification on 2p24-25 in human neuroblastoma is directly depending on the physical distance to *MYCN* in our population of 98 *MYCN* amplified neuroblastomas (correlation coefficient, -0.857; $P = .007$, Spearman-Rho test; Fig 2).

Coamplification Status of the Investigated Genes Does Not Correlate to Stage or Age at Diagnosis

As clinical parameters such as age at diagnosis and stage of disease are of interest, even in *MYCN* amplified neuroblastoma in respect to prognosis, we looked for statistical correlations of these parameters to the coamplification status of the investigated genes. We found no significant correlation between coamplification of an investigated gene and a clinical parameter as stage (stages 1, 2, and 4S *v* 3 and 4, or stages 1, 2, 3, 4S *v* 4) or age at diagnosis ($<$ 12 months *v* $>$ 12 months; data not shown), with exception of *SMC6*, which was found to be coamplified more frequently in infants (age $<$ 12 months at diagnosis) compared with older patients ($P = .017$, Fisher's exact test).

Coamplification of DDX1 Correlates Significantly With an Enhanced Survival Probability in Patients With MYCN Amplification

The large number of investigated patients and the long follow-up time of surviving patients in our cohort allowed the evaluation of the prognostic impact for the coamplified genes. Kaplan-Meier survival analyses using the log-rank test were performed to determine the clinical relevance of coamplification status of the investigated genes. Differences in the 6-year survival probability and median survival time are shown in Table 1. A statistically significant difference in the survival probability was found only for coamplification status of *DDX1*. Patients with *DDX1* coamplified tumors showed a significantly better outcome compared with patients without *DDX1* coamplification ($P = .027$; Table 1; Fig 3). No significant differences in survival probability were found in analyses for coamplification status of the other investigated genes (Table 1).

Survival analysis of 1,443 neuroblastoma tumors of different stage, age, and *MYCN* amplification status indicate no more statistical relevant change in survival probability after a 6-year follow-up time (probability to die of the disease after surviving 72 months after diagnosis $<$ 1%; authors' own data, not shown). Thus, to focus on a definitively observed cohort, we excluded patients with a short time follow-up ($<$ 72 months) and perfomed survival analysis only for patients diagnosed before 1996 (Fig 3; n = 51; minimum follow-up time, 72 months after initial diagnosis). In this group, *DDX1* coamplification identifies patients

Information downloaded from jco.ascopubs.org and provided by at UNIVERSITAETSKLINIKUM LEIPZIG on August 27, 2016 from 139.18.235.208
Copyright © 2004 American Society of Clinical Oncology. All rights reserved.

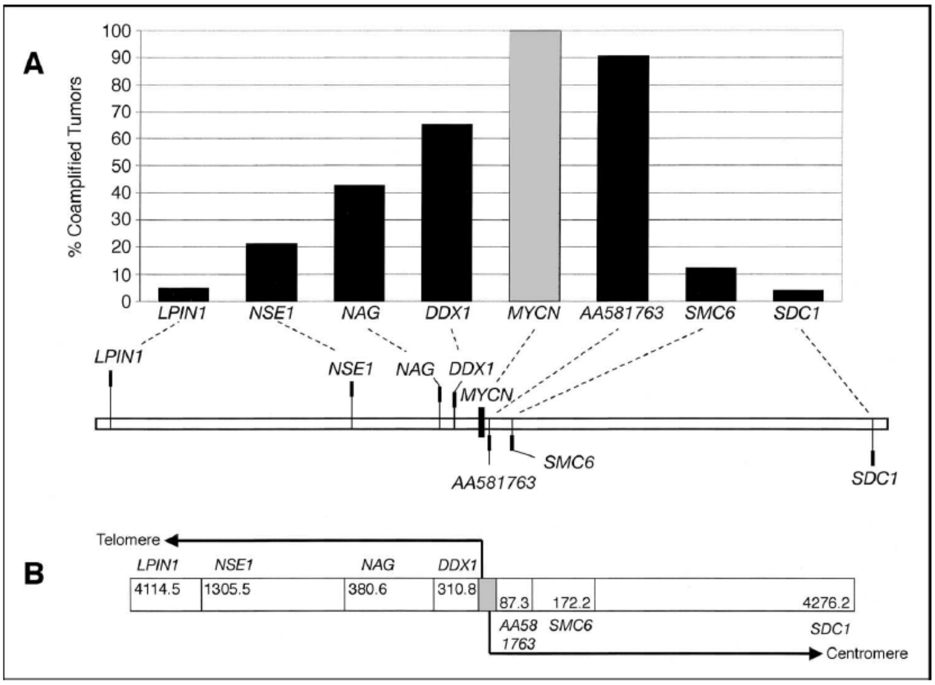

Fig 2. Gene coamplification directly depends on the physical distance to *MYCN.* (A) Coamplification frequence of the seven investigated genes on chromosome 2p24-25 in 98 primary neuroblastoma tumors; (B) physical distance of the seven investigated genes in relation to *MYCN,* based on current BLAT assignment information.[13]

with a 35% chance of long-time survival. In contrast, all patients without *DDX1* coamplification died within 28 months after initial diagnosis (Fig 3; $P = .01$, Kaplan-Meier analysis).

As survival rates of *DDX1* coamplified or noncoamplified patients showed no difference within the first 24 months after diagnosis, the prognostic relevance of *DDX1* coamplification status was of particular interest for patients with *MYCN*-amplified neuroblastoma that survived the first 2 years after diagnosis. A reason for this finding might be the advanced stage of disease for most patients at the time of diagnosis and the intensive therapy protocol for *MYCN*-amplified neuroblastoma patients independent of the gene coamplification status. A re-evaluation of survival analysis for the mentioned patients (survivors 24 months after diagnosis, $n = 46$) resulted in a survival probability for the next 4 years of 78.9% with *DDX1* coamplification compared with 30.4% without *DDX1* coamplification ($P < .0005$, Kaplan and Meier analysis).

Multivariate Cox regression analysis showed that prognostic relevance of *DDX1* coamplification is independent of age at diagnosis ($P = .033$) or stage of disease (1, 2, 3, and 4S *v* 4; $P = .05$) in our investigated group (Table 2). Thus, coamplification of *DDX1* defines a better prognostic subtype of *MYCN*-amplified neuroblastoma independent of clinical prognostic factors.

However, patients with *DDX1* coamplified *MYCN*-amplified neuroblastomas are still at increased risk when compared with patients with *MYCN*-nonamplified tumors. Survival analysis of 1,149 neuroblastoma patients without *MYCN* amplification diagnosed from 1981 to 2000 out of our database revealed a median survival of 187.8 months (95% CI, 138.3 to 236.3 months) and a 6-year survival probability of 60.4% (compare with Table 1). The 64 patients with *MYCN* amplification and *DDX1* coamplification have a worse prognosis compared with the patients without *MYCN* amplification ($P = 1.8 \times 10^{-9}$, Kaplan-Meier analysis). The 34 patients with *MYCN* amplification but without *DDX1* coamplification show even worse prognosis compared with patients without *MYCN* amplification, respectively ($P = 5.6 \times 10^{-19}$, Kaplan-Meier analysis).

Amplification Correlates With Elevated Gene Expression Level for DDX1 and NAG

In addition to the coamplification status, we investigated 19 of the 98 tumors for expression pattern of DDX1 and NAG. We found a significant higher expression of DDX1 mRNA in neuroblastomas with *DDX1* coamplification. Thus, high expression level of DDX1 mRNA was found in eight of 10 coamplified tumors, but only in one of nine tumors lacking *DDX1* coamplification ($P < .005$, Fisher's exact test). For *NAG,* we found a trend towards a higher expression level in coamplified tumors, as five of eight coamplified tumors expressed NAG mRNA on a high level, whereas only two of 11 tumors without *NAG* coamplification showed elevated NAG expression ($P = .06$, Fisher's exact test).

Expression of DDX1 mRNA Is Associated With an Improved Survival

Kaplan-Meier analysis using the log-rank test was performed to determine the clinical relevance of mRNA expression level of *DDX1* and *NAG,* as these two genes showed

Information downloaded from jco.ascopubs.org and provided by at UNIVERSITAETSKLINIKUM LEIPZIG on August 27, 2013 from 139.18.235.208
Copyright © 2004 American Society of Clinical Oncology. All rights reserved.

Table 1. Ninety-Eight Investigated Neuroblastoma Patients With *MYCN*-Amplified Tumors

Variable	No. of Patients	6-Year Survival (%)	Median Survival Time (months)	95% CI (months)	*P* (log-rank test)	6-Year Survival Probability*	
						No. of Patients	%
MYCN							
Amplified	98	30.2	28.3	18.1 to 38.6	—	51	24.8
DDX1							
Noncoamplified	34	14.9	20.6	8.6 to 32.6		15	0
Coamplified	64	39.6	33.3	11.8 to 54.8	.027	36	35.2
NAG							
Noncoamplified	56	19.1	20.6	9.0 to 32.2		29	13.8
Coamplified	42	42.6	30.1	4.4 to 55.8	.09	12	39.8
NSE1							
Noncoamplified	77	28.7	28.4	17.1 to 39.6		41	23.5
Coamplified	21	33.3	21.0	0.0 to 53.7	.40	10	30.0
LPIN1							
Noncoamplified	93	30.3	28.6	17.5 to 39.7		49	25.9
Coamplified	5	26.7	20.8	7.4 to 34.2	.75	2	0
AA581763							
Noncoamplified	9	14.3	20.6	17.9 to 23.3		6	11.1
Coamplified	89	31.3	29.7	17.5 to 42.0	.34	45	26.7
SMC6							
Noncoamplified	86	27.7	21.0	10.2 to 31.8		48	27.1
Coamplified	12	0.0	29.7	26.9 to 32.6	.34	3	0
SDC1							
Noncoamplified	94	31.9	28.3	17.3 to 39.4		49	25.9
Coamplified	4	0.0	20.8	0.0 to 61.0	.94	2	0

*Analysis of neuroblastoma patients with a minimum follow-up time of 72 months.

highest relevance for clinical outcome based on the coamplification status. Patients with tumors that express *DDX1* on higher levels showed a trend towards a better survival probability that nearly reached statistical significance ($P = .058$), whereas *NAG* expression was not correlated with a better clinical outcome ($P = .47$, Kaplan-Meier analysis).

DISCUSSION

It is generally accepted that the *MYCN* oncogene represents the core of the chromosomal region on 2p24-25, frequently amplified in human neuroblastoma tumors as no genes in this region have been reported to be amplified independent of the *MYCN* gene locus.[10,12] Mechanisms of gene amplification are complex. Thus, it is yet unclear whether it is possible for a highly proliferating clone of cells to control the size and structure of resulting amplicons, as we can see a variety of amplicon sizes, rearrangments, deletions, and resulting structures in *MYCN* amplicons in neuroblastoma tumors.[12] In accordance to these previous observations, we can see a high number of gene coamplification combinations in our investigated population defining differences in amplicon size and structure and, in a subset of amplicons, deleted regions. Most of the investigated *MYCN* amplicons (66 of 98) span shorter distances telomeric and centromeric of the *MYCN* locus, including *DDX1*, *NAG*, and EST-*AA581763*. Genes located in farther distances from *MYCN* are coamplified less frequently (Fig 2). For all investigated genes, we can show that frequency of gene coamplification within the 2p24-25 amplicon in neuroblastoma is directly correlated to the physical distance to *MYCN*. These results underline the role for *MYCN* as the core gene within the 2p24-25 amplicon, and make a superordinated, controlled determination of the amplicon size and structure unlikely.

Coamplification of *DDX1*, *NAG*, *SDC1*, *LPIN1*, and *NSE1* within the *MYCN* amplicon have been reported previously[7,8,33] and our data are in accordance with the reported coamplification frequencies and maximal amplicon sizes. Despite these genes, we can first describe the coamplification of *SMC6* and a locus in centromeric vincinity to *MYCN* as EST-*AA581763*. Interestingly, *SMC6* belongs to the same DNA organizing SMC complex as *NSE1*,[22] thus, two genes encoding for proteins involved in DNA damage repair lie within 3,000 kb distance telomeric and centromeric to *MYCN* and are coamplified in a subset of tumors.[34] As expected, investigated genes located most distantly to *MYCN* in our study (*SDC1* and *LPIN1*) are coamplified in only 4% and 5%, respectively. Thus, we could show that these genes statistically earmark the maximal expansion of the *MYCN* amplicon, as almost 95% of the investigated

Information downloaded from jco.ascopubs.org and provided by at UNIVERSITAETSKLINIKUM LEIPZIG on August 27, 2013 from 139.18.235.208
Copyright © 2004 American Society of Clinical Oncology. All rights reserved.

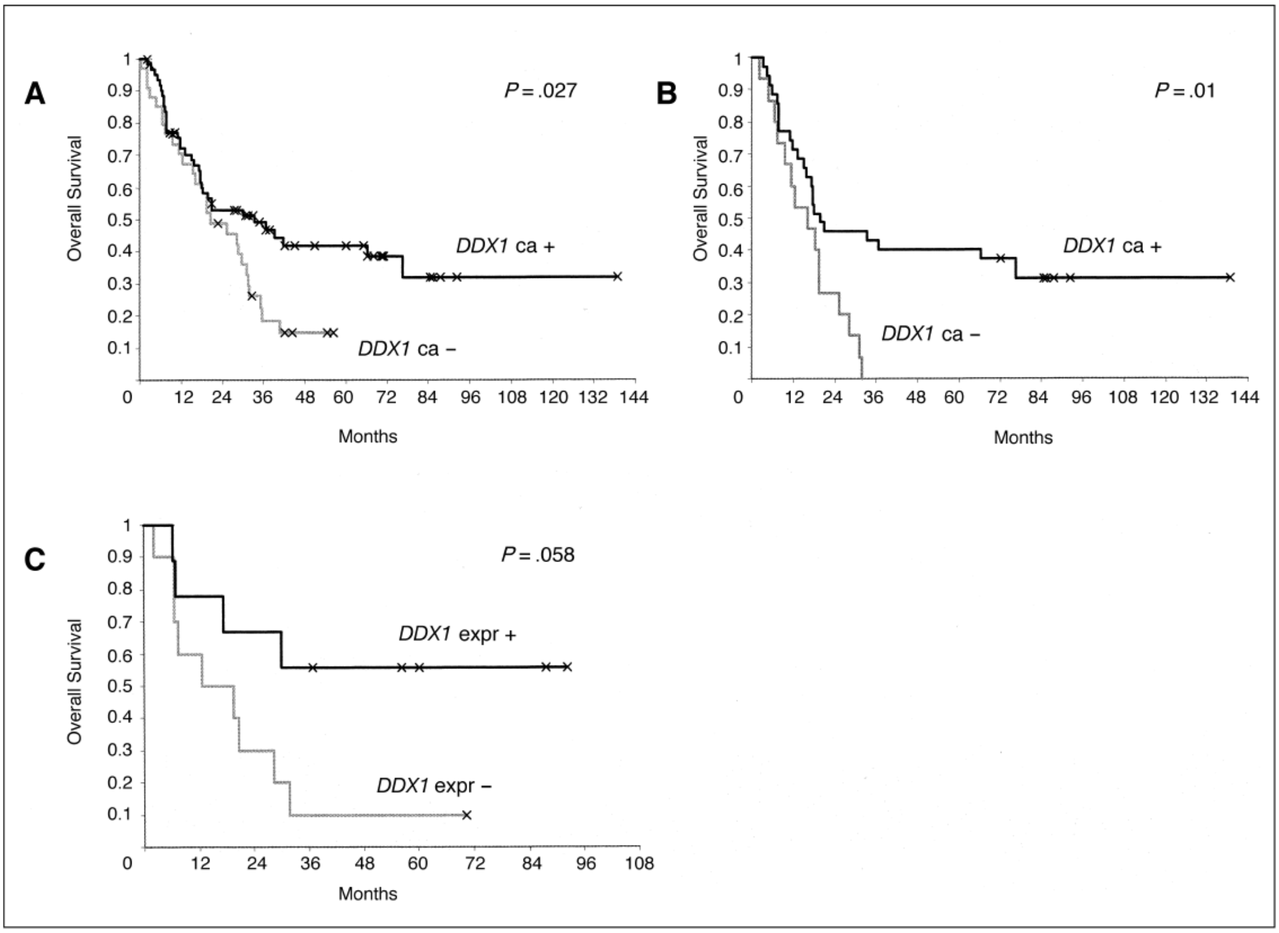

Fig 3. Kaplan-Meier survival analyses for *DDX1* coamplification in the (A) population of all 98 investigated tumors (n = 98) and (B) in tumors with a long-term follow-up ≥ 72 months (n = 51) after initial diagnosis and (C) for *DDX1* mRNA expression in a subset of patients (n = 19).

neuroblastoma tumors showed amplicon sizes of smaller extension. We hypothesize that genes in farther distances telomeric or centromeric to *MYCN* have to be found even more rarely coamplified with *MYCN*.

Reiter and Brodeur[12] found a high frequency of rearrangements in investigated *MYCN* amplicons. They hypothesized that most of the coamplified sequences belonging to normally functional genes would lack their genomic function, because genes would not lie within a physiological genomic context in the DNA amplicons compared with their context (eg, promotor regions) in the wild type chromosomal region. They defined a 130 kb core region for the *MYCN* amplicon containing the *MYCN* gene and a region of 125 kb centromeric and 5 kb telomeric to *MYCN* that is amplified in 32 (97%) of 33 *MYCN* amplified tumors. However, recent studies by Chen et al[35] could show that rearrangements, even at the *MYCN* locus, occur late in amplicon formation, as they could be found less frequently compared with the according unrearranged sequences in the same cell line. These results indicate that even the case of existing rearranged sequences within an amplicon structure does not exclude the existence of coamplified functional regions in far distance to the amplicon's core.

Based on recent BLAT alignment data, *DDX1* and *NAG* are the closest yet known functional sequences telomeric to *MYCN* on 2p24-25, but they do not lie within the formerly defined core region. The coamplification frequency for both genes based on our data is in accordance to this finding, as both genes are coamplified less often compared with sequences within the defined core region (Fig 2). We found EST-*AA581763* coamplified in 91% of all 98 investigated cases according to the close genomic localization 87.3 kb centromeric to *MYCN* and thus, within the defined amplicon core region. Conspicuously, the centromeric gene *SCM6* is coamplified less often than the telomeric genes *DDX1* or *NAG,* although it is assigned in a closer distance to *MYCN*. This finding might be explained as a result of the high variety of amplicon borders and rearrangements described outside the defined core region by Reiter and Brodeur.[12] Another argument for functionality of coamplified

Information downloaded from jco.ascopubs.org and provided by at UNIVERSITAETSKLINIKUM LEIPZIG on August 27, 2013 from 139.18.235.208
Copyright © 2004 American Society of Clinical Oncology. All rights reserved.

Table 2. Analyses of 98 MYCN-Amplified Neuroblastoma Patients

	P
Univariate Kaplan-Meier analysis	
DDX1-coamplification*	.027
Stage†	.016
Age at diagnosis	.27
Multivariate Cox-regression analysis	
First variable	
DDX1-coamplification	
Second variable	
Stage†	.05
Age at diagnosis‡	.033

*Coamplification versus noncoamplification.
†Stages 1, 2, 3, 4S versus 4.
‡$<$ 12 versus $>$ 12 months.

genes is given by the frequent finding of an upregulated mRNA expression level of the respective amplified gene.[35]

For neuroblastoma tumors, most data concerning correlation of gene amplification and expression exist for *MYCN*, *DDX1*, and *NAG*.[9,36,37] Our expression analysis of 19 out of the 98 primary neuroblastomas with *MYCN* amplification also revealed significantly higher mRNA expression levels for DDX1 and NAG in tumors with coamplification for the according gene, compared with noncoamplified tumors.

It is thought that genetic alterations, deletions of chromosomal regions, amplification, and coamplification of genes in tumor cells could lead to a growth advantage for the malignant cell clone through either loss of tumor suppressor genes or alteration of gene products with oncogenic potential. Both aberrations qualify the malignant clone to overcome physiological growth control mechanisms. Thus, it does not seem to be conclusive that coamplification and resulting overexpression of a gene might be responsible for a better prognosis in malignant disease. However, we can show that coamplification of *DDX1* within the *MYCN* amplicon correlates with an improved long-term survival probability in neuroblastoma patients (Table 1; Fig 3). These data are, in part, contrary to previous investigations of smaller sample studies that describe no correlations or trends towards a worse prognosis in case of *DDX1* coamplification ($n = 13$, 16, 27, 35, 66, and 45 respectively).[6-11] Interestingly, the survival analysis of 66 neuroblastoma patients recently published by De Preter et al[10] shows a trend toward a better prognosis for patients in the groups of DDX1 and DDX1/NAG coamplified neuroblastomas, which is in accordance with our investigation. However, their analysis did not reach statistical significance, probably because of the shorter follow-up time and the smaller cohort size ($n = 66$).

DDX1 is a putative RNA helicase containing the characteristic D(Asp)-E(Glu)-A(Ala)-D(Asp)-box highly conserved sequence motif. The DDX family proteins share function by altering RNA secondary structure, thus they are found to influence translation initiation, splicing, and ribosome and splicesome assembly. Godbout et al[19] identified a homologous region in the amino acid sequence for DDX1 to heterogenous nuclear ribonucleoprotein-U (hnRNP-U), a RNA binding and processing protein.[38] Furthermore, DDX1 has recently been identified as an interaction partner for heterogenous nuclear ribonucleoprotein K (hnRNP-K), and the authors can show that the ability of RNA unwinding of DDX1 is dependent on complex formation with hnRNP-K in vitro.[39] hnRNP-K is a multifunctional protein involved in regulation of transcription, translation, nuclear transport, and signal transduction.[40-42] Recent findings identify translational silencing of differentiation regulating proteins as a major specific function of active hnRNP-K. This translation control activity is regulated by c-Src kinase.[43] Thus, DDX1 might be directly involved in RNA processing by its local homology to hnRNP-U, and in translational silencing processes by its interaction with hnRNP-K.

Our data also provide a trend towards a better prognosis in patients with neuroblastomas coamplified for *NAG*. Scott et al[11] recently characterized the *NAG* transcript and genomic structure. These authors found a significant association between coamplification of *NAG* and lower stage of the *MYCN*-amplified tumors. These data are in accordance to our findings for a better survival in the *NAG*-coamplified group of tumors, although there is no correlation in *MYCN*-amplified neuroblastoma between stage and survival, per se. In our group of 98 neuroblastoma patients, we can see a significantly better outcome for patients with tumors of stage 1, 2, 3, and 4S at the time of diagnosis compared with stage 4 ($n = 98$; $P = .016$, Kaplan and Meier analysis; Table 2). In contrast to our *DDX1* coamplification data, this analysis loses statistical significance with exclusion of patients with a short time-to-follow-up period ($<$ 72 months; $n = 51$; $P = .44$, Kaplan and Meier analysis).

As coamplification of a gene involved in mechanisms of cell proliferation and/or division (eg, RNA processing like DDX1) may lead primarily to a growth advantage for the according cells, it may also lead to a better chemotherapy response in these tumors. Thus, more than a direct antiproliferative effect on tumor growth, enhanced chemosensibility should be discussed as a more likely reason for the better outcome of patients with DDX1 coamplification. Comparable findings in childhood acute lymphoblastic leukemia demonstrate that amplification of the AML1 gene or involvement of AML1 in a gene fusion product, as a result of a translocation t(12;22), results in a better response to chemotherapy treatment of the leukemic cells and thus a better prognosis for the patients.[44-49] These data emphasize the possibility for a factor-mediating clonal growth advantage to sensitize cells to chemotherapy treatment.

Information downloaded from jco.ascopubs.org and provided by at UNIVERSITAETSKLINIKUM LEIPZIG on August 27, 2016 from 139.18.235.208
Copyright © 2004 American Society of Clinical Oncology. All rights reserved.

Taken together, our data show that coamplification frequency of genes in primary human neuroblastoma tumors with *MYCN* amplification is directly correlated with the physical distance to the core region of the amplified chromosomal region on chromosome 2p24-25. Our findings strongly imply a role for *DDX1* in tumorigenesis and further tumor development of *MYCN*-amplified human neuroblastoma tumors. Thus, we show that coamplification of *DDX1* identifies a subgroup of patients with a significantly better survival probability. Furthermore, the prognostic impact of *DDX1* coamplification is statistically independent of tumor stage and patient's age at diagnosis. One possible mechanism for our findings might be a functional interaction of DDX1 with hnRNP-K in influencing the translational control of genes involved in cellular differentation processes.

More information about the regulation of these differentiation influencing pathways is needed for future therapeutic approaches that may aim at influencing DDX1 and hnRNP-K pathways contributing differentiation induction in human neuroblastomas. Our findings are of substantial clinical interest for patients with *MYCN*-amplified neuroblastoma for evaluation of survival probability and reevaluation after initial treatment. However, further confirmation of our correlated data is needed to evaluate a possible practical usage for the coamplification and expression status of DDX1 as an additional prognostic marker for *MYCN*-amplified neuroblastoma.

■ ■ ■

Acknowledgment

The acknowledgment is included in the full-text version of this article, available on-line at www.jco.org. It is not included in the PDF (via Adobe® Acrobat Reader®) version.

Authors' Disclosures of Potential Conflicts of Interest

The authors indicated no potential conflicts of interest.

REFERENCES

1. Schwab M, Alitalo K, Klempnauer KH, et al: Amplified DNA with limited homology to myc cellular oncogene is shared by human neuroblastoma cell lines and a neuroblastoma tumour. Nature 305:245-248, 1983

2. Brodeur GM, Seeger RC, Schwab M, et al: Amplification of N-myc in untreated human neuroblastomas correlates with advanced disease stage. Science 224:1121-1124, 1984

3. Brodeur GM, Maris JM, Yamashiro DJ, et al: Biology and genetics of human neuroblastomas. J Pediatr Hematol Oncol 19:93-101, 1997

4. Kawa K, Ohnuma N, Kaneko M, et al: Long-term survivors of advanced neuroblastoma with MYCN amplification: A report of 19 patients surviving disease-free for more than 66 months. J Clin Oncol 17:3216-3220, 1999

5. Brodeur GM, Seeger RC: Gene amplification in human neuroblastomas: Basic mechanisms and clinical implications. Cancer Genet Cytogenet 19:101-111, 1986

6. Squire JA, Thorner PS, Weitzman S, et al: Co-amplification of MYCN and a DEAD box gene (DDX1) in primary neuroblastoma. Oncogene 10:1417-1422, 1995

7. George RE, Kenyon RM, McGuckin AG, et al: Investigation of co-amplification of the candidate genes ornithine decarboxylase, ribonucleotide reductase, syndecan-1 and a DEAD box gene, DDX1, with N-myc in neuroblastoma. United Kingdom Children's Cancer Study Group. Oncogene 12:1583-1587, 1996

8. George RE, Kenyon R, McGuckin AG, et al: Analysis of candidate gene co-amplification with MYCN in neuroblastoma. Eur J Cancer 33:2037-2042, 1997

9. Manohar CF, Salwen HR, Brodeur GM, et al: Co-amplification and concomitant high levels of expression of a DEAD box gene with MYCN in human neuroblastoma. Genes Chromosomes Cancer 14:196-203, 1995

10. De Preter K, Speleman F, Combaret V, et al: Quantification of MYCN, DDX1, and NAG gene copy number in neuroblastoma using a real-time quantitative PCR assay. Mod Pathol 15:159-166, 2002

11. Scott DK, Board JR, Lu X, et al: The neuroblastoma amplified gene, NAG: Genomic structure and characterisation of the 7.3 kb transcript predominantly expressed in neuroblastoma. Gene 307:1-11, 2003

12. Reiter JL, Brodeur GM: High-resolution mapping of a 130-kb core region of the MYCN amplicon in neuroblastomas. Genomics 32:97-103, 1996

13. Kent WJ: BLAT—The BLAST-like alignment tool. Genome Research 12:656-664, 2002

14. Tanner NK, Linder P: DExD/H box RNA helicases: From generic motors to specific dissociation functions. Mol Cell 8:251-262, 2001

15. Hashimoto K, Nakagawa Y, Morikawa H, et al: Co-overexpression of DEAD box protein rck/p54 and c-myc protein in human colorectal adenomas and the relevance of their expression in cultured cell lines. Carcinogenesis 22:1965-1970, 2001

16. Klappacher GW, Lunyak VV, Sykes DB, et al: An induced Ets repressor complex regulates growth arrest during terminal macrophage differentiation. Cell 109:169-180, 2002

17. Godbout R, Squire J: Amplification of a DEAD box protein gene in retinoblastoma cell lines. Proc Natl Acad Sci U S A 90:7578-7582, 1993

18. Amler LC, Schurmann J, Schwab M: The DDX1 gene maps within 400 kbp 5′ to MYCN and is frequently coamplified in human neuroblastoma. Genes Chromosomes Cancer 15:134-137, 1996

19. Godbout R, Hale M, Bisgrove D: A human DEAD box protein with partial homology to heterogeneous nuclear ribonucleoprotein U. Gene 138:243-245, 1994

20. Pandita A, Godbout R, Zielenska M, et al: Relational mapping of MYCN and DDXl in band 2p24 and analysis of amplicon arrays in double minute chromosomes and homogeneously staining regions by use of free chromatin FISH. Genes Chromosomes Cancer 20:243-252, 1997

21. Wimmer K, Zhu XX, Lamb BJ, et al: Co-amplification of a novel gene, NAG, with the N-myc gene in neuroblastoma. Oncogene 18:233-238, 1999

22. Fujioka Y, Kimata Y, Nomaguchi K, et al: Identification of a novel non-structural maintenance of chromosomes (SMC) component of the SMC5-SMC6 complex involved in DNA repair. J Biol Chem 277:21585-21591, 2002

23. Peterfy M, Phan J, Xu P, et al: Lipodystrophy in the fld mouse results from mutation of a new gene encoding a nuclear protein, lipin. Nat Genet 27:121-124, 2001

24. Taylor EM, Moghraby JS, Lees JH, et al: Characterization of a novel human SMC heterodimer homologous to the Schizosaccharomyces pombe Rad18/Spr18 complex. Mol Biol Cell 12:1583-1594, 2001

25. Ala-Kapee M, Nevanlinna H, Mali M, et al: Localization of gene for human syndecan, an integral membrane proteoglycan and a matrix receptor, to chromosome 2. Somat Cell Mol Genet 16:501-505, 1990

26. Alexander CM, Reichsman F, Hinkes MT, et al: Syndecan-1 is required for Wnt-1-induced mammary tumorigenesis in mice. Nat Genet 25:329-332, 2000

27. Brodeur GM, Pritchard J, Berthold F, et al: Revisions of the international criteria for neuroblastoma diagnosis, staging, and response to treatment. J Clin Oncol 11:1466-1477, 1993

28. Berthold F, Burdach S, Kremens B, et al: The role of chemotherapy in the treatment of children with neuroblastoma stage IV: The GPO (German Pediatric Oncology Society) experience. Klin Padiatr 202:262-269, 1990

29. Berthold F, Hero B: Neuroblastoma: Current drug recommendations as part of the total treatment approach. Drugs 59:1261-1277, 2000

30. Chomczynski P, Sacchi N: Single-step method of RNA isolation by acid guanidinium

Information downloaded from jco.ascopubs.org and provided by at UNIVERSITAETSKLINIKUM LEIPZIG on August 27, 2010 from 139.18.235.208
Copyright © 2004 American Society of Clinical Oncology. All rights reserved.

thiocyanate-phenol-chloroform extraction. Anal Biochem 162:156-159, 1987

31. Christiansen H, Sahin K, Berthold F, et al: Comparison of DNA aneuploidy, chromosome 1 abnormalities, MYCN amplification and CD44 expression as prognostic factors in neuroblastoma. Eur J Cancer 31A:541-544, 1995

32. Livak KJ, Schmittgen TD: Analysis of relative gene expression data using real-time quantitative PCR and the 2(-Delta Delta C(T)) Method. Methods 25:402-408, 2001

33. Beheshti B, Braude I, Marrano P, et al: Chromosomal localization of DNA amplifications in neuroblastoma tumors using cDNA microarray comparative genomic hybridization. Neoplasia 5:53-62, 2003

34. Hirano T: The ABCs of SMC proteins: Two-armed ATPases for chromosome condensation, cohesion, and repair. Genes Dev 16:399-414, 2002

35. Chen B, Jhanwar SC, Ladanyi M: Rearrangement in the coding region of the MYCN gene in a subset of amplicons in a case of neuroblastoma with MYCN amplification. Diagn Mol Pathol 10:100-104, 2001

36. Schwab M, Ellison J, Busch M, et al: Enhanced expression of the human gene N-myc consequent to amplification of DNA may contribute to malignant progression of neuroblastoma. Proc Natl Acad Sci U S A 81:4940-4944, 1984

37. Godbout R, Packer M, Bie W: Overexpression of a DEAD box protein (DDX1) in neuroblastoma and retinoblastoma cell lines. J Biol Chem 273:21161-21168, 1998

38. Kiledjian M, Dreyfuss G: Primary structure and binding activity of the hnRNP U protein: Binding RNA through RGG box. EMBO J 11:2655-2664, 1992

39. Chen HC, Lin WC, Tsay YG, et al: An RNA helicase, DDX1, interacting with poly(A) RNA and heterogeneous nuclear ribonucleoprotein K. J Biol Chem 277:40403-40409, 2002

40. Michael WM, Eder PS, Dreyfuss G: The K nuclear shuttling domain: A novel signal for nuclear import and nuclear export in the hnRNP K protein. EMBO J 16:3587-3598, 1997

41. Takimoto M, Tomonaga T, Matunis M, et al: Specific binding of heterogeneous ribonucleoprotein particle protein K to the human c-myc promoter, in vitro. J Biol Chem 268:18249-18258, 1993

42. Ostareck DH, Ostareck-Lederer A, Wilm M, et al: mRNA silencing in erythroid differentiation: HnRNP K and hnRNP E1 regulate 15-lipoxygenase translation from the 3′ end. Cell 89:597-606, 1997

43. Ostareck-Lederer A, Ostareck DH, Cans C, et al: C-Src-mediated phosphorylation of hnRNP K drives translational activation of specifically silenced mRNAs. Mol Cell Biol 22:4535-4543, 2002

44. Borkhardt A, Cazzaniga G, Viehmann S, et al: Incidence and clinical relevance of TEL/AML1 fusion genes in children with acute lymphoblastic leukemia enrolled in the German and Italian multicenter therapy trials. Associazione Italiana Ematologia Oncologia Pediatrica and the Berlin-Frankfurt-Munster Study Group. Blood 90:571-577, 1997

45. Busson-Le Coniat M, Nguyen Khac F, et al: Chromosome 21 abnormalities with AML1 amplification in acute lymphoblastic leukemia. Genes Chromosomes Cancer 32:244-249, 2001

46. Dal Cin P, Atkins L, Ford C, et al: Amplification of AML1 in childhood acute lymphoblastic leukemias. Genes Chromosomes Cancer 30:407-409, 2001

47. Maloney K, McGavran L, Murphy J, et al: TEL-AML1 fusion identifies a subset of children with standard risk acute lymphoblastic leukemia who have an excellent prognosis when treated with therapy that includes a single delayed intensification. Leukemia 13:1708-1712, 1999

48. Ramakers-van Woerden NL, Pieters R, Loonen AH, et al: TEL/AML1 gene fusion is related to in vitro drug sensitivity for L-asparaginase in childhood acute lymphoblastic leukemia. Blood 96:1094-1099, 2000

49. Krishna Narla R, Navara C, Sarquis M, et al: Chemosensitivity of TEL-AML1 fusion transcript positive acute lymphoblastic leukemia cells. Leuk Lymphoma 41:615-623, 2001

Information downloaded from jco.ascopubs.org and provided by at UNIVERSITAETSKLINIKUM LEIPZIG on August 27, 2016 from 139.18.235.208
Copyright © 2004 American Society of Clinical Oncology. All rights reserved.

The Coamplification Pattern of the *MYCN* Amplicon Is an Invariable Attribute of Most *MYCN*-Amplified Human Neuroblastomas

Axel Weber, Sven Starke, Eckhard Bergmann, and Holger Christiansen

Abstract **Purpose:** Fifteen percent to 20% of human neuroblastomas show amplification of the *MYCN* oncogene physiologically located at chromosome 2p24-25, indicating an aggressive subtype of human neuroblastoma with a poor clinical outcome. Recent findings revealed that the structure of the amplicon differs interindividually and that coamplification of genes in telomeric proximity to *MYCN* might play a relevant role in neuroblastoma development and response to treatment, respectively. We now asked if the amplicon structure is an invariable attribute of an individual tumor or if the coamplification pattern could change during progress or in case of recurrent disease.

Experimental Design: We used a previously described multiplex PCR approach to analyze the coamplification status of *MYCN*-amplified human neuroblastomas ($n = 33$) in tumor tissue at the time of initial diagnosis and in consecutive tissue specimens at later time points after initial treatment or from relapsing disease. The *MYCN* copy number per haploid genome (Mcn/hg) in these specimens was determined in a separate duplex PCR.

Results: In 32 of the 33 investigated tumors, the amplicon structure showed no changes after initial chemotherapy and in recurrent disease. Mcn/hg showed a decrease after initial treatment ($n = 23$), whereas we found a significant increase in recurrent disease ($n = 10$).

Conclusion: Our data indicate that the initial determined structure of the 2p24-25 amplicon is a consistent attribute in the great majority of the individual *MYCN*-amplified neuroblastomas and shows no plasticity during or after chemotherapy. Observed changes in the Mcn/hg over the course of disease are in line with preexisting cell culture findings.

Amplification of the *MYCN* oncogene is the most extensively studied biological marker for an unfavorable prognostic outcome in patients with neuroblastoma (1–3). The overall survival probability for patients with *MYCN* amplification is <30% in the first 6 years after initial diagnosis (own data of 216 patients with *MYCN*-amplified neuroblastoma). Within this population, patients that show no metastatic disease at initial diagnosis (stages I, II, and III) respond better to current therapy strategies, including high-dose chemotherapy, autologous stem cell transplantation, and treatment with 13-*cis*-retinoic acid compared with patients with initial stage IV disease. Examining primary tumor samples of a large cohort of patients for coamplification pattern of different genes telomeric and centromeric to *MYCN*, we recently showed that the coamplification of the *DDX1* gene, in proximal telomeric vicinity to *MYCN*, identifies a subgroup of patients with an improved survival probability compared with patients without this coamplification, independently of stage and age (4).

However, not all of the long-time-surviving patients harbored *DDX1* coamplification and not every patient that underwent rapid progression of disease lacked *DDX1* coamplification. Other investigators found only a trend toward a better prognosis (5) or even described a trend toward a worse prognosis for patients with *DDX1*-coamplified tumors (6–9). Because of the relative homogeneity regarding prognosis of the patients in these studies and the small numbers of investigated patients, statistical significance was not obtained. We hypothesized that DDX1 might influence the response of neuroblastoma cells to chemotherapy under certain conditions but does not serve as a warrant for survival per se.

In cell culture studies on methotrexate-treated Chinese hamster and mouse cells, Hahn et al. (10, 11) showed that an elevation in the amplification number of the amplified *dihydrofolate reductase* gene occurs under increasing selective pressure. Furthermore, the authors described a trend to a reduction in the amplicon size under these strong selective conditions. In general, the size of the amplified DNA fragments in those cell models is described to be a stable attribute independent of the manner of amplification as double-minute chromosomes or homogenously staining regions (11, 12).

These findings and our previously determined data of coamplification pattern in primary neuroblastoma prompted us to ask if the structure and the copy number of the chromosome 2p24-25 amplicon, once determined at initial neuroblastoma development, are invariable attributes for each

---

Authors' Affiliation: Children's Hospital, Pediatric Hematology and Oncology, University of Marburg, Marburg, Germany

Received 4/4/06; revised 8/15/06; accepted 10/6/06.

The costs of publication of this article were defrayed in part by the payment of page charges. This article must therefore be hereby marked *advertisement* in accordance with 18 U.S.C. Section 1734 solely to indicate this fact.

Note: Supplementary data for this article are available at Clinical Cancer Research Online (http://clincancerres.aacrjournals.org/).

Requests for reprints: Holger Christiansen, Universitaetskinderklinik, Baldinger Strasse, D-35049 Marburg, Germany. Phone: 49-6421-28-62671; Fax: 49-6421-28-66824; E-mail: holger.christiansen@mailer.uni-marburg.de.

©2006 American Association for Cancer Research.

doi:10.1158/1078-0432.CCR-06-0837

individual *MYCN*-amplified neuroblastoma. To answer that question, we analyzed the coamplification pattern of subsequent tissue specimens taken at initial diagnosis and at different time intervals after treatment initiation of 33 patients with *MYCN*-amplified neuroblastoma using the two multiplex PCRs previously described (4). Furthermore, we determined the number of amplified copies of *MYCN* in relation to ***inhibin-β-b*** in a separate, semiquantitative duplex PCR (Supplementary Fig. S1).

Patients and Methods

Patients. We studied primary tumor specimens from 33 children with *MYCN*-amplified neuroblastomas diagnosed in Germany from 1986 to 2003. The 33 neuroblastomas were selected out of a total number of 174 tumor specimens with *MYCN* amplification within this period of time. The selection criterion was the availability of tumor tissue of comparable quality to different time points during therapy of each individual patient for DNA isolation.

All neuroblastoma diagnoses were confirmed by histologic assessment of a tumor specimen obtained at surgery. The tumors were classified according to the International Neuroblastoma Staging System criteria (13). All patients were treated according to previously described protocols with confirmed consent for therapy and study procedures (14, 15). Therapy included surgery, polychemotherapy, and, dependent on the randomization procedure, high-dose chemotherapy with autologous stem cell transplantation, anti-GD2 antibody, and retinoic acid treatment.

Our study group consisted of 1 stage I, 0 stage II, 10 stage III, 17 stage IV, and 5 stage IV-S tumors. The median patient age at diagnosis was 30.8 months (range 0.6-163.3 months). The median follow-up time for all 33 patients was 25.2 months (range 7.5-150.1 months). The median follow-up time of the patients that died of the disease was 18.4 months (n = 21) compared with 82.6 months for patients alive (n = 12).

The mean time interval between first and second biopsy of all investigated patients (n = 33) was 4.6 months (range 1.0-76.9 months). The mean time between first and third biopsy (n = 3) was 22.5 months. Most of the second biopsies were taken from the site of the initial tumor during operation after initial chemotherapy treatment. The mean time between first and second biopsy of these patients (n = 23) was 4.1 months (range 1.0-20.3 months). For 10 patients, recurrent disease was diagnosed based on the clinical criteria that before relapse, a full remission of the initial disease occurred during therapy. The mean time between first and second biopsy of these patients (n = 10) was 17.2 months (range 5.2-76.9 months). Clinical data and amplification pattern of all investigated patients are presented in Table 1.

Methods. Isolation of genomic DNA and the two multiplex PCR was done as previously described (4). The mean tumor cell content of investigated *MYCN*-amplified neuroblastoma in the last 6 years in our laboratory was 80% (range 98% maximum to 60% minimum, n = 173). The mean tumor cell content of the investigated specimens in this study was 80% (range 95% maximum to 65% minimum) at initial diagnosis. The mean tumor cell content of the investigated specimens was 80% (range 90% maximum to 60% minimum) at second biopsy (Table 1).

For quantification of the *MYCN* copy number per haploid genome (Mcn/hg), a separate duplex PCR approach was established. Because the band intensities of the investigated genes were, in addition to the amplicon number, dependent on the coamplification pattern in both multiplex PCR, it was essential to design a separate duplex PCR for determination of the *MYCN* copy number relative to a control gene (*inhibin-β-b*) located on the same chromosome (primer used: *MYCN*-upper, CATCCACCAGCAGCACAACTATG; *MYCN*-lower, CCAGAGGCTCCCAACCGT-CAC; *inhibin-β-b*-upper, CATTGCCTTGTGTTCTCCTT; *inhibin-β-b*-lower, GAATGCGGTGCCTG-CTGTC; denaturation 20 s, 95°C; annealing 20 s, 63°C; elongation 60 s, 72°C). The amplified PCR fragments (10 µL of the PCR reaction) were separated on a 2% agarose gel by electrophoresis, visualized by ethidium bromide staining and UV light exposure, and finally documented and analyzed with the Image Master VDS software [GE-Healthcare(Amersham-Pharmacia), Munich, Germany]. The relative level of the PCR bands was determined by densitometry. Moreover, a ratio of the *MYCN* band intensity to the intensity of the *inhibin-β-b* band was determined.

A standard curve was created using a dilution series of genomic DNA from a neuroblastoma with high copy number *MYCN*-amplified neuroblastomas, with known diploid karyotype and known Mcn/hg determined by Southern blot as described previously (4). The tumor DNA (~ 250 Mcn/hg) was diluted stepwise with human placental DNA; thus, the Mcn/hg was halved with each dilution step. The obtained standard curve was used to deduce the Mcn/hg for each patient's tumor specimens (Supplementary Fig. S1).

The coamplification pattern of the investigated genes on chromosome 2p24-25 and the Mcn/hg for each investigated tumor are given in Table 1.

Statistics. Fisher's exact test was used to compare the amplification status for each gene determined at initial diagnosis and at later time points. The paired t test was used to compare the Mcn/hg determined at initial diagnosis and at later time points. Statistical analyses were done with the SPSS version 10.0 software (SPSS, Inc., Chicago, IL). P values of ≤0.05 were regarded as significant.

Results

The coamplification pattern within the **MYCN** *amplicon is an invariable attribute of most neuroblastoma tumors.* In the present cohort besides *MYCN* amplification, 15 (46%) of the investigated tumors showed coamplification for *DDX1*, 11 (33%) for *NAG*, 5 (15%) for *NSE1*, 2 (6%) for *LPIN1*, 31 (94%) for EST-*AA581763*, 2 (6%) for *SMC6*, and 1 (3%) for *SDC1* (Fig. 1; Table 1) The coamplification of genes located telomeric to *MYCN* (*DDX1*, *NAG*, and *NSE1*) was less frequent compared with our previously published data that were determined on a larger cohort (n = 98 patients; ref. 4). However, the differences were not statistically significant and could be explained by the smaller patient numbers in the present study and the relatively high number of patients with recurrent disease selected for investigation within this study.

In the cohort of 33 patients investigated in this study, all patients except one did not show any change in the coamplification pattern during the course of disease, which means that the amplicon structure was invariable at the different time points of subsequent biopsies.

Patient 18 showed a loss of primarily coamplified genes (*NSE1*, *NAG*, and *DDX1*) within the amplicon at the second biopsy date, 76.9 months after the initial diagnosis. This patient was initially diagnosed as a stage I tumor at the age of 6.6 months. At the age of 6.4 years (83.5 months), a recurrent tumor was diagnosed that again was defined as stage I. To the date of our investigation, the patient was still alive (114 months after initial diagnosis; Fig. 2).

In three patients, three consecutive tumor biopsies were investigated. In DNA isolated from third biopsy tissue (n = 3), no change in the amplicon structure was found compared with the first or second biopsy in all three patients. Coamplification of *DDX1* was found in only one of these three specimens. No tumor showed amplification of genes located further telomeric to *MYCN* (Table 1).

The number of amplified **MYCN** *copies decreases after initial chemotherapy and increases in recurrent disease.* Unlike the

Table 1. Clinical data and coamplification pattern of the 33 neuroblastoma patients investigated

Patient no.	Age at diagnosis[*]	Stage[†]	% Viab. t.c.	Mcn/hg	Second biopsy[‡]	Age at second biopsy[*]	% Viab. t.c.	Mcn/hg	Third biopsy[‡]	Age at third biopsy[*]
1	161.6	III	90	120	Rec	180.5	80	120	Rec	184.1
2	36.4	IV	NA	32	Rec	NA	80	32		
3	59.9	III	70	32	Rec	65.6	80	30		
4	0.6	V	90	10	Tu	3.7	90	20		
5	20.8	IV	80	30	Tu	25.7	70	30		
6	49.6	IV	70	10	Tu	52.3	NA	10		
7	11.9	V	75	4	Rec	24.7	90	30	Rec	62.6
8	32.1	IV	80	64	Tu	35.8	80	25		
9	33.5	IV	80	30	Tu	37.6	80	4	Tu	55.4
10	31.0	III	70	30	Tu	35.1	70	30		
11	98.9	III	90	20	Tu	102.3	80	15		
12	66.5	IV	95	5	Tu	70.8	8	5		
13	4.6	V	80	25	Tu	12.4	70	15		
14	163.3	IV	80	20	Tu	167.2	70	20		
15	6.6	IV	80	40	Rec	66.2	90	32		
16	18.9	IV	90	25	Tu	23.2	80	25		
17	26.7	IV	NA	10	Tu	31.4	NA	10		
18	6.6	I	65	20						
18					Rec	83.5	75	64		
19	6.6	V	80	10	Rec	11.7	80	20		
20	46.0	IV	90	10	Rec	53.2	80	60		
21	4.6	III	80	40	Tu	24.9	NA	10		
22	23.7	IV	80	15	Tu	28.5	70	30		
23	19.2	IV	80	30	Rec	33.8	90	60		
24	18.7	III	90	30	Tu	36.0	70	30		
25	33.2	III	80	40	Tu	36.7	70	10		
26	30.8	IV	90	16	Tu	33.5	80	4		
27	33.9	IV	70	16	Tu	36.1	80	10		
28	1.7	V	90	16	Tu	6.6	80	4		
29	29.9	IV	75	24	Rec	53.9	80	64		
30	54.6	III	65	64	Tu	57.9	60	64		
31	27.6	IV	NA	24	Tu	28.6	NA	24		
32	57.5	III	80	64	Tu	61.6	NA	16		
33	21.5	IV	80	64	Tu	25.8	70	32		

NOTE: Only patient 18 showed a change in amplification pattern. The amplification pattern for all other patients is given only once and showed no changes in subsequent specimens.

Abbreviations: Tu, primary tumor; Rec, recurrent tumor; % Viab. t.c., % viable tumor cells; NA, not available; Ampl., amplified gene; s.c., single copy per haploid genome.

[*] Age at different time points in months.

[†] Stage of disease at diagnosis (according to International Neuroblastoma Staging System criteria).

[‡] Tissue for coamplification investigation from primary or recurrent tumor.

coamplification pattern, a significant change in amplification number was observed in the investigated cohort (Fig. 3).

Thus, we found the Mcn/hg to be decreased after initial chemotherapy (n = 23; Fig. 3A). The median Mcn/hg at initial diagnosis was 25 Mcn/hg compared with 20 Mcn/hg after initial chemotherapy (25-75% percentile: 25-40 Mcn/hg compared with 20-30 Mcn/hg, respectively).

In contrast, we found an increase of Mcn/hg in tumor samples of recurrent disease compared with their primary counterparts (n = 10; Fig. 3B). The median *MYCN* copy number at primary diagnosis was 27 Mcn/hg compared with 46 Mcn/hg in recurrent disease (25-75% percentile: 10-36 Mcn/hg compared with 30-64 Mcn/hg, respectively). Both alterations are statistically significant ($P < 0.05$, paired t test).

Discussion

Not much is known about the initiation and genesis of the *MYCN* amplicon in neuroblastoma development. Cheng et al. (16) revealed that, preferentially, the paternal allele undergoes the amplification process. Referring to patient age, recent data indicate that amplification of *MYCN* occurs to a defined point of time in neuroblastoma development as 65% of patients with *MYCN*-amplified neuroblastomas are between 12 and 40 months of age (17). Our data from about 247 patients are in consent with this age distribution, as, in our cohort, 55% *MYCN*-amplified tumors are initially diagnosed at an age between 12 and 40 months.

The amplicon size varies between 350 and >1,000 kb in length, including different coamplified genes telomeric and centromeric of *MYCN* (4, 18). The amplicon number varies from 2 to 256, and, in some cases, more copies per haploid genome in neuroblastoma cells at that time of diagnosis. In the great majority of *MYCN*-amplified neuroblastomas, the amplified genomic regions are initially present in the form of extrachromosomal double minutes rather than in homogeneously staining regions, which can be found mainly in recurrent disease (19, 20).

Table 1. Clinical data and coamplification pattern of the 33 neuroblastoma patients investigated (Cont'd)

Patient no.	% Viab. t.c.	Mcn/hg	Amplified genes							
			LPIN1	*NSE1*	*NAG*	*DDX1*	*MYCN*	*44_332*	*SMC6*	*SDC1*
1	NA	200	s.c.	s.c.	s.c.	s.c.	Ampl.	Ampl.	s.c.	s.c.
2			Ampl.	Ampl.	Ampl.	Ampl.	Ampl.	Ampl.	s.c.	s.c.
3			s.c.	s.c.	s.c.	s.c.	Ampl.	Ampl.	s.c.	s.c.
4			s.c.	s.c.	Ampl.	Ampl.	Ampl.	Ampl.	s.c.	s.c.
5			s.c.	s.c.	Ampl.	Ampl.	Ampl.	Ampl.	s.c.	s.c.
6			s.c.	s.c.	s.c.	Ampl.	Ampl.	Ampl.	s.c.	s.c.
7	NA	20	s.c.	s.c.	s.c.	Ampl.	Ampl.	Ampl.	Ampl.	Ampl.
8			s.c.	s.c.	s.c.	s.c.	Ampl.	Ampl.	s.c.	s.c.
9			s.c.	s.c.	s.c.	s.c.	Ampl.	Ampl.	s.c.	s.c.
10	NA	15	s.c.	s.c.	s.c.	s.c.	Ampl.	Ampl.	s.c.	s.c.
11			s.c.	s.c.	s.c.	s.c.	Ampl.	Ampl.	s.c.	s.c.
12			s.c.	s.c.	s.c.	s.c.	Ampl.	Ampl.	s.c.	s.c.
13			s.c.	s.c.	Ampl.	Ampl.	Ampl.	Ampl.	Ampl.	s.c.
14			s.c.	s.c.	s.c.	s.c.	Ampl.	Ampl.	s.c.	s.c.
15			s.c.	s.c.	s.c.	s.c.	Ampl.	Ampl.	s.c.	s.c.
16			s.c.	s.c.	s.c.	s.c.	Ampl.	Ampl.	s.c.	s.c.
17			s.c.	s.c.	s.c.	s.c.	Ampl.	Ampl.	s.c.	s.c.
18			s.c.	Ampl.	Ampl.	Ampl.	Ampl.	Ampl.	s.c.	s.c.
18			s.c.	s.c.	s.c.	s.c.	Ampl.	Ampl.	s.c.	s.c.
19			s.c.	s.c.	s.c.	s.c.	Ampl.	Ampl.	s.c.	s.c.
20			s.c.	s.c.	Ampl.	Ampl.	Ampl.	Ampl.	s.c.	s.c.
21			s.c.	s.c.	s.c.	s.c.	Ampl.	Ampl.	s.c.	s.c.
22			s.c.	s.c.	s.c.	s.c.	Ampl.	s.c.	s.c.	s.c.
23			s.c.	s.c.	s.c.	s.c.	Ampl.	Ampl.	s.c.	s.c.
24			s.c.	Ampl.	Ampl.	Ampl.	Ampl.	Ampl.	s.c.	s.c.
25			s.c.	Ampl.	Ampl.	Ampl.	Ampl.	Ampl.	s.c.	s.c.
26			s.c.	s.c.	s.c.	Ampl.	Ampl.	s.c.	s.c.	s.c.
27			s.c.	s.c.	Ampl.	Ampl.	Ampl.	Ampl.	s.c.	s.c.
28			Ampl.	s.c.	s.c.	s.c.	Ampl.	Ampl.	s.c.	s.c.
29			s.c.	s.c.	Ampl.	Ampl.	Ampl.	Ampl.	s.c.	s.c.
30			s.c.	s.c.	Ampl.	Ampl.	Ampl.	Ampl.	s.c.	s.c.
31			s.c.	s.c.	s.c.	s.c.	Ampl.	Ampl.	s.c.	s.c.
32			s.c.	s.c.	s.c.	s.c.	Ampl.	Ampl.	s.c.	s.c.
33			s.c.	Ampl.	s.c.	Ampl.	Ampl.	Ampl.	s.c.	s.c.

Extensive DNA rearrangements can be found within the amplified region, leading in part to the phenomenon that coamplified genes might be presented not equally in copy number compared with *MYCN* in either homogenously staining regions or double-minute chromosomes (21, 22).

Yoshimoto et al. (20) described the possibility of coexisting double-minute chromosomes and homogenously staining regions in single tumor cells besides cells with either double-minute chromosomes or homogenously staining regions in one neuroblastoma tumor. They claim a possible transition from double-minute chromosomes to homogenously staining regions during tumor development based on the finding that cells that reintegrate amplified oncogenes into the genome show a growth advantage over cells harboring the amplified gene copies in extrachromosomal double-minute chromosomes (23).

A change or evolution of the amplicon structure has not yet been reported for neuroblastoma. Our findings show that a change of the amplicon structure is uncommon during the course of disease but is possible in neuroblastoma recurrent disease. In the great majority of cases, we found the amplicon structure to be an invariable attribute of the individual tumor that does not undergo rearrangement during therapy. The observed change in the coamplification pattern in one patient could be explained by subsequent selection of more therapy-resistant neuroblastoma cell clones harboring the *MYCN* amplicon of smaller extent (Fig. 2B). As a prerequisite for this explanation, a heterogeneous ancestor cell population, which contains cells harboring *MYCN* amplicons of different sizes at determination of the individual neuroblastoma, has to be presumed. Alternatively, a successive change of the amplicon structure, caused coincidentally in highly proliferating cells or by DNA interfering agents and favoring cells with amplicons of smaller size over a given period of time, could be a possible mechanism. The latter explanation is more consistent with observations in common cell culture models (reviewed in ref. 23).

We previously showed coamplification and overexpression of *DDX1* to occur preferentially in long-time-surviving patients and discussed a possible influence on the response to chemotherapeutics (4). Hypothetically, cells that lose this coamplification telomeric to *MYCN* should become more resistant to chemotherapeutic treatment. Our finding in the neuroblastoma of patient 18 that lost coamplification of *NSE1*, *NAG*, and *DDX1* in the relapsing tumor is consistent with this hypothesis.

Interestingly, for amplified copies of the *c-myc* and *MYCN* genes occurring in double-minute chromosomes, a reduction in copy number after treatment with hydroxyurea can be observed, but not for copies in homogenously staining regions. After hydroxyurea treatment, the amplicon number can recur to the initial count (24). These findings show a possibility to influence gene amplification by medical treatment but also

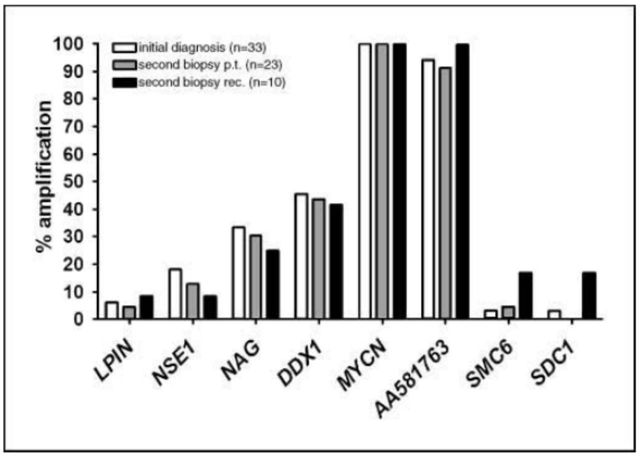

Fig. 1. Frequency of coamplification of the investigated genes on chromosome 2p24-25 in primary tumor tissue at the time of initial diagnosis (*white columns*, *n* = 33) and at the time of the second biopsy [*gray columns*, primary tumor site (*p.t.*; *n* = 23) and *black columns*, recurrent disease (*rec.*; *n* = 10)].

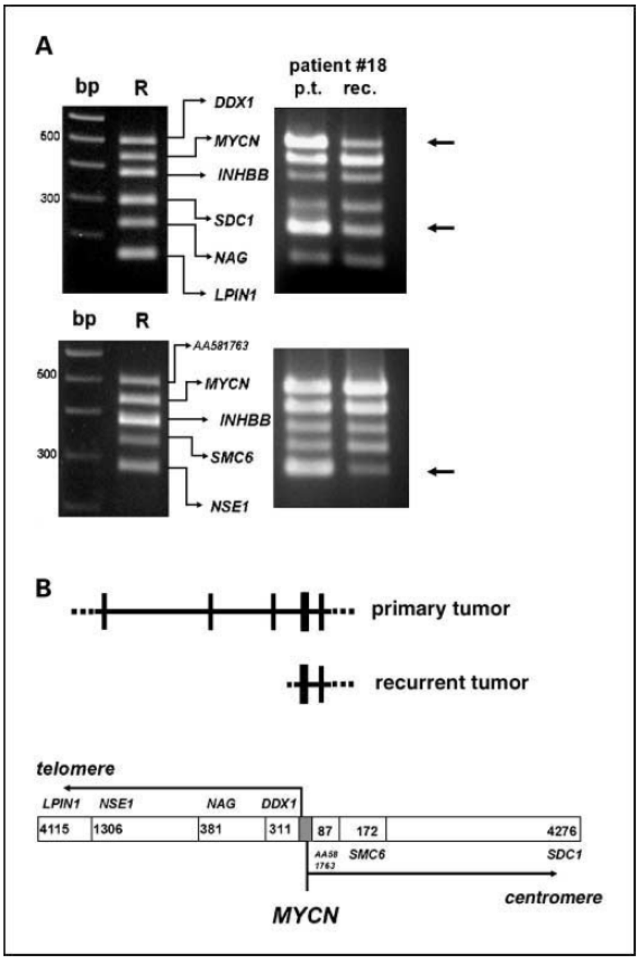

Fig. 2. *A*, different coamplification pattern of patient 18 as indicated by the two described multiplex PCR (*bp*, molecular weight marker; *R*, healthy human kidney DNA was used as single copy reference). *B*, different amplicon structures of patient 18 derived from the two multiplex PCR. Distance (kbp) of the seven investigated genes in relation to *MYCN* (BLAT assignment information).

indicate that these exogenously induced genomic changes are not irreversible. In 1987, Brodeur et al. (25) investigated consecutive tumor samples of 12 patients with *MYCN*-amplified neuroblastomas and describe no change in the amplicon number for their investigated cohort. However, considering the given data of each individual patient, the findings of Brodeur et al. are strongly consistent with our findings. In their study, the Mcn/hg was found to be increased in tumor tissue of four of the seven patients with recurrent disease when compared with the primary tumor tissue. In consecutive specimens of patients during treatment, the Mcn/hg decreased in three of four reported patients.

These findings and our own observation of a reduction of the Mcn/hg after initial chemotherapeutic treatment indicate that the reported observations in cell culture regarding elimination of extrachromosomal amplified *MYCN* in response to treatment is also a possible mechanism of adaptation in primary *MYCN*-amplified neuroblastomas. In a cellular context, this regulation is reasonable as cells that eliminate extrachromosomal copies of *MYCN* might decelerate MYCN-induced proliferation. This is an observed mechanism to avoid massive apoptosis triggered by chemotherapy and enforced by *myc* oncogenes (26). As we lack the information if *MYCN* amplification is present in double-minute chromosomes or homogenously staining regions in neuroblastomas of our investigated patients, a correlation of the molecular phenotype of amplification to a decline of the amplification number is not possible. On the other hand, we observed a significant increase in the Mcn/hg in recurrent disease compared with the initially diagnosed primary neuroblastoma. These cells might represent highly proliferating clones that could bypass myc-enforced apoptosis and, thus, have benefit from harboring a higher Mcn/hg. We have to annotate that the observed changes of the Mcn/hg could also result from a different content of viable tumor cells within the subsequent tissue specimens, based on the used PCR method. However, the tumor cell content of the investigated specimens in this study is interindividually and intraindividually comparable (Table 1).

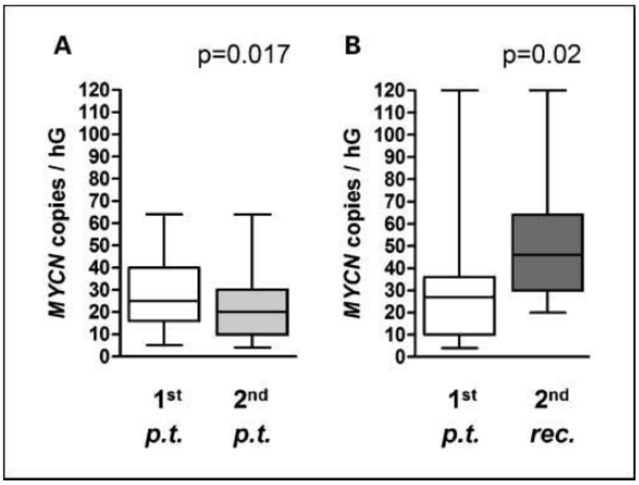

Fig. 3. Copy number of *MYCN* per haploid genome at the time of initial diagnosis (*1st*) and time of second biopsy (*2nd*; *box-whisker plot*). *A*, patients (*n* = 23) with second biopsy at the primary tumor site after initial chemotherapy ($P = 0.017$, paired *t* test). *B*, patients (*n* = 10) with recurrent disease ($P = 0.02$, paired *t* test).

The observed changes in the amplicon copy number over time might reflect abided regulatory mechanisms in neuroblastoma cells comparable with cell culture models of acquired gene amplification. In contrast to an acquired gene amplification under selective pressure, a reason for an initialization of the *MYCN* amplification in developing neuroblastic cells, with the possibility to lead to *MYCN*-amplified neuroblastoma, remains unclear. Once initiated, the *MYCN* amplification is found to be irreversible in neuroblastoma tumors, and, once determined at time of initial amplification, the structure of the *MYCN* amplicon is invariable during the course of disease, including chemotherapy with DNA-damaging agents, in the majority of neuroblastoma tumors.

A fundamental question arises from our findings. Is there a cellular program superior to *MYCN* amplification that advises a cell, deriving from the neural crest, to amplify *MYCN* in a certain developmental condition, which then could lead to *MYCN*-amplified neuroblastoma if this genomic condition becomes an irreversible attribute?

Acknowledgments

We thank Monika Faulhaber for performing many of the PCR experiments, our colleagues from about 100 German pediatric centers for providing us with neuroblastoma tumor material since 1981, Prof. Berthold and Dr. Hero (University of Cologne, Cologne, Germany) for providing clinical data, and Prof. Lampert (University of Gießen, Gießen, Germany) for support of our research group.

References

1. Schwab M, Alitalo K, Klempnauer KH, et al. Amplified DNA with limited homology to myc cellular oncogene is shared by human neuroblastoma cell lines and a neuroblastoma tumour. Nature 1983;305:245–8.

2. Brodeur GM, Seeger RC, Schwab M, Varmus HE, Bishop JM. Amplification of N-myc in untreated human neuroblastomas correlates with advanced disease stage. Science 1984;224:1121–4.

3. Brodeur GM, Maris JM, Yamashiro DJ, Hogarty MD, White PS. Biology and genetics of human neuroblastomas. J Pediatr Hematol Oncol 1997;19:93–101.

4. Weber A, Imisch P, Bergmann E, Christiansen H. Coamplification of DDX1 correlates with an improved survival probability in children with MYCN-amplified human neuroblastoma. J Clin Oncol 2004;22:2681–90.

5. De Preter K, Speleman F, Combaret V, et al. No evidence for correlation of DDX1 gene amplification with improved survival probability in patients with MYCN-amplified neuroblastomas. J Clin Oncol 2005;23:3167–8; author reply 3168–70.

6. Squire JA, Thorner PS, Weitzman S, et al. Co-amplification of MYCN and a DEAD box gene (DDX1) in primary neuroblastoma. Oncogene 1995;10:1417–22.

7. George RE, Kenyon R, McGuckin AG, et al. Analysis of candidate gene co-amplification with MYCN in neuroblastoma. Eur J Cancer 1997;33:2037–42.

8. Manohar CF, Salwen HR, Brodeur GM, Cohn SL. Co-amplification and concomitant high levels of expression of a DEAD box gene with MYCN in human neuroblastoma. Genes Chromosomes Cancer 1995;14:196–203.

9. De Preter K, Speleman F, Combaret V, et al. Quantification of MYCN, DDX1, and NAG gene copy number in neuroblastoma using a real-time quantitative PCR assay. Mod Pathol 2002;15:159–66.

10. Hahn P, Nevaldine B, Morgan WF. X-ray induction of methotrexate resistance due to dhfr gene amplification. Somat Cell Mol Genet 1990;16:413–23.

11. Hahn PJ, Nevaldine B, Longo JA. Molecular structure and evolution of double-minute chromosomes in methotrexate-resistant cultured mouse cells. Mol Cell Biol 1992;12:2911–8.

12. Pauletti G, Lai E, Attardi G. Early appearance and long-term persistence of the submicroscopic extrachromosomal elements (amplisomes) containing the amplified DHFR genes in human cell lines. Proc Natl Acad Sci U S A 1990;87:2955–9.

13. Brodeur GM, Pritchard J, Berthold F, et al. Revisions of the international criteria for neuroblastoma diagnosis, staging, and response to treatment. J Clin Oncol 1993;11:1466–77.

14. Berthold F, Burdach S, Kremens B, et al. The role of chemotherapy in the treatment of children with neuroblastoma stage IV: the GPO (German Pediatric Oncology Society) experience. Klin Padiatr 1990;202:262–9.

15. Berthold F, Hero B. Neuroblastoma: current drug recommendations as part of the total treatment approach. Drugs 2000;59:1261–77.

16. Cheng JM, Hiemstra JL, Schneider SS, et al. Preferential amplification of the paternal allele of the N-myc gene in human neuroblastomas. Nat Genet 1993;4:191–4.

17. London WB, Castleberry RP, Matthay KK, et al. Evidence for an age cutoff greater than 365 days for neuroblastoma risk group stratification in the Children's Oncology Group. J Clin Oncol 2005;23:6459–65.

18. Hiemstra JL, Schneider SS, Brodeur GM. High-resolution mapping of the N-myc amplicon core domain in neuroblastomas. Prog Clin Biol Res 1994;385:51–7.

19. Brodeur GM, Green AA, Hayes FA, Williams KJ, Williams DL, Tsiatis AA. Cytogenetic features of human neuroblastomas and cell lines. Cancer Res 1981;41:4678–86.

20. Yoshimoto M, Caminada De Toledo SR, et al. MYCN gene amplification. Identification of cell populations containing double minutes and homogeneously staining regions in neuroblastoma tumors. Am J Pathol 1999;155:1439–43.

21. Schneider SS, Hiemstra JL, Zehnbauer BA, et al. Isolation and structural analysis of a 1.2-megabase N-myc amplicon from a human neuroblastoma. Mol Cell Biol 1992;12:5563–70.

22. Pandita A, Godbout R, Zielenska M, Thorner P, Bayani J, Squire JA. Relational mapping of MYCN and DDXI in band 2p24 and analysis of amplicon arrays in double minute chromosomes and homogeneously staining regions by use of free chromatin FISH. Genes Chromosomes Cancer 1997;20:243–52.

23. Hahn Peter J. Molecular biology of double minute chromosomes. Bioessays 1993;15:477–84.

24. Von Hoff DD, McGill JR, Forseth BJ, et al. Elimination of extrachromosomally amplified MYC genes from human tumor cells reduces their tumorigenicity. Proc Natl Acad Sci U S A 1992;89:8165–9.

25. Brodeur GM, Hayes FA, Green AA, et al. Consistent N-myc copy number in simultaneous or consecutive neuroblastoma samples from sixty individual patients. Cancer Res 1987;47:4248–53.

26. Fulda S, Lutz W, Schwab M, Debatin KM. MycN sensitizes neuroblastoma cells for drug-induced apoptosis. Oncogene 1999;18:1479–86.

2.5 Strukturelle Untersuchung des *MYCN* Amplikons und Entwicklung eines MRD Markers

Hintergrund:

Die Ergebnisse der Multiplex-PCR Untersuchungen *MYCN* amplifizierter Neuroblastome (Abschnitt 2.4) zeigten eine deutliche Variabilität in der Ausdehnung der amplifizierten Genomabschnitte (ampGA) sowohl telomer- als auch centromerwärts zu *MYCN*.
Um die Grenzen der ampGA genau identifizieren zu können wurde genomische DNA von n=40 primären Neuroblastomen und 3 Zelllinien mit bekannter *MYCN* Amplifikation mittels eines hochauflösenden Tiling-Arrays (HR-TA) untersucht. Aufgrund der Fokussierung der Untersuchung auf einen Bereich um *MYCN* von insgesamt 20 Megabasen konnten die auf den Array hybridisierten DNA Oligos in einem durchschnittlichen Abstand von 50 (+/- 8bp) Basen designt werden (Bereiche mit hoher Repeatdichte ausgenommen). Diese hohe Auflösung ermöglichte es uns erstmals die Grenzbereiche der einzelnen amplifizierten Chromosomenabschnitte genau miteinander zu vergleichen und Gemeinsamkeiten in den Sequenzen und/oder spezifischer Motive auszuarbeiten. Diese Untersuchung lieferte folgende Ergebnisse:
1) Die Ausdehnung der ampGA und damit deren telomer- und centromerseitigen Grenzen sind eine individuelle Eigenschaft jedes einzelnen untersuchten Neuroblastom Genoms.
2) Die Wahrscheinlichkeit der telomer- und centromerseitigen ampGA-Grenzen nimmt mit zunehmenden Entfernungen zu *MYCN* ab (kleinere ampGA sind häufiger, als ausgedehnte ampGA).
3) Es gibt *MYCN* Amplikons, die aus nur einem ampGA bestehen (Typ-1) und solche, die aus mehreren ampGA aufgebaut sind (Typ-2)
4) die Grenzen der ampGA (Amplikon-Fusions-Stellen (AFS)) lassen sich mittels PCR validieren (AFS-PCR).
5) Durch Untersuchung von genomischer DNA aus zugehörigen residualen Tumoren nach Therapiebeginn bzw. Rezidiven (n=3) konnten wir die Konstanz der ampGA in diesen Fällen nachweisen.
Durch Sequenzierung der PCR Fragmente, die die AFS beinhalten konnten die Grenzen der ampGA letztlich basengenau beschrieben werden. Eine bioinformatische Auswertung dieser Sequenz-Daten wird zur Zeit durchgeführt. Wir erhoffen uns dadurch eventuell vorhandene Konsensussequenzen, die Start- und Endpunkte genomischer Amplifikationsprozesse definieren könnten, beschreiben zu können.

Die Individualität der Grenzbereiche der ampGA, die einfache Etablierung einer spezifischen PCR über einen AFS Bereich und die Konstanz der ampGA im Verlauf der Erkrankung prädestinieren für den Einsatz in der klinischen Diagnostik, insbesondere für den hochsensitiven Nachweis von Tumorzellen bzw. Tumorzell-DNA im Sinne einer minimalen Resterkrankung (minimal residual disease (MRD)).

In der Pädiatrie liegen für die praktischen Anwendung hochsensitiver Tumorzell-Nachweisverfahren die meisten Daten für Kinder mit akuten Leukämieen (vor allem akuten lymphatischen Leukämien (ALL)) vor. Der Nachweis von residualen, leukämischen Blasten (MRD) zu definierten Zeitpunkten der Therapieprotokolle gibt eine direkte Information über das Ansprechen auf die durchgeführte Therapie und hat eine hohe prognostische Relevanz. Damit ist eine Stratifizierung der im weiteren Verlauf durchzuführenden Therapie unabhängig von weiteren Parametern (Alter, genomischen Aberrationen, etc.) möglich. In zunehmendem Maße findet die MRD Diagnostik auch Einsatz zur Beurteilung des Remissionsstatus verschiedener solider Tumore.

Weitere, potentielle Anwendungsmöglichkeiten hochsensitiver Nachweisverfahren neben der MRD Diagnostik in Blut und KM sind der Nachweis von Tumorzellen bzw. Tumorzell-DNA in Aszites und Pleurapunktat, wie es z.B. auf mikroskopischer Ebene für die Stadieneinteilung der Lymphome relevant ist, der Nachweis von Tumorzellen in Liquor (Leukämieen), Urin (Blasen-, Nierenkarzinom, Nephroblastom) sowie im Stuhl (Kolonkarzinom).

Genexpressionsprofile, die im KM und PB von Patienten mit humanen Neuroblastomen aktuell in einer prospektiven Studie als potentielle MRD Marker untersucht werde beinhalten die mRNA Expression von PHOX2B, TH, DDC, CHRNA3, GAP43 und DBH (*Stutterheim et al. 2008 und 2009*). In einer retrospektiven Untersuchung konnte eine hohe Tumorzellspezifität vor allem für PHOX2B gezeigt werden. Der Nachteil bei dieser Form der MRD Diagnostik besteht in der nicht genau zu kalkulierenden Tumorzellspezifität der Expression vieler Gene im Vergleich zu den gesunden, umliegenden Geweben und einem dadurch bedingten erheblichen Unsicherheitsfaktor, vor allem bei niedriger Tumorzellzahl. Ein weiterer Unsicherheitsfaktor ist das nicht zu Kalkulierende Genexpressionsverhalten unter und nach stattgehabter Chemotherapie. Die Untersuchung gleich mehrerer mRNAs vermindert das Risiko falsch negativer und falsch positiver Befunde, kann diese jedoch nicht vollständig ausschließen. Die Sensitivität des Verfahrens wurde in den durchgeführten Zellkulturexperimenten mit $1/10^6$ – $1/10^7$ Zellen angegeben.

Die Nutzung genomischer Marker (z.B. AFS-PCR) bietet eine Möglichkeit bei ebenfalls sehr hoher Sensitivität auch eine absolute Tumorzell-Spezifität zu garantieren.

Eigene Publikationen:

Weber A, Taube S, Starke S, Bergmann E, Christiansen NM, Christiansen H. Detection of tumor cells by amplicon-fusion-site polymerase-chain-reaction (AFS-PCR).
J Clin Invest., 2010 accepted for publication 2010
IF (Stand 2010): 15,387

Diese Arbeit stellt die Erstbeschreibung der Etablierung einer AFS-PCR dar. Die Vorgehensweise umfasste:
1) Die amplifizierten genomischen Abschnitte (ampGA) um *MYCN* (Chr.2p24-25) von n=40 primären Neuroblastomen und 3 Neuroblastomzelllinien wurden mittels Tiling-Array hochauflösend dargestellt.
2) Die telomer- und centromerseitigen Grenzen der ampGA wurden virtuell fusioniert. Diese virtuellen AFS dienten als Sequenzvorlage zur Etablierung von Primerpaaren für eine AFS überbrückende PCR.
3) Die resultierenden PCR Produkte wurden sequenziert, um die basengenauen Fusionsstellen beschreiben zu können.
4) Basierend auf der genauen Beschreibung der AFS konnten hoch sensitive, quantitative Realtime-PCR Assays für die entsprechenden individuellen Tumore entwickelt werden.

Alle ampGA und damit alle AFS waren absolut tumorzell-spezifisch und individuell für jeden untersuchten Patienten. In Zellverdünnungsexperimenten konnte mittels AFS-PCR eine Tumorzelle in einem Hintergrund von 10^6-10^7 Kontrollzellen identifiziert werden. Des Weiteren konnten wir erfolgreich AFS-DNA in Knochenmark und peripherem Blut verschiedener Patienten mit *MYCN* amplifizierten Neuroblastomen nachweisen und damit die Möglichkeit einer praktischen Anwendbarkeit beweisen.
Der Einsatz der AFS-PCR kann einen wichtigen Beitrag zur exakten Beschreibung des initialen Tumorstadiums, zur Verlaufsbeurteilung des Therapieanspreches sowie zur möglichst frühen Identifizierung residueller oder rezidivierender Erkrankungsverläufe (minimal residual disease (MRD)) leisten. Mittels AFS-PCR ist der Nachweis von Tumorzellgenom in diversen Gewebeproben (Primärtumor, Metastasen, Lymphknoten, Knochenmark) oder Köperflüssigkeiten (Blut, Liquor, Urin) möglich.
Das Verfahren wurde beispielhaft an *MYCN* amplifizierten Neuroblastomen entwickelt. Die mögliche Übertragbarkeit auf andere amplifizierte Genomabschnitte eröffnet die Möglichkeit diese Methode auch für viele andere Tumorentitäten als Diagnostikum einzusetzen. Die Wertigkeit eines Nachweises geringster Mengen von Tumorzellen bzw. Tumorzellgenom sollte für jede Malignomentität studienbegleitend überprüft werden.

Weber A, Christiansen H. Verfahren und Mittel zum patienten- und tumorspezifischen Nachweis von Malignomzellen.*Deutsche Patentanmeldung Nr. 10 2009 047 549.4-41*

Der Untersuchungsalgorithmus, der zur Etablierung einer patientenindividuellen AFS-PCR führen kann wurde im Dezember 2009 beim Deutschen Patent- und Markenamt (DPMA) als Patent angemeldet.

Detection of human tumor cells by amplicon fusion site polymerase chain reaction (AFS-PCR)

Axel Weber, Sylvia Taube, Sven Starke, Eckhard Bergmann,
Nina Merete Christiansen, and Holger Christiansen

Department of Pediatric Oncology, Hematology, and Hemostaseology, Children's Hospital, University of Leipzig, Leipzig, Germany.

Reliable diagnostic strategies for individuals with cancer demand practical methods for highly sensitive and specific detection of tumor cells. Amplification of genomic regions that include putative oncogenes is common in tumor cells of various types. Genomic array platforms offer the opportunity to identify and precisely map amplified genomic regions (ampGRs). The stable existence of these tumor cell–specific genomic aberrations during and after therapy, in theory, make ampGRs optimal targets for cancer diagnostics. In this study, we mapped ampGRs around the proto-oncogene *MYCN* of human neuroblastomas using a high-resolution tiling array (HR-TA). Based on the HR-TA data, we were able to precisely describe the telomeric and centromeric borders of the ampGRs and deduce virtual fusion sites of the joined ampGRs (amplicon fusion sites [AFSs]). These AFSs served as blueprints for the subsequent design of AFS bridging PCR assays (AFS-PCRs). Strikingly, these assays were absolutely tumor cell specific and capable of detecting 1 tumor cell in 1×10^6 to 8×10^6 control cells. We successfully proved the in vivo practicability of AFS-PCR by detecting and quantifying the specific AFS DNA of human *MYCN*-amplified neuroblastomas in the patients' corresponding peripheral blood and bone marrow samples. Thus, we believe AFS-PCR could become a powerful and nevertheless feasible personalized diagnostic tool applicable to a large number of cancer patients, including children with *MYCN*-amplified neuroblastomas.

Introduction

The detection of minimal amounts of tumor cells within putative metastatic sites — LNs, BM, peripheral blood (PB), and cerebral fluid — is becoming indispensable for thorough stage classification and therapy stratification for all different kinds of malignancies. Most evidence that a very small residual population of tumor cells during or after therapy can significantly influence the final outcome of a patient is given from hematological malignancies. The early detection of such minimal amounts of residual or recurrent malignoma cells has been shown to be a major prognostic factor for adult and childhood acute lymphoblastic leukemia (1, 2). Among solid tumors, the clinical relevance of minimal residual disease (MRD) during and after therapy has been most extensively studied in breast cancer patients (3, 4). Smaller studies report a significant impact on prognosis for minimal numbers of tumor cells or tumor cell DNA detected in the BM or PB, respectively, for different types of nonhematological malignancies (3, 5, 6).

Besides their use in clinical diagnostics, another important application for highly sensitive methods of tumor cell tracking is the screening of autologous stem cell or BM grafts for residual, potentially viable tumor cells to avoid retransfusion following myeloablative therapy (7). However, the current literature lacks feasible diagnostic strategies for most solid tumor entities with tumor cell specificity and sensitivity comparable to that commonly described for leukemia diagnostics.

Absolute tumor cell specificity is a characteristic of particular parts of the sequence of genomic amplifications, in which single copies of amplified genomic regions (ampGRs) directly attach, forming amplicon fusion sites (AFSs). A major advantage of identifying genomic amplifications compared with other genetic aberrations is the possibility of an easy-to-perform screen for ampGRs via whole-genome comparative genomic hybridization (CGH) analysis. ampGRs are easily detectable in primary tumor specimens, even in those containing a high content of stromal tissue. Moreover, ampGRs are found in a wide variety of tumor entities, emphasizing the relevance of a diagnostic tool targeting these numerical aberrations (8). Recent integrated genomic analyses of breast cancer, colorectal cancer, and glioblastoma multiforme describe detectable ampGRs in almost every individual malignoma (9, 10). At least 1 ampGR (>12 copies per haploid genome) was found in 41 of 45 (91%) breast cancer, 27 of 36 (75%) colon cancer, and 18 of 22 (82%) glioblastoma specimens. The described attributes suggest genomic amplifications may be a predetermined target for cancer diagnostics.

Since its discovery in 1983 (11), amplification of the *MYCN* locus on chromosome 2p24-25 in human neuroblastomas has emerged as one of the most intensively studied examples of gene amplification. We used human neuroblastoma cell lines and primary neuroblastomas harboring chromosome 2p24-25 amplifications as a model to describe a diagnostic algorithm to detect and map the ampGRs, and to use them as blueprints for the subsequent design of an AFS bridging, and thus absolute tumor cell specific, PCR assay (AFS-PCR; Figure 1).

Results

High-resolution tiling array (HR-TA) mapping of ampGRs. Based on HR-TA analysis of the DNA of 3 *MYCN*-amplified neuroblastoma cell lines and 40 primary neuroblastomas, we could describe 2 main types of amplicons (Figure 2 and Supplemental Figures 1

Conflict of interest: The authors have declared that no conflict of interest exists.
Citation for this article: *J Clin Invest* doi:10.1172/JCI44415.

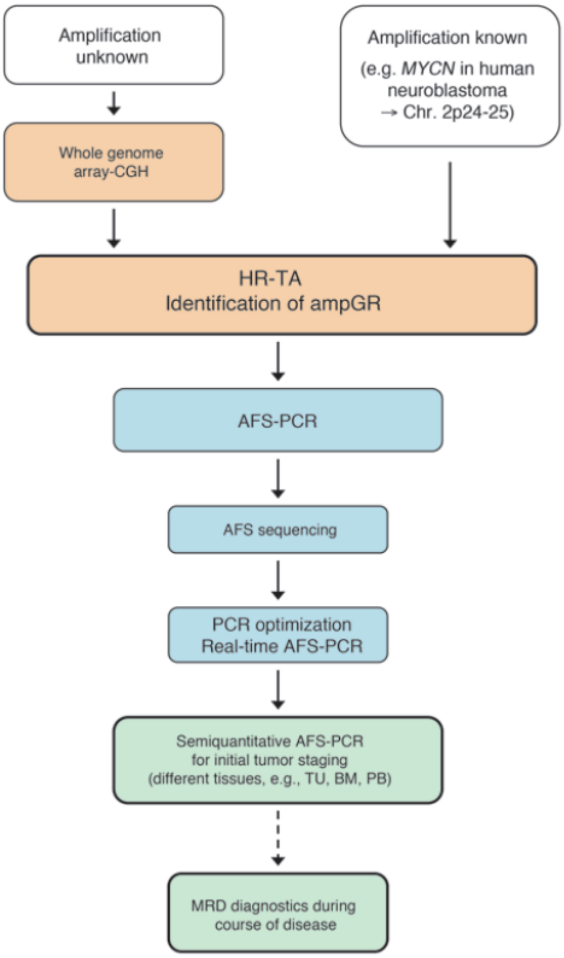

Figure 1
Identification and diagnostic use of AFSs in newly diagnosed malignomas. The diagnostic algorithm combines the possibility of screening for ampGRs by whole-genome CGH analysis, the precision of HR-TA as a platform for subsequent base-exact AFS mapping, the absolute specificity of the AFSs for the respective malignoma cells, and the high sensitivity of real-time PCR. For malignomas with already described ampGRs, isolated genomic DNA can be hybridized directly on the corresponding HR-TA, covering the region of interest. If no ampGRs are described, or common ampGRs are not found in preliminary investigations, whole-genome CGH analysis could be used to screen for regions with ampGRs for further fine mapping on a HR-TA. Once the borders of the ampGRs are mapped, AFS-PCR, and subsequently AFS-RQ-PCR, can be designed. AFS-PCR can be used as a feasible tool in the initial staging of malignoma diseases and, furthermore, for highly sensitive and absolutely specific tracking of remaining or recurrent malignoma cells during the course of the diseases.

and 2; supplemental material available online with this article; doi:10.1172/JCI44415DS1). Of the 43 investigated *MYCN* amplicons, 27 consisted of 1 single ampGR (type 1 amplicons; Supplemental Figure 1), whereas the remaining 16 were assembled of 2 or more ampGRs (type 2 amplicons) that appeared to be separated by nonamplified genomic regions, potentially reflecting a more complex amplicon formation (Supplemental Figure 2).

Telomeric and centromeric borders of the identified ampGRs were unique for each tumor and cell line investigated. The ampGRs including the *MYCN* gene were defined as core ampGRs. The additional ampGRs of the type 2 amplicons were defined as satellite ampGRs. The telomeric borders of the core ampGRs extended from bp 10,446,277 to bp 15,994,874 (median, bp 15,717,248). The centromeric borders extended from bp 16,041,166 to bp 21,821,063 (median, bp 16,474,239). We found the *MEIS1* gene amplified within 1 ampGR of the IMR-32 cell line, as previously described (12–14). Just one other *MYCN* amplicon (tumor no. TU-26) showed integration of an ampGR in relative proximity to, but not including, the *MEIS1* gene (bp 63,352,423 to bp 63,921,178; Supplemental Table 1). The intensities of the array signal of the ampGRs correlated with the copy numbers of the ampGRs estimated by comparative PCR, as described in our previous publication (15), with a Pearson correlation of 0.70 (Supplemental Table 2). The unique dimensions of the ampGRs permitted the design of individual PCR assays for the corresponding tumor cells, and thus for each investigated patient or cell line.

Creation of virtual AFSs and first primer design. Based on the exact information about the chromosomal location of the oligonucleotides that were printed on the HR-TA slides, we were able to assess virtual centromeric and telomeric borders of the ampGRs for each investigated neuroblastoma DNA. The virtual ampGR borders were predicted with a mean accuracy of 65 bp that was given by the HR-TA resolution. Based on the hypothesis that the single amplicons consist of consecutively joined copies of ampGRs, we were able to estimate possible resulting AFSs. Figure 3 shows an example of type 1 amplicons, with the KELLY cell line. In the first step, the AFSs were virtually simulated by joining the first 1,000 amplified bp of the virtual telomeric border to the last 1,000 amplified bp of the virtual centromeric ampGR border (Figure 3B). The sequences of these virtual junctions served as templates for the AFS-PCR primer design. A first generation of PCR primers was designed by setting one primer within the centromeric border region and the other within the telomeric border region of the ampGR. Thus, a successful AFS-PCR was only possible with the AFS bridging sequence present in the input DNA (Figure 3C). These AFSs were defined as type 1 AFSs. Interestingly, in all identified type 1 AFSs, the ampGRs were found to be joined in the head-to-tail orientation (Supplemental Figure 3A).

Type 2 amplicons offered additional opportunities to design specific AFS-PCRs. Joining the virtual borders of 2 different ampGRs led to different possible virtual AFSs that could be used to design PCR primers analogously to type 1 AFSs. An example is given with the IMR-32 cell line (Figure 4). In type 2 AFSs, the ampGRs were found to be arranged in head-to-tail, head-to-head, or tail-to-tail orientation (Supplemental Figure 3B). Thus, in some cases, we found 2 different ampGRs to be joined inversely in their orientation. This resulted in a joining of the coding and noncoding DNA strands of 2 different ampGRs in opposite directions. Interestingly, additional short sequences were found between ampGRs in the 2 identified AFSs of IMR-32 and in different primary neuroblastomas, most of which were too short to identify their chromosomal origin with any precision (Figure 4C). Not all possible AFSs could have been successfully verified by PCR for the IMR-32 cell line and for primary neuroblastomas with complex type 2 amplicons (Supplemental Table 1).

Finally, the generation of at least 1 AFS-PCR leading to a specific PCR product was successful in 34 of 40 (85%) primary neuroblas-

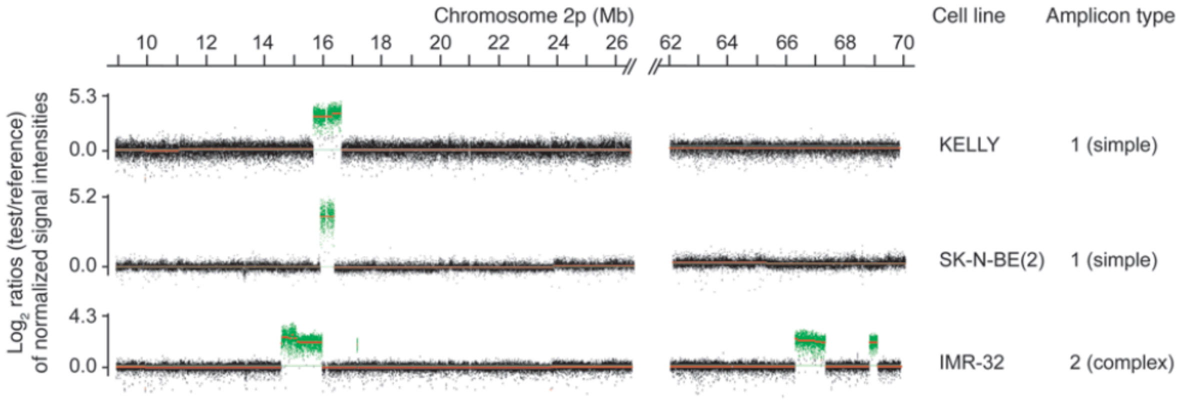

Figure 2
ampGRs of the 3 *MYCN*-amplified neuroblastoma cell lines around the *MYCN* gene on human chromosome 2. Signal-Map software (see Methods) was used for visualization of the HR-TA data. The relative copy number for each printed oligonucleotide is presented as fluorescence intensity of the Cy5-labeled test DNA (cell lines) normalized to the Cy3-labeled reference DNA (healthy human female) ($\log_2$ ratios). The mean signal intensity values of the continuous genomic regions calculated are indicated by red lines. The 0 baseline is indicated by the green line. AmpGRs are highlighted green. Each cell line harbored an individual amplicon composed of different copy numbers of 1 (type 1) or more (type 2) ampGRs with unique telomeric and centromeric borders. See Supplemental Figures 1 and 2 for ampGRs of the 40 *MYCN*-amplified primary neuroblastomas.

tomas. Including AFS-PCR for the 3 *MYCN*-amplified cell lines, overall success was 37 of 43 (86%) *MYCN* amplicons investigated. The design of AFS-PCR was more successful in type 1 amplicons (26 of 27) compared with type 2 amplicons (11 of 16). A detailed description of the single amplicons is given in Supplemental Figures 1 and 2 and Supplemental Tables 1 and 2.

AFS sequencing. By sequencing the AFS-PCR products, we were able to exactly describe individual AFSs on the level of sequence. The coordinates of the ampGR borders of all successfully sequenced AFSs are available in Supplemental Table 1. A comparison of the sequenced AFSs with the AFSs predicted by the array CGH revealed a mean difference of 56 bp, which nearly matched the average array resolution of 65 bp between the printed oligonucleotides. The maximum difference found was 354 bp.

Based on the exact sequences we were able to design primers located closer to the AFSs for real-time quantitative PCR (RQ-PCR).

Specificity of AFS-RQ-PCR. Based on the uniqueness of the individual ampGRs, each AFS-PCR product was absolutely specific for the neuroblastoma cell line or tumor on whose virtual AFS sequence it was designed. For the 3 *MYCN*-amplified cell lines, the specificity of AFS-PCR products is shown in Figure 5. Every AFS-PCR primer pair for the amplicons of the primary neuroblastomas were tested with control DNA isolated from human placental tissue. Strikingly, specific AFS-PCR product could only be identified with the corresponding tumor DNA (Supplemental Figure 3).

Sensitivity of AFS-RQ-PCR. The sensitivity of AFS-RQ-PCR was tested with dilution series of 3 human neuroblastoma cell lines with *MYCN* amplification [IMR-32, KELLY, and SKnBE(2)] with a line without *MYCN* amplification (SH-EP; see Methods for details). These *MYCN*-amplified cell lines and SH-EP cells harbor almost identical DNA content per cell. The ΔCt values of the specific AFS-PCR products relative to the control PCR product, a fragment of inhibin-β-b (*INHBB*), were additionally set in relation to the DNA of the nondiluted *MYCN*-amplified cell lines, calculated according to the $2^{-\Delta\Delta Ct}$ method (see Methods and ref. 16). Strikingly, the calculated values of the successive dilution steps reflected the single dilution steps of the input DNA (Figure 6 and Supplemental Figures 4 and 5). For all 3 cell lines, AFS-PCR products were reliably detectable in the last dilution step: 1 *MYCN*-amplified cell per 10^6 SH-EP cells. We further escalated testing for sensitivity with a successive dilution of DNA of the 1×10^{-6} dilution steps with SH-EP control DNA at a ratio of 1:1. Finally, the method provided suitable to track the AFS from 1 *MYCN*-amplified cell of 8×10^6 control cells. The control for a specific AFS-PCR product, as assessed by agarose gel electrophoresis, was positive down to the highest dilution step (Supplemental Figure 4). Thus, we estimated the sensitivity for AFS-PCR to detect 1 *MYCN*-amplified cell of 1×10^6 to 8×10^6 control cells within our experimental setting.

Practicability for MRD diagnostics in primary neuroblastomas. For 3 of the 40 primary neuroblastomas investigated, we were able to investigate DNA from tissue of a second biopsy or of recurrent disease by HR-TA (Supplemental Figure 7). In all 3 cases, we found absolute consistent borders of the ampGRs in the primary tumor tissues and the tissue of each secondary specimen, evidence supporting the structural stability of the ampGRs over time.

To test the practicability of AFS-PCR to identify tumor cells or tumor cell DNA in tissues other than primary tumor tissue, we investigated genomic DNA of BM, PB, and residual tumor tissue during the treatment of 3 different neuroblastoma patients. Strikingly, we were able to detect AFS DNA in different sample types from all 3 neuroblastoma patients investigated (Figure 7 and Supplemental Figure 6). From patient TU-23, we were able to investigate BM samples from the time of the initial diagnosis as well as from BM aspirations after the first cycle of chemotherapy. The relative decrease of the number of tumor cells detected in the secondary BM samples of this patient (Figure 7) might indicate a therapeutic effect. Because of the lack of exact information, the content of tumor cells in the initial tumor samples of patients TU-20, TU-21, and TU-23 was assumed to be 100% analogous to that of the described cell culture experiments. By general agreement, this does not reflect the situation in primary tumor specimens. The tumor cell content in the initial tumor sample is a variable attribute and depends on malignoma type and histological grading. Because for AFS-PCR, the number of tumor cells or tumor cell

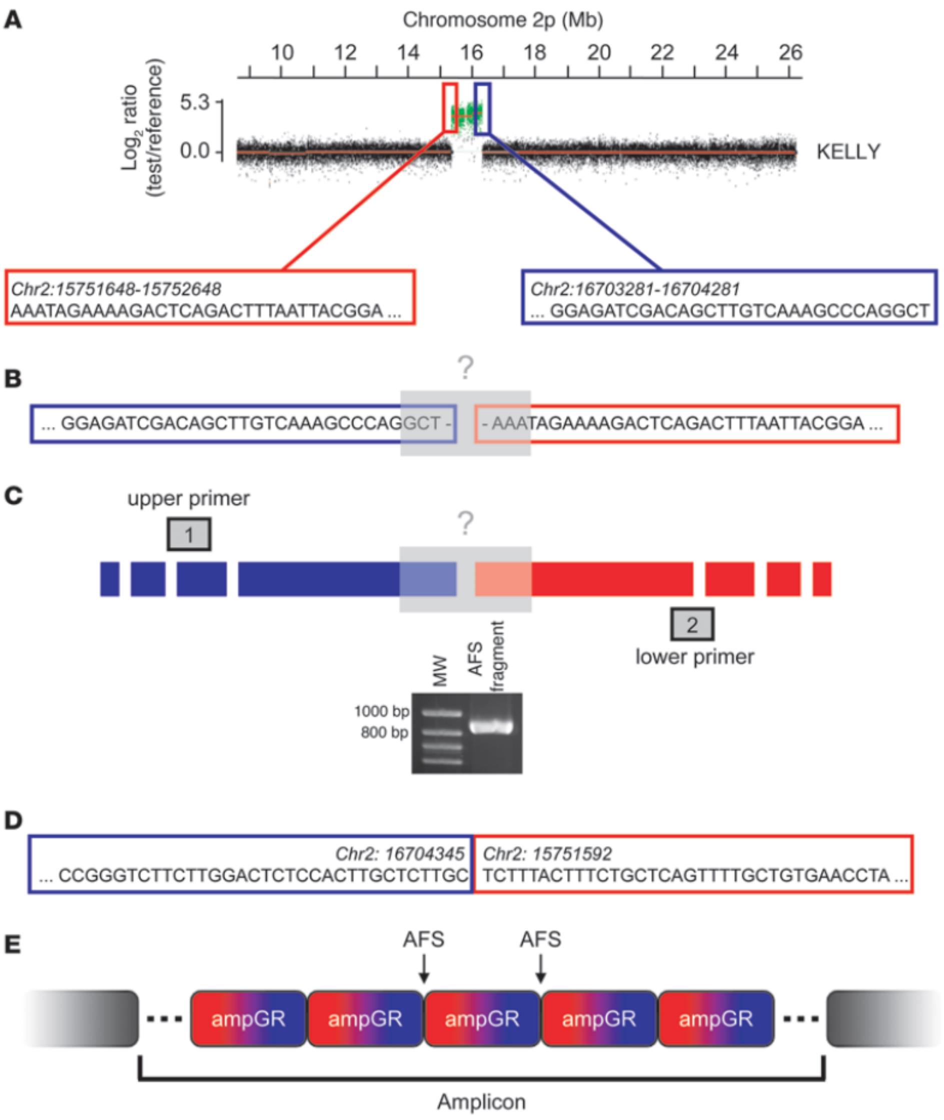
A
Chromosome 2p (Mb)
10
12
14
16
18
20
22
24
26
Log2 ratio (test/reference)
5.3
0.0
KELLY
Chr2:15751648-15752648
AAATAGAAAAGACTCAGACTTTAATTACGGA ...
Chr2:16703281-16704281
... GGAGATCGACAGCTTGTCAAAGCCCAGGCT
B
?
... GGAGATCGACAGCTTGTCAAAGCCCAGGCT -
- AAATAGAAAAGACTCAGACTTTAATTACGGA ...
C
upper primer
1
?
2
lower primer
MW
AFS fragment
1000 bp
800 bp
D
Chr2: 16704345
... CCGGGTCTTCTTGGACTCTCCACTTGCTCTTGC
Chr2: 15751592
TCTTTACTTTCTGCTCAGTTTTGCTGTGAACCTA ...
E
AFS
AFS
ampGR
ampGR
ampGR
ampGR
ampGR
Amplicon

Figure 3

Identification of the AFS sequence in the type 1 amplicon of the KELLY cell line. (**A**) HR-TA data indicate the virtual telomeric and centromeric borders of the ampGR of the KELLY cell line by referring to the first and last amplified oligonucleotide. The relative copy number for each printed oligonucleotide is presented as fluorescent intensity of the Cy5-labeled test DNA (cell lines) normalized to the Cy3-labeled reference DNA (healthy human female) (log_2 ratios). The mean signal intensity values of the continuous genomic regions calculated are indicated by red lines. The ampGR is highlighted green. (**B**) The last (red) and first (blue) 1,000 amplified bps are fused together, resulting in a virtual AFS. (**C**) Primers for a first AFS-PCR are designed up- and downstream of the virtual AFS. (**D**) Sequencing of the excised AFS fragment from both sides, using the previously designed primers, results in the exact AFS. (**E**) Simplified model of the architecture of a simple type 1 amplicon. ampGRs are subsequently joined together in head-to-tail orientation, resulting in a tumor cell–specific AFS.

genomes relative to nonmalignant cell genomes in a given sample (e.g., BM and PB) is calculated directly in relation to the ΔCt values of the primary tumor sample, it must be corrected for the tumor cell content of the primary tumor. This correction (see Methods for details) is needed in order to obtain interindividually comparable results. For example, this calculation is of importance to define threshold values of total cell numbers in a given compartment (e.g., BM) that might be of potential clinical relevance, like for a decision about changing a therapeutic strategy. Corrected results, taking into account different hypothetical tumor cell contents of the primary tumors investigated (Figure 7), are displayed in Supplemental Table 3.

Discussion

Once established from tissue of the primary tumor site, an individual AFS-PCR offers a powerful tool to track tumor cells or tumor cell DNA in potential metastatic sites of any tissue origin as well as in BM aspirates, in PB samples, and even in cerebral fluid, urine, or any other sample of the corresponding patient. Hence, AFS-PCR could significantly improve the exact definition of the tumor stage at the time of initial diagnosis, the monitoring of response to therapy by quantification of tumor cells in subsequent samples, and the early detection of MRD or recurrent disease over time.

As fused ampGRs are a prerequisite for the development of an AFS-PCR, the diagnostic algorithm is limited to patients with malignancies harboring genomic amplifications (Figure 1). However, current publications give evidence that ampGRs could be found in a large percentage of different types of malignomas (9, 10). A second prerequisite is the stability of the borders of the ampGRs. There are very few data about possible flexibility in the structure of ampGRs during the course of malignant diseases. Our own prior data from *MYCN*-amplified neuroblastomas showed a stable coamplification pattern in almost all investigated subjects (15). However, the multiplex PCR used in this setting was characterized by low resolution and thus lacked satisfactory information on possible smaller changes in the amplicon structure. Nonetheless, it is unlikely that a complex architecture of consecutively repeated ampGRs might change its structure on the level of sequence dur-

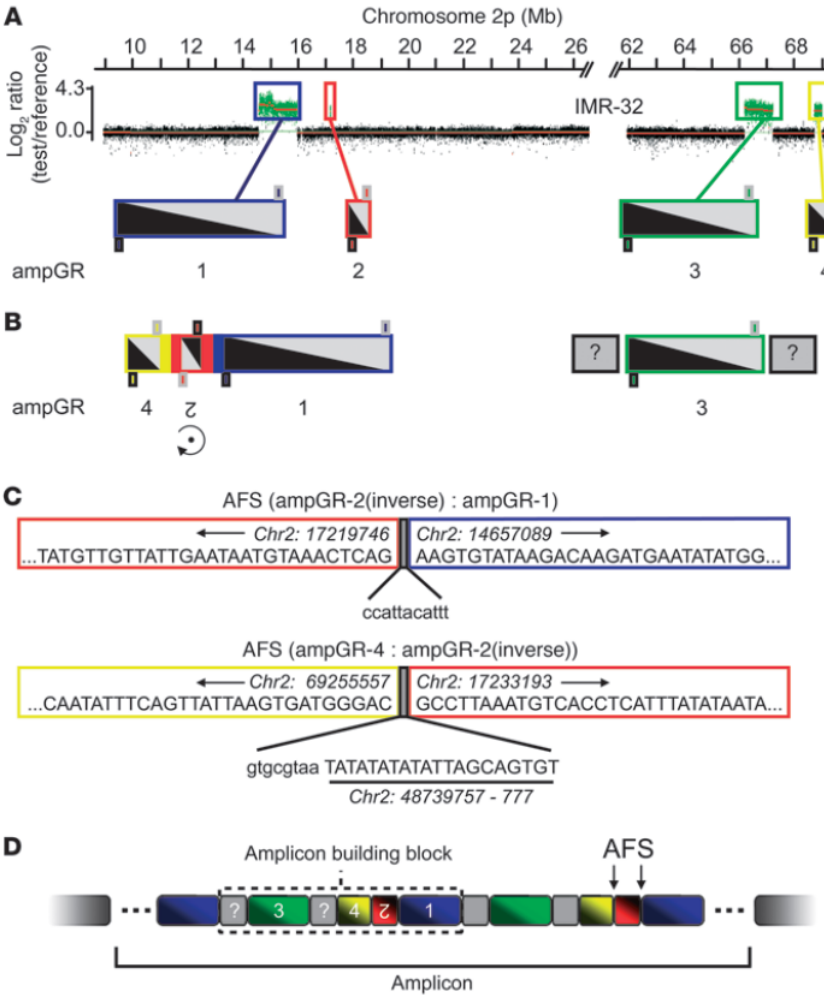
A
Chromosome 2p (Mb)
10
12
14
16
18
20
22
24
26
62
64
66
68
70
Log2 ratio (test/reference)
4.3
0.0
IMR-32
ampGR
1
2
3
4
B
?
?
ampGR
4
2
1
3
C
AFS (ampGR-2(inverse) : ampGR-1)
Chr2: 17219746
...TATGTTGTTATTGAATAATGTAAACTCAG
Chr2: 14657089
AAGTGTATAAGACAAGATGAATATATGG...
ccattacattt
AFS (ampGR-4 : ampGR-2(inverse))
Chr2: 69255557
...CAATATTTCAGTTATTAAGTGATGGGAC
Chr2: 17233193
GCCTTAAATGTCACCTCATTTATATAATA...
gtgcgtaa TATATATATATTAGCAGTGT
Chr2: 48739757 - 777
D
Amplicon building block
AFS
?
3
?
4
2
1
Amplicon

Figure 4

Identification of AFS sequences in the type 2 amplicon of the IMR-32 cell line. (**A**) HR-TA data indicate the virtual telomeric and centromeric borders of 4 ampGRs that appear to be separated by nonamplified genomic regions. (**B**) ampGR order within a single building block. ampGR-2 is fused between ampGR-1 and ampGR-4 inversely, as identified by different combinations of PCR primers and subsequent sequencing. No combination of primers for the known ampGRs successfully integrated ampGR-3 in the amplicon. Most likely, additional ampGRs that were not covered by the HR-TA are adjacent to both sides of ampGR-3, avoiding a successful PCR. (**C**) Sequencing of the AFS-PCR products from both sides resulted in the exact AFS. In both AFSs, additional short sequences were found between the ampGR borders. In the AFS between ampGR-4 and ampGR-2 (inverse), an additional ampGR, 20 bp long, was identified. For shorter sequences (lower case) of both AFSs, it was not possible to identify the definite chromosomal origin. (**D**) Simplified model of the architecture of a complex type 2 amplicon. Different ampGRs are joined together in head-to-tail, head-to-head, or tail-to-tail orientation, resulting in different tumor cell–specific AFSs. The different ampGRs build single building blocks that are subsequently joined together. The entirety of all ampGRs corresponds to the whole, individual amplicon.

ing the course of disease and therapy, resulting in a change of all AFSs that were initially present.

Hypothetically, the monitoring of malignancies that obviously develop from more than 1 clonal cellular population could be at the limits of AFS-PCR. However, current publications indicate an initially monoclonal origin for different kinds of malignomas, even though a rising diversity of different subclones could be found during the course of disease (17, 18). Compared with other genomic aberrations, ampGRs showed high stability between different arising subclones in those studies. One of the neuroblastomas investigated (patient TU-19) harbored 2 different core ampGRs detected by HR-TA. There are 2 possible explanations for this finding: either the different ampGRs were existent in 1 single tumor cell clone, leading to a complex amplicon pattern with the different possible AFSs, or 2 independent cell clones were present in the initial tumor. Because it is impossible to easily discriminate between these 2 conditions, it is imperative to design PCR for the AFSs of all potential cell clones, since it might be possible that during the course of disease and therapy, one clone might become privileged, and thus only a single AFS-PCR could be of use for subsequent diagnostic steps. For tumor TU-19, we were able to successfully design AFS-PCRs for both possible amplicons, but because we lacked consecutive tissue probes of the corresponding patient, it was not possible to assess whether 1 of the 2 AFSs disappeared during the course of disease.

Different conditions may influence the ability to successfully establish an AFS-PCR for an individual malignancy. The most important prerequisite is DNA of good quality from the initial tumor site for HR-TA, as DNA quality directly influences the exact mapping of the ampGR borders. Depending on the resolution of the HR-TA, it is also possible to miss small additional ampGRs and thus fail to successfully design AFS bridging primers. In general, it is more difficult to identify the exact ampGR borders of tumors with just a few copies of ampGRs (gain) compared with high-copy amplifications. An example for a low-copy gain is given with tumor TU-4 (Supplemental Figure 1). Performing the HR-TA more than once in such cases could increase the reliability of the array-based prediction of the ampGR borders. Moreover, each AFS-PCR has to be optimized prior to its use for semiquantitative diagnostics based on the individual sequences flanking each AFS. For the complex type 2 amplicons, it is theoretically possible to design primers for all potential AFSs. For these cases, it is important to keep in mind that 2 different ampGRs could be merged in the same or the opposite direction with regard to the coding DNA strand (Supplemental Figure 3).

The used HR-TA with a custom design covering 8 megabases (Mb) telomeric and 10 Mb centromeric to *MYCN* (and additional

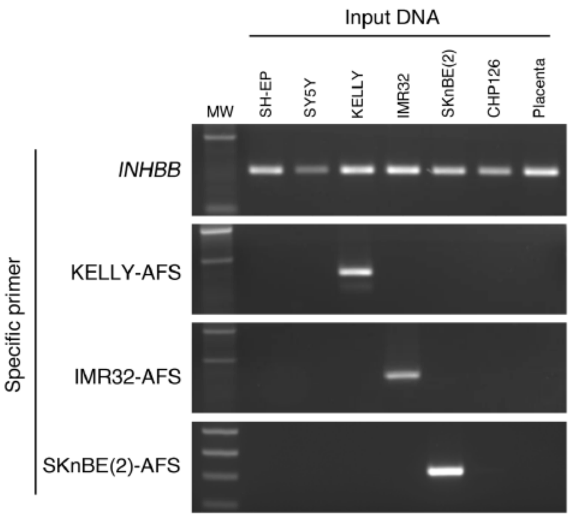

Figure 5
Specificity of AFS-PCR. PCRs with genomic DNA of different neuroblastoma cell lines or human placenta tissue were performed with either specific AFS primers of 1 of the 3 investigated cell lines, or primers for a fragment of *INHBB* that served as control. 15 µl of the PCR was separated in a 3% agarose gel by electrophoresis and visualized under UV light after ethidium bromide staining. AFS-PCR was absolutely specific for the respective cell line DNA harboring the individual ampGR.

10 Mb around *MEIS1*) was suitable to design AFS bridging primers for at least 85% of all amplicons investigated. As shown for the *MYCN* amplicon of the IMR-32 cell line, ampGRs situated far from the core ampGRs were found integrated within an amplicon building block (ref. 14 and Figure 4). For some of the investigated neuroblastomas, 1 ampGR — or even more — might have been missed simply because the HR-TA did not cover the corresponding chromosomal regions. This would explain why it was impossible to design an AFS-PCR in these cases. Although successful in most cases in this study, the described identification of the AFSs was based on a simplified model of amplicon formation; thus, it is not possible to exclude the possibility that amplicons may be composed in a complex pattern that does not allow the investigator to successfully identify 1 single AFS based on the given HR-TA data (19).

If the described requirements are fulfilled, AFS-PCR offers remarkable benefits over applications currently used for the detection of minimal amounts of tumor cells (20). Compared with flow cytometry, which is mainly used for the detection of leukemic cells (21–23), AFS-PCR — like other PCR-based strategies — is characterized by higher sensitivity. However, even compared with different commonly used PCR applications, AFS-PCR is characterized by certain advantages. Thus, RQ-PCR strategies targeting the mRNA of genes that are primarily expressed in transformed cells lack the reliable specificity that fundamentally has to be claimed for MRD diagnostics (24, 25). PCR assays designed to bridge the fusion sites of gene fusion products (e.g., BCR/ABL) are, like AFS-PCR, tumor cell specific (22, 23, 26). However, in contrast to AFSs, the fusion sites of such gene fusion transcripts are not individual for each patient: cross-contamination between different patients' specimens is a known problem for these MRD

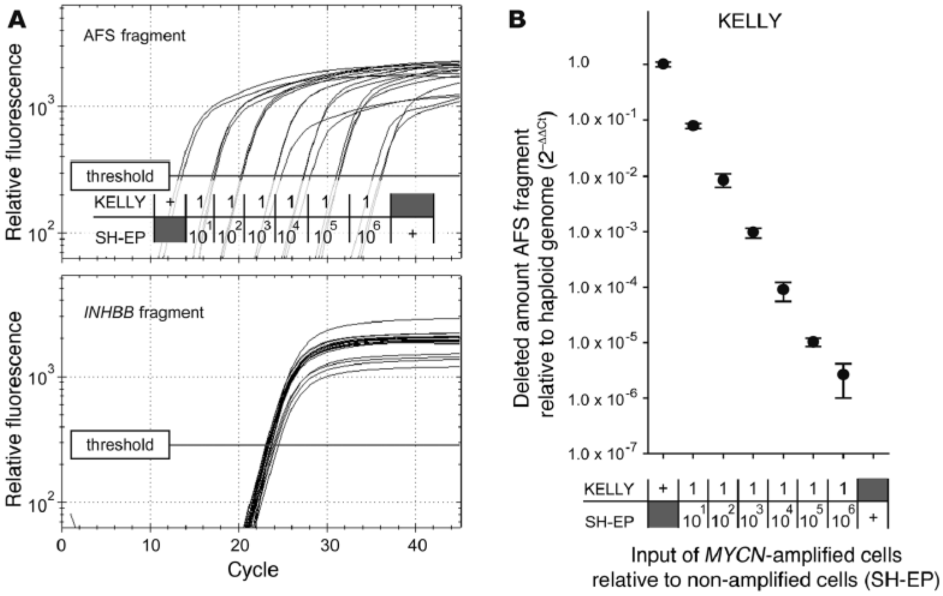

Figure 6
Sensitivity of AFS-PCR. (**A**) RQ-PCR traces of 1 representative dilution series of KELLY cells with SH-EP cells. A $\log_{10}$ dilution series of suspended *MYCN*-amplified cells (KELLY) with non–*MYCN*-amplified control cells (SH-EP) was performed in triplicate prior to DNA isolation. Undiluted KELLY cells (+) served as 100% tumor cell control; SH-EP cells (+) served as negative control. 200 ng DNA isolated from 3×10^6 cells of each dilution step or control served as templates for RQ-PCR with either specific AFS primers or *INHBB* control primers. (**B**) Calculated $2^{-\Delta\Delta Ct}$ of all 3 independent dilution series. Mean and SD are indicated by points and horizontal bars, respectively. The values reflected almost exactly the corresponding dilution steps of the KELLY cell line. See Supplemental Figures 4 and 5 for IMR-32 and SKnBE(2) cell lines and further dilution steps.

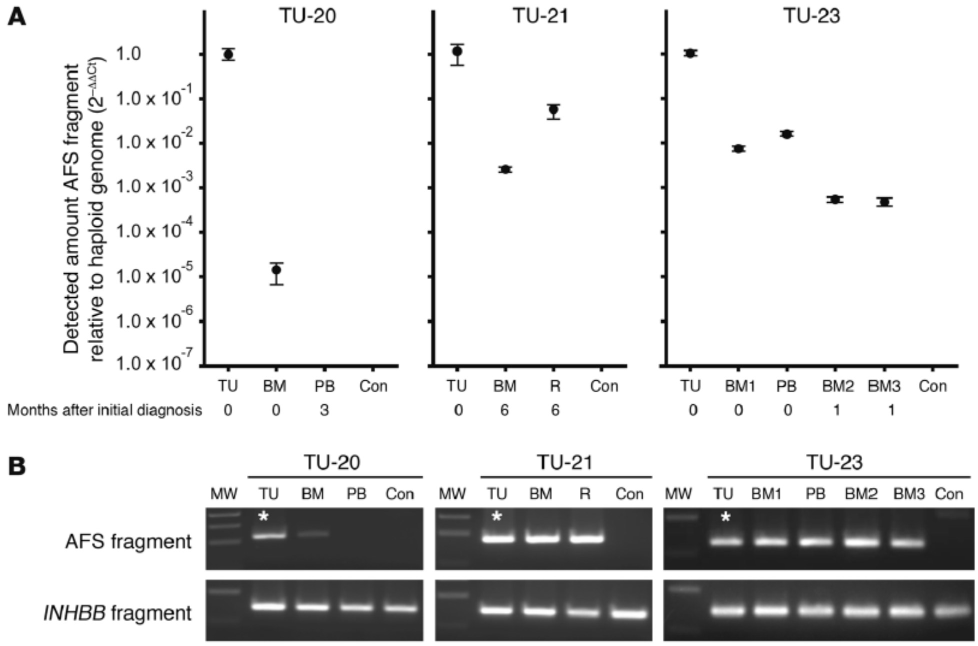

Figure 7

Specific AFS fragments are detectable in samples of different tissue origin of neuroblastoma patients at the time of initial diagnosis and during therapy. (**A**) Tumor cell contents of the primary tumors (TU) were estimated at 100%. Tumor cell contents of the different probes were quantified according to the $2^{-\Delta\Delta Ct}$ calculation. Each PCR was performed in triplicate. Mean and SD are indicated by points and horizontal bars, respectively. DNA from human placenta tissue served as negative control (Con). AFS-PCR identified a weak BM infiltration for patient TU-20 at the time of diagnosis. This infiltration was not detectable cytologically. Patient TU-21 had considerable BM infiltration in a control aspiration after 6 months of therapy. AFS-PCR of a secondary biopsy sample of the residual tumor (R) showed a 10-fold decrease of tumor cells compared with the initial tumor specimen. Patient TU-23 had BM infiltration and circulating tumor cells in the PB at the time of diagnosis (BM1). The secondary BM aspirations, taken from 2 independent anatomical locations after 1 month of therapy (BM2 and BM3), showed a 10-fold decrease of tumor cells compared with the initial BM sample, giving evidence for a response to therapy. (**B**) AFS fragments and *INHBB* control fragments of the RQ-PCR separated in a 3% agarose gel. RQ-PCR had been running for 40 cycles. Asterisks denote lines of the tumor probe loaded with half the PCR product of the other lines.

targets. The dependency on mRNA as starting material for MRD diagnostics instead of genomic DNA is an additional disadvantage with regard to its stability and its isolation from tissue specimens. Furthermore, the identification of specific mRNA expression pattern, gene fusion products, or tumor cell–specific mutations, such as in putative tumor suppressor genes (27–29), may be hindered by a high content of stromal tissue in the specimen of interest, whereas the identification of ampGRs could still be possible. PCR strategies targeting rearrangements in genes encoding for immunoglobulin chains are of high specificity and sensitivity but, like flow cytometry, suffer from limitations in the detection of MRD in different kinds of leukemias (30).

Currently, the designs of genomic microarrays are becoming progressively higher in resolution, which results in several advantages. The gaps between the printed oligonucleotides on the available standard whole-genome arrays will be small enough for a direct AFS-PCR design, and customized tiling arrays for each single genomic region of interest will become dispensable. To reach this goal, arrays with 10^7 or more printed oligonucleotides are required, whereas the recently available CGH arrays consist of a standard resolution of 2.1 × 10^6 printed probes resulting in gaps of 1.5–2.0 kilobases. Those arrays would be efficient in reflecting larger genomic regions around the core regions of interest, increasing the possibility of complete amplicon mapping even for type 2 amplicons. Decreasing costs of high-resolution array approaches will make this method more affordable for use in routine diagnostics. In the long term, next-generation sequencing has the potential to substitute for the array CGH. With this technique, it is still possible to directly sequence AFSs or other specific junction sites in the tumor cell genome, making them affordable for a direct PCR design (31, 32). However, this approach is so far too expensive and time intensive for use in routine diagnostics.

Fulfilling the qualitative requirements of different analytical methods, the malignoma cell–specific AFSs could also be useful for designing PCR primers or other types of probes targeting the AFSs directly (e.g., labeled probes for fluorescence in situ hybridization). Besides these diagnostic approaches, AFSs could also be of interest as a target for different malignoma cell–specific therapy strategies like double-strand DNA binding antisense oligonucleotides.

In summary, our approach gives rise to a feasible tool for absolutely specific and highly sensitive detection of tumor cells, suitable for a large number of patients suffering from different malignancies. Once established, it should be possible to easily perform AFS-PCR in every laboratory capable of performing RQ-PCR. The possibility to reliably detect ampGRs in a primary tumor specimen even with low tumor cell content by AFS-

PCR represents a major advantage over other methods recently described. Its prognostic impact on MRD diagnostics and its role as a criterion for clinical decision making has to be evaluated for each single type of malignoma.

Methods

Patients. We studied primary tumor specimens from 40 children with *MYCN*-amplified neuroblastomas diagnosed in Germany from 1986 to 2003. The 40 neuroblastomas were selected from a total of 230 tumor specimens with *MYCN* amplification within this time period based on the availability of tumor tissue of comparable quality for DNA isolation.

All neuroblastoma diagnoses were confirmed by histological assessment of a tumor specimen obtained from surgery. The tumors were classified according to INSS criteria (33). All patients were treated according to previously described protocols (34, 35), and informed consent for therapy and study procedures was obtained. The studies were reviewed and approved by the Ethics Committee of the medical faculty of the University of Cologne (Cologne, Germany).

Our study group consisted of 3 stage 1, 0 stage 2, 13 stage 3, 20 stage 4, and 4 stage 4S tumors. The median patient age at diagnosis was 23.7 months (range, 0.03 to 78.6 months). The median follow-up time for all 40 patients was 31.9 months (range, 0.4 to 87.6 months). The median follow-up time of the patients that died from the disease was 11.5 months ($n = 21$), compared with 56.4 months for surviving patients ($n = 19$). Age, tumor stage, and survival data for each investigated patient are given in Supplemental Table 2.

Cell culture. Human neuroblastoma cell lines SH-EP, IMR32, KELLY, and SKnBE(2) were grown under standard cell culture conditions in RPMI Medium (Gibco; Invitrogen) containing 10% fetal calf serum (Sigma-Aldrich), glutamine (2 mM), penicillin-G (100 U/ml), and streptomycin (100 μg/ml) at 37°C and 5% CO_2. Cells were trypsinized and harvested at 80% confluence. For dilution series, the cells were counted, and *MYCN*-amplified cells [IMR32, KELLY, and SKnBE(2)] were stepwise diluted with non–*MYCN*-amplified SH-EP cells according to the following dilution steps: 1 *MYCN*-amplified cell per 10 SH-EP cells (1:10), 1 *MYCN*-amplified cell per 100 SH-EP cells ($1:10^2$), followed by $1:10^3$, $1:10^4$, $1:10^5$, and $1:10^6$. For all *MYCN*-amplified cell lines, the dilution series were performed in independent triplicates. 3×10^6 cells of each dilution step were then used for DNA isolation.

DNA isolation and further dilution steps. Isolation of genomic DNA was performed using the DNA-Blood and Tissue Kit (QIAGEN). DNA quality and concentration was measured spectrometrically (Nanodrop, Amersham).

To test the sensitivity, we further diluted the DNA of each $1:10^6$ dilution step with SH-EP control DNA at a ratio of 1:1 down to $1:80^6$ for each cell line investigated.

HR-TA design. Design of the printed oligos and manufacturing of the array slides was performed by Roche NimbleGen. 384,599 DNA oligos of 35–50 nucleotides in length were printed on 1 array slide. The genomic regions of interest were located on chromosome 2p (region 1 [around *MYCN*], bp 8,502,655 to bp 26,522,939; region 2 [around *MEIS1*], bp 59,390,222 to bp 66,064,884; region 3 [control], bp 120,730,406 to bp 120,948,861), covering 24,913,401 bp in total. We obtained bp coordinates from the UCSC Genome Bioinformatics Database, March 2006 (NCBI36/hg18) assembly (http://genome.ucsc.edu/). The average resolution was 1 DNA oligo every 65 bp. The specific resolution for a genomic section was dependent on the underlying sequence. Thus, sections with long sequence repeats were represented in a lower resolution, while sections containing highly specific chromatin (e.g., gene encoding euchromatin) were represented in a higher resolution. Hybridization of the tiling array required a total of 5 μg DNA (DNA quality criteria and hybridization methods were according to Ima-Genes). The DNA of the neuroblastoma cell lines and primary tumors were hybridized together with control DNA (healthy human being) on the array slides. The DNA of the neuroblastoma specimens were labeled with Cy5, whereas the control DNA was labeled with Cy3. SignalMap Software (version 1.9; NimbleGen) was used for analysis of the HR-TA data.

Primer design. All primers for standard PCR and RQ-PCR were designed using OLIGO Primer analysis software (version 6.41; Molecular Biology Insights Inc.). See Results and the Figure 2 and Figure 3 legends for details of primer design. The sequences of all primers used are listed in Supplemental Table 4.

PCR and sequencing. The PCR for validation of the virtual AFSs was performed under standardized conditions. We used the QIAGEN HotStarTaq-Plus PCR Mastermix (12.5 μl), 200 ng DNA, 2 primers at a final concentration of 1 pmol each, 1.5 μl DMSO (Sigma-Aldrich), and Aqua-dest (Braun) at 25 μl. Cycler conditions were as follows: 5 minutes initial denaturation at 95°C, followed by 38 cycles with 20 seconds at 95°C, 20 seconds at 57°C, and 40 seconds at 72°C. Electrophoresis was performed in 1%–3% agarose gels dependent on the PCR fragment length. Gels were stained with ethidium bromide, and bands were visualized under UV light (Image Master VDS; Pharmacia).

Bands of estimated length were excised from the gel, and PCR fragments were isolated using the QIAGEN gel extracting kit following the manufacturer's instructions. Each AFS fragment was sequenced from both sides using a BigDye Terminator 3.1 Ready Reaction Cycle Seq Kit (Applied Biosystems) following the manufacturer's instructions. We used a 16 Capillary Sequenzer Genetic Analyzer 3100 from Applied Biosystems. 250 ng of DNA and 10 pmol of 1 primer were put in 1 sequencing reaction.

RQ-PCR conditions were as follows: QIAGEN HotStarTaq-Plus PCR Mastermix (12.5 μl), 200 ng DNA, 2 primers at a final concentration of 1 pmol each, 1.5 μl DMSO, 2.5 μl SYBR-Green (10× concentration; Roche), and Aqua-dest at 25 μl. Cycler conditions were as follows: 5 minutes initial denaturation at 95°C, followed by 40 cycles with 20 seconds at 95°C, 20 seconds at 56°C–58°C, and 40 seconds at 70°C–72°C (depending on individual primer binding conditions). All real-time PCR was performed on a BIORAD iQ5-Cycler. Each real-time PCR, including the internal control *INHBB*, was performed in triplicate.

Statistics. Relative amounts of *MYCN*-amplified tumor cells within the different steps of the dilution series of the cell lines, or in the samples of different tissue origin from the neuroblastoma patients investigated, were calculated using the $2^{-\Delta\Delta Ct}$ method (16). Therefore, the Ct values of the specific AFS fragments were normalized to the corresponding Ct values of the *INHBB* control PCR fragments. Each resulting ΔCt value was further normalized to the median ΔCt of the corresponding 100% *MYCN*-amplified cell line DNA or primary tumor DNA specimen. This calculation resulted in triplicate $2^{-\Delta\Delta Ct}$ values for each specimen investigated. RQ-PCR data in Figure 7 present the mean and SD of these $2^{-\Delta\Delta Ct}$ triplicates. Each dilution series of *MYCN*-amplified cell lines was performed in independent biological triplicates. Thus, RQ-PCR data in Figure 6 and Supplemental Figure 4 present the mean and the SD of all 3 corresponding $2^{-\Delta\Delta Ct}$ triplicates (i.e., 9 values).

To correct the Ct value of the specific AFS-PCR fragment of the primary tumor DNA to the histological assessed tumor cell content, we used the equation $\text{AFS-Ct}_{corrected} = \text{AFS-Ct}_{native} + \log_2 X$; where X is the relative tumor cell content of the primary tumor specimen (e.g., 0.8 for 80%). All other Ct values stayed unchanged. ΔCt values were then calculated in relation to the corrected ΔCt value of the primary tumor specimen according to the $2^{-\Delta\Delta Ct}$ method (Supplemental Table 3).

Acknowledgments

We thank our colleagues from about 100 German pediatric centers for providing us with neuroblastoma tumor material since 1981.

We thank F. Berthold and B. Hero (University of Cologne, Cologne, Germany) for providing clinical data and F. Lampert (University of Giessen, Giessen, Germany) for supporting our research group. This work was substantially supported by the Deutsche Forschungsgemeinschaft (project no. WE-4324/1-1). We thank Steffi Meyer (University of Leipzig) for valuable comments on the manuscript.

Received for publication July 18, 2010, and accepted in revised form November 10, 2010.

Address correspondence to: Axel Weber, Liebigstrasse 20a, D-04103 Leipzig, Germany. Phone: 49.0341.9726114; Fax: 49.0341.9726099; E-mail: axel.weber@medizin.uni-leipzig.de.

1. Mortuza FY, et al. Minimal residual disease tests provide an independent predictor of clinical outcome in adult acute lymphoblastic leukemia. *J Clin Oncol*. 2002;20(4):1094–1104.
2. Flohr T, et al. Minimal residual disease-directed risk stratification using real-time quantitative PCR analysis of immunoglobulin and T-cell receptor gene rearrangements in the internationalmulticenter trial AIEOP-BFM ALL 2000 for childhood acute lymphoblastic leukemia. *Leukemia*. 2008;22(4):771–782.
3. Ignatiadis M, et al. Different prognostic value of cytokeratin-19 mRNA positive circulating tumor cells according to estrogen receptor and HER2 status in early-stage breast cancer. *J Clin Oncol*. 2007;25(33):5194–5202.
4. Janni W, Rack B, Lindemann K, Harbeck N. Detection of micrometastatic disease in bone marrow: is it ready for prime time? *Oncologist*. 2005;10(7):480–492.
5. Cristofanilli M, et al. Circulating tumor cells, disease progression, and survival in metastatic breast cancer. *N Engl J Med*. 2004;351(8):781–791.
6. Diehl F, et al. Circulating mutantDNA to assess tumor dynamics. *Nat Med*. 2008;14(9):985–990.
7. Spyridonidis A, Bernhardt W, Fetscher S, Behringer D, Mertelsmann R, Henschler R. Minimal residual disease in autologous hematopoietic harvests from breast cancer patients. *Ann Oncol*. 1998;9(8):821–826.
8. Santarius T, Shipley J, Brewer D, Stratton MR, Cooper CS. A census of amplified and overexpressed human cancer genes. *Nat Rev Cancer*. 2010;10(1):59–64.
9. Leary RJ, et al. Integrated analysis of homozygousdeletions, focal amplifications, and sequence alterations in breast andcolorectal cancers. *Proc Natl Acad Sci U S A*. 2008;105(42):16224–16229.
10. Parsons DW, et al. An integrated genomicanalysis of human glioblastoma multiforme. *Science*. 2008;321(5897):1807–1812.
11. Schwab M, et al. Amplified DNA with limited homology to myc cellular oncogene is shared by human neuroblastoma cell lines and a neuroblastoma tumour. *Nature*. 1983;305(5931):245–248.
12. Jones TA, Flomen RH, Senger G, Nizetic D, Sheer D. The homeobox gene MEIS1 is amplified in IMR-32 and highly expressed in other neuroblastoma cell lines. *Eur J Cancer*. 2000;36(18):2368–2374.
13. Spieker N, et al. The MEIS1 oncogene is highly expressed in neuroblastoma and amplified in cell line IMR32. *Genomics*. 2001;71(2):214–221.
14. Oberthuer A, et al. Characterization of a complex genomic alteration on chromosome 2pthat leads to four alternatively spliced fusion transcripts in the neuroblastoma cell lines IMR-5, IMR-5/75 and IMR-32. *Gene*. 2005;363:41–50.
15. Weber A, Starke S, Bergmann E, Christiansen H. The coamplification pattern of the MYCN amplicon is an invariable attribute of most MYCN-amplified human neuroblastomas. *Clin Cancer Res*. 2006;12(24):7316–7321.
16. Livak KJ, Schmittgen TD. Analysis of relative gene expression data using real-time quantitative PCR and the 2(-Delta Delta C(T)) method. *Methods*. 2001;25(4):402–408.
17. Liu W, et al. Copy number analysis indicates monoclonal origin of lethal metastatic prostate cancer. *Nat Med*. 2009;15(5):559–565.
18. Wang X, et al. Evidence for common clonal origin of multifocal lung cancers. *J Natl Cancer Inst*. 2009;101(8):560–570.
19. Bignell G, et al. Architectures of somatic genomic rearrangement in human cancer amplicons at sequence-level resolution. *Genome Res*. 2007;17(9):1296–1303.
20. Szczepanski T, Orfão A, van der Velden VH, San Miguel JF, van Dongen JJ. Minimal residual disease in leukaemia patients. *Lancet Oncol*. 2001;2(7):409–417.
21. Borowitz MJ, et al. Minimal residual disease detection in childhood precursor-B-cell acute lymphoblastic leukemia: relation to other risk factors. *Leukemia*. 2003;17(8):1566–1572.
22. Thörn I, et al. Monitoring minimal residual disease with flow cytometry, antigen-receptor gene rearrangements and fusion transcript quantification in Philadelphia-positive childhood acute lymphoblastic leukemia. *Leuk Res*. 2009;33(8):1047–1054.
23. Kern W, Haferlach C, Haferlach T, Schnittger S. Monitoring of minimal residual disease in acute myeloid leukemia. *Cancer*. 2008;112(1):4–16.
24. Lambooy LH, et al. Real-time analysis of tyrosine hydroxylase gene expression: a sensitive and semiquantitative marker for minimal residual disease detection of neuroblastoma. *Clin Cancer Res*. 2003;9(2):812–819.
25. Stutterheim J, et al. PHOX2B is a novel and specific marker for minimal residual disease testing in neuroblastoma. *J Clin Oncol*. 2008;26(33):5443–5449.
26. Scholl C, et al. The prognostic value of MLL-AF9 detection in patients with t(9;11)(p22;q23)-positive acute myeloid leukemia. *Haematologica*. 2005;90(12):1626–1634.
27. Schnittger S, et al. Minimal residual disease levels assessed by NPM1 mutation- pecific RQ-PCR provide important prognostic information in AML. *Blood*. 2009;114(11):2220–2231.
28. Hirt C, Schüler F, Dölken G. Minimal residual disease (MRD) in follicular lymphoma in the era of immunotherapy with rituximab. *Semin Cancer Biol*. 2003;13(3):223–231.
29. Diehl F, et al. Detection and quantification of mutations in the plasma of patients with colorectal tumors. *Proc Natl Acad Sci U S A*. 2005;102(45):16368–16373.
30. Van der Velden VH, et al. Prognostic significance of minimal residual disease in infants with acute lymphoblastic leukemia treated within the Interfant-99 protocol. *Leukemia*. 2009;23(6):1073–1079.
31. Stephens PJ, et al. Complex landscapes of somatic rearrangement in human breast cancer genomes. *Nature*. 2009;462(7276):1005–1010.
32. Leary RJ, et al. Development of personalized tumor biomarkers using massively parallel sequencing. *Sci Transl Med*. 2010;2(20):20ra14.
33. Brodeur GM, et al. Revisions of the international criteria for neuroblastoma diagnosis, staging, and response to treatment. *J Clin Oncol*. 1993;11(8):1466–1477.
34. Berthold F, et al. The role of chemotherapy in the treatment of children with neuroblastoma stage IV: the GPO (German Pediatric Oncology Society) experience. *Klin Padiatr*. 1990;202(4):262–269.
35. Berthold F, Hero B. Neuroblastoma: Current drug recommendations as part of the total treatment approach. *Drugs*. 2000;59(6):1261–1277.

Verfahren und Mittel zum patienten- und malignomspezifischen Nachweis von Malignomzellen

Deutsche Patentanmeldung Nr. 10 2009 047 549.4-41

Die Erfindung betrifft die Malignomdiagnostik, insbesondere die Diagnostik von Malignomen mit amplifizierten (in mehreren Kopien vorliegenden) Genomabschnitten, welche Onkogene enthalten können, wie z.B. *MYCN* (Chromosom 2p24-25) in humanen Neuroblastomen.

Der Nachweis minimaler Mengen an Malignomzellen innerhalb gesunden Gewebes (z.B. innerhalb des Knochenmarkes) ist ein wichtiger diagnostischer Baustein unter Anderem im Rahmen der Untersuchung auf das Vorliegen einer minimalen Resterkrankung (Minimal residual disease = MRD) vornehmlich hämatologischer Malignome aber auch solider, bösartiger Tumore geworden. Der möglichst sensitive und spezifische, quantitative Nachweis einer minimalen Resterkrankung gibt einen Hinweis auf das Ansprechverhalten der malignen Zellen auf die bis zu diesem Zeitpunkt durchgeführte Therapie.

Die PCR stellt eine der grundlegenden Methoden im Rahmen dieser Diagnostik dar. Bezogen auf eine generell zu erwartende Tumorspezifität kann man 2 verschiedene Formen der genomischen MRD-PCR Methoden unterscheiden. 1.) Die klonspezifische PCR in Rearrangementbereichen von Genen, die für Immunglobulinketten kodieren und 2.) PCRs, die über einen Translokationsbereich (z.B. BCR/ABL) gelegt werden und somit ebenfalls klonspezifisch sind, falls es sich nicht um eine Keimbahnmutation handelt.

Während die erste Methode ausschließlich für hämatologische Malignome einzusetzen ist, da nur in diesen Zellen die klonspezifischen Rearrangements in den Immunglobulinkettengenen stattfinden, ist die zweite Methode grundsätzlich auch für jedes andere Malignom denkbar, wenn entsprechende Translokationen vorliegen. Sind die entsprechenden Translokationspunkte genau definiert, wie bei den exakten Translokationen, die notwendig sind, um sinnvolle Fusionsproteine zu generieren, können spezifische PCRs gut etabliert werden. Ein Nachteil dieser Methode liegt in der schlechten Abgrenzbarkeit der Translokationspunkte, wenn diese Translokationspunkte nicht genau definiert sind. Aufgrund der limitierten Reaktionsweite der PCR Reaktion ist es dann schwer eine funktionierende PCR zu etablieren, da es keine Methode gibt, die genau genug ist die Translokationsfusionsbereiche zuvor mittels Screening einzugrenzen. Die Erarbeitung entsprechender, individueller PCRs ist daher zeitaufwendig und kostspielig, da viele Primer nötig sind, um sich an den exakten Translokationspunkt heranzutasten.

Weitere Methoden zur MRD-Diagnostik umfassen die quantitative Bestimmung möglichst malignomspezifischer Genexpressionsmuster. Der Nachteil besteht in der nicht genau zu kalkulierenden Malignomzellspezifität der Expression vieler Gene im Vergleich zu den gesunden, umliegenden Geweben und einem dadurch bedingten erheblichen Unsicherheitsfaktor, vor allem bei niedriger Malignomzellzahl.

Der Nachweis minimaler Mengen von Malignomzellen ist außerdem von großem Interesse bei der Erstdiagnose bösartiger Erkrankungen, um eine initiale, minimale Infiltration anderer Gewebe (z.B. Knochenmark oder Lymphknoten) bzw. minimale Mengen von in peripherem Blut zirkulierenden Malignomzellen zu detektieren. Dieser Nachweis kann einen direkten Einfluss auf die notwendige, zu planende Therapie und damit die Heilungschancen des individuellen Patienten haben. Ebenso ist es von Interesse, ob in Stammzell- bzw.

Knochenmarkpräparaten, die für eine eventuelle autologe Transplantation/Retransfusion des erkrankten Indivuduums benutzt werden können, minimale Mengen von Malignomzellen enthalten sind.

Aufgabe der Erfindung ist ein Verfahren anzugeben, welches eine malignomzellspezifische und patientenindividuelle Erkennung von Tumorzellen erlaubt.

Erfindungsgemäß wird die Aufgabe gelöst durch ein Verfahren welches es ermöglicht malignomzellspezifische und patientenindividuelle Diagnostika (Proben oder Sonden) für Malignomzellen bereitzustellen. Das erfindungsgemäße Verfahren ermöglicht es vorteilhaft absolut malignomzellspezifische und patientenidividuelle DNA Sequenzen basengenau zu detektieren und diese für diagnostische Anwendungen, z. B. in einem hoch sensitiven PCR Assay (AFS-PCR) zu verwenden.

Die Erfindung baut dabei auf der Erkenntnis auf, dass viele Malignome amplifizierte Genomabschnitte (ampGA) enthalten. Unter ampGA werden Bereiche des Genoms (eine bestimmte DNA-Sequenz) verstanden, welche in mehr als zwei Kopien pro haploidem Genom (häufig 4 bis über 120) in einer Zelle vorliegen. Diese ampGA liegen in so genannten „Amplikons" meist in streng hintereinander aufgereihter Form (repetitiv) vor.
Ein Amplikon ist somit das Gesamtgebilde, das aus den vielen Kopien eines (oder mehrerer unterschiedlicher) Genomabschnittes aufgebaut ist. Falls mehrere genomische Abschnitte amplifiziert sind können diese in unterschiedlichen Formen aneinander fusioniert sein, so dass z. T. sehr komplexe Amplikons entstehen.
Die Amplikons können in separaten, kleinen, zirkulären DNA Strukturen, den so genannten „Double-minute Chromosomen (dMin)" vorliegen, oder an unterschiedlicher Stelle wieder als so genannte „Homogenously staining regions (HSRs)" in das Genom reintegriert sein.
In Malignomen sind häufig Genomabschnitte amplifiziert, die Onkogene enthalten (z.B. MYCN in humanen Neuroblastomen, c-myc in Brustkrebs, AURKA in Blasenkarzinomen, etc.). Der genetische Inhalt der amplifizierten Bereiche spielt für die vorliegende Erfindung und die Etablierung einer AFS-PCR allerdings keine Rolle.

Der oder die ampGA sind bei jedem Malignom und damit auch bei jedem Patienten unterschiedlich groß und haben dementsprechend unterschiedliche telomerseitige und centromerseitige Grenzen. Ein Amplikon enthält zwischen 4 bis zu >120 Kopien der ampGA. Die Amplikon-Fusionsstellen (AFS) sind die Sequenzabschnitte innerhalb eines Amplikons, an denen die Kopien der ampGA aufeinander folgen. D.h. die Amplikon-Fusionsstelle (AFS) ist die Stelle in der Sequenz eines Amplikons, an der auf das letzte Nukleotid eines ampGA wieder das erste Nukleotid des nächsten ampGA folgt. Dadurch entsteht über diese AFS eine DNA Sequenzfolge (Fusionsbereich), die in keiner Zelle zu finden ist, die diese ampGA nicht enthält. Der Fusionsbereich ist der Sequenzbereich (bevorzugt mit einer Länge von 30 bis 300 Nukleotiden), welcher die AFS umgibt und diese beinhaltet. Da es sich bei Tumorerkrankungen vornehmlich um klonale Erkrankungen handelt, sind die AFS und damit die Fusionsbereiche in jeder Malignomzelle aber nicht in gesunden Zellen zu finden. Die AFS und damit die Fusionsbereiche sind in jedem Malignom unterschiedlich und damit absolut malignomspezifisch und patientenindividuell.

Die Insertionsstellen an denen ein Amplikon potentiell wieder in das Genom reintegriert ist, sind zwar genauso spezifisch und patientenindividuell, wie die AFS der hintereinander geschalteten DNA Abschnitte, jedoch lassen diese sich nur schwer identifizieren, da diese nur einmal in der Zelle vorliegen. Die AFS liegen jedoch in mehreren Kopien vor, so dass durch Bestimmung der telomer- und centromerseitigen Grenzen der ampGA mittels CGH und Tiling-Array auf die AFS gescreent werden kann.

Das erfindungsgemäße Verfahren ermöglicht einerseits die Herstellung eines Diagnostikums zur spezifischen Detektion von Malignomzellen eines Individuums und anderseits die darauf aufbauende Bereitstellung eines malignomzellspezifischen und patientenindividuellen Nachweisverfahrens.

Das erfindungsgemäße Verfahren zeichnet sich durch folgende Schritte aus:

a.) Hochauflösende Darstellung amplifizierter Genomabschnitte (ampGA) in einer isolierten Tumorprobe mittels Fine-Tiling Array,
bevorzugt nach Detektion des/der ampGA durch Gesamtgenomanalyse, bevorzugt durch CGH (Comparative Genomic Hybridization), falls diese nicht schon zuvor bekannt sind,

b.) Vervielfältigung, bevorzugt per PCR und anschließende Sequenzierung der Fusionsbereiche,

c.) Bereitstellen einer Probe (eine Sonde oder ein Primerpaar) welche es erlaubt, spezifisch den Fusionsbereich zu detektieren oder zu amplifizieren,

d.) bevorzugt Anwendung des Primerpaars in einer PCR (nachfolgend AFS-PCR), bevorzugt einer Realtime PCR, welche den Fusionsbereich bevorzugt überlappt und vorteilhaft die Möglichkeit der anschließenden relativen Quantifizierung der Zellen mit entsprechenden Amplikons bietet.

Die Probe ist entweder eine Nukleinsäuresonde, welche spezifisch mit dem Fusionsbereich durch komplementäre Basenpaarung hybridisiert. Eine solche Sonde hat bevorzugt eine Länge von 15 bis 35 Nukleotiden, bevorzugt 20 bis 30 Nukleotiden. Eine solche Sonde kann beispielsweise nach einer geeigneten Markierung in einem Southern- oder Northernblot oder in einer Realtime-PCR oder auch auf einem DNA-Array oder in Zellkulturexperimenten eingesetzt werden. Die Sonde kann nur dann an die DNA binden, wenn diese den malignomspezifischen Fusionsbereich (AFS) enthält.

Alternativ ist die Probe ein Primerpaar, welches in einer PCR (Polymerasekettenreaktion) spezifisch den Fusionsbereich vervielfältigt. Dazu bindet bevorzugt der eine Primer jeweils spezifisch den Genomabschnitte links und der andere rechts des Fusionsbereichs. D. h. die Primer werden bevorzugt so designt, dass jeweils ein Primer im telomerseitigen und ein Primer im centromerseitigen Sequenzbereich des ampGA liegt. Eine PCR kann also nur zu einem Produkt führen, wenn diese Bereiche aneinander fusioniert sind. Bevorzugt überbrückt die PCR den Fusionsbereich, wobei ein Primer vollständig auf der einen Seite und der zweite Primer auf der anderen Seite des Fusionsbereichs bindet (**Figur 3**). Alternativ kann ein Primer exakt auf die Fusionsstelle gelegt werden. Dies ist aus Primerdesigngründen jedoch nicht immer möglich, da bestimmte Bedingungen (wie z. B. G/C-Gehalt) eingehalten werden müssen, damit die PCR optimal funktioniert.

Eine weitere Möglichkeit zum Design einer malignomzellspezifischen AFS-PCR besteht in der Überbrückung von nicht amplifizierten Bereichen, die auf der Arraydarstellung wie Lücken innerhalb eines ampGA wirken. Hierbei handelt es sich nicht um wirkliche „Lücken“, sondern um nicht-amplifizierte Genomabschnitte, die zwischen zwei ampGA liegen. Es gibt sehr komplex aufgebaute Amplikons, in denen mehrere, verschiedene ampGA fusioniert sind, die damit eine übergeordnete Einheit darstellen, die dann wiederum repetitiv hintereinander fusioniert ist, um das Amplikon zu bilden. Hier besteht die Möglichkeit, dass die einzelnen ampGA in gleicher, oder in inverser Richtung miteinander fusioniert sind, d. h., dass zwei aufeinander folgende ampGA so angeordnet sind, dass an ampGA 1 in „Telomer → Centromer“ Ausrichtung ampGA 2 in „Centromer → Telomer“ Ausrichtung fusioniert ist. Dies kommt dadurch zustande, dass es sich bei genomischer DNA um einen Doppelstrang handelt, der sowohl in gleicher, als auch in inverser Richtung (dann allerdings mit vertauschten Strängen) aneinander fusioniert werden kann (vergleiche hierzu **Figur 4**).

In der PCR kann alternativ zu den spezifischen Primern oder zusätzlich eine Sonde eingesetzt werden, die spezifisch den Fusionsbereich bindet (z. B. für eine entsprechende Realtime-PCR). Alternativ kann einer der beiden Primer so gestaltet werden, dass er spezifisch den Fusionsbereich bindet. Die Bindung der Probe (Sonde und/oder Primer) erfolgt jeweils durch komplementäre Basenpaarung. Die Primer haben bevorzugt jeweils eine Länge von 15 bis 35 Nukleotiden, bevorzugt 18 bis 24 Nukleotiden.

Das erfindungsgemäße Verfahren ermöglicht vorteilhaft in kurzer Zeit, einen absolut malignomzellspezifischen und patientenindividuellen Genombereich (den Fusionsbereich mit der AFS) basengenau zu identifizieren und diesen mittels hochsensitiver PCR Verfahren, bzw. Verfahren, die eine Probe auf genau diesen Bereich legen, für die Verlaufsbeurteilung verschiedenster Malignome einzusetzen.

Voraussetzung für das erfindungsgemäße Verfahren ist das Vorhandensein von amplifizierten Genomabschnitten. Diese können in einem vorbekannten, definierten Bereich liegen. Wenn über die mögliche Amplifikation noch nichts bekannt ist, erfolgt in Schritt a.) zunächst eine Gesamtgenomanalyse, bevorzugt durch Gesamtgenom-CGH (Comparative Genomic Hybridization)-Array, d. h. einem DNA-Chip der Proben für das gesamte Genom enthält.
Ist der Genomabschnitt, in dem die Amplifikation vorkommt, bekannt oder durch die zuvor beschriebene Gesamtgenomanalyse ermittelt, wird der entsprechende Genomabschnitt bevorzugt in einer Fine-Tiling-CGH-Arrayuntersuchung hochauflösend abgegrenzt. Dazu erfolgt in Schritt b.) bevorzugt eine Hybridisierung mit einem so genannten Tiling Array, d. h. einem DNA-Chip der Proben für einzelne Chromosomen oder Chromosomabschnitte enthält.

Durch die höhere Auflösung der Tiling-Array Untersuchung werden durch die genaue Beschreibung der telomer- und centromerseitigen Grenzen der ampGA auch die potentiellen AFS innerhalb des Amplikon ermittelt.

In Schritt b.) wird der in Schritt a.) ermittelte Fusionsbereich sequenziert. Dazu erfolgt bevorzugt zunächst eine Vervielfältigung des Fusionsbereichs. Bevorzugt wird dazu eine konventionelle PCR über den in Schritt a.) ermittelten Fusionsbereich gelegt. Bevorzugt nach Erhalt eines spezifischen PCR-Fragmentes wird der Fusionsbereich durch Sequenzierung basengenau beschrieben. Nach ggf. notwendiger Optimierung der den Fusionsbereich übergreifenden PCR bzgl. Sensitivität und Anwendbarkeit für semiquantitative Verfahren (z. B. Real-Time PCR) erhält man eine patientenindividuelle und 100% malignomzellspezifische PCR. Je nach Aufbau des Amplikons kann die PCR dabei auch mehrere (z.B. sehr kurze) ampGA und damit ggf. mehrere Fusionsbereiche überbrücken, zwischen denen auch nicht amplifizierte Bereiche liegen können.

Das Bereitstellen der Probe in Schritt c.) erfolgt basierend auf der in Schritt b.) erhaltenen Sequenz des Fusionsbereichs. Dies kann durch manuelles Primer bzw. Sondendesign oder auch computergestützt mit Programmen erfolgen (wie z. B. Beacon Designer™, Premier Biosoft, Palo Alto CA, USA oder PrimerQuest, Integrated DNA Technologies, Inc., Coralville, IA, USA).

Der Begriff Nukleinsäuren im Sinne der Erfindung umfasst neben Desoxyribonukleinsäuren (DNA) und Ribonukleinsäuren (RNA) auch alle anderen linearen Polymeren in denen die Basen Adenin (A), Cytosin (C), Guanin (G) und Thymin (T) oder Uracil (U) (oder andere komplementär zu verwendenden, modifizierten Basen) in entsprechender Abfolge angeordnet sind, insbesondere Nukleinsäuren mit verändertem Rückgrat oder 3' oder 5'-Terminus, wie z. B. einem Phosphothioat-, Phosphoramidat- oder O-Methyl-derivatisierten Rückgrat, Peptid-Nukleinsäuren (PNA), und locked nucleic acids (LNA) oder gemischtem Rückgrat. Der Begriff „modifizierter 3' oder 5' Terminus" umfasst dabei sowohl Modifikationen, die der Stabilisierung dienen als auch das Anbinden von Markern. Beispiele für Marker sind Enzyme, Farbstoff- oder Fluoreszenzfarbstoffe, Radionukleotide, sowie Haptene, wie z. B. Digoxigenin oder Biotin. Bei den Enzymen wird der Nachweis meist über eine von dem Enzym katalysierte Farbbildungsreaktion geführt. Farbige oder fluoreszierende Moleküle können direkt photometrisch oder fluorometrisch nachgewiesen werden. Hapten-Liganden werden meist mit einem entsprechenden enzym- oder farbstoffmarkierten Rezeptor, der eine Affinität für den Liganden hat, in Kontakt gebracht und darüber nachgewiesen.

Die mit dem erfindungsgemäße Verfahren erhaltene Probe kann vorteilhaft (beispielsweise in einer semiquantitaiven PCR) zur Detektion von Malignomzellen in unterschiedlichen Gewebe, wie z. B. dem Tumor selbst (TU), potentiellen Metastasen (M), Knochenmark (KM) und peripherem Blut (pB), aber auch in Körperflüssigkeiten wie Aszites, Pleuraerguss, Liquor, Urin (interessant z.B. bei Blasenkarzinom) oder auch Stuhl eingesetzt werden.

Das erfindungsgemäße Verfahren bzw. die damit erhaltenen Proben ermöglichen vorteilhaft, die hochspezifische Detektion von Malignomzell-DNA und damit Malignomzellen. Das Verfahren ist absolut malignomzell- und patientenspezifisch und hochsensitiv. Es ermöglicht die qualitative Detektierung und Quantifizierung von Malignomzell-DNA und Malignomzellen. Damit kann z. B. nach einer Malignombehandlung (z. B. durch Resektion, Chemotherapie und/oder Strahlentherapie) überprüft werden, ob tatsächlich alle Malignomzellen entfernt wurden. Die Erfindung liefert daher einen wichtigen Beitrag für die Initial- und Verlaufsdiagnostik im Rahmen diverser Malignomerkrankungen, bei denen Amplifikationen von Genomabschnitten vorliegen.

Die erfindungsgemäße hochspezifische Detektion von Malignomzellen ermöglicht auch den Nachweis oder Ausschluss von Metastasen oder einer Minimal Residue Disease (MRD). Eine andere wichtige Anwendung ist die Knochenmarkstransplantation, insbesondere die autologe Knochenmarkstransplantation. Das erfindungsgemäße Verfahren bzw. die damit erhaltenen Proben ermöglichen vorteilhaft, zu überprüfen, ob die dem Patienten entnommen Knochenmark- / Stammzellpräparate Malignomzellen enthalten, bevor sie nach der Malignombehandlung (Hochdosischemotherapie mit/ohne Ganzkörperbestrahlung) dem Patienten zurückgegeben werden.

Die einzelnen bevorzugten Schritte des erfindungsgemäßen Verfahrens werden näher durch das Schema in **Figur 1** erläutert.

Ein Malignom ist eine Erkrankung, bei der Zellen des Körpers autonom und grenzüberschreitend, teilweise destruierend wachsen und ohne Behandlung zum Tod des Organismus führen können. Diese beinhalten

Erkrankungen des blutbildenden Systemes (Leukämien und Lymphome) sowie Erkrankungen, die aus Zellen aller anderen Organen hervorgehen können (solide, bösartige Tumore).

Der Begriff Malignom umfasst alle bösartigen Neoplasien, insbesondere Leukämien, Lymphome und solide maligne Tumore. Im Folgenden wird die die Erfindung am Beispiel der in humanen Neuroblastomen amplifizierten Region des Chromosomes 2 (Chr. 2p24-25) näher erläutert. Die Erfindung ist jedoch auf alle Formen maligner Erkrankungen, die ampGA aufweisen, anwendbar, unabhängig von der Sequenz und der Lokalisation der ampGA innerhalb des Gesamtgenomes. Für viele Malignome sind ampGA bekannt (z.B. *MYCN* in Neuroblastomen, *c-myc, HER-2* und *ERBB2* in Brustkarzinomen; *c-myc* und *MYCN* in Medulloblastomen; *c-myc, AR (Androgen Rezeptor)* und *PIK3CA*, in Prostatakarzinomen etc.). In transformierten Zellen finden sich zudem häufig ampGA, die nicht regelmäßig bei diesen Erkrankungen vorkommen und, anders als z.B. beim Neuroblastom, somit keine Aussage über eine prognostische Bedeutung per se zulassen (z.B. Magenkarzinom). Alle diese ampGA können mit dem erfindungsgemäßen Verfahren als diagnostisches Werkzeug benutzt werden, um hochselektiv Malignomzellen identifizieren zu können. Die Erfindung ist grundsätzlich auf alle Malignome anwendbar, welche amplifizierte Genomabschnitte enthalten. Diese können, müssen aber kein spezifisches Gen (wie *MYCN*, *AURKA* oder andere) enthalten. Der genetische Inhalt des ampGA und die Frage, ob die Amplifikation dieses Bereiches eine prognostische Relevanz für das entsprechende Malignom besitzt oder nicht, spielen in der Erfindung keine Rolle. Auch die die Ausdehnung und Struktur des ampGA sind von geringer Relevanz. Weitere Beispiele für Malignome die häufig amplifizierte Genomabschnitte enthalten sind Leukämien, Lungen- und Magenkarzinome.

Mit Hilfe der Erfindung kann z.B. ein initialer Knochenmarkbefall eines Malignomes bzw. in peripherem Blut zirkulierende Malignomzellen äußerst sensitiv diagnostiziert werden. Malignomzellen können in Körperflüssigkeiten wie Liquor, Urin, Aszites, Pleuraflüssigkeit, Gelenkergüssen oder Stuhl nachgewiesen werden. Des weiteren kann in definierten Verlaufskontrollen eine Aussage über ein quantitatives Ansprechen der Erkrankung auf die Therapie gemacht werden (Tumorzellnachweis in Knochenmark oder Tumorrestgewebe, Lokalrezidivdiagnostik (Primärtumorlokalisation, Metastasen, Lymphknoten)). Eine weitere Anwendungsmöglichkeit besteht in dem äußerst sensitiven Nachweis von Tumorzellen in patienteneigenen Stammzell-/Knochenmarkpräparaten vor einer eventuell notwendigen autologen Stammzell-/Knochenmarktransplantation z. B. im Rahmen einer Hochdosis-Chemotherapie.

Die Erfindung wir nachfolgend anhand von Figuren und Ausführungsbeispielen näher erläutert, ohne auf diese beschränkt zu sein.

Die prinzipielle Vorgehensweise des erfindungsgemäßen Verfahrens zur Etablierung einer Amplikon-Fusionsstellen-PCR wird anhand zweier primärer, humaner Neuroblastomzellinien beschrieben, die eine Amplifikation des genomischen Bereiches um *MYCN* aufweisen.
Da das Vorhandensein der Amplifikation des genomischen Berreiches um *MYCN* in beiden Zellinien bekannt ist konnte die DNA gleich auf einem Tiling-Array hybridisiert werden, der den genomischen Bereich um das *MYCN*-Gen entsprechend hoch auflöst.

Figur 1: Dargestellt ist der mögliche Untersuchungsablauf im Falle einer neu diagnostizierten Malignomerkrankung. Sind für die entsprechende Erkrankung bereits ampGA vorbeschrieben, kann direkt mit einer Fine-Tiling Array Untersuchung begonnen werden. Sind keine Gen-Amplifikationen bekannt, kann zuvor im Gesamtgenom mittels CGH Untersuchung gescreent werden. Folgend sind die weiteren Schritte zur Etablierung einer AFS-PCR beschrieben.

Figur 2: Dargestellt sind die Ergebnisse der Fine-Tiling Array Untersuchung von genomischer DNA aus den Neuroblastomzellinien KELLY und IMR32. In beiden Fällen ist die Amplifikation des Bereiches um *MYCN* (genomische Lokalisation um 16Mb) darstellbar und gut nach telomer- und centromerwärts abgrenzbar. Die Amplifikationshöhe ist als Log2-Ratio bezogen auf die Basallinie dargestellt.

Figur 3: A) Tiling-Array Darstellung des ampGA der KELLY Zellinie und dessen virtuellen telomerseitigen und centromerseitigen Grenzen. B) Virtuelle Fusionierung der ampGA-Grenzen. Damit wird die Aneinanderreihung „simuliert“, ohne die basengenaue Grenze zu kennen. C) Mit Abstand zu der virtuellen Fusionsstelle werden die Primer für die nachfolgende PCR designt. In Einzelfällen kann es notwendig sein mehrere Primerpaare zu designen, abhängig von der Qualität der Arrayuntersuchung und der Arrayauflösung an den Grenzbereichen (s. Haupttext). Nach erfolgreichem Primerdesign erhält man eine spezifische PCR Bande. D) Nach Sequenzierung des PCR Produktes erhält man die basengenaue Amplikonfusionstelle (AFS) und den Fusionsbereich, anhand derer eine hochsensitive Realtime PCR mit geringerem Abstand zur AFS designt werden kann.

Figur 4: A) Tiling-Array Darstellung der ampGA der IMR-32 Zellinie und deren virtuellen telomerseitigen und centromerseitigen Grenzen. B) Darstellung der durch PCR validierten AFS. Für drei der vier im Array dargestellten ampGA konnte eine direkte Fusion gezeigt werden. Dabei ist interessant, dass in diesem Fall die ampGA auch in inverser Richtung fusioniert sein können. Für ein ampGA konnte keine direkte Fusion mit den übrigen, auf dem Array dargestellten ampGA gezeigt werden. Mögliche Ursache ist das Vorhandensein weiterer ampGA in Bereichen des Genomes, die von der Tiling-Array Untersuchung nicht erfasst wurden und noch zwischen diese ampGA fusioniert sind. Für die Etablierung einer tumorspezifischen AFS-PCR reicht jedoch der Nachweis einer einzelnen AFS aus. C) Nach Sequenzierung des PCR Produktes erhält man die basengenaue Amplikonfusionstelle (AFS), anhand derer eine hochsensitive Realtime PCR mit geringerem Abstand zur AFS designt werden kann.

Figur 5: A) Darstellung der Realtime PCR Daten der spezifischen Real time-AFS PCRs für die beiden Neuroblastomzellinien KELLY und IMR-32. Auf die X-Achse sind die zunehmenden Verdünnungsschritte der Zellverdünnungsreihe aufgetragen. Die Y-Achse zeigt die relative Kopienzahl der Amplikons der Verdünnungsschritte, die mittels Realtime PCR nachgewiesen werden konnten bezogen auf die Kopienzahl der Amplikons in DNA aus den jeweils unverdünnten, *MYCN* amplifizierten Zellinien, die entsprechend =1 gesetzt wurden. B) Auftrag der AFS-PCR Fragmente in ein 3% Agarosegel und Färbung mit Ethidiumbromid. C) Weitere Verdünnung der isolierten DNA aus dem Zellverdünnungsschritt 1:10^6 mit DNA aus SH-EP Zellen in log2 -Schritten. Der Nachweis von AFS ist bis zu einer DNA Verdünnung von 1:80^6 deutlich möglich. Inhibin-Beta-B (IBB, ein Gen auf dem langen Arm von Chromosom2) wurde als Kontrollgen vervielfältigt. Für dieses Gen ist keine genomische Amplifikation bekannt.

Figur 6: Darstellung der Spezifität der AFS-PCRs für die Neuroblastomzellinien KELLY und IMR-32. Durchgeführte PCRs mit den jeweiligen Primern führen nur mit den DNAs der jeweiligen Zellinien zu spezifischen PCR Fragmenten. Die Zelllinien SH-EP, SY5Y, SK-N-BE(2) und CHP126 sowie natives gesundes Plazentagewebe sind Vergleichsproben.

Figur 7a/7b: Dargestellt sind die Ergebnisse der Fine-Tiling Array Untersuchung von genomischer DNA aus 40 unterschiedlichen, primären, *MYCN* amplifizierten Neuroblastomen. In allen Fällen ist die Amplifikation des/der ampGA um *MYCN* (genomische Lokalisation um 16Mb) darstellbar und gut nach temomer- und centromerwärts abgrenzbar. Die Amplifikationshöhe ist als Log2-Ratio bezogen auf die Basallinie dargestellt.

Figur 8: Dargestellt sind die Ergebnisse der Fine-Tiling Array Untersuchung von genomischer DNA aus 4 primären, *MYCN* amplifizierten Tumoren und deren zugehörigen Rezidiven. In allen Fällen ist die Amplifikation des Bereiches um *MYCN* (genomische Lokalisation um 16Mb) darstellbar und gut nach temomer- und centromerwärts abgrenzbar. Die Amplifikationshöhe ist als Log2-Ratio bezogen auf die Basallinie dargestellt. Die Untersuchung zeigt deutlich, daß die Amplikonstruktur in den Primärtumorzellen und den jeweiligen Zellen der Rezidivtumore exakt übereinstimmt.

Figur 9: A) Quantitative Realtime AFS-PCR am Beispiel zweier Primärtumoren (TU20 und TU21) und der dazugehörigen DNA aus primärem Tumor (TU), Knochenmark (KM) zum Zeitpunkt der Initialdiagnose, peripherem Blut (pB) und Rezidivtumorgewebe (Rez.). Als Negativkontrolle wurde DNA aus humanem Plazentagewebe eingesetzt (Kontr.). B) Nachweis der spezifischen AFS-PCR Fragmente in 3% Argarosegelen.

Zellen und Zellkultur

Für die Untersuchung wurden die humanen Neuroblastomzelllinien „IMR32“ (DSMZ No. ACC 165) und „KELLY“ (DSMZ No. ACC 355) mit vorbekannter *MYCN* Amplifikation, sowie die humane Neuroblastomzellinie SH-EP (keine DSMZ No. vorhanden) ohne *MYCN* Amplifikation in Kultur genommen. Die Zellen wurden unter Standardzellkulturbedingungen kultiviert (5% CO2, 37°C, RPMI-Medium mit 10% fötalem Kälberserum, Penicillin [100U/ml], Streptomycin [100µg/ml] und Glutamin [2mmol/L]). Vitale, in

Teilung befindliche Zellen wurden bei Erreichen einer Konfluenz von ca. 80% trypsinisiert, geerntet und abzentrifugiert und bis zur DNA Isolation bei -20°C gelagert.

DNA Isolation

Dazu wurde mittels eines Säulenaufreinigungsverfahrens die genomische DNA aus jeweils 5 x 10^6 Zellen isoliert (QIAGEN DNA-Blood an Tissue Kit; nach Anleitung des Herstellers). Die DNA-Konzentration und -Qualität wurden photospektrometrisch gemessen (Nanodrop, Fa. Amersham). Ausgangsbedingung für eine Arrayhybridisierung war eine DNA - Konzentration von 250ng/µl, eine DNA Gesamtmenge von 5µg DNA und eine 280/260nm Ratio von 1,85 – 1,95 (Angaben der Firma ImaGenes, Berlin).

Array

Die DNA wurde zusammen mit einer Kontroll-DNA (DNA eines gesunden, humanen, gleichgeschlechtlichen Individuums) auf den entsprechenden Arrayslide hybridisiert. Die Färbung der Proben DNA erfolgte mit dem Fluoreszenzfarbstoff Cy5, die Färbung der Kontroll DNA erfolgte mit Cy3. Das Arraydesign und die Arrayhybridisierung erfolgte als Auftragsleistung bei der Firma ImaGenes (Berlin, Deutschland).

Auf dem Arrayslide wurden DNA-Oligonukleotide (16-20 Basen Länge) des zu untersuchenden Bereiches geprintet. Die Auflösung errechnet sich dabei aus der möglichen Anzahl der zu hybridisierenden Oligonukleotide und der gewünschten Ausdehnung des zu untersuchenden Bereiches. In unserem Fall wurde ein Arrayslide mit 384.599 DNA-Oligonukleotide bestückt. Die Ausdehnung des zu untersuchenden Bereiches auf Chromosom 2p (inclusive der Kontrollbereiche) umfasste 24.913.401 Basen. Daraus ergibt sich eine Auflösung unseres Array von durchschnittlich 65 Basen Abstand zwischen 2 aufeinander folgenden DNA-Oligonukleotide. Zu Beachten ist dabei, dass in Bereichen des Genomes mit hochspezifischen Sequenzfolgen (z.B. für Gene kodierendes Euchromatin) die spezifischen DNA-Oligonukleotide in einer höheren Auflösung (kleinerer Abstand zueinander) designt werden können. In Bereichen des Genomes, in denen z.B. längere Repeatfolgen vorkommen ist die Auflösung entsprechend niedriger. Die Ergebnisse der Arrayhybridisierung der beiden Zelllinien-DNAs sind in **Figur 2** dargestellt.

Primerdesign

Die Angabe der exakten Position der auf den Array geprinteten Oligonukleotide ermöglicht es per Datenbanksuche (z.B. BLAT - The BLAST-Like Alignment Tool, *Genome Res* 12:4 656-664. http://genome.ucsc.edu/cgi-bin/hgBlat?command=start) die Sequenzen der telomerseitigen und zentromerseitigen Grenzen des ampGA zu erhalten.

Die jeweils ersten und letzten 1000 Basen des auf dem Array als ampGA dargestellten Bereiches wurden in eine Textdatei kopiert und so aneinandergereiht, dass jeweils an das Ende eines ampGA ein neuer Anfang des nächsten ampGA folgt. Damit wird virtuell der Fusionsbereich simuliert, in dem, in gleichgerichteter Orientierung, die amplifizierte Sequenz wieder aufeinander folgt. Diese Amplikonfusionsstelle (AFS) und damit der Fusionsbereich sind absolut spezifisch für das Tumorzellgenom und in keiner anderen Zelle zu finden, da ausschließlich die Tumorzellen die Amplifikation des exakt gleichen Bereiches aufweisen. Der so ermittelte Fusionsbereich dient nun zum Primerdesign für die nachfolgenden AFS-PCR Reaktionen. Die Primer werden so designt, dass jeweils ein Primer im telomerseitigen und ein Primer im centromerseitigen Sequenzbereich des ampGA liegt. Eine PCR kann also nur zu einem Produkt führen, wenn diese Bereiche aneinander fusioniert sind. Ein Beispiel bietet das *MYCN*-Amplikon der KELLY Zellinie (**Figur 3**).

Eine weitere Möglichkeit zum Design einer malignomzellspezifischen AFS-PCR besteht in der Überbrückung von nicht amplifizierten Bereichen, die auf der Arraydarstellung wie Lücken innerhalb eines amplifizierten Genomabschnittes wirken. Hier besteht die Möglichkeit, dass die einzelnen ampGA in gleicher, oder in inverser Richtung miteinander fusioniert sind. (D.h., dass zwei aufeinander folgende, ampGA so angeordnet sein können, dass an ampGA-1 in „Telomer → Centromer“ Ausrichtung der nächste ampGA-2 in „Centromer →Telomer“ Ausrichtung fusioniert ist. Dies kommt dadurch zustande, dass es sich bei genomischer DNA um einen Doppelstrang handelt, der sowohl in gleicher, als auch in inverser Richtung (dann allerdings mit vertauschten Strängen) aneinander fusioniert werden kann.) Ein Beispiel bietet das *MYCN*-Amplikon der IMR32 Zellinie. Dieses Amplikon zeigt einen sehr komplexen Aufbau, da noch weitere amplifizierte Genomabschnitte aus einer Entfernung von 50 Megabasen (um das *MEIS1*-Gen) in die Amplikonstruktur integriert sind. (**Figur 4**) Am Beispiel des IMR32 Amplikons wird deutlich, dass die Lokalisation, die Ausdehnung und der genomische „Inhalt“ des amplifizierten Bereiches zur Etablierung einer AFS-PCR unerheblich sind.

		Primer für die Zellinien PCRs	SEQ ID No.
Zellinie		Sequenz (5´→3´)	
		Zellinien AFS-PCR (vor Sequenzierung):	
IMR32	F	GGTTGTTGAGAGGATAATGGA	1
	R	TAGGAAAGGCTTTGGGTTAT	2
Kelly	F	TCTACCCAAGACACATGCTAA	3
	R	GCTGTCTGGTGCTACTCAA	4
		Zellinien quantitative Realtime-AFS-PCR (nach Sequenzierung):	
IMR32	F	CCCAGGATTAGACGGAAAAT	5
	R	CTACTGGTGATGCTTGACTC	6
Kelly	F	TCTGCCAAGCTGGGGTAAG	7
	R	TGTAAGTGGGCAGCGTGAC	8

PCR

Die PCR zur Validierung der virtuellen Fusionsbereiche erfolgte unter folgenden Bedingungen: QIAGEN-HotStarTaq Plus PCR Mastermix 12,5µl, DNA der entsprechenden Zellinie/Tumor 200ng, je 2 amplikonspezifische Primer oder 2 Kontrollprimer (je [25pMol]), DMSO 1,5µl, Aqua-dest. ad 25µl.

Cyclerbedingungen: 5 Minuten initiale Denaturierung bei 95°C, anschließend 38 Zyklen mit 20 Sekunden Denaturierung bei 95°C, 20 Sekunden Annealing bei 57°C, 60 Sekunden Elongation bei 72°C, danach Abkühlen auf 4°C bis zum Auftragen auf des Agarosegel.

Agarosegelelektrophorese in 1% – 3% Agarosegel (je nach Produktlänge). Anschließend Färbung der Gele mit Ethidiumbromid. Die Banden wurden unter UV Durchleuchtung sichtbar gemacht und dokumentiert (**Figur 3c**).

Isolation der DNA der PCR Banden

Im Anschluß wurden die PCR-Fragmente unter UV-Durchleuchtung aus dem Agarosegel ausgeschnitten und mit dem QIAGEN DNA Gel Extraktion Kit nach Herstellerangaben isoliert.

Sequenzierung

Die Sequenzierung der PCR-Fragmente erfolgte von beiden Seiten mit den entsprechenden, zuvor in der PCR eingesetzten Primern. (Einsatz in die Reaktion: 20ng/100bp DNA-Fragment, je 10pmol Primer). Ansatz der Sequenzierreaktion mit dem „ABI Prism BigDye Terminator 3.1 Ready Reaction Cycle Seq. Kit“ von Applied Biosystems. Reaktionsablauf unter Bedingungen nach Angaben des Herstellers. Als Sequenzer wurde ein „16 Capillary Sequenzer Genetic Analyzer 3100“ von Applied Biosystems benutzt.

Design von Primern für eine Realtime PCR

Nach Sequenzierung der PCR Fragmente ist die basengenaue Fusionsstelle (AFS) des entsprechenden Amplikons identifiziert. Es können nun Primer designt werden, die zu einem PCR-Produkt führen, das die exakte AFS überbrückt. (Entsprechend der Kriterien für eine Realtime PCR sollte das Produkt 100-200bp Länge nicht überschreiten. Daher ist die Sequenzierung des Fusionsbereichs mit der genauen Fusionsstelle (AFS) für das RT-Primer Design obligat.)

Durchführung der Realtime PCR

Die PCR zur Validierung der virtuellen Fusionsbereiche erfolgte unter folgenden Bedingungen: QIAGEN-HotStarTaq Plus PCR Mastermix 12,5µl, SYBR-Green-I [0,5x] (Molecular Probes), DNA der entsprechenden Zellinie/Tumor 200ng, je 2 amplikonspezifische Primer oder 2 Kontrollprimer (*Inhibin-beta-B*) (je 25pmol), Formamid 0,3µl, DMSO 1,5µl, Aqua-dest. ad 25µl.

Cyclerbedingungen: 5 Minuten initiale Denaturierung bei 95°C, anschließend 38 Zyklen mit 20 Sekunden Denaturierung bei 95°C, 20 Sekunden Annealing bei 57°C, 30 Sekunden Elongation bei 72°C, danach Abkühlen auf 4°C.

Der SYBR-Green Ansatz für die Realtime AFS-PCR wurde gewählt, da mit Hilfe einer anschließenden Schmelzkurvenanalyse eine qualitative Aussage über die Spezifität des PCR Produktes gemacht werden kann.

Testung der Sensitivität des Verfahrens (Zell-Verdünnungsreihe)

Mittels der etablierten Realtime PCR wurde anhand einer Verdünnungsreihe von Tumorzellen die Sensitivität des Verfahrens ermittelt. Tumorzellen der entsprechenden Neuroblastomzellinien mit *MYCN* Amplifikation (KELLY und IMR-32) wurden in Zellen einer Neuroblastomzellinie ohne *MYCN* Amplifikation (SH-EP) mit annähernd identischem DNA Gehalt/Zelle verdünnt. Dabei wurden folgende Verdünnungsstufen hergestellt: Eine Tumorzelle auf 10 Kontrollzellen (1/10), Eine Tumorzelle auf 100 Kontrollzellen ($1/10^2$) und im Weiteren ($1/10^3$), ($1/10^4$), ($1/10^5$), ($1/10^6$). Von jeder *MYCN* amplifizierten Tumorzellinie wurden drei unabhängige Verdünnungsreihen angelegt. Aus diesen Zellverdünnungsschritten wurde von jeweils 2 x 10^6 Zellen genomische DNA isoliert. Von der isolierten DNA wurden 200ng in eine Realtime AFS-PCR eingesetzt. Als

Positivkontrolle diente DNA der spezifischen, *MYCN* amplifizierten Zelllinie (IMR32, KELLY). Als Negativkontrolle diente DNA der nicht *MYCN* amplifizierten Kontrollzelllinie (SH-EP). Jede Verdünnungsreihe wurde im Triplikat untersucht. Die Ergebnisse sind in relative AFS-Kopienzahl in Bezug auf die Positivkontrolle dargestellt (**Figur 5**). Mittels Realtime PCR konnten so tumorspezifische AFS-PCR Produkte aus einer Zellverdünnung von $1/10^6$ sicher dargestellt werden. Dieser Wert entspricht der ermittelten Sensitivität des Verfahrens. Die experimentell nachgewiesenen, relativen Kopienzahlen entsprechen dabei fast exakt den angesetzten Verdünnungsschritten (bei KELLY exakter als bei IMR-32). Dieses Ergebnis unterstreicht die Anwendbarkeit und Interpretationsfähigkeit des Verfahrens.

Qualitativ wurden spezifische AFS-PCR Fragmente aus einer weiteren DNA Verdünnung, ausgehend von der DNA aus dem Zellverdünnungsschritt $1:10^6$, in Bereichen von $1/10^6$ - $1/10^7$ detektiert. Dazu wurde die DNA aus dem Zellverdünnungsschritt $1:10^6$ mit SH-EP DNA schrittweise 1:1 weiter verdünnt und anschließend in die AFS-PCR eingesetzt. Dabei ist der letzte Verdünnungsschritt ($1/10^7$) teilweise nur noch sehr schwach nachweisbar. Eine Quantifizierung mittels Realtime PCR ist aufgrund der großen Standardabweichungen in diesem Bereich nur noch ungenau möglich. Aufgrund der 100%igen Spezifität der AFS-Fragmente ist dieser qualitative Nachweis jedoch immer als positiver Befund zu werten (**Figur 5 C**).

Testung der Spezifität des Verfahrens 1 (Spezifität der AFS-PCR Primer)

Die Spezifität der AFS-PCR wurde überprüft, indem die AFS spezifischen Primer mit DNA der jeweiligen amplifizierten Zellinien und weiteren Kontrollzellinien/Geweben eingesetzt wurden. Dabei können AFS spezifische PCR-Fragmente nur aus DNA der entsprechenden Zellinien generiert werden (**Figur 6**).

Testung der Spezifität des Verfahrens 2 (Hybridisierung von DNA aus 40 primären MYCN amplifizierten Neuroblastomen)

Die Spezifität der AFS wird anhand einer Untersuchung von DNA aus 40 primären, *MYCN* amplifizierten Neuroblastomen dargestellt (**Figur 7a, 7b**). Für jedes Amplikon finden sich individuelle telomer- und centromerseitige Grenzen der ampGA. Damit sind die Fusionsbereiche nicht nur innerhalb eines Individuums malignomzellspezifisch, sondern auch interindividuell einzigartig. Die etablierten AFS-PCRs sind somit sowohl malignomzellspezifisch als auch patientenindividuell.

Testung der Spezifität des Verfahrens für die Verlaufskontrolle

Von 4 Tumoren lag ausreichend Material von Tumorgewebe aus einem zugehörigen Rezidiv vor. Aus diesem Material wurde wie zuvor beschrieben DNA isoliert und auf einen gleich designten Array hybridisiert. Die Grenzen der ampGA entsprechen exakt denen der entsprechenden Primärtumoren (**Figur 8**).

Von einigen Tumoren wurde DNA aus zugehörigen Blut- und Knochenmarkproben sowie aus Tumormaterial von Rezidivtumoren isoliert. Die individuellen AFS-PCRs wurden mit diesen DNAs durchgeführt. In einigen Fällen konnte damit das Vorhandensein von Tumorgenom in diesen Proben und damit der Beweis der Praktikabilität der Methode für die Verlaufskontrollen in der klinischen Praxis dargestellt werden (**Figur 9**).

Figur 1

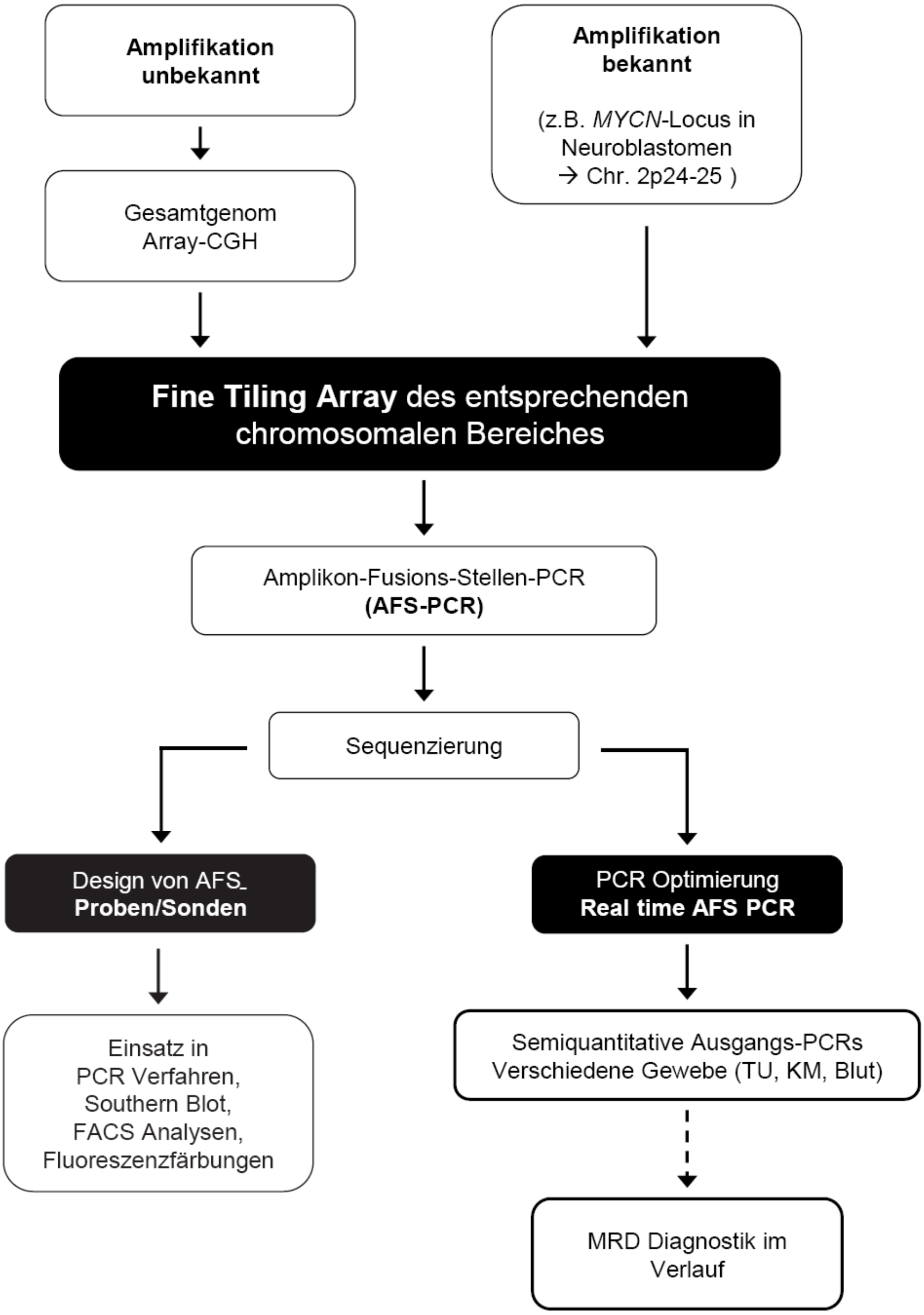
Amplifikation unbekannt
Gesamtgenom Array-CGH
Amplifikation bekannt
(z.B. *MYCN*-Locus in Neuroblastomen → Chr. 2p24-25)
Fine Tiling Array des entsprechenden chromosomalen Bereiches
Amplikon-Fusions-Stellen-PCR **(AFS-PCR)**
Sequenzierung
Design von AFS_ **Proben/Sonden**
Einsatz in PCR Verfahren, Southern Blot, FACS Analysen, Fluoreszenzfärbungen
PCR Optimierung **Real time AFS PCR**
Semiquantitative Ausgangs-PCRs Verschiedene Gewebe (TU, KM, Blut)
MRD Diagnostik im Verlauf

Figur 2

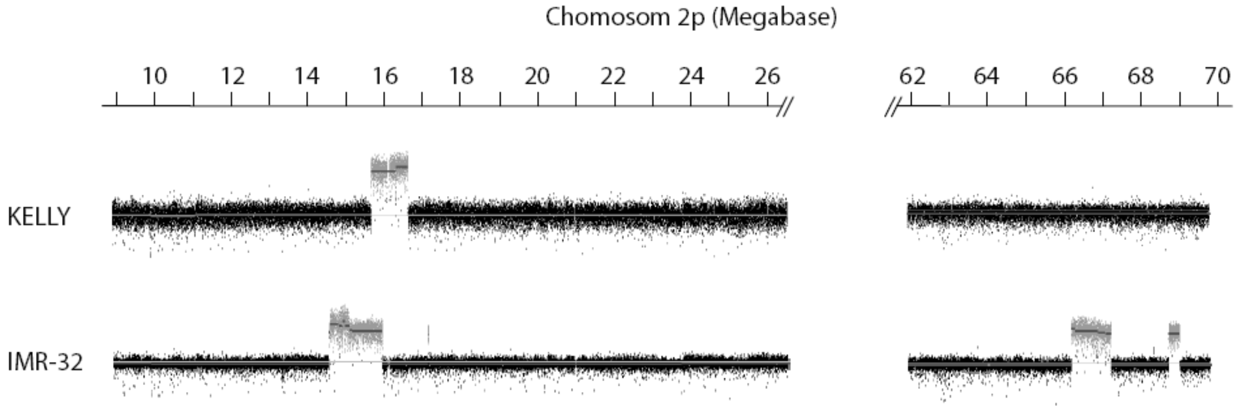
Chomosom 2p (Megabase)
10
12
14
16
18
20
22
24
26
62
64
66
68
70
KELLY
IMR-32

Figur 3

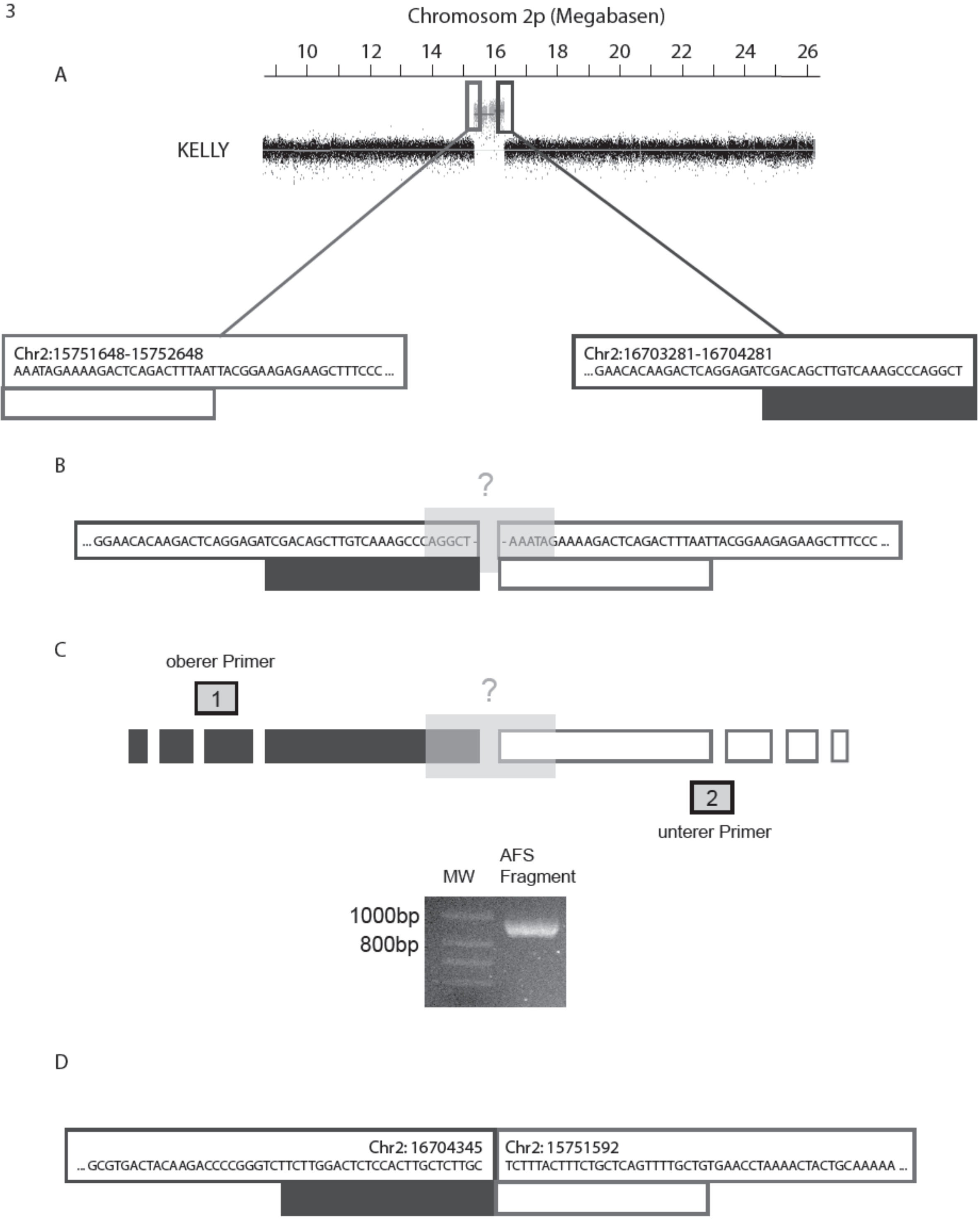
Chromosom 2p (Megabasen)
10
12
14
16
18
20
22
24
26
A
KELLY
Chr2:15751648-15752648
AAATAGAAAAGACTCAGACTTTAATTACGGAAGAGAAGCTTTCCC ...
Chr2:16703281-16704281
...GAACACAAGACTCAGGAGATCGACAGCTTGTCAAAGCCCAGGCT
B
?
... GGAACACAAGACTCAGGAGATCGACAGCTTGTCAAAGCCCAGGCT -
- AAATAGAAAAGACTCAGACTTTAATTACGGAAGAGAAGCTTTCCC ...
C
oberer Primer
1
?
2
unterer Primer
MW
AFS Fragment
1000bp
800bp
D
Chr2: 16704345
... GCGTGACTACAAGACCCCGGGTCTTCTTGGACTCTCCACTTGCTCTTGC
Chr2: 15751592
TCTTTACTTTCTGCTCAGTTTTGCTGTGAACCTAAAACTACTGCAAAAA ...

Figur 4

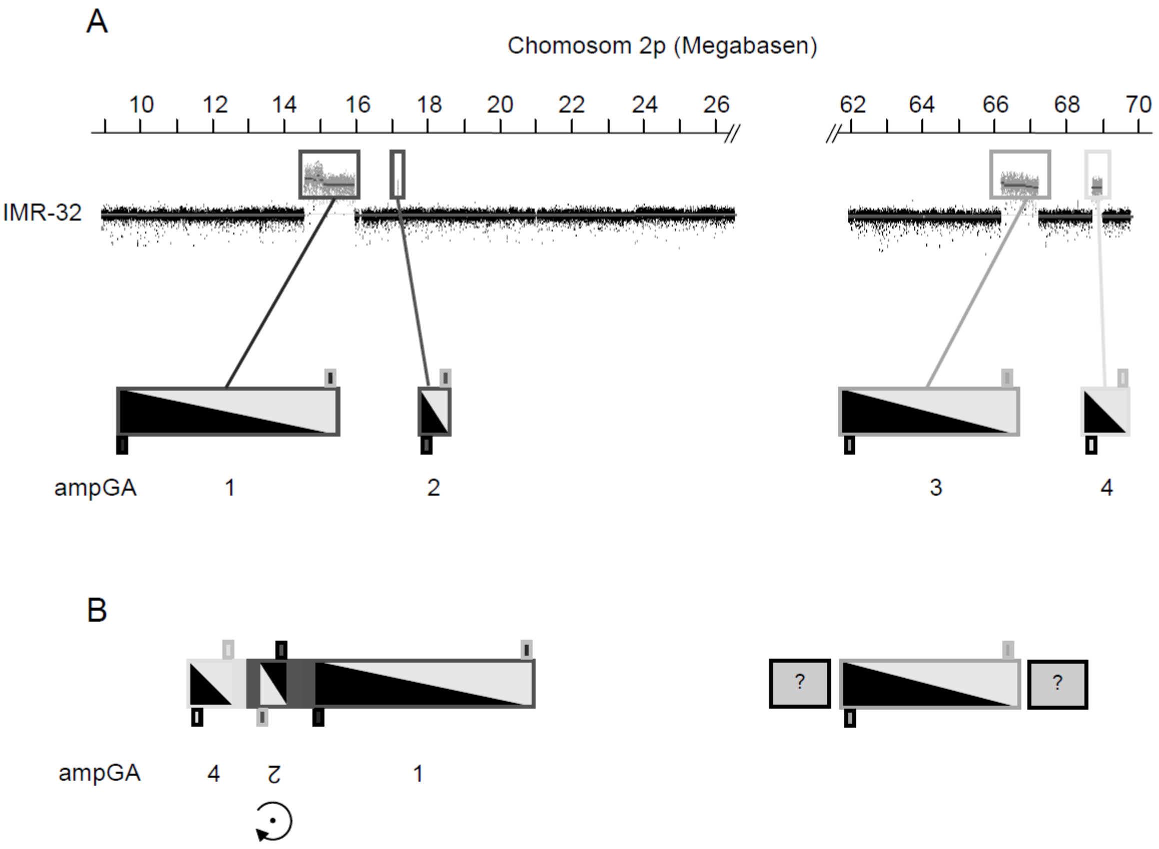
A
Chomosom 2p (Megabasen)
10
12
14
16
18
20
22
24
26
62
64
66
68
70
IMR-32
ampGA
1
2
3
4
B
?
?
ampGA
4
2
1

C

AFS 1 (ampGA 1 : 2(invers))

← Chr2: 17219746 TTATTCTAAGTTACTCCATGCTATGTTGTTATTGAATAATGTAAACTCAG	Chr2: 14657089 → AAGTGTATAAGACAAGATGAATATATGGATATACTCTAAATGTTAATAGT

AFS 2 (ampGA 4 : 2(invers))

← Chr2: 69255557 GTCCCATCACTTAATAACTGAAATATTGGGGCCACTGGTATTTTAATCTC	Chr2: 17233193 → TTGATTGTGATATTCTGTAAATATTATATAAATGAGGTGACATTTAAGGC

ampGA = amplifizierter genomischer Abschnitt

Figur 5

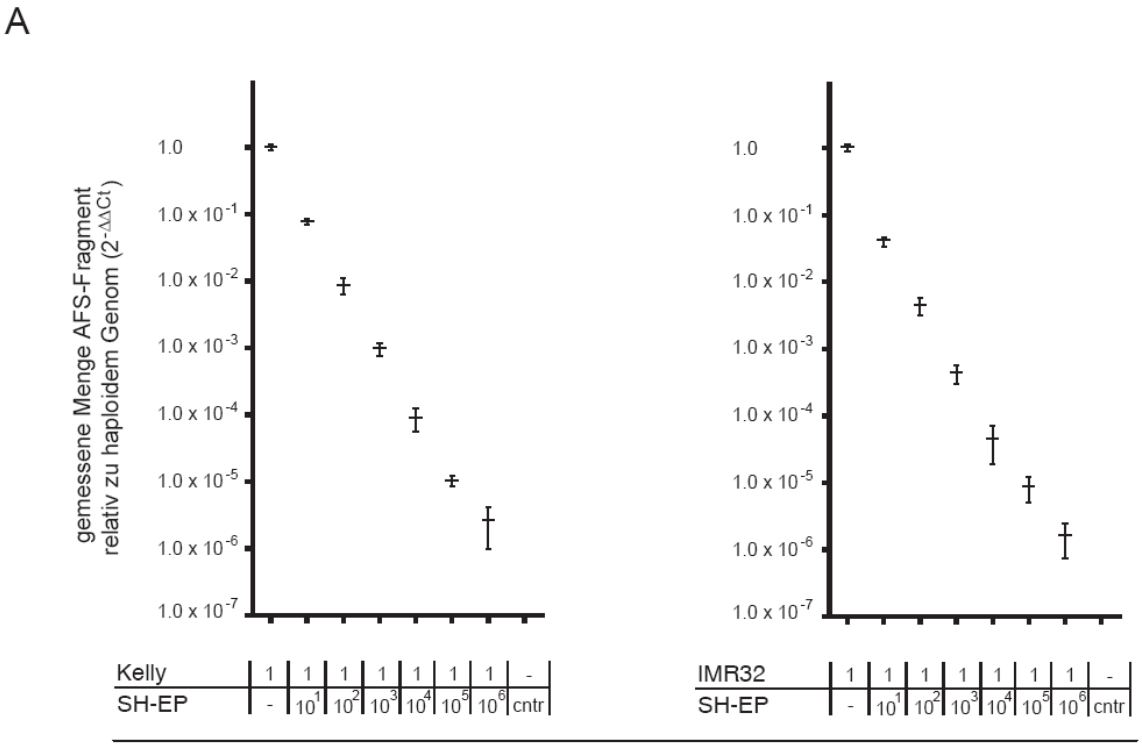

Einsatz *MYCN* amplifizierter Zellen relativ zu nicht amplifizierten Zellen (SH-EP) in die jeweiligen PCRs

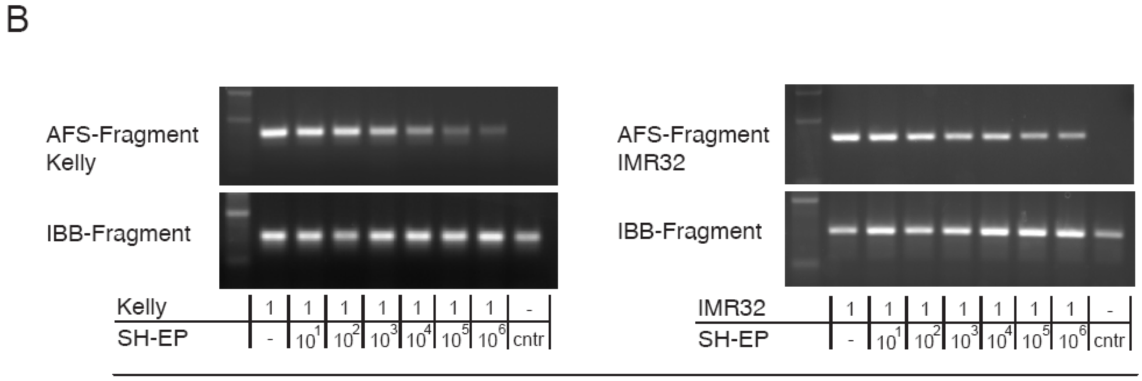
B
AFS-Fragment Kelly
IBB-Fragment
AFS-Fragment IMR32
IBB-Fragment
Kelly | 1 | 1 | 1 | 1 | 1 | 1 | 1 | -
SH-EP | - | 10^1 | 10^2 | 10^3 | 10^4 | 10^5 | 10^6 | cntr
IMR32 | 1 | 1 | 1 | 1 | 1 | 1 | 1 | -
SH-EP | - | 10^1 | 10^2 | 10^3 | 10^4 | 10^5 | 10^6 | cntr

Einsatz *MYCN* amplifizierter Zellen relativ zu nicht amplifizierten Zellen (SH-EP) in die jeweiligen PCRs

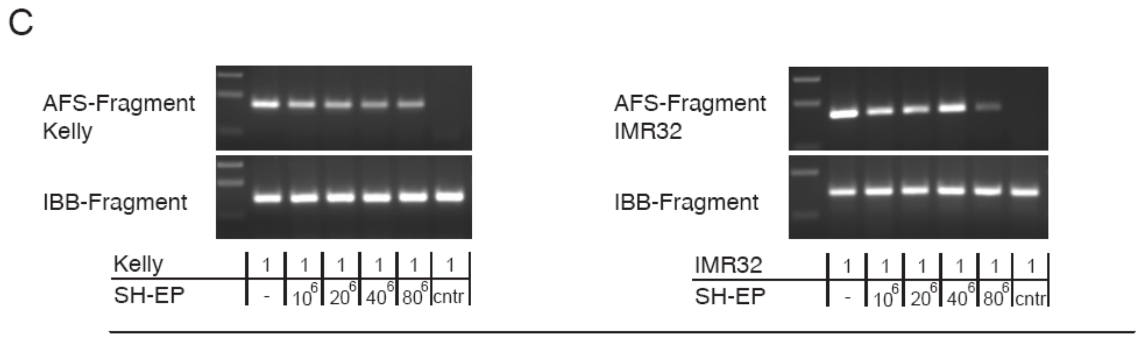
C
AFS-Fragment Kelly
IBB-Fragment
AFS-Fragment IMR32
IBB-Fragment
Kelly | 1 | 1 | 1 | 1 | 1 | 1
SH-EP | - | 10^6 | 20^6 | 40^6 | 80^6 | cntr
IMR32 | 1 | 1 | 1 | 1 | 1 | 1
SH-EP | - | 10^6 | 20^6 | 40^6 | 80^6 | cntr

Einsatz Genom *MYCN* amplifizierter Zellen relativ zu nicht amplifizierter Zellen (SH-EP) in die jeweiligen PCRs

Figur 6

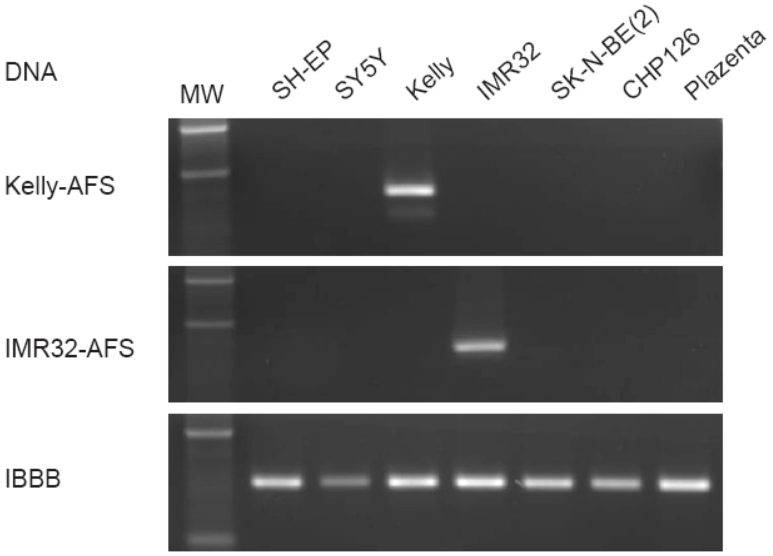
DNA
MW
SH-EP
SY5Y
Kelly
IMR32
SK-N-BE(2)
CHP126
Plazenta
Kelly-AFS
IMR32-AFS
IBBB

Figur 7a

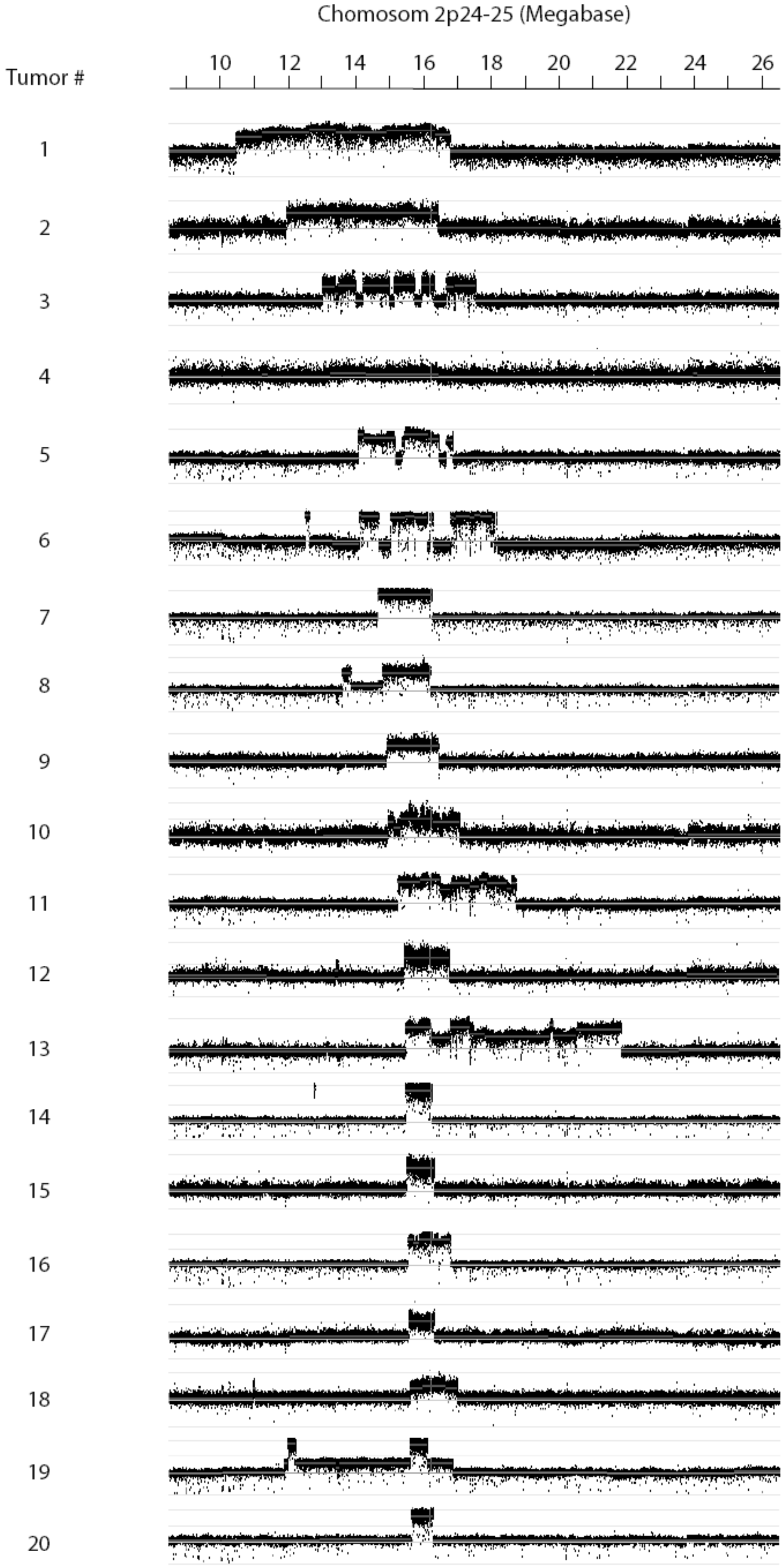
Chomosom 2p24-25 (Megabase)
Tumor #
10
12
14
16
18
20
22
24
26
1
2
3
4
5
6
7
8
9
10
11
12
13
14
15
16
17
18
19
20

Figur 7b

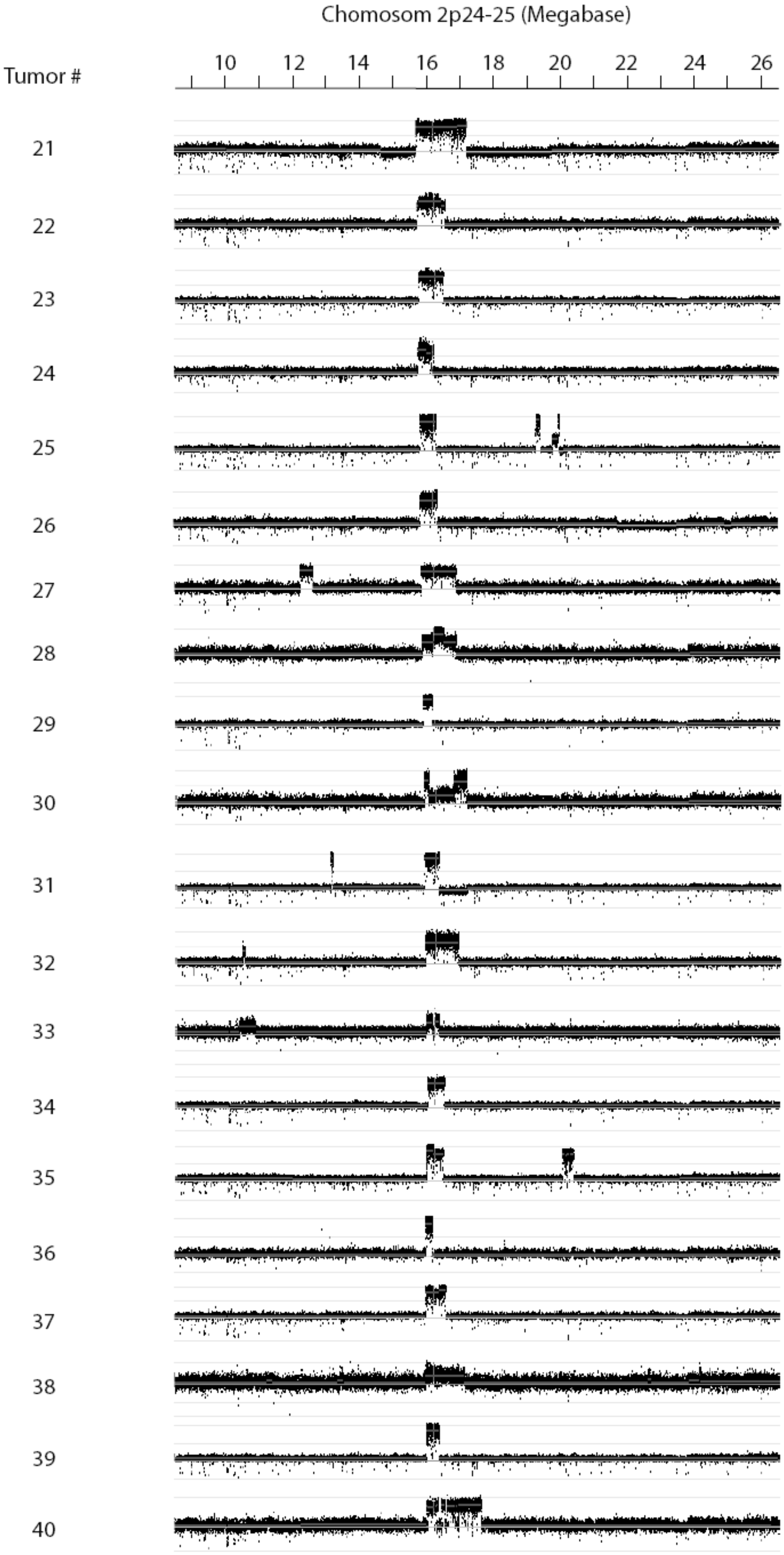
Chomosom 2p24-25 (Megabase)
Tumor #
10
12
14
16
18
20
22
24
26
21
22
23
24
25
26
27
28
29
30
31
32
33
34
35
36
37
38
39
40

Figure 8

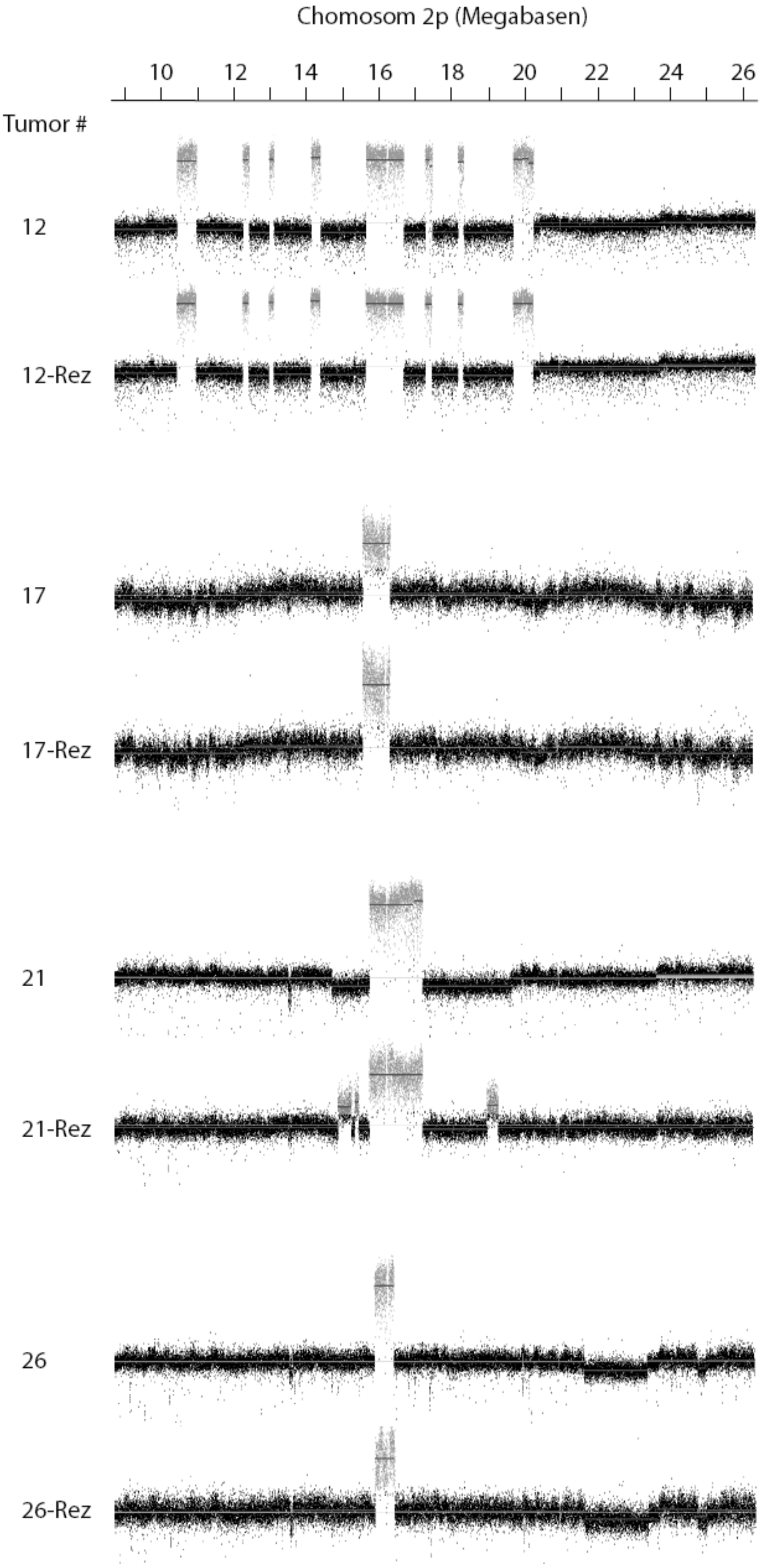
Chomosom 2p (Megabasen)
10
12
14
16
18
20
22
24
26
Tumor #
12
12-Rez
17
17-Rez
21
21-Rez
26
26-Rez

Figur 9

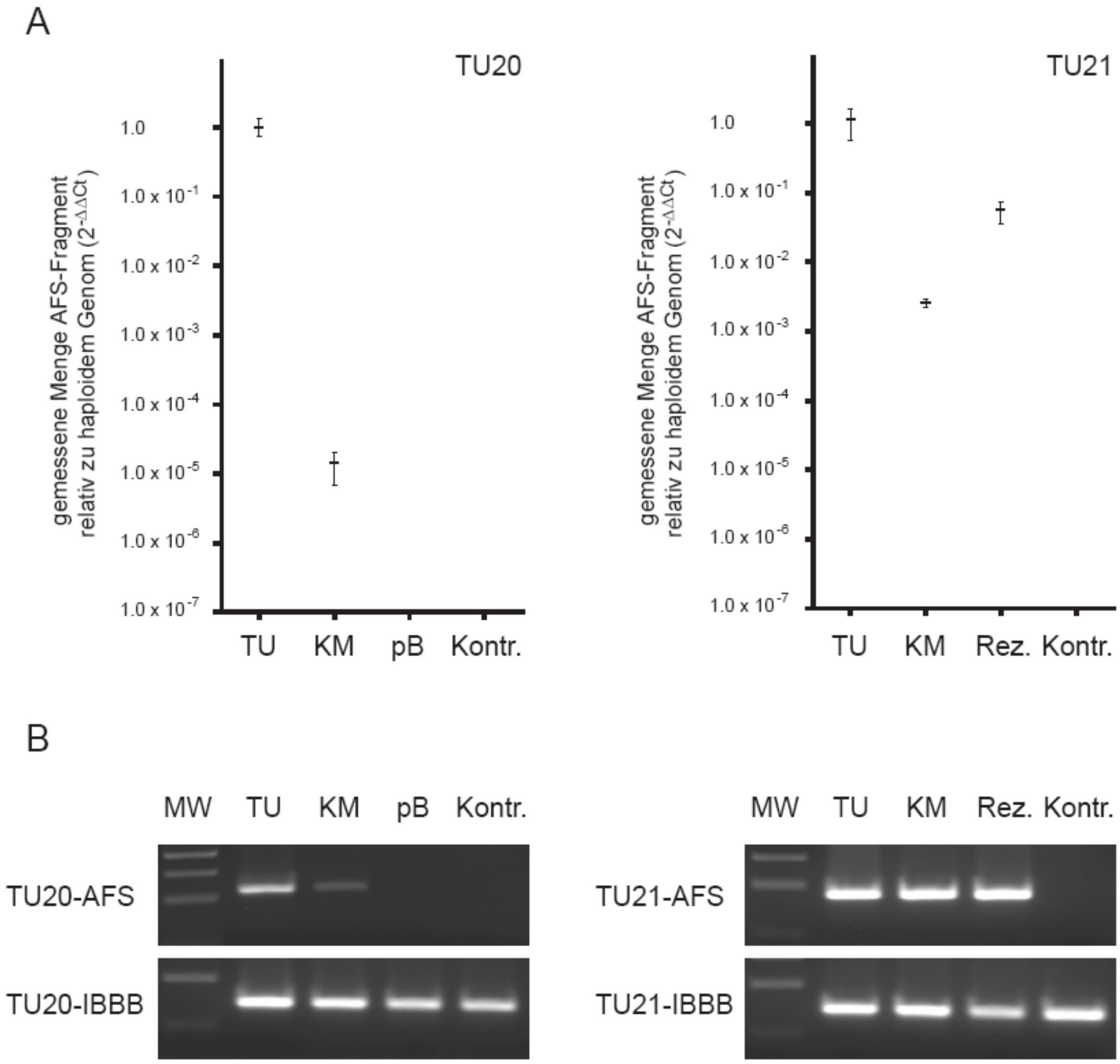
A
TU20
gemessene Menge AFS-Fragment relativ zu haploidem Genom ($2^{-\Delta\Delta Ct}$)
1.0
1.0 x 10^{-1}
1.0 x 10^{-2}
1.0 x 10^{-3}
1.0 x 10^{-4}
1.0 x 10^{-5}
1.0 x 10^{-6}
1.0 x 10^{-7}
TU
KM
pB
Kontr.
TU21
gemessene Menge AFS-Fragment relativ zu haploidem Genom ($2^{-\Delta\Delta Ct}$)
1.0
1.0 x 10^{-1}
1.0 x 10^{-2}
1.0 x 10^{-3}
1.0 x 10^{-4}
1.0 x 10^{-5}
1.0 x 10^{-6}
1.0 x 10^{-7}
TU
KM
Rez.
Kontr.
B
MW
TU
KM
pB
Kontr.
TU20-AFS
TU20-IBBB
MW
TU
KM
Rez.
Kontr.
TU21-AFS
TU21-IBBB

2.6 Diskussion und Ausblick

Molekulare Marker nehmen in der onkologische Diagnostik einen immer größeren Stellenwert ein. Neben den Leukämieen können in fast allen Formen solider Tumoren genomische Veränderungen beschrieben werden, die zur Diagnostik, Stratifizierung und Etablierung von MRD Markern genutzt werden können (siehe hierzu: *Atlas of Genetics and Cytogenetics in Oncology and Haematology.* URL http://AtlasGeneticsOncology.org).

Im Falle des Neuroblastomes hat die Entdeckung der *MYCN* Amplifikation und deren prognostische Bedeutung die risikoadaptierte Therapiestratifizierung revolutioniert (*Schwab et al., 1983*). Im weiteren Verlauf konnte auch für weitere genomische Veränderungen eine Korrelation zu einem schlechteren Therapieansprechen und damit verbunden, zu einer schlechteren Prognose beschrieben werden (*Maris et al 1999; Fischer et al 2008*). Für die Risikostratifizierung werden zusätzlich zur *MYCN* Amplifikation noch Deletionen auf Chromosom 1p und 11q herangezogen.

Neben genomischen Veränderungen unterscheiden sich Neuroblastome verschiedener Risikogruppen auch in Ihren Genexpressionsmustern. Durch vergleichende Untersuchung solcher Genexpressionsprofile können teilweise Rückschlüsse auf das biologische Verhalten von Tumorzellen wie Proliferationskompetenz oder ein potentielles Ansprechen auf bestimmte Zytostatika gezogen werden. Exemplarisch wurden im Rahmen dieser Arbeit die Expression von dem CDK Inhibitor p27kip, der Rezeptor-Tyrosinkinase IRR und des Transkriptionsfaktors Zbtb4 (KL1) untersucht. Die Arbeiten ließen Rückschlüsse auf die funktionelle Bedeutung dieser Proteine in der Genese des humanen Neuroblastomes zu. Für das in unserer Arbeitsgruppe zuvor erstmals klonierte Zinc-Finger Protein Zbtb4 konnten Protein-Interaktionspartner identifiziert und die Auswirkung auf die Bindung dieses Proteinkomplexes an dem Promotor des Zellzyklusinhibitors p21cip analysiert werden. Durch Aufklärung dieser Mechanismen konnte nicht nur die prognostische Bedeutung der Zbtb4 Expression in humanen Neuroblastomen erklärt werden. Die Identifizierung des Zusammenspieles des Transkriptionsfaktor-Komplexes um Zbtb4 mit Histonacetylasen (HDAC) lässt auch eine potentielle therapeutische Beeinflussung denkbar erscheinen.

Neben der Identifizierung einzelner, für die Genese des Neuroblastomes wichtiger Gene aus einer Screeninguntersuchung (z.B. Microarray basiert) kann die Betrachtung der gesamten Genexpressionsprofile auch benutzt werden, um Risikogruppen zu stratifizieren. Dies ist durch die Etablierung des PAM Classifiers zumindest für einen Großteil der Neuroblastompatienten möglich. Gerade die Hochrisiko-Patienten, für die weitere Stratifizierungswerkzeuge dringend notwendig wären, scheinen jedoch am wenigsten von der Einteilung über den PAM Classifier zu profitieren.

Es bleibt abzuwarten, inwieweit Genexpressionsmarker oder ganze Genexpressionsprofile wirklich Anwendung in der klinischen Routine finden werden. RNA ist wesentlich instabiler als genomische DNA und der hohe logistische Aufwand bei der Materialgewinnung, -aufbereitung, dem -transport und letztlich der RNA Isolation spricht derzeit noch gegen einen routinemäßigen Einsatz.

Für die Hochrisiko-Patienten mit Amplifikation des *MYCN* Genes konnte gezeigt werden, dass die ampGA in Ihrer Ausdehnung her von Patient zu Patient sehr unterschiedlich sind. Dies wurde zuerst mittels Multiplex-PCR durch Nachweis von Koamplifikationsmustern gezeigt. In dem untersuchten Patientenkollektiv zeigte sich ein Überlebensvorteil für Patienten, deren ampGA telomerwärts von *MYCN* auch das *DDX1* Gen mit einschließt. Mit den etablierten Multiplex-PCR Ansätzen konnte ebenfalls gezeigt werden, dass sich die Ausdehnung der ampGA im Verlauf der Erkrankung (nach Chemotherapie bzw. im Falle eines Rezidives) nicht ändert. Lediglich die Kopieenzahl zeigte eine begrenzte Variabilität. In einer Folgeuntersuchung konnten wir mittels HR-TA die ampGA hochauflösend darstellen und die absolute Individualität deren Ausdehnung beschreiben. Die Grenzbereiche der ampGA konnten mittels PCR validiert werden. Die dafür entwickelten PCRs wurden über Fusionsbereiche der ampGA gelegt und waren damit absolut Tumorzell-spezifisch und Patienten-individuell (AFS-PCR). Dieses Verfahren wurde eingehend auf seine Spezifität und Sensitivität hin untersucht und scheint sich nach unseren Daten ideal als Diagnostikum zum Nachweis minimaler Tumorzellmengen zu eignen. Dies ist zum Beispiel für einen Einsatz in der MRD-Diagnostik denkbar, die aktuell einen immer größer werdenden, therapiebegleitenden Stellenwert für Patienten mit soliden Tumoren einnimmt.

Die Weiterentwicklung geeigneter, molekularer Marker, die für die routinemäßige Anwendung bei Neuroblastompatienten geeignet sind, ist das vorrangige Ziel weiterer Forschungsprojekte, die auf den Arbeiten, die die Grundlage dieser Habilitationsschrift bilden, aufbauen. Dabei spielt die Praktikabilität eine große Rolle. Der Einsatz der AFS-PCR ist sehr viel versprechend und soll in prospektiven Untersuchungen auf seine Anwendbarkeit hin untersucht werden. Das Verfahren wurde beispielhaft an *MYCN* amplifizierten Neuroblastomen entwickelt. Die mögliche Übertragbarkeit auf andere amplifizierte Genomabschnitte eröffnet die Möglichkeit diese Methode auch für viele andere Tumorentitäten als Diagnostikum zu etablieren. Die Wertigkeit eines Nachweises geringster Mengen von Tumorzellen bzw. Tumorzellgenom muss allerdings für jede Malignomentität studienbegleitend überprüft werden.

2.7 Abkürzungen

AFS (Amplikon-Fusions-Stelle); AI (Apoptotic-Index); ALL (akute lymphatische Leukämie); ampGA (amplifizierten Genomabschnitte); ChIP (Chromatin-Immunoprezipitation); DI (DNA-Index); dMin (double-minute-chromosome-bodies); DPMA (Deutschen Patent- und Markenamt); EFS (event free survival); HDAC (Histondeacetylasen); HR-TA (hochauflösenden Tiling-Arrays); HSR (homogeneously staining regions); INPC (International Neuroblastoma Pathology Committee); INSS (Internationale Stadieneinteilung für Neuroblastome); IRR (Insulin-Rezeptor-related-Rezeptor); LOH (loss of heterozygosity); LZÜ (Langzeitüberleben); MRD (minimal residual disease); MYCN (Avian Myelozytomatosis viral-related oncogene, Neuroblastoma-derived); NB (Neuroblastom); OS (overall survival); PAM (Prediction analysis for microarrays); PCR (Polymerase Chain Reaction); RTK (Rezeptor-Tyrosinkinase); Zbtb4 (Zinc-Finger and BTB-Poz Domain containing Protein 4)

2.8 Literatur

Adida C, Berrebi D, Peuchmaur M, Reyes-Mugica M, Altieri DC. Anti-apoptosis gene, survivin, and prognosis of neuroblastoma. *Lancet*. 1998 Mar 21;351(9106):882-3.

Berwanger B, Hartmann O, Bergmann E, Bernard S, Nielsen D, Krause M, Kartal A, Flynn D, Wiedemeyer R, Schwab M, Schäfer H, Christiansen H, Eilers M. Loss of a FYN-regulated differentiation and growth arrest pathway in advanced stage neuroblastoma. *Cancer Cell*. 2002 Nov;2(5):377-86.

Bown N, Cotterill S, Lastowska M, O'Neill S, Pearson AD, Plantaz D, Meddeb M, Danglot G, Brinkschmidt C, Christiansen H, Laureys G, Speleman F. Gain of chromosome arm 17q and adverse outcome in patients with neuroblastoma. *N Engl J Med*. 1999 Jun 24;340(25):1954-61.

Brodeur GM, Sekhon G, Goldstein MN. Chromosomal aberrations in human neuroblastomas. *Cancer*. 1977 Nov;40(5):2256-63.

Brodeur GM. Neuroblastoma: clinical significance of genetic abnormalities. *Cancer Surv*. 1990;9(4):673-88.

Brodeur GM. Molecular basis for heterogeneity in human neuroblastomas. *Eur J Cancer*. 1995;31A(4):505-10.

Caron H, van Sluis P, Buschman R, Pereira do Tanque R, Maes P, Beks L, de Kraker J, Voute PA, Vergnaud G, Westerveld A, Slater R, Versteeg R. Allelic loss of the short arm of chromosome 4 in neuroblastoma suggests a novel tumour suppressor gene locus. *Hum Genet*. 1996 Jun;97(6):834-7.

Castle VP, Heidelberger KP, Bromberg J, Ou X, Dole M, Nunez G. Expression of the apoptosis-suppressing protein bcl-2, in neuroblastoma is associated with unfavorable histology and N-myc amplification. *Am J Pathol*. 1993 Dec;143(6):1543-50.

Christiansen H, Lampert F. Tumour karyotype discriminates between good and bad prognostic outcome in neuroblastoma. *Br J Cancer*. 1988 Jan;57(1):121-6.

Christiansen, H., Christiansen, N. M., Wagner, F., Altmannsberger, M., and Lampert. F. Neuroblastoma: inverse relationship between expression of N-myc and NGF-r. *Oncogene*, *5:* 437–440, 1990.

Christiansen, N. M., Christiansen, H., Berthold, F., and Lampert, F. Transcriptional activity of N-myc and ngf-r in 50 primary human neuroblastomas as predictor for clinical outcome. *Int. J. Oncol*., *3:*853–857, 1993.

Cohn SL, Pearson AD, London WB, Monclair T, Ambros PF, Brodeur GM, Faldum A,Hero B, Iehara T, Machin D, Mosseri V, Simon T, Garaventa A, Castel V, Matthay KK; INRG Task Force. The International Neuroblastoma Risk Group (INRG) classification system: an INRG Task Force report. *J Clin Oncol*. 2009 Jan 10;27(2):289-97.

Combaret V, Gross N, Lasset C, Frappaz D, Peruisseau G, Philip T, Beck D, Favrot MC. Clinical relevance of CD44 cell-surface expression and N-myc gene amplification in a multicentric analysis of 121 pediatric neuroblastomas. *J Clin Oncol*. 1996 Jan;14(1):25-34.

Defferrari R, Tonini GP, Conte M, Papio F, Sementa AR, Valent A, Schena F, Perri P, Mazzocco K. Concomitant DDX1 and MYCN gain in neuroblastoma. *Cancer Lett*. 2007 Oct 18;256(1):56-63.

Dhooge CR, De Moerloose BM, Benoit YC, Van Roy N, Philippe, Laureys GG. Expression of the MDR1 gene product P-glycoprotein in childhood neuroblastoma. Cancer. 1997 Oct 1;80(7):1250-7.

Dole M, Nunez G, Merchant AK, Maybaum J, Rode CK, Bloch CA, Castle VP. Bcl-2 inhibits chemotherapy-induced apoptosis in neuroblastoma. *Cancer Res*. 1994 Jun 15;54(12):3253-9.

Eggert A, Ho R, Ikegaki N, Liu XG, Brodeur GM. Different effects of TrkA expression in neuroblastoma cell lines with or without MYCN amplification. *Med Pediatr Oncol*. 2000 Dec;35(6):623-7.

Evans AE, D'Angio GJ, Randolph J. A proposed staging for children with neuroblastoma. Children's cancer study group *A. Cancer*. 1971 Feb;27(2):374-8.

Fischer M, Spitz R, Oberthür A, Westermann F, Berthold F. Risk estimation of neuroblastoma patients using molecular markers. *Klin Padiatr*. 2008 May-Jun;220(3):137-46.

Fong CT, Dracopoli NC, White PS, Merrill PT, Griffith RC, Housman DE, Brodeur GM. Loss of heterozygosity for the short arm of chromosome 1 in human neuroblastomas: correlation with N-myc amplification. *Proc Natl Acad Sci U S A*. 1989 May; 86(10):3753-7.

Franke F, Rudolph B, Christiansen H, Harbott J, Lampert F. Tumour karyotype may be important in the prognosis of human neuroblastoma. *J Cancer Res Clin Oncol*. 1986;111(3):266-72.

Giannakakou P, Sackett DL, Ward Y, Webster KR, Blagosklonny MV, Fojo T (2000) p53 is associated with cellular microtubules and is transported to the nucleus by dynein. *Nat Cell Biol* 2:709–717

Godbout R, Squire J. Amplification of a DEAD box protein gene in retinoblastoma cell lines. *Proc Natl Acad Sci U S A* 1993 90(16):7578-7582

Gross N, Beck D, Beretta C, Jackson D, Perruisseau G. CD44 expression and modulation on human neuroblastoma tumours and cell lines. *Eur J Cancer*. 1995;31A(4):471-5.

Hahn PJ, Nevaldine B, Longo JA. Molecular structure and evolution of double-minute chromosomes in methotrexate-resistant cultured mouse cells. *Mol Cell Biol*. 1992 Jul;12(7):2911-8.

Hallstensson K, Thulin S, Aburatani H, Hippo Y, Martinsson T. Representational difference analysis and loss of heterozygosity studies detect 3p deletions in neuroblastoma. *Eur J Cancer*. 1997 Oct;33(12):1966-70.

Hughes M, Marsden HB, Palmer MK. Histologic patterns of neuroblastoma related to prognosis and clinical staging. *Cancer*. 1974 Nov;34(5):1706-11

Kaneko S, Ohira M, Nakamura Y, Isogai E, Nakagawara A, Kaneko M. Relationship of DDX1 and NAG gene amplification/overexpression to the prognosis of patients with MYCN-amplified neuroblastoma. *J Cancer Res Clin Oncol*. 2007 Mar;133(3):185-92.

Keim DR, Hailat N, Kuick R, Reynolds CP, Brodeur GM, Seeger RC, Hanash SM. PCNA levels in neuroblastoma are increased in tumors with an amplified N-myc gene and in metastatic stage tumors. *Clin Exp Metastasis*. 1993 Jan;11(1):83-90.

Kogner, P., Barbany, G., Dominici, C., Castello, M. A., Raschella, G., and Persson, H. Coexpression of messenger RNA for TRK protooncogene and low affinity nerve growth factor receptor in neuroblastoma with favorable prognosis. *Cancer Res., 53:* 2044–2050, 1993

Look AT, Hayes FA, Nitschke R, McWilliams NB, Green AA. Cellular DNA content as a predictor of response to chemotherapy in infants with unresectable neuroblastoma. *N Engl J Med*. 1984 Jul 26;311(4):231-5.

Look AT, Hayes FA, Shuster JJ, Douglass EC, Castleberry RP, Bowman LC, Smith EI, Brodeur GM. Clinical relevance of tumor cell ploidy and N-myc gene amplification in childhood neuroblastoma: a Pediatric Oncology Group study. *J Clin Oncol*. 1991 Apr;9(4):581-91.

Maris JM, Matthay KK. Molecular biology of neuroblastoma. *J Clin Oncol*. 1999 Jul;17(7):2264-79

Matsunaga T, Takahashi H, Ohnuma N, Tanabe M, Yoshida H, Iwai J, Shirasawa H, Simizu B. Expression of N-myc and c-src protooncogenes correlating to the undifferentiated phenotype and prognosis of primary neuroblastomas. *Cancer Res*. 1991 Jun 15;51(12):3148-52.

Monclair T, Brodeur GM, Ambros PF, Brisse HJ, Cecchetto G, Holmes K, Kaneko M, London WB, Matthay KK, Nuchtern JG, von Schweinitz D, Simon T, Cohn SL, Pearson AD; INRG Task Force. The International Neuroblastoma Risk Group (INRG) staging system: an INRG Task Force report. *J Clin Oncol*. 2009 Jan 10;27(2):298-303.

Moroz V, Machin D, Faldum A, Hero B, Iehara T, Mosseri V, Ladenstein R, Bernardi BD, Rubie H, Berthold F, Matthay KK, Monclair T, Ambros PF, Pearson AD, Cohn SL, London WB. Changes over three decades in outcome and the prognostic influence of age-at-diagnosis in young patients with neuroblastoma: A report from the International Neuroblastoma Risk Group Project. *Eur J Cancer*. 2010 Nov 26.

Nakagawara A, Kadomatsu K, Sato S, Kohno K, Takano H, Akazawa K, Nose Y, Kuwano M. Inverse correlation between expression of multidrug resistance gene and N-myc oncogene in human neuroblastomas. *Cancer Res*. 1990 May 15;50(10):3043-7.

Nakagawara, A., Arima-Nakagawara, M., Scavarda, N. J., Azar, C. G., Cantor, A. B., and Brodeur, G. M. Association between high levels of expression of the trk gene and favorable outcome in human neuroblastoma. *N. Engl. J. Med*., *328:* 847–854, 1993

Oberthuer A, Berthold F, Warnat P, et al: Customized oligonucleotide microarray gene expressionbased classification of neuroblastoma patients outperforms current clinical risk stratification. *J Clin Oncol* 24:5070-5078, 2006

Schwab M, Alitalo K, Klempnauer KH, Varmus HE, Bishop JM, Gilbert F, Brodeur G, Goldstein M, Trent J. Amplified DNA with limited homology to myc cellular oncogene is shared by human neuroblastoma cell lines and a neuroblastoma tumour. *Nature*. 1983 Sep 15-21;305(5931):245-8.

Seeger RC, Wada R, Brodeur GM, Moss TJ, Bjork RL, Sousa L, Slamon DJ. Expression of N-myc by neuroblastomas with one or multiple copies of the oncogene. Prog Clin Biol Res. 1988;271:41-9. No abstract available. Cohn SL, London WB, Huang D, Katzenstein HM, Salwen HR, Reinhart T, Madafiglio J, Marshall GM, Norris MD, Haber M. MYCN expression is not prognostic of adverse outcome in advanced-stage neuroblastoma with nonamplified MYCN. *J Clin Oncol*. 2000 Nov 1;18(21):3604-13.

Seoane J, Le HV, Massague J (2002) Myc suppression of the p21(Cip1) Cdk inhibitor influences the outcome of the p53 response to DNA damage. *Nature* 419: 729–734

Shimada H, Chatten J, Newton WA Jr, Sachs N, Hamoudi AB, Chiba T, Marsden HB, Misugi K. Histopathologic prognostic factors in neuroblastic tumors: definition of subtypes of ganglioneuroblastoma and an age-linked classification of neuroblastomas. *J Natl Cancer Inst*. 1984 Aug;73(2):405-16.

Shimada, H, I M Ambros, L P Dehner, et al. Terminology and morphologic criteria of neuroblastic tumors: recommendations by the International Neuroblastoma Pathology Committee. *Cancer* 1999; 86: 349-63

Srivatsan ES, Murali V, Seeger RC. Loss of heterozygosity for alleles on chromosomes 11q and 14q in neuroblastoma. *Prog Clin Biol Res*. 1991;366:91-8.

Stutterheim J, Gerritsen A, Zappeij-Kannegieter L, Kleijn I, Dee R, Hooft L, van Noesel MM, Bierings M, Berthold F, Versteeg R, Caron HN, van der Schoot CE, Tytgat GA. PHOX2B is a novel and specific marker for minimal residual disease testing in neuroblastoma. *J Clin Oncol*. 2008 Nov 20;26(33):5443-9.

Stutterheim J, Gerritsen A, Zappeij-Kannegieter L, Yalcin B, Dee R, van Noesel MM, Berthold F, Versteeg R, Caron HN, van der Schoot CE, Tytgat GA. Detecting minimal residual disease in neuroblastoma: the superiority of a panel of real-time quantitative PCR markers. *Clin Chem*. 2009 Jul;55(7):1316-26.

Suzuki T, Yokota J, Mugishima H, Okabe I, Ookuni M, Sugimura T, Terada M. Frequent loss of heterozygosity on chromosome 14q in neuroblastoma. *Cancer Res*. 1989 Mar 1;49(5):1095-8.

Tanaka T, Slamon DJ, Shimoda H, Waki C, Kawaguchi Y, Tanaka Y, Ida N. Expression of Ha-ras oncogene products in human neuroblastomas and the significant correlation with a patient's prognosis. *Cancer Res*. 1988 Feb 15;48(4):1030-4.

Takita J, Hayashi Y, Kohno T, Yamaguchi N, Hanada R, Yamamoto K, Yokota J. Deletion map of chromosome 9 and p16 (CDKN2A) gene alterations in neuroblastoma. *Cancer Res*. 1997 Mar 1;57(5):907-12.

Weber A, Huesken C, Bergmann E, Kiess W, Christiansen NM, Christiansen H. Coexpression of insulin receptor-related receptor and insulin-like growth factor 1 receptor correlates with enhanced apoptosis and dedifferentiation in human neuroblastomas. *Clin Cancer Res*. 2003 Nov 15;9(15):5683-92.

3. Erklärung

Hiermit erkläre ich, dass ich die Habilitationsordnung anerkenne.

Die Habilitationsschrift wurde von mir selbstständig verfasst. Es wurden keine anderen als die angegebenen Quellen und Hilfsmittel benutzt sowie die wörtlich oder inhaltlich übernommenen Stellen als solche gekennzeichnet.

Die Habilitationsschrift wurde in dieser oder ähnlicher Form an keiner anderen Stelle zum Zweck eines Graduierungsverfahrens vorgelegt.

Leipzig, den 11. Januar 2011

Dr. med. Axel Weber

4.1 Curriculum Vitae

Persönliche Daten:

Dr. med. Axel Weber Geboren am 10.05.1974 in Hanau

Schulausbildung:

Zivildienst:

Studium:

Famulaturen:

Promotionsarbeit:

Beruflicher Werdegang:

Weiterbildungen:

Eingeworbene Drittmittel:

Durchgeführte Lehrtätigkeit:

4.2 Publikationen

Originalarbeiten:

Bergmann E, Wanzel M, **Weber A**, Shin I, Christiansen H, Eilers M. Expression of P27(KIP1) is prognostic and independent of *MYCN* amplification in human neuroblastoma. Int J Cancer. 2001 May 20;95(3):176-83.

Weber A, Huesken C, Bergmann E, Kiess W, Christiansen NM, Christiansen H. Coexpression of insulin receptor-related receptor and insulin-like growth factor 1 receptor correlates with enhanced apoptosis and dedifferentiation in human neuroblastomas. *Clin Cancer Res*. 2003 Nov 15;9(15):5683-92. PMID: 14654552

Weber A, Imisch P, Bergmann E, Christiansen H. Coamplification of *DDX1* correlates with an improved survival probability in children with *MYCN*-amplified human neuroblastoma. *J Clin Oncol*. 2004 Jul 1;22(13):2681-90.

Weber A, Imisch P, Bergmann E, Christiansen H. In reply:. *J Clin Oncol*. 2005 May 1;23(13):3168-70

Weber A, Starke S, Bergmann E, Christiansen H. The coamplification pattern of the *MYCN* amplicon is an invariable attribute of most *MYCN*-amplified human neuroblastomas. *Clin Cancer Res*. 2006 Dec 15;12(24):7316-21.

Weber A, Marquardt J, Elzi D, Forster N, Starke S, Glaum A, Yamada D, Defossez PA, Delrow J, Eisenman RN, Christiansen H, Eilers M. Zbtb4 represses transcription of P21CIP1 and controls the cellular response to p53 activation. *EMBO J.* 2008 Jun 4;27(11):1563-74. Epub 2008 May 1.

Ferrandiz N, Martin-Perez J, Blanco R, Donertas D, **Weber A**, Eilers M, Dotto P,Delgado MD, Leon J. HCT116 cells deficient in p21(Waf1) are hypersensitive to tyrosine kinase inhibitors and adriamycin through a mechanism unrelated to p21 and dependent on p53. *DNA Repair* (Amst). 2009 Mar 1;8(3):390-9.

Bergmann E, Bierbach U, Fischer L, Frenzel K, **Weber A**, Starke S, Christiansen NM, Christiansen H. Therapie höhergradiger Gliome mit dem onkolytischen Stamm MTH-68/H des Newcastle-Disease-Virus in der pädiatrischen Onkologie. *Kinder und Jugendmedizin*. 3/2010; 10: 171-175.

Oberthuer A, Hero B, Berthold F, Juraeva D, Faldum A, Kahlert Y, Asgharzadeh S, Seeger R, Scaruffi P, Tonini GP, Janoueix-Lerosey I, Delattre O, Schleiermacher G, Vandesompele J, Vermeulen J, Speleman F, Noguera R, Piqueras M, Bénard J, Valent A, Avigad S, Yaniv I, **Weber A**, Christiansen H, Grundy RG, Schardt K, Schwab M, Eils R, Warnat P, Kaderali L, Simon T, Decarolis B, Theissen J, Westermann F, Brors B, Fischer M. Prognostic impact of gene expression-based classification for neuroblastoma. *J Clin Oncol*. 2010 Jul 20;28(21):3506-15.

Weber A, Taube S, Starke S, Bergmann E, Christiansen NM, Christiansen H. Detection of tumor cells by amplicon-fusion-site polymerase-chain-reaction (AFS-PCR). *J Clin Invest*., Published online January 10, 2011

Publikation von Gensequenzen:

Weber A, Glaum A, Klinkhammer B, Bergmann E, Berwanger B, Eilers M and Christiansen H; Homo sapiens Syntaxin binding protein 1 like 1 (STXBP1-L1) mRNA, GenBank accession AY299407

Weber A, Klinkhammer B, Glaum A, Bergmann E, Berwanger B, Eilers M and Christiansen H; KAISO like zinc finger (KAISO-L1) mRNA, complete cds. GenBank accession AY302699

Patentanmeldungen:

Weber A, Christiansen H; Verfahren und Mittel zum patienten- und tumorspezifischen Nachweis von Malignomzellen. *Deutsche Patentanmeldung Nr. 10 2009 047 549.4*
(eingereicht im Dezember 2009, angenommen Dezember 2010, Erteilung geplant für April 2011)

Weber A, Christiansen H; Verfahren und Mittel zur patienten- und tumorspezifischen Therapie von Malignomzellen. *Deutsche Patentanmeldung Nr. 10 2010 001 332.2*
(eingereicht im Januar 2010)

Danksagung

Wissenschaftliche Ziele konsequent zu verfolgen und sinnvoll umzusetzen, so dass sie zu erfolgreichen Publikationen und einer solchen Habilitationsschrift führen können, bedeutet viel Zeit zu investieren. Da die klinische Arbeit und Ausbildung eigentlich den Hauptteil ärztlichen Handelns bestimmt, ist es oft schwierig die wissenschaftlichen Interessen adäquat realisieren zu können. Hierfür ist es zwingend notwendig, neben räumlichen und technischen auch ausreichend zeitliche und finanzielle Möglichkeiten zur Verfügung gestellt zu bekommen.

Ich hatte das Glück, in Herrn Prof. Holger Christiansen einen Mentor zu finden, der mir in den vielen Jahren unserer gemeinsamen Arbeit den Freiraum geben konnte, der für die Projektgestaltung und -umsetzung notwendig war. Hierfür bin ich Ihm gegenüber zu großem Dank verpflichtet und ich freue mich, in Ihm neben unserer gemeinsamen Arbeit auch einen guten Freund gefunden zu haben.

Ich möchte an dieser Stelle auch allen weiteren Personen danken, die mich auf meinem bisherigen, wissenschaftlichen Weg unterstützt haben, allen voran Herrn Prof. Martin Eilers, in dessen Arbeitsgruppe am IMT in Marburg ich das Glück hatte 2 Jahre lang mitarbeiten zu dürfen. In dieser Zeit habe ich sehr viel gelernt und tiefe Einblicke in konsequentes molekolarbiologisches und biochemisches Arbeiten bekommen können. Herrn Prof. Hansjörg Seyberth gebührt mein Dank, dass er mir in seiner Zeit als Klinikdirektor der Universitäts-Kinderklinik in Marburg die Möglichkeit gab, neben meiner allgemeinpädiatrischen Ausbildung auch meine Forschungsprojekte weiter verfolgen zu können.

Allen aktuellen und ehemaligen Mitarbeitern in unserem kinderonkologischen Labor (dem „Neuroblastom-Labor“) danke ich für die immerwährende, tatkräftige Unterstützung. Im Besonderen sei hier Herrn Dr. Sven Starke und Frau Sylvia Taube gedankt.

Ein besonderer Dank gebührt meiner Frau und meinen beiden Töchtern, die mit großer Geduld mein berufliches Engagement unterstützt haben und gerade in der „Leipziger“ Zeit viel auf meine Unterstützung zu Hause verzichten mussten. Ohne die Kraft und den Einsatz meiner Frau wäre diese Arbeit nicht möglich gewesen.

Meinen Eltern und meiner Schwester Christiane möchte ich für den immer vorhandenen Rückhalt und die niemals in Frage gestellte Unterstützung unserer Familie danken. Dies ist ein Geschenk, das leider in vielen Momenten nicht die Schätzung erfährt, die ihm eigentlich gebührt.

All diese Menschen hatten damit Ihren unverzichtbaren Anteil an dieser Arbeit.

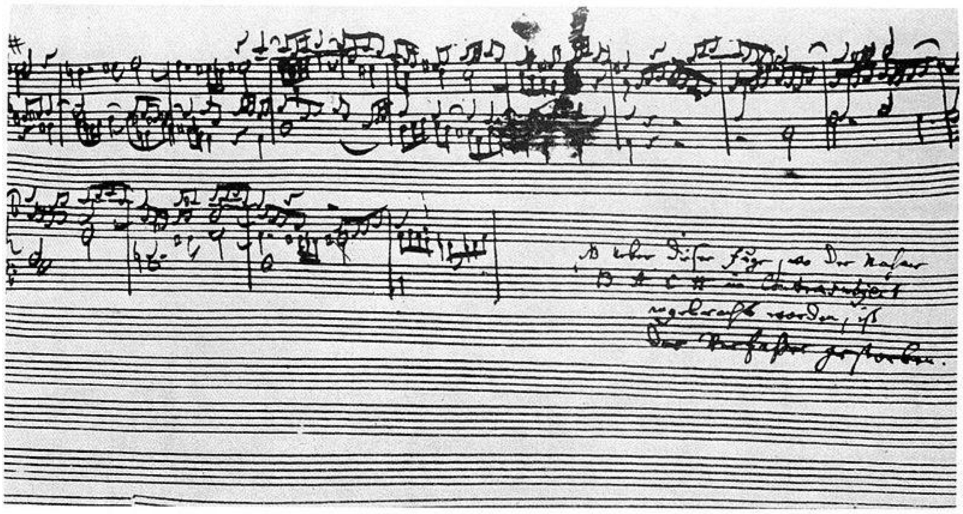
NB uber dieser Fuge, wo der Nahme
B A C H im Contrasubject
angebracht worden, ist
der Verfaßer gestorben.

J.S. Bach (1685-1750); die letzte Seite des Autographen „Die Kunst der Fuge“

(komponiert am Ende seiner Schaffensperiode als Kantor an der Thomaskirche zu Leipzig)